Aus der Klinik für Gefäß- und Endovaskularchirurgie
(Direktor Univ. Prof. Dr. med. Hubert Schelzig)
Der Medizinischen Fakultät der
Heinrich-Heine-Universität Düsseldorf

Die pathogenetische Relevanz des Geweberemodelings für gefäßchirurgische Krankheitsbilder

---

Habilitationsschrift zur Erlangung der Venia legendi für das Fach Chirurgie
an der Medizinischen Fakultät der Heinrich-Heine-Universität Düsseldorf
vorgelegt von

Dr. med. Markus Wagenhäuser
aus Würzburg

Düsseldorf 2020

Meinen geliebten Eltern in größter Dankbarkeit

Inhaltsverzeichnis

1. Zugrundeliegende Originalarbeiten

1) **Wagenhäuser MU**, Garabet W, van Bonn M, Ibing W, Mulorz J, Rhee YH, Spin JM, Dimopoulos C, Oberhuber A, Schelzig H, Simon F. Time-dependent effects of cellulose and gelatin-based hemostats on cellular processes of wound healing. Arch Med Sci. 2020; doi:10.5114/aoms.2020.92830.

2) **Wagenhäuser MU**, Dimopoulos C, Antakyali K, Meyer-Janiszewski YK, Mulorz J, Ibing W, Ertas N, Spin JM, Schelzig H, Duran M. Clinical outcomes after direct and indirect surgical venous thrombectomy for inferior vena cava thrombosis. J Vasc Surg Venous Lymphat Disord. 2019;7(3):333-343.e2.

3) Nguyen DM, **Wagenhäuser MU**, Mehrkens D, Adam M, Tsao PS, Ramasubramanian AK. An Automated Algorithm to Quantify Collagen Distribution in Aortic Wall. J Histochem Cytochem. 2019;67(4):267-274.

4) **Wagenhäuser MU***, Schellinger IN*, Yoshino T, Toyama K, Kayama Y, Deng A, Guenther SP, Petzold A, Mulorz J, Mulorz P, Hasenfuß G, Ibing W, Elvers M, Schuster A, Ramasubramanian AK, Adam M, Schelzig H, Spin JM, Raaz U*, Tsao PS*. Chronic Nicotine Exposure Induces Murine Aortic Remodeling and Stiffness Segmentation-Implications for Abdominal Aortic Aneurysm Susceptibility. Front Physiol. 2018;31;9:1459.

5) **Wagenhäuser MU**, Sadat H, Dueppers P, Meyer-Janiszewski YK, Spin JM, Schelzig H, Duran M. Open surgery for iliofemoral deep vein thrombosis with temporary arteriovenous fistula remains valuable. Phlebology. 2018;33(9):600-609.

6) Adam M, Kooreman NG, Jagger A, **Wagenhäuser MU**, Mehrkens D, Wang Y, Kayama Y, Toyama K, Raaz U, Schellinger IN, Maegdefessel L, Spin JM, Hamming JF, Quax PHA, Baldus S, Wu JC, Tsao PS. Systemic Upregulation of IL-10 (Interleukin-10) Using a Nonimmunogenic Vector Reduces Growth and Rate of Dissecting Abdominal Aortic Aneurysm. Arterioscler Thromb Vasc Biol. 2018;38(8):1796-1805.

7) **Wagenhäuser MU**, Mulorz J, Ibing W, Simon F, Spin JM, Schelzig H, Oberhuber A. Oxidized (non)-regenerated cellulose affects fundamental cellular processes of wound healing. Sci Rep. 2016;25;6:32238.

8) **Wagenhäuser MU,** Duran M, Dueppers P, Witte M, Schelzig H, Oberhuber A. Preliminary results of transcutaneous oxygen pressure measurement as effective monitoring for conservative therapy in peripheral occlusive disease. Ital J Vasc Endovasc Surg. 2015;22(4):163-70.

2. Einleitung

Die extrazelluläre Matrix (EZM) ist eine komplexe multimolekulare Struktur, die u.a. aus Kollagenbündeln, Elastinlamellen, verschiedenen Glykoproteinen und Mukopolysacchariden besteht. Zur Aufrechterhaltung der Gewebehämostase befinden sich Synthese- und Degradationsprozesse von EZM Bestandteilen in einem „steady-state“[1]. Kommt es zu einem Ungleichgewicht zwischen Synthese und Degradation kann diese Dysbalance Krankheitswert gewinnen.

In das 3-dimensionale Rahmenwerk der EZM eingebettet liegen verschiedene Zellarten, wie Fibroblasten oder glatte Muskelzellen, die sich je nach Gewebefunktion in Quantität und Zusammensetzung unterscheiden[2]. Die zelluläre Funktionalität und Integrität ist unmittelbar mit der Synthese und Degradation der EZM verknüpft. Die Beziehung zwischen der EZM und den eingebetteten Zellen ist reziprok. Zellen sind für die Synthese und Organisation verschiedener Bestandteile der EZM verantwortlich und regulieren die strukturelle Zusammensetzung der synthetisierten Proteine[3]. Dagegen fungieren zelluläre Oberflächenrezeptoren, wie Integrine, als Bindeglied zwischen Proteinen der EZM und den Zellen[4]. Durch eine Phosphorylierungskaskade können Integrine die Zellproliferation, -differenzierung und Genexpression steuern, wodurch die EZM durch das so genannte „outside-in signaling“ Einfluss auf zelluläre Prozesse nehmen kann[5,6].

Neben den stationären Zellen existieren nicht residente inflammatorische Zellen, die bei entsprechendem Reiz rekrutiert werden und in das Gewebe einwandern können[7]. Sie spielen somit für die Organisation und Struktur der EZM eine entscheidende Rolle und können auf dieser Grundlage maßgeblichen Einfluss für die Krankheitsentstehung gewinnen[8,9].

Im gefäßmedizinischen Krankengut spielt das dysfunktionale Geweberemodeling bei der Entstehung verschiedener Erkrankungen eine substantielle Rolle. So ist ein fehlgesteuertes Geweberemodeling strukturgebender Proteine der aortalen Gefäßwand in der Pathogenese des infrarenalen abdominellen Aortenaneurymsa (AAA) von hoher Relevanz[10]. Weiterhin sind stromale Remodelingprozesse, die sowohl auf der Interaktion verschiedener Zelltypen basieren als auch auf dem geordneten Wechselspiel biologisch aktiver Mediatoren beruhen, für die physiologische Wundheilung entscheidend[11,12]. Auch Folgeerkrankungen einer venösen Thrombose mit hoher Morbidität, wie das post-

thrombotische Syndrom (PTS), gründen kausal auf durch Inflammation initiierten Remodulierungsprozessen der Venenklappen/-wand[13,14]. Auf das jeweils krankheitsspezifische Geweberemodeling dieser Pathologien soll im Folgenden näher eingegangen werden.

2.1. Das abdominelle Aortenaneurysma

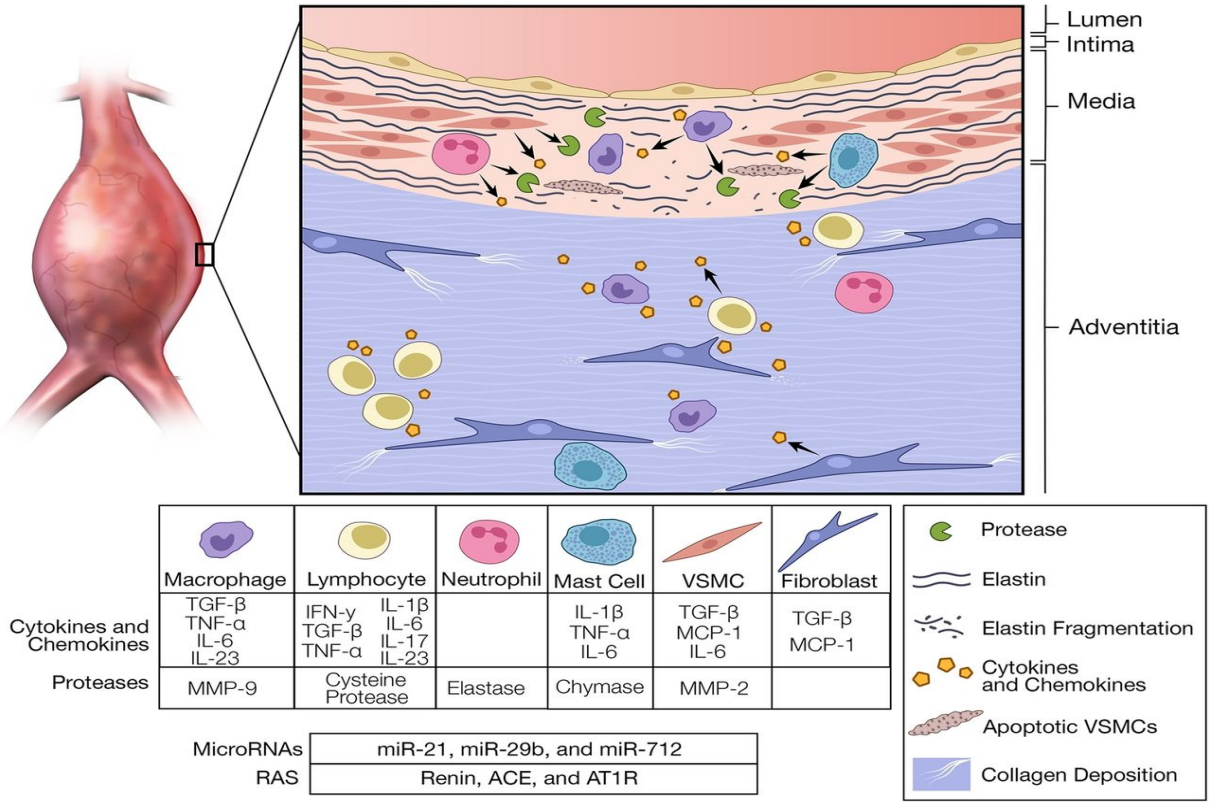

Abbildung 1: Pathogenese der Entwicklung eines abdominellen Aortenaneurysma (AAA). Die Rekrutierung von inflammatorischen Zellen etabliert ein chronisch inflammatorisches Milieu. Eine gesteigerte Aktivität von Matrix-Metalloproteinasen (MMP) und weiteren Enzymen führt zur Degradation von Kollagenen und zur Fragmentierung von Elastinfasern. Der sukzessive Stabilitätsverlust der Aortenwand wird begleitet von einer Apoptose glatter Muskelzellen. Aus Davis, F. M., Rateri, D. L. & Daugherty, A. *Mechanisms of aortic aneurysm formation: translating preclinical studies into clinical therapies.* Heart. Oct;100(19):1498-505 (2014). (Mit freundlicher Genehmigung von British Medical Journal, lizenziert, Nummer: 4666450372939).

Das AAA ist eine häufige Erkrankung des alten Menschen und besitzt bei Ruptur eine hohe Letalitätsrate von bis zu 80%[15,16]. Ein AAA ist definiert als pathologische Dilatation des Aortendiameters auf > 30 mm (> 1,5-fach des normalen Diameters) und tritt zumeist im infrarenalen Aortensegment auf[17]. Ein hohes Lebensalter (> 65 Jahre), männliches Geschlecht, genetische Prädisposition, stammbetonte Fettleibigkeit und das Rauchen von Zigaretten sind allgemein anerkannte Risikofaktoren[18]. Obwohl die Implantation

eines Stentgraft für das vornehmlich betroffene ältere Patientengut zu einer deutlichen Reduktion der Krankenhausmortalität geführt hat, existiert bis heute keine primäre Präventionsstrategie[19]. Zur Entwicklung solcher Behandlungsansätze ist das Wissen um die zugrundeliegenden Pathomechanismen elementar.

Präklinische AAA Modelle zeichnen ein komplexes Bild der Krankheitsentstehung und Diameterprogression, das eine chronische lokale Inflammation innerhalb der Aortenwand nahelegt. Beschrieben wurde die Einwanderung von Monozyten/Makrophagen, polymorphkernige Leukozyten und/oder T- und B-Lymphozyten in die Adventitia und Tunica Media. Durch diese Rekrutierung kommt es zur Etablierung eines chronisch inflammatorischen Milieus, in dem Zytokine, Leukotriene und Immunoglobuline stetig weitere Immunzellen rekrutieren[20]. Diese Prozesse leiten ein pathologisches Geweberemodeling ein, an dessen Ende bei fehlender operativer Therapie die AAA Ruptur steht.

Die proteolytische Destruktion der Tunica Media und der stabilitätssichernden Tunica Adventitia basiert fundamental auf der Aktivität von Matrix-Metalloproteinasen (MMP) und Serinproteasen, die überwiegend von residenten Zelltypen der Aortenwand und rekrutierten Makrophagen gebildet werden[20,21]. In Tiermodellen wird so die initial kompensatorisch gesteigerte Kollagensynthese durch eine vermehrte Degradation abgelöst und so eine Dysbalance zwischen Neusynthese und Degradation geschaffen[22]. Basierend auf derselben pathologisch gesteigerten enzymatischen Aktivität, findet simultan eine vermehrte Fragmentierung des Elastins statt[20].

Neben diesen Remodelingsprozessen der EZM sind auf zellulärer Ebene glatte Muskelzellen für die Progression des AAA entscheidend. So können glatte Muskelzellen der Aortenwand in einen proliferativ-sekretorischen und migratorischen Phänotyp differenzieren, der zur vermehrten Freisetzung und Aktivitätszunahme der zuvor beschriebenen MMPs führt[23]. Im weiteren Fortgang der Erkrankung kommt es schließlich zur Apoptose von glatten Muskelzellen, was zu einem weiteren signifikanten Stabilitätsverlust der Aortenwand und Diameterexpansion führt[20,24].

Verschiedene regulative Vorgänge können diese grundlegenden Prozesse der AAA Entstehung und Progression modifizieren. So sind kleine, nicht kodierende Ribonukleinsäuren, so genannte mikro-RNA (miRNA), effektive intrazelluläre

Regulatoren inflammatorischer Prozesse. Hier zeigte sich miR-24 als wesentlicher Regulator der Inflammation in der AAA Progression[25]. Neben der Inflammation wird auch die quantitative und qualitative Zusammensetzung verschiedener Kollagentypen sowie von Elastin durch miR-29b[26] gesteuert. Die Modifikation intrazellulärer Konzentrationen dieser miRNAs stellt einen vielversprechenden Therapieansatz dar, der jedoch aktuell noch nicht klinisch verfügbar ist.

Des Weiteren scheint der innerhalb des Aneurysmasacks häufig auftretende intraluminale Thrombus (ILT) von hoher Relevanz für die Destabilisierung der AAA-Wand zu sein, was sich in einer gesteigerten Rupturrate bei hoher Thrombuslast widerspiegelt[27]. Dem folgend erscheint der ILT als biologisch aktives Kompartiment, das aktiv Einfluss auf fundamentale Prozesse der AAA Entwicklung nimmt.

Es bleibt festzuhalten, dass stromale Umbauprozesse und zelluläre Dedifferenzierungen, die durch eine chronische Inflammation getriggert werden, fundamentale Bedeutung für die Krankheitsentstehung besitzen.

2.2. Wundheilungsstörungen/chronische Wunden

Postoperative Wundheilungsstörungen, sowie Wunden, die durch eine chronisch kritische Beinischämie induziert werden stellen ein stetig wachsendes gesamtgesellschaftliches und insbesondere spezifisch gefäßmedizinisches Problem dar[28,29]. Das Lebenszeitrisiko, eine chronische Wunde zu entwickeln, beträgt in Industrieländern ca. 1-2%[30]. Im gefäßchirurgischen Patientenkollektiv beträgt das Risiko einer postoperativen Wundheilungsstörung je nach Lokalisation des operativen Zugangs zwischen 3-44%[31–33]. Aufgrund multipler Lymphbahnen im chirurgischen Zugangsgebiet ist die Leistenregion einem besonders hohen Risiko ausgesetzt. Gleichfalls epidemiologisch relevant sind chronische Wunden im Endstadium einer peripheren arteriellen Verschlusskrankheit (pAVK)[34]. Die Versorgungskosten ischämisch bedingter Ulzerationen und chronischer Wunden sind in westlichen Industrieländern hoch und stellen sozioökonomisch eine enorme Herausforderung dar[35].

Dem pathophysiologischen Verständnis um relevante Einflussfaktoren, die zur Entwicklung nicht heilender Wunden beitragen, kommt folglich ein großes Interesse zu.

Die physiologische Wundheilung beruht auf einem hierarchisch gegliederten Prozess mit sich teilweise überlappenden Einzelphasen. In der Inflammationsphase formieren sich aktivierte Thrombozyten und bilden ein zunächst instabiles Fibringerüst. Durch die Ausschüttung pro-inflammatorischer Zytokine wandern neutrophile Granulozyten ein, die ein inflammatorisches Milieu etablieren[36,37].

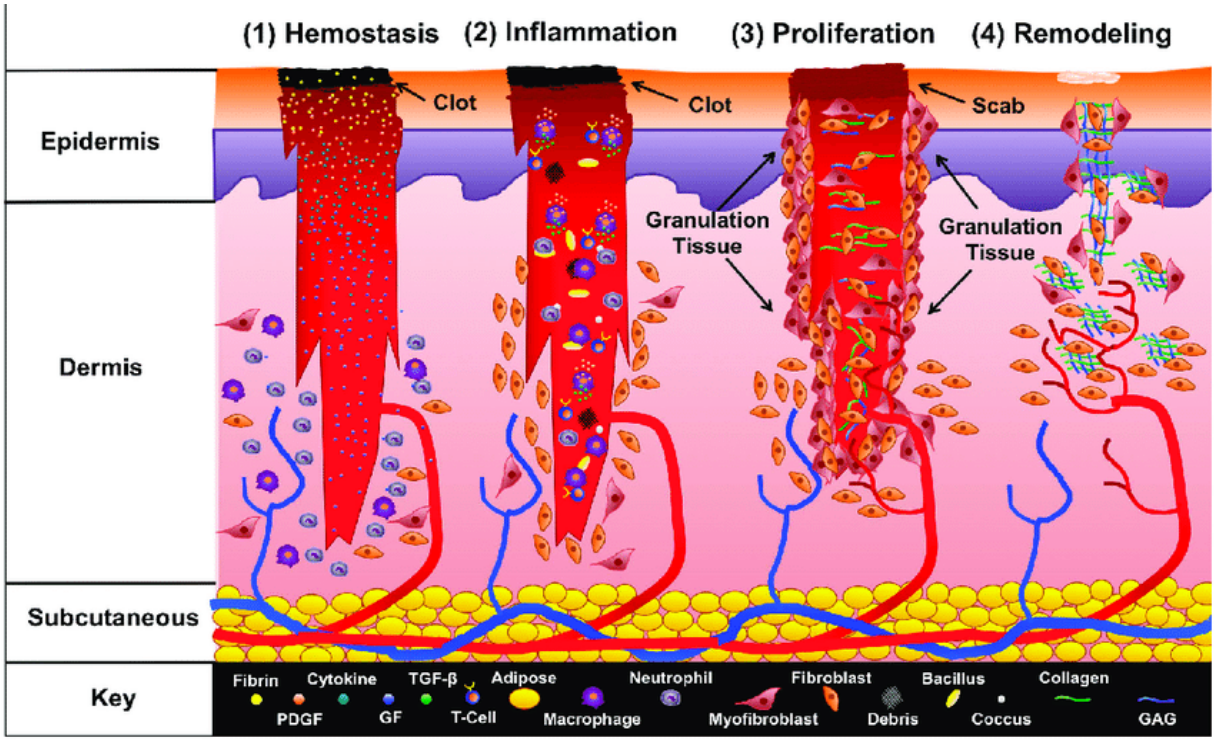

Abbildung 2: Zeitlicher Ablauf der einzelnen Wundheilungsphasen. Nach einer initialen Inflammationsphase kommt es zur Proliferation von Fibroblasten. Diese etablieren durch Produktion von strukturgebenden Kollagenen ein vorläufiges Granulationsgewebe. Zur Erhöhung des Nährstoffangebots in diesem Granulationsgewebe findet eine gesteigerte Angiogenese statt. Schließlich differenzieren Fibroblasten zu Myofibroblasten, die für den definitiven Wundverschluss wesentlich sind. Im weiteren Verlauf folgt eine Remodulierungsphase, die durch weitere stromale Umbauvorgänge zur langfristigen Stabilisation des Narbengewebes führt. Aus Mellott AJ. *Negative Pressure Wound Therapy in Maxillofacial Applications.* Dent J (Basel). Sep; 4(3): 30. (2016). (Mit freundlicher Genehmigung des Multidisciplinary Publishing Institute (MDPI), lizenziert, Creative Commons Attribution (CC-BY) license (http://creativecommons.org/licenses/by/4.0/).

In der nachfolgenden Proliferationsphase erfolgt die Bildung eines Granulationsgewebes sowie eines vaskulären Netzwerks. Die Phase wird häufig auch als Reparationsphase bezeichnet[38]. Es kommt zu einer Proliferation von Fibroblasten und Keratinozyten, die teils in das Wundgebiet migrieren und durch gesteigerte Synthese zur Formierung einer provisorischen Matrix führen. Diese besteht überwiegend aus Kollagen, Glykosaminoglykanen und Fibronektin[38,39]. Die so entstandene schlichte Matrix imponiert

rötlich, da die überlappend gesteigerte Angiogenese noch nicht vollständig abgeschlossen ist[38].

Die Neubildung von Gefäßen beruht sowohl auf der Angiogenese als auch auf einer Vaskulogenese[40]. Während die Angiogenese auf einem Aus- bzw. Einwachsen bereits vorhandener Gefäße in nicht vaskularisiertes Gewebe beruht, kommt es bei der Vaskulogenese zu einer de novo Gefäßformation aus Progenitorzellen[40]. Durch beide Prozesse kommt es zur Ausbildung eines profunden vaskulären Netzwerkes, das ein ausreichendes Nährstoffangebot für das Granulationsgewebe sicherstellt[39].

Die Re-epithelialsierung der Wunde erfolgt ausgehend von den Rändern. Von hier wandern lokale Keratinozyten in die Wunde ein und nehmen zusammen mit epithelialen Stammzellen die Reepithelialisierung vor[38].

Die Remodulierungsphase schließt sich diesen Vorgängen final an und kann Jahre fortdauern[41]. Langfristig wird das Kollagen Typ III durch das mechanisch mehr beanspruchbare Kollagen Typ I ersetzt, wodurch die Wunde belastbarer wird[38,42]. Die Kontraktion der Wunde wird durch den maßgeblichen Einfluss von „transforming growth factor β“ (TGF-β) reguliert. Es kommt zur Synthese von „α-smooth muscle actin“ (α-SMA) wodurch Myofibroblasten eine Kontraktion im gesamten Wundgebiet ausüben[43]. Die Kontraktion führt die Wundränder zusammen und sorgt für einen definitiven Wundverschluss[44,45]. Schließlich erfolgt die Apoptose der Myofibroblasten, was zur Bildung einer definitiven azellulären Narbe führt[39].

Ist das Zusammenspiel der einzelnen Gewebeumbauprozesse gestört bzw. werden zelluläre Subprozesse durch externe Einflüsse gestört, kann sich eine verlangsamte oder gar insuffizienten Wundheilung entwickeln bzw. können sich chronische Wunden etablieren.

2.3. Post-thrombotisches Syndrom (PTS)

Das PTS ist nach stattgehabter tiefer Beinvenenthrombose (TVT) ein sozioökonomisch hoch relevantes Krankheitsbild. Es besitzt 8 Jahre nach einer TVT eine kumulative Inzidenz von ca. 7%[46]. Insbesondere deszendierende Beckenvenenthrombosen haben ein deutlich höheres Risiko der PTS Entwicklung[47]. Bei einer schweren Verlaufsform kann es zu Ulzerationen an der betroffenen unteren Extremität kommen, was die

krankheitsspezifische Lebensqualität („Health-related quality of life“ (HRQOL)) der betroffenen Patienten signifikant reduziert[47,48]. Die Entwicklung dieser Spätkomplikation ist komplex.

Ein durch den Thrombus hervorgerufenes dysfunktionales Geweberemodeling der Venenklappen und der -wand in betroffenen Venensegmenten, das auch nach erfolgter Auflösung des Thrombus noch fortwirkt scheint für die Pathogenese hohe Relevanz zu besitzen[49]. Der Übergang von einer akuten Verlegung der venösen Strombahn hin zu einer chronischen Fibrosierung und Obstruktion in betroffenen Venensegmente mit Venenklappeninsuffizienz ist jedoch nur unzureichend verstanden.

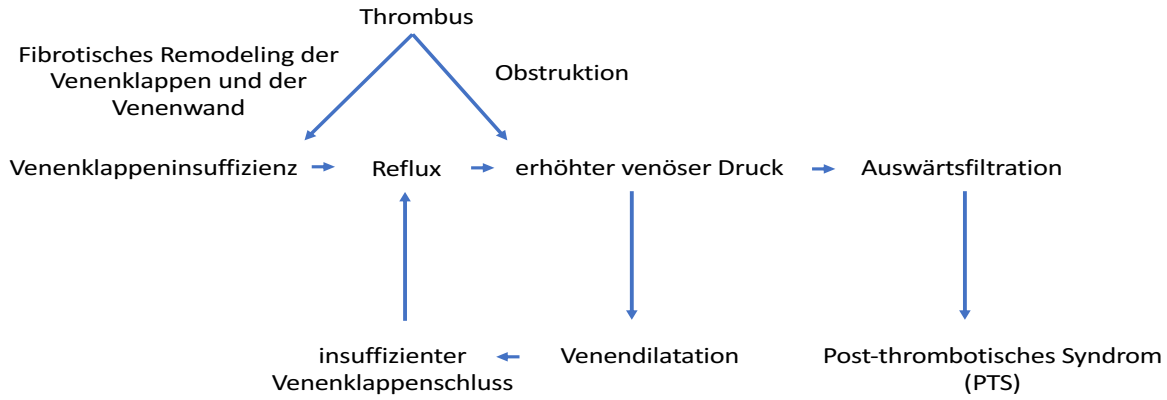

Abbildung 3: Pathomechanismus der Entwicklung eines post-thrombotischen Syndroms (PTS). Der Thrombus führt zu einem fibrotischen Umbau der Venenklappen und der -wand und obstruiert im Extremfall das betroffene Venensegment. Dies erzeugt eine Diametererweiterung der vorgeschalteten Venensegmente, was zu einem insuffizienten Schluss der Venenklappen und folglich zu einem Reflux führt. Dieser Reflux erhöht den venösen Druck und bedingt eine Auswärtsfiltration mit Entstehung eines chronischen Gewebeödems. Besteht dieser Zustand über längere Zeit können venös-bedingte Ulzerationen entstehen. Modifiziert aus Phillips, L. J. & Sarkar, R. *Molecular characterization of post-thrombotic syndrome*. J Vasc Surg. 45 Suppl A, A116-22 (2007). (Mit freundlicher Genehmigung des Elsivier Verlags, lizenziert, Nummer: 4666470129960)

Auf molekularer Ebene bedingt der Thrombus eine Extravasation von Monozyten/Makrophagen in die Venenwand. Dies führt zu einer substantiellen Erhöhung pro-inflammatorischer Zytokine, wie „tumor necrosis factor-alpha“ (TNF-α) und Interleukin-6 (IL-6) und etabliert ein lokal inflammatorisches Milieu[50]. Parakrine Signalkaskaden führen zu einer Erhöhung der MMP-9 Expression in der Frühphase und der MMP-2 Expression im weiteren Fortgang. Dies geht sowohl mit einer vermehrten Kollagenproduktion als auch mit einer Degradation von Elastinfasern einher, was funktionell zu einer Erhöhung der Rigidität führt[51–53]. Die Prozesse bedingen einen lokal fibrotischen Umbau der segmental betroffenen Venenwand und ihrer Klappen. Die

Degradation von strukturgebendem hochwertigem Kollagen wird überlagert von einer vermehrten Transkription und Translation an weniger organisierten Kollagen Typ I und III, das in die Tunica Media der Venenklappen und der -wand eingelagert wird. Die dysfunktionalen Geweberemodelingprozesse, die denen der physiologischen Wundheilung ähnlich sind, führen in tierexperimentellen Versuchen zu einer, durch Fibrose bedingten, erhöhten Steifigkeit in den betroffenen Venensegmenten[53]. Diese Beobachtungen werden auch durch klinische Untersuchungen an TVT Patienten unterstützt, die eine 1,5- bis 1,8-fache Verdickung der Venenwand in betroffenen Segmenten, sowie eine 4- bis 5-fache Erhöhung der MMP-9 Serumspiegel aufwiesen[49].
Die Erhöhung des venösen Abflusswiderstands erzeugt eine venöse Hypertension[54,55]. Diese ambulatorische venöse Hypertension bedingt eine Erhöhung der venösen Auswärtsfiltration und provoziert ein chronisches Gewebeödem. Final kommt es zur Entstehung venöser Ulzerationen[56–58].
Die zuvor beschrieben fibrotischen thrombusbasierenden Remodulierungsprozesse der Venenwand tragen, neben hämodynamischen Überlegungen, entscheidend zur venösen Obstruktion und Etablierung der ambulatorischen venösen Hypertension bei. Durch eine frühe und effektive Entfernung des obstruierenden Thrombus mit früher Rekanalisation des iliofemoralen Stromgebiets sollte gemäß der „open vein“ Hypothese eine Reduktion der akuten und später auch chronischen venösen Obstruktion, des valvulären Refluxes und schließlich auch der PTS Inzidenz erreicht werden können[59].

3. Zielsetzung

Dysfunktionales Geweberemodeling ist bei der Entstehung verschiedener Krankheitsbilder im gefäßmedizinischen Krankengut bedeutsam. Insbesondere besitzt es bei der Entstehung eines AAA, der physiologischen Wundheilung sowie bei der PTS Entwicklung entscheidende pathogenetische Relevanz. Das übergeordnete Ziel der Arbeiten ist es, krankheitsspezifische Geweberemodelingprozesse und assoziierte zelluläre Subprozesse zu untersuchen, um Angriffspunkte für Präventionsstrategien herauszuarbeiten. Außerdem soll das Potential konservativer und chirurgischer Therapien, krankheitsspezifisches Geweberemodeling zu modulieren durch Analyse patientenzentrierter objektiver Endpunkte abgeschätzt werden.

4. Originalarbeiten

4.1. Abdominelles Aortenaneurysma

4.1.1. Zitationen

Adam M, Kooreman NG, Jagger A, **Wagenhäuser MU**, Mehrkens D, Wang Y, Kayama Y, Toyama K, Raaz U, Schellinger IN, Maegdefessel L, Spin JM, Hamming JF, Quax PHA, Baldus S, Wu JC, Tsao PS. *Systemic Upregulation of IL-10 (Interleukin-10) Using a Nonimmunogenic Vector Reduces Growth and Rate of Dissecting Abdominal Aortic Aneurysm.* Arterioscler Thromb Vasc Biol. 2018;38(8):1796-1805.

Wagenhäuser MU*, Schellinger IN*, Yoshino T, Toyama K, Kayama Y, Deng A, Guenther SP, Petzold A, Mulorz J, Mulorz P, Hasenfuß G, Ibing W, Elvers M, Schuster A, Ramasubramanian AK, Adam M, Schelzig H, Spin Jm, Raaz U*, Tsao PS*. *Chronic Nicotine Exposure Induces Murine Aortic Remodeling and Stiffness Segmentation – Implications for Abdominal Aortic Aneurysm Susceptibility.* Front Physiol. 2018;31;9:1459.

Nguyen DM, **Wagenhäuser MU**, Mehrkens D, Adam M, Tsao PS, Ramasubramanian AK. *An Automated Algorithm to Quantify Collagen Distribution in Aortic Wall.* J Histochem Cytochem. 2019;67(4):267-274.

4.1.2. Spezifische Fragestellung/Methodik

Um die Mechanismen der Entstehung und Progression eines AAA zu verstehen, bedarf es geeigneter Mausmodelle, auch um phänotypische Unterschiede in verschiedenen Versuchsgruppen festzustellen. Außerdem werden nachgeschaltete laborexperimentelle Methoden benötigt, um gewonnene Erkenntnisse zu verifizieren und spezifische Signaltransduktionswege und zelluläre Interaktionen zu entschlüsseln.

Um die Effekte gesicherter Risikofaktoren der AAA Entwicklung valide untersuchen zu können, sind krankheitsspezifische Tiermodelle unerlässlich. Nikotin ist der Hauptbestandteil von Tabak- und E-Zigaretten. Der signifikante Anstieg von E-Zigaretten-Konsumenten in den Mitgliedsstaaten der europäischen Union zwingt zur Erforschung krankheitsspezifischer Risiken von Nikotin[60]. Die Auswirkungen von Nikotin auf das Gefäßsystem sind jedoch nur unzureichend verstanden.

Ein innovativer und interessanter Erklärungsansatz der AAA Entstehung ist die differente segmentale aortale Steifigkeitsentwicklung. Durch eine Erhöhung des Steifigkeitsgradienten in sich angrenzenden Aortensegmenten kommt es in

tierexperimentellen Arbeiten zu einem schnelleren Voranschreiten des AAA Diameters[61,62]. Auf diesen Beobachtungen basierend, könnte die Etablierung eines erhöhten Steifigkeitsgradienten in sich angrenzenden aortalen Segmenten (thorakal/abdominell) durch Nikotin risikofaktorspezifische pathogenetische Relevanz gewinnen. Eine solche Entwicklung würde substantiell auf unterschiedlichem Geweberemodeling beruhen.

In einem nicht AAA-spezifischen Mausmodell wurden nikotingefüllte osmotische Minipumpen (25 mg kg/Tag) C57BL/6 Wildtyp-Mäusen implantiert. Durch *in-vivo* Sonographien zur Bestimmung der aortalen Pulswellengeschwindigkeit (PWV) und *ex-vivo* Myographmessungen, in denen der Diameterzuwachs pro Druckdifferenz standardisiert bestimmt werden kann, konnte die globale und segmental aortale Steifigkeitsentwicklung in der thorakalen und abdominellen Aorta indirekt untersucht werden. Grundlage einer differenten Entwicklung der Steifigkeit in abdominellen und thorakalen Aortensegmenten könnte ein unterschiedliches Geweberemodeling sein. Steifigkeitsändernde Parameter, wie die Fragmentierung von Elastinfasern und die quantitative und qualitative Verteilung verschiedener Kollagentypen in den einzelnen Schichten der Aortenwand, sind von besonderem Interesse. Durch Immunhistochemie (IHC), *in-situ* Zymographien und polarisierte Lichtmikroskopie von Pikro-Siriusrot (PSR)-gefärbten histologischen Aortenpräparaten konnten steifigkeitsassoziierte bzw.-ändernde Parameter untersucht bzw. automatisierte Auswertungsmethoden entwickelt werden.

Für das AAA existieren zwei anerkannte krankheitsspezifische Mausmodelle. Neben dem „Porcine Pancreas Elastase“ (PPE) Modell mit segmental transienter Elastaseperfusion eines ausgeklemmten Aortensegments findet das Angiotensin II (ANG II) Infusionsmodell breite Anwendung[63,64]. In diesem Modell wird Apolipoprotein E-defizienten (Apoe−/−) Mäusen über subkutan implantierte osmotische Minipumpen eine ANG II Lösung (1 000 ng/min/kg) infundiert , was zur Entwicklung eines AAA im viszero-renalen Aortensegment nach durchschnittlich 5-7 Tagen führt[64]. Das Modell eignet sich, um detaillierte Erkenntnisse über krankheitsspezifische Inflammation und das damit zusammenhängende Geweberemodeling zu gewinnen. Der maximale Diameter des entstandenen Dissektionsaneurysma kann in diesem experimentellen Modell durch

Ultraschall über einen Zeitraum von 28 Tage gemessen werden. So können Phänotypänderungen erfasst und Rückschlüsse auf essentielle Signaltransduktionswege in der Pathogenese der Erkrankung gewonnen werden. Das Modell wurde genutzt, um einen genbasierten anti-inflammatorischen auf Interleukin-10 (IL-10) Augmentation beruhenden Therapieansatz auf seine Effektivität zu prüfen.

4.1.3. Synopsis der Ergebnisse/Diskussion

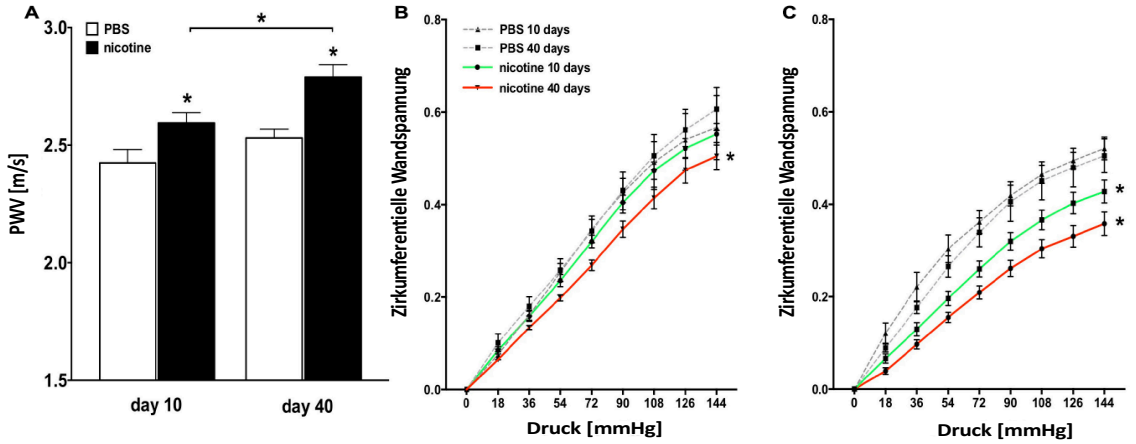

Abbildung 4: Veränderung der Gefäßsteifigkeit durch Nikotin Exposition. A: Nikotin-infundierte Mäuse zeigen im Vergleich „phosphate-buffered saline“ (PBS)-infundierten Mäusen eine Erhöhung der aortalen globalen Pulswellengeschwindigkeit (PWV) nach 10 und 40 Tagen unter Verwendung der „time“delay“ Sonographiemethode. Die PWV nikotin-infundierter Mäuse steigt im zeitlichen Verlauf zwischen Tag 10 und Tag 40. **B und C:** In thorakalen (**B**) und abdominellen (**C**) Aortensegmenten steigt im Vergleich zu PBS Kontrollen die lokale aortale Steifigkeit unter Nikotininfusion in ex-vivo Myographemssungen im zeitlichen Verlauf. Die Effekte sind im abdominellen Segment früher und stärker ausgeprägt. *p<.05 vs. PBS Kontrolle bzw. 10 Tage vs. 40 Tage. 2-way ANOVA mit „Holm–Sidak’s multiple comparison Test “. Modifiziert aus Wagenhäuser, M. U. et al. *Chronic Nicotine Exposure Induces Murine Aortic Remodeling and Stiffness Segmentation—Implications for Abdominal Aortic Aneurysm Susceptibility.* Front Physiol. *Oct 31;9:1459* (2018). (Mit freundlicher Genehmigung von Frontiers Media SA, lizenziert, CC-BY Creative Commons attribution license (CC-BY, version 4.0 http://creativecommons.org/licenses/by/4.0/))

Nikotin erzeugt eine globale Erhöhung der murinen aortalen PWV, die ein etabliertes indirektes Maß der Gefäßsteifigkeit ist (***Abbildung 4A***). Ähnliche Beobachtungen wurden bei Rauchern beschrieben. So konnte eine kurzfristige Erhöhung der aortale PWV nach Exposition gezeigt werden, die mit einer Steigerung der Herzfrequenz und des Blutdrucks einhergeht und damit auch teilweise erklärbar ist[65]. Gleichgerichtete kurzfristige Effekte konnten kürzlich auch für Nutzer von E-Zigaretten beschrieben werden, was die tierexperimentellen Ergebnisse plausibel erscheinen lässt[66].

Neben der globalen aortalen Steifigkeitserhöhung bedingt Nikotin eine segmental differenzielle Steifigkeitsentwicklung in sich angrenzenden Aortenabschnitten. So ist eine

unterschiedliche Entwicklung der Steifigkeit in der thorakalen und abdominellen Aorta über einen Untersuchungszeitraum von 6 Wochen zu beobachten (***Abbildung 4B und C)***. Es kommt zu einer primären Steifigkeitszunahme der abdominellen Aorta, während die thorakale Aorta später und schwächer an Steifigkeit gewinnt. Dies etabliert sowohl nach 10 Tagen als auch nach 40 Tagen einen erhöhten Steifigkeitsgradienten zwischen diesen beiden Aortenabschnitten.

Eine Steifigkeitszunahme kann kausal auf unterschiedlichen Geweberemodelingprozessen beruhen. Sowohl eine gesteigerte Degradation und Fragmentierung von Elastinfasern mit Elastizitätsverlust als auch eine Fibrose durch Zunahme des Kollagengehalts mit Rigiditätszunahme können ursächlich sein. Weiterhin kann eine Steifigkeitszunahme auch auf einer Seneszenz und Apoptose von glatten Muskelzellen oder Kalzifizierungen in der Gefäßwand beruhen[67]. Soll die Fibrose in der Gefäßwand untersucht werden, so ist eine schichtspezifische Bestimmung des Kollagengehalts entscheidend. Für differenzierte Fragestellungen ist die prozentuale Verteilung des Kollagens in der Media und Adventitia essentiell. Die Proteinbestimmung aus Gewebeproben erlaubt jedoch nur die Bestimmung des globalen gesamten Kollagengehalts, weshalb eine differenzierte schichtspezifische Analyse nur an histologischen Präparaten erfolgen kann. Hier kommt der PSR Färbung besondere Bedeutung zu. Die anionische Struktur des PSR Moleküls, das parallel zu den kationischen Kollagenbündeln bindet, verstärkt die Doppelbrechung der Kollagenbündel[68]. Unter polarisiertem Licht erscheinen Kollagen innerhalb eines Farbsprektrums von grün, gelb und rot[69]. Während früher angenommen wurde, dass die Dicke der Kollagenbündel die Farbgebung beeinflusst und so von der Farbe auf den Kollagensubtyp rückgeschlossen werden kann, konnte inzwischen gezeigt werden, dass die Orientierung und Ausrichtung der Kollagenfasern für die Farbgebung essentiell ist[70,71].

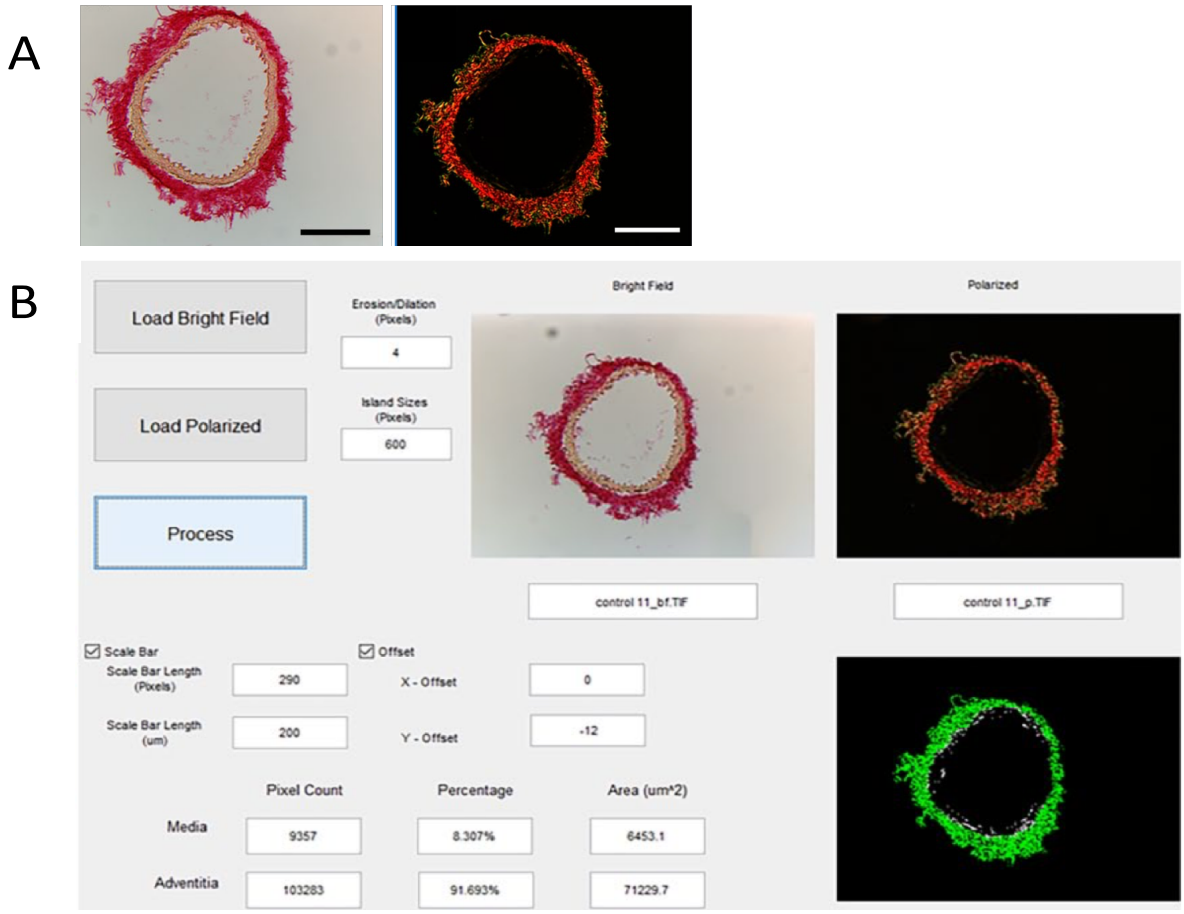

Abbildung 5: Graphical User Interface (GUI) zur semi-automatisierten Quantifizierung der Kollagenverteilung innerhalb der einzelnen aortalen Gefäßwandschichten. A: Repräsentative Bilder einer mit Pikro-Siriusrot (PSR) gefärbten Mausaorta in einer Lichtbildaufnahme (rechts) und einer Aufnahme unter polarisiertem Licht (links). **B: „**Graphical User Interface“ (GUI) zur indirekten Errechnung des prozentualen Kollagengehalts in der Tunica media und adventitia (links). Modifiziert aus Nguyen, DM, Wagenhäuser MU, Mehrkens D et al. *An Automated Algorithm to Quantify Collagen Distribution in Aortic Wall.* J Histochem Cytochem. Apr;67(4):267-274 (2019). (Mit freundlicher Genehmigung von SAGE Publications im Rahmen der „re-use and archiving policies“).

Anhand von histologischen Schnitten von Mausaorten konnte in einem kollaborativen Projekt ein „Graphical User Interface“ (GUI) entwickelt werden, mit Hilfe dessen die einzelnen Wandschichten automatisch definiert und von der residualen Intensität der Farbgebung der Kollagengehalt indirekt automatisiert errechnet werden kann (***Abbildung 5A und B***). Zur Verifizierung wurden die automatisch errechneten Ergebnisse mit manuell prozessierten Bildern durch lineare Regression verglichen. Der Korrelationskoeffizienten betrug hier R^2=0,94 (nicht gezeigte Daten). Die automatisierte Auswertung kann auf unterschiedliche Fragstellungen, für die eine schichtspezifische Kollagenverteilung innerhalb der Gefäßwand wesentlich ist, angewendet werden.

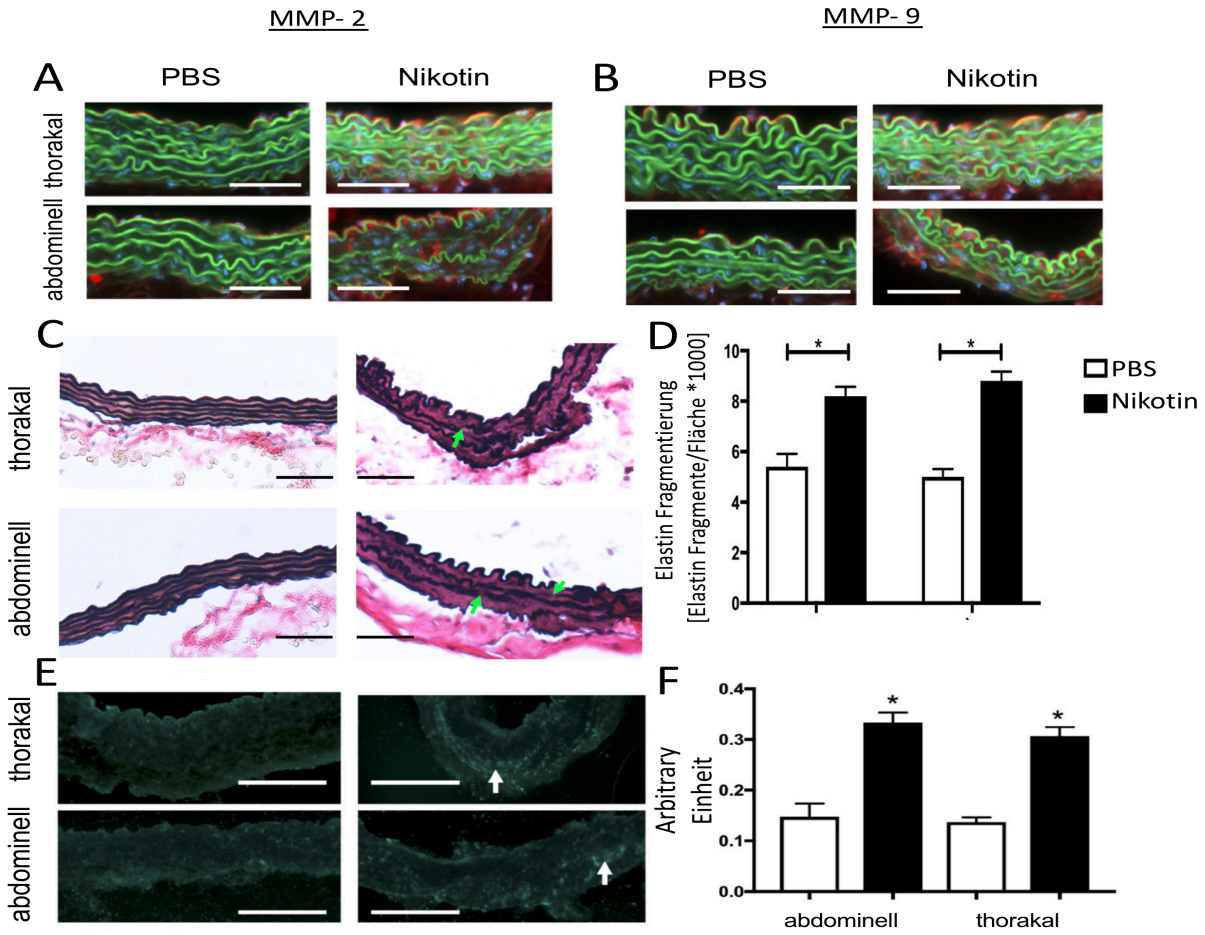

Abbildung 6: Molekulare Auswirkungen einer Nikotinexposition in der murinen Aortenwand. A und B: Repräsentative Immunfluoreszenzfärbungen zeigen eine erhöhte Expression von Matrix-Metalloproteinase (MMP)-2 (rot) (**A**) und -9 (rot) (**B**) in thorakalen und abdominellen Aortensegmenten Nikotin-infundierter Mäuse nach 40 Tagen. **C:** Repräsentative Bilder einer Elastin Verhoeff's Van Gieson Färbung. Nikotin-infundierte Aorten zeigen im Vergleich zu „phosphate-buffered saline" (PBS)-infundierten Aorten eine vermehrte Fragmentierung von Elastin (grüne Pfeile). **D:** Die Häufung an Brüchen in den Elastinlamellen kann sowohl im thorakalen als auch im abdominellen Aortensegmenten gesehen werden. **E:** *In-situ* Zymographien zeigen eine erhöhte MMP Aktivität in Nikotin-infundierten Aorten, was anhand einer gesteigerten Fluoreszenz gesehen werden kann (weiße Pfeile) **F:** Die Quantifizierung der blau-grünen Fluoreszenz zeigt eine gleichgerichtete Erhöhung der MMP Aktivität in thorakalen und abdominellen Aortensegmenten Nikotin-infundierter Aorten nach 40 Tagen. D und F: *p<.05 Nikotin vs. PBS Infusion. One-way ANOVA mit Holm–Sidak's multiple comparison Test. Modifiziert aus *Wagenhäuser, M. U. et al. Chronic Nicotine Exposure Induces Murine Aortic Remodeling and Stiffness Segmentation—Implications for Abdominal Aortic Aneurysm Susceptibility.* Front Physiol. *Oct 31;9:1459* (2018). (Mit freundlicher Genehmigung von Frontiers Media SA, lizenziert, CC-BY Creative Commons attribution license (CC-BY, version 4.0 http://creativecommons.org/licenses/by/4.0/))

Die aortale Steifigkeitszunahme durch Nikotininfusion beruhte jedoch nicht auf einer Fibrose der Gefäßwand, sondern auf vermehrter Fragmentierung von Elastinfasern. Auf molekularer Ebene bedingt Nikotin sowohl in der thorakalen als auch in der abdominellen Aorta eine gleichgerichtete Expressions- und Aktivitätserhöhung von MMP-2 und -9. Beide Enzyme degradieren Elastinfasern und können diese fragmentieren. Die

Beobachtungen sind über der Aorta uniform verteilt (***Abbildung 6A-D***). Zellkulturexperimente an glatten Muskelzellen und Endothelzellen zeigten eine ähnliche Regulation der MMP-Genexpression unter Nikotinexposition, so dass diese Zelltypen maßgeblich für das durch Nikotin hervorgerufene aortale Geweberemodeling der Aortenwand erscheinen[72,73].

Die Aktivitätszunahme von MMP-2 und -9 sowie die damit einhergehende Elastinfragmentierung sind durch experimentelle Hemmung von MMP-2 und -9 durch den kompetitiven „small-molecule inhibitor“ SB-3CT umkehrbar (***Abbildung 7A-G)***.

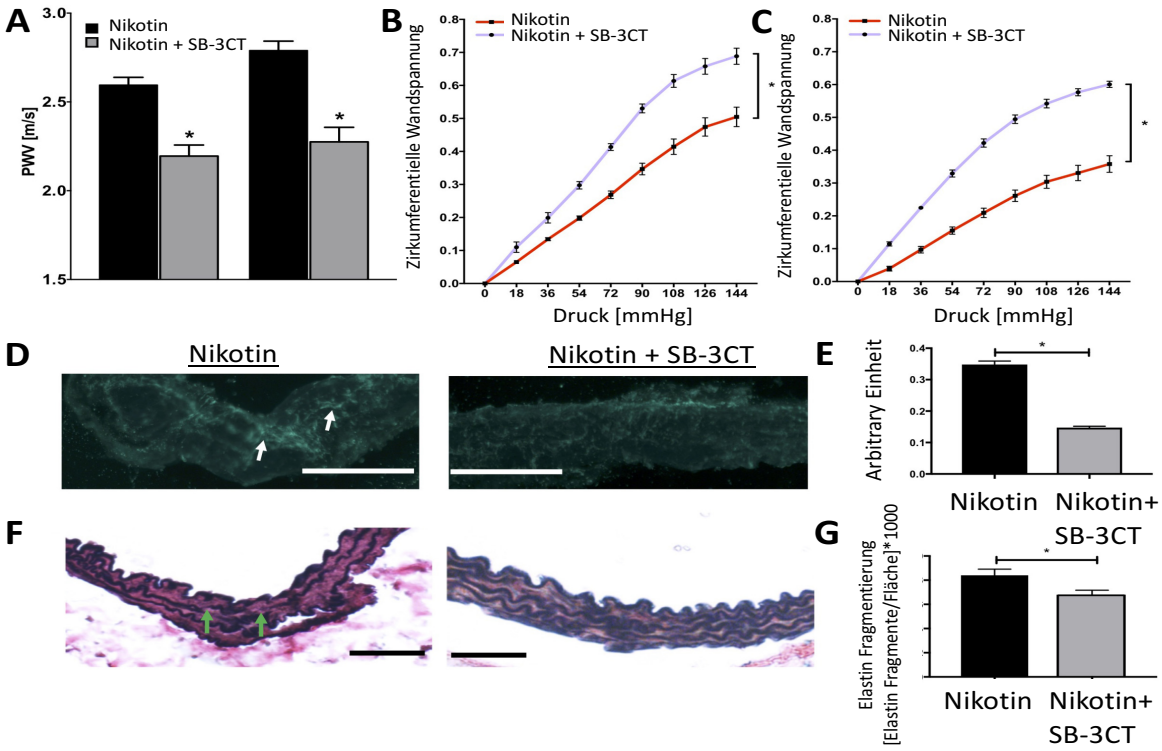

Abbildung 7: Aufhebung der durch Nikotin hervorgerufenen Effekte durch SB-3CT. SB-3CT führt zu einer Hemmung von Matrix-Metalloproteinase (MMP)-2 und -9**.** SB-3CT wurde Nikotin-infundierten Mäusen alle 2 Tage durch intraperitoneale Injektion appliziert. **A:** SB-3CT reduziert die durch Nikotin gesteigerte aortale Pulswellengeschwindigkeit (PWV) nach 10 und 40 Tagen. Die PWV ist ein indirektes Maß der globalen aortalen Steifigkeit. **B und C:** *Ex-vivo* Druck*m*yographmessungen zeigen die Kompensation bzw. Verhinderung, der durch Nikotin bedingten Steifigkeitszunahme in thorakalen (**B**) und abdominellen (**C**) Aortensegmenten durch SB-3CT Injektion. **D und E:** *In-situ* Zymographien zeigen eine Reduktion, der durch Nikotin gesteigerten MMP Aktivität durch SB-3CT Injektion (**D**). Quantitativ kann durch SB-3CT Injektion ein geringeres blau-grünes Fluoreszenzsignal gesehen werden (weiße Pfeile) (**E**). **F und G:** SB-3CT Injektion führt zu einer Reduktion der durch Nikotin gesteigerten Fragmentierung von Elastinfasern (**F**). Quantitativ zeigt sich durch SB-3CT Injektion eine Reduktion, der durch Nikotin erhöhten Anzahl an Strangbrüchen in Elastinlamellen (grüne Pfeile) (**G**). E und G: *p<.05 Nokotin vs. Nikotin + SB-3CT. One-way ANOVA mit Holm–Sidak's multiple comparison Test. Modifiziert aus *Wagenhäuser, M. U. et al. Chronic Nicotine Exposure Induces Murine Aortic Remodeling and Stiffness Segmentation—Implications for Abdominal Aortic Aneurysm Susceptibility.* Front Physiol. *Oct 31;9:1459* (2018). (Mit freundlicher Genehmigung von Frontiers Media SA, lizenziert, CC-BY Creative Commons attribution license (CC-BY, version 4.0 http://creativecommons.org/licenses/by/4.0/))

Kausal erklärend für den primären Steifigkeitszuwachs in der abdominellen Aorta bei uniformer Aktivitätszunahme vom MMPs und ähnlicher Erhöhung der Fragmentierung von Elastinfasern in beiden Aortensegmenten könnte der höhere Basisgehalt an Elastin in der thorakalen Aorta sein. Auf dieser Grundlage könnte eine erhöhte Kompensationsfähigkeit gegenüber der Degradation von Elastin bestehen und der verlangsamte bzw. zeitversetzte Steifigkeitszuwachs im thorakalen Aortensegment erklärbar sein[74,75]. Da eine unterschiedliche Steifigkeitsentwicklung in den angrenzenden Aortenabschnitten zur Entwicklung eines Steifigkeitsgradienten zwischen diesen Segmenten führt, könnte dieser Gradient die Rolle von Nikotin in der Pathogenese des AAA teilweise erklären. Interessanterweise konnte eine unterschiedliche Entwicklung der aortalen Steifigkeit durch primäre Zunahme im abdominellen Segment als ein Wesensmerkmal der alternden, von der Entstehung eines AAA vornehmlich betroffenen Aorta, beschrieben werden[62,76,77].

Zusammenfassend bleibt festzuhalten, dass eine unterschiedliche Entwicklung der Steifigkeitszunahme in der thorakalen und der abdominellen Aorta unter Nikotin durch die charakteristisch unterschiedliche Zusammensetzung der EZM in diesen Aortensegmenten bedingt sein könnte, wenngleich Nikotin ein ähnliches Geweberemodeling über der gesamten Aorta hervorruft.

Neben dem Geweberemodeling durch den wesentlichen Risikofaktor Nikotin spielt insbesondere die Inflammation in der Pathogenese des AAA eine gesicherte Rolle. Inflammation und Geweberemodeling innerhalb der Aortenwand bedingen und regulieren sich gegenseitig[78]. IL-10 ist das bekannteste anti-inflammatorisches Zytokin der Klasse II[79,80]. Es ist für seine immunsupressive Wirkung durch Inhibierung der Produktion pro-inflammatorischer Zytokine in Makrophagen und dentrischen Zellen bekannt[81,82]. Der Einsatz von rekombinantem IL-10 im humanen System erbrachte keine wesentlichen Nebenwirkungen bei Erhalt der immunsuppresiven Wirkung[83]. Die Wirkung von IL-10 als potentielles Therapeutikum bei einem AAA ist bislang nicht erforscht. Die einmalige Injektion eines IL-10 tragenden „minicircle“, der verglichen mit herkömmlichen Plasmiden kleiner und weniger immunogen ist, kann im ANG II-Infusionsmodell zu einer verminderten Inzidenz an AAA bzw. zu einem verlangsamten AAA-Wachstum beitragen (***Abbildung 8A-C***). Auf zellulärer Ebene führt IL-10 zu einer Verschiebung der Ratio von

T_{reg}-Zellen/$CD8^+$ zytotoxischen T-Zellen (CTL) zugunsten der T_{reg}-Zellen, ohne die absolute Zellzahl in der Aneurysmawand zu verändern (***Abbildung 9A und B)***.

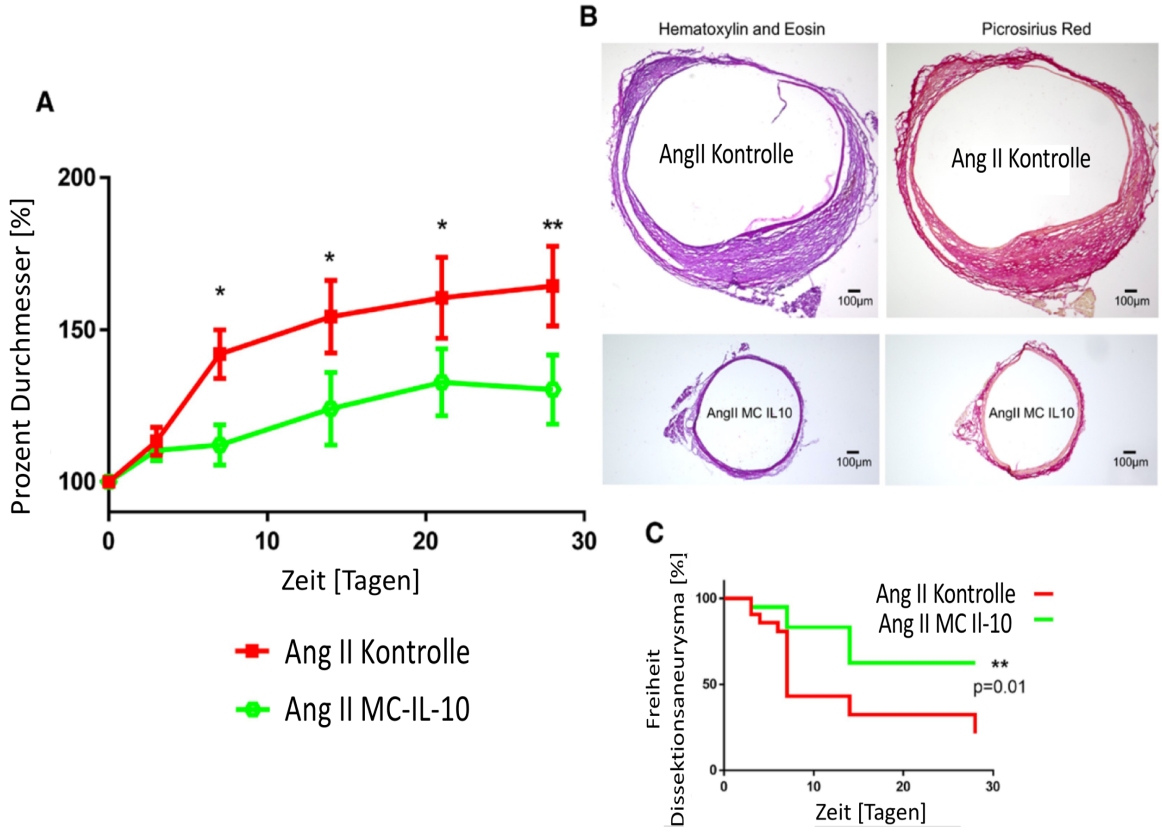

Abbildung 8: Inzidenz und Progression des abdominellen Aortenaneurysma (AAA) nach Interleukin-10 (IL-10) minicircle Injektion. A: Geringere Diameterprogression nach Injektion eines Interleukin-10 (IL-10) „minicircle" verglichen mit Kontrollmäusen bei Verwendung des Angiotensin II (ANG II)-Infusionsmodells. **B:** Repräsentative Hematoxylin und Eosin (H&E) sowie Picrosirius Red Färbungen von Aortenaneurysmen vor (untere Reihe) und 28 Tage (obere Reihe) nach IL-10 minicircle Injektion. **C:** Kaplan-Meier-Schätzung der AAA Inzidenz (bzw. Freiheit von einem AAA) nach IL-10 minicircle Injektion. IL-10 senkt die Auftretenswahrscheinlichkeit eines AAA im ANG II-Infusionsmodell. A-D: *p<.05 IL-10 minicricle vs. Kontrollen. Ungepaarter Student's t-Test bzw. Log-rank (Mantel-Cox) Test. Modifiziert aus *Adam M, Kooreman NG, Jagger A, Wagenhäuser MU et al. Systemic Upregulation of IL-10 (Interleukin-10) Using a Nonimmunogenic Vector Reduces Growth and Rate of Dissecting Abdominal Aortic Aneurysm.* Arterioscler Thromb Vasc Biol. Aug;38(8):1796-1805 (2018). (Mit freundlicher Genehmigung von Lippincott Williams & Wilkins (LWW), lizenziert, Nummer: 4666480525311).

T_{reg}-Zellen können Makrophagen in Gewebe wie die Aortenwand rekrutieren[84]. Insbesondere die M2c Makrophagen-Subpopulation ist besonders in das Geweberemodeling eingebunden und kann in späten Phasen eine Progression des AAA eindämmen[85,86]. Im Gegensatz führt die Rekrutierung von $CD8^+$ zytotoxischen T-Lymphozyten zu Zellschäden und Apoptose, was einen beschleunigten Stabilitätsverlust der Aneurysmawand bedeutet[87,88].

Gestützt werden die experimentellen Ergebnisse durch Beobachtungen, die eine dosisabhängige Reduktion der AAA Progression durch T_{reg}-Zelltransfer unter Verwendung des ANG II Infusionsmodells fanden[89]. Auch Zellkulturexperimente zeigten gleichgerichtete Ergebnisse. So führte die direkte Behandlung von Makrophagen mit T_{reg}-Zellen zu einer akzentuierten Differenzierung in den M2-Phänotyp, einer geringeren Makrophagenzahl und einer Reduktion an pro-inflammatorischen Zytokinen in der Aneurysmawand[84,86]. Diese Beobachtungen legen sowohl einen auf Zell-Zell Interaktion beruhenden Wirkungsmechanismus als auch parakrine Effekte, die auf T_{reg}-Zellen beruhen, nahe. Da Makrophagen eine unbestrittene Signifikanz für das Geweberemodeling in der Pathogenese der AAA Erkrankung besitzen, stellt insbesondere die Interaktion von T_{reg}-Zellen mit Makrophagen ein wichtiges Bindeglied zwischen Inflammation und Geweberemodeling dar.
Zusammenfassend unterstreichen die Beobachtungen die Relevanz der Immunregulation für die AAA Progression.

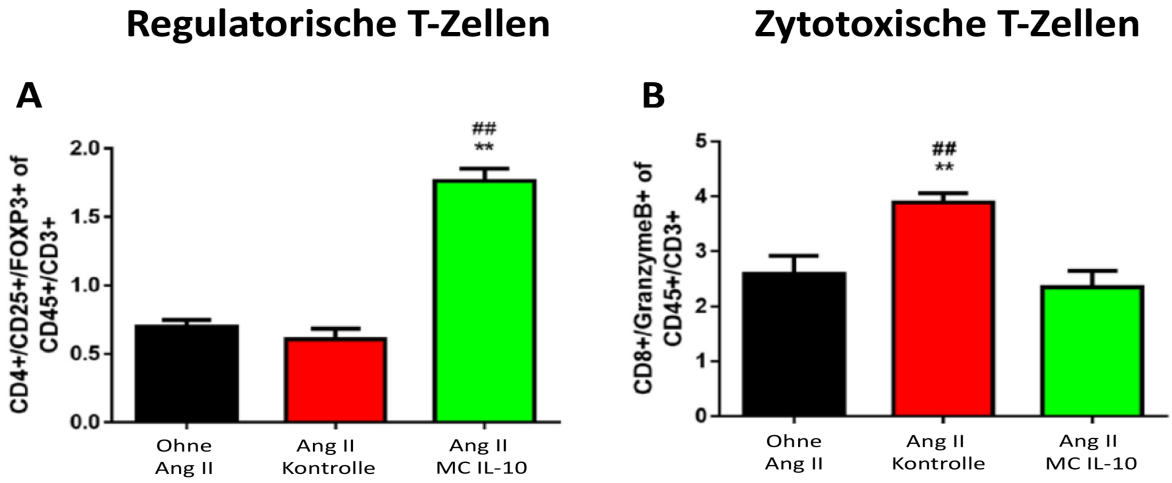

Abbildung 9: Auswirkungen der Interleukin-10 (IL-10) minicircle Injektion auf regulatorische und zytotoxische T-Zellen. IL-10 bewirkt in durchflusszytometrischen Messungen eine Verschiebung der T-Zellpopulation zugunsten regulatorischer T-Zellen. Diese regulatorischen T-Zellen sind für die Rekrutierung von Makrophagen wesentlich, die wiederum signifikant das Geweberemodeling beeinflussen. **A:** Anteil CD4+/CD25+/Foxp3 (forkhead box P3) an CD45+/CD3+ Zellen in unbehandelten, Angiotensin-II (ANG II)- infundierten und ANG II-infundierten+IL-10 minicircle injizierten Mausaortenaneurysmen 7 Tage nach Induktion. **B:** Anteil von CD8+/GZMB+ (granzyme B) an CD45+/CD3+ cells in unbehandelten, ANG II-infundierten und ANG II-infundierten+IL-10 minicircle injizierten Mausaortenaneurysmen 7 Tage nach AAA Induktion. **p≤0.01 vs. Ang II, ## p≤0.01 vs. untreated. One-way ANOVA mit Fisher Least Significant Difference Tests. Modifiziert aus *Adam M, Kooreman NG, Jagger A, Wagenhäuser MU et al. Systemic Upregulation of IL-10 (Interleukin-10) Using a Nonimmunogenic Vector Reduces Growth and Rate of Dissecting Abdominal Aortic Aneurysm.* Arterioscler Thromb Vasc Biol. Aug;38(8):1796-1805 (2018). (Mit freundlicher Genehmigung von Lippincott Williams & Wilkins (LWW), lizenziert, Nummer: 4666480525311).

4.1.4. Zusammenfassung/Ausblick

Das Geweberemodeling ist für die Entwicklung und Progression eines AAA von hoher Relevanz. Nikotin führt in der Frühphase der AAA Entstehung zu einer Steifigkeitszunahme durch erhöhte MMP Aktivität und Fragmentierung der Elastinfasern. Die Steifigkeitszunahme im thorakalen und abdominellen Aortensegment erfolgt zeitlich versetzt. Die gewonnen Erkenntnisse sollen zunächst im humanen System verifiziert werden. Besondere Beachtung soll E-Zigarettenkonsumenten zukommen. Es bleibt abzuwarten, ob in diesem zumeist jungen Patientenkollektiv ähnliche Beobachtungen der aortalen Steifigkeitsentwicklung gemacht werden können.

Ein steifigkeitserhöhender Faktor ist neben der Fragmentierung von Elastin die Fibrose der Aortenwand durch Vermehrung des Kollagengehalts. Eine spezifische Bestimmung des Kollagengehalts für einzelne Aortenwandschichten gelingt nur anhand histologischer Präparate, für die eine automatisierte prozentuale Verteilung anhand eines GUI ermöglicht wurde. Das Analysetool kann für künftige Fragestellungen flexibel eingesetzt werden.

Eng mit dem Geweberemodeling verbunden, bzw. dieses direkt beeinflussend, ist die Inflammation. Anti-inflammatorische therapeutische Ansätze erschienen vielversprechend, da eine systemische IL-10 Erhöhung experimentell zu einer Verlangsamung der Diameterprogression führt. Die Translation der Beobachtungen am Menschen sind zur definitiven Etablierung anti-inflammatorischer Therapieansätze zwingend.

frontiers in Physiology

ORIGINAL RESEARCH
published: 31 October 2018
doi: 10.3389/fphys.2018.01459

Chronic Nicotine Exposure Induces Murine Aortic Remodeling and Stiffness Segmentation—Implications for Abdominal Aortic Aneurysm Susceptibility

Markus U. Wagenhäuser[1,2,3†], Isabel N. Schellinger[4,5,6†], Takuya Yoshino[1,2], Kensuke Toyama[1,2], Yosuke Kayama[1,2], Alicia Deng[1,2], Sabina P. Guenther[7,8], Anne Petzold[4], Joscha Mulorz[1,2,3], Pireyatharsheny Mulorz[1,2], Gerd Hasenfuß[5], Wiebke Ibing[3], Margitta Elvers[3], Andreas Schuster[4,5,9], Anand K. Ramasubramanian[10], Matti Adam[1,2], Hubert Schelzig[3], Joshua M. Spin[1,2], Uwe Raaz[4,5†] and Philip S. Tsao[1,2†]*

[1] Cardiovascular Institute, Stanford University School of Medicine, Stanford, CA, United States, [2] VA Palo Alto Health Care System, Palo Alto, CA, United States, [3] Department of Vascular and Endovascular Surgery, University Hospital Düsseldorf, Heinrich-Heine-University, Düsseldorf, Germany, [4] Molecular and Translational Vascular Medicine, Department of Cardiology and Pneumology, Heart Center at the University Medical Center Göttingen, Göttingen, Germany, [5] German Center for Cardiovascular Research e.V., Göttingen, Germany, [6] Department of Endocrinology and Nephrology, University of Leipzig, Leipzig, Germany, [7] Department of Cardiac Surgery, University Hospital Munich, Ludwig-Maximilian-University, Munich, Germany, [8] Department of Surgery, University of California, San Francisco, San Francisco, CA, United States, [9] Department of Cardiology, Royal North Shore Hospital, The Kolling Institute, Northern Clinical School, University of Sydney, Sydney, NSW, Australia, [10] Department of Biomedical, Chemical and Materials Engineering, San Jose State University, San Jose, CA, United States

Aim: Arterial stiffness is a significant risk factor for many cardiovascular diseases, including abdominal aortic aneurysms (AAA). Nicotine, the major active ingredient of e-cigarettes and tobacco smoke, induces acute vasomotor effects that may temporarily increase arterial stiffness. Here, we investigated the effects of long-term nicotine exposure on structural aortic stiffness.

Methods: Mice (C57BL/6) were infused with nicotine for 40 days (20 mg/kg/day). Arterial stiffness of the thoracic (TS) and abdominal (AS) aortic segments was analyzed using ultrasound (PWV, pulse wave velocity) and *ex vivo* pressure myograph measurements. For mechanistic studies, aortic matrix-metalloproteinase (MMP) expression and activity as well as medial elastin architecture were analyzed.

Results: Global aortic stiffness increased with nicotine. In particular, local stiffening of the abdominal segment occurred after 10 days, while thoracic aortic stiffness was only increased after 40 days, resulting in aortic stiffness segmentation. Mechanistically, nicotine exposure enhanced expression of MMP-2/-9 and elastolytic activity in both aortic segments. Elastin degradation occurred in both segments; however, basal elastin levels were higher in the thoracic aorta. Finally, MMP-inhibition significantly reduced nicotine-induced MMP activity, elastin destruction, and aortic stiffening.

OPEN ACCESS

Edited by:
Michael A. Hill,
University of Missouri, United States

Reviewed by:
Jessica E. Wagenseil,
Washington University in St. Louis, United States
Chetan P. Hans,
University of Missouri, United States
Ying Hu Shen,
Baylor College of Medicine, United States

***Correspondence:**
Philip S. Tsao
ptsao@stanford.edu

[†] These authors have contributed equally to this work

Specialty section:
This article was submitted to Vascular Physiology, a section of the journal Frontiers in Physiology

Received: 21 July 2018
Accepted: 26 September 2018
Published: 31 October 2018

Citation:
Wagenhäuser MU, Schellinger IN, Yoshino T, Toyama K, Kayama Y, Deng A, Guenther SP, Petzold A, Mulorz J, Mulorz P, Hasenfuß G, Ibing W, Elvers M, Schuster A, Ramasubramanian AK, Adam M, Schelzig H, Spin JM, Raaz U and Tsao PS (2018) Chronic Nicotine Exposure Induces Murine Aortic Remodeling and Stiffness Segmentation—Implications for Abdominal Aortic Aneurysm Susceptibility. Front. Physiol. 9:1459. doi: 10.3389/fphys.2018.01459

Conclusion: Chronic nicotine exposure induces aortic MMP expression and structural aortic damage (elastin fragmentation), irreversibly increasing aortic stiffness. This process predominantly affects the abdominal aortic segment, presumably due in part to a lower basal elastin content. This novel phenomenon may help to explain the role of nicotine as a major risk factor for AAA formation and has health implications for ECIGs and other modes of nicotine delivery.

Keywords: nicotine, AAA, stiffness, segmentation, e-cigarettes, mouse model

INTRODUCTION

In United States and globally, the use of ECIGs has increased annually across all age groups, and recently ECIGs have become more commonly used among 12th graders than tobacco cigarettes (Arrazola et al., 2015; Bunnell et al., 2015; Gravely et al., 2015; McMillen et al., 2015). One reason for this rising popularity may be the general misconception that ECIGs are a relatively harmless alternative to conventional smoking that lacks toxic tobacco combustion products. In particular, ECIGs are promoted as a "healthy" smoking cessation aid among nicotine-dependent young adult conventional smokers, however recent research suggests a potential to damage DNA at a chromosomal and a gene level in urine (Canistro et al., 2017). In this context, a more complete understanding of the risks of nicotine is mandatory, particularly given that ECIGs can exceed the nicotine delivery profile of tobacco cigarettes (Talih et al., 2015; Dawkins et al., 2016).

In the realm of cardiovascular medicine, a recent study found that ECIG use acutely increases arterial stiffness (Lundbäck et al., 2017). Notably, stiff conduit arteries lose their capability to mechanically buffer against the pulsatile nature of cardiac ejection, resulting in widespread augmentation of hemodynamic stress on end-organs. As such, arterial stiffness has been identified as a strong independent risk factor for many cardiovascular conditions, e.g., heart failure, myocardial infarction, stroke, and AAA formation (Lyle and Raaz, 2017).

The aforementioned acute effects on arterial stiffness appeared to be transient, and due to nicotine's short-term effects on vascular function. However, the chronic and potentially irreversible progressive effects on arterial stiffness that may result from structural vascular alterations due to long-term nicotine exposure are unknown.

Here, we report that prolonged nicotine exposure in mice induces fragmentation of the elastic layers of the aortic wall, irreversibly increasing structural arterial stiffness in mice. Importantly, we find that nicotine-induced aortic stiffening predominantly affects the abdominal aortic segment—thereby revealing a novel mechanism to explain the role of nicotine as a major risk factor for AAA formation.

Abbreviations: AAA, abdominal aortic aneurysms; AS, abdominal aortic segment; AUC, area-under-curve; bif, aortic bifurcation; ddH_2O, double-distilled water; DNA, complementary deoxyribonucleic acid; ECG, electrocardiogram; ECIGs, e-cigarettes; ECM, extracellular matrix; LSA, left subclavian artery; MLUs, medial lamellar units; MMP, matrix-metalloproteinase; MMP-2, matrix-metalloproteinase-2; MMP-9, matrix-metalloproteinase-9; mRNA, messenger ribonucleic acid; PBS, phosphate buffered saline; PWV, pulse wave velocity; ROI, region of interest; RNA, ribonucleic acid; SB-3CT, SB-3CT (2-[[(4-Phenoxyphenyl)sulfonyl]methyl]thiirane); TS, thoracic aortic segment; VVG, Verhoeff–Van Gieson.

MATERIALS AND METHODS

The authors declare that all supporting data are available within the article and its online **Supplementary Files**.

Animals

C57BL/6 wild-type male mice were purchased from the Jackson Laboratory. Animals were housed in a temperature-controlled and humidity-controlled room under a 12-h light/dark cycle (6:30 am/6:30 pm). All animal protocols were approved by the VA Institutional Animal Care and Use Committee and followed the National Institutes of Health and U.S. Department of Agriculture Guidelines for Care and Use of Animals in Research.

Osmotic Mini-Pump Implantation

10-week-old male C57BL/6J mice (24–26 g) were anesthetized with inhaled 2% isoflurane and osmotic mini pumps (ALZET, United States) were implanted subcutaneously slightly posterior to the scapulae. Animals were examined after 10 and 40 days. Nicotine (Sigma-Aldrich, United States) was diluted with PBS (Gibco, United States) and the perfusion rate was set to (25 mg/kg/day). The control group was infused with PBS. Effectiveness of nicotine delivery was confirmed by cotinine levels (Calbiotech, United States, CO096D-100).

SB-3CT Treatment

SB-3CT was purchased from ApexBio Technology, United States and administrated by i.p. injection at day 0 and every other day thereafter at a concentration of 25 mg/kg in 65% polyethylene glycol 200 (Fisher Scientific, United States), 25% dimethyl sulfoxide (Sigma-Aldrich, United States), and 10% ddH_2O. SB-3CT possesses an inhibitory constant (Ki) of 14 nM for MMP-2 and 600 nM for MMP-9 and is metabolized to an even more potent and competitive gelatinase inhibitor *in vivo*. Off-target effects are unknown and Ki-values for other MMPs are within a micromolar range (206 μM for MMP-1, 15 μM for MMP-3, and 96 μM for MMP-7).

In vivo Ultrasound Studies (PWV)

PWV was examined to globally [including both the TS and AS (**Supplementary Figure 1A**)] assess aortic stiffness by simultaneous tracking of the R-wave of the ECG and the

pulse wave at two specific locations: the LSA and the bif. We determined the PVW as a ratio of the distance (d) and time (t) delay of the pulse wave between both locations. PWV was calculated as PWV = [d(bif)-d(LSA)]/[t(bif)-t(LSA)]. All measurements have been conducted following the two-mean principle.

Ex vivo Pressure Myography

Pressure myography was performed as previously described (Raaz et al., 2015a). In short, TS and AS were explanted from post-treatment male C57BL/6J mice. The midparts of the descending TS and AS were dissected and further processed (**Supplementary Figure 1A**). TS and AS samples both approximately 0.6–0.8 cm in length were placed on specially designed stainless-steel cannulas and secured with silk surgical suture (10-0). Aortic segments were mounted in the heated vessel chamber of a pressure arteriograph system (Model 100P, Danish Myotechnology, Copenhagen, Denmark) and extended to *in vivo* length. Physiological saline solution at 37°C, aerated with 5% CO_2/95% O_2 was used to fill the vessel chamber and for aortic perfusion. Subsequently, aortic segments were pressurized from 0 to 144 mmHg in 18 mmHg increments, and the vessel's outer diameter was simultaneously tracked by continuous computer video analysis. The strain (S) was calculated as a ratio of outer diameter at baseline (D_b) to outer diameter at every given pressure level (D_p) ($S = (D_p - D_b)/D_b$).

Immunofluorescence Staining of Aortic Tissue

Aortic cross sections (7 µm) were incubated with rabbit anti-MMP-2 antibody (Abcam, dilution 1:500, ab37150) and rabbit anti-MMP-9 antibody (dilution 1:500; Abcam, ab38898) at 4°C overnight. Goat anti-rabbit IgG secondary antibody (Alexa Fluor 633, Thermo Fisher, dilution 1:1,000, A-21070) was performed at room temperature for 1 h. Counterstaining was performed with Hoechst reagent (Thermo Fisher). Negative controls were performed with the omission of the primary antibody. Imaging was performed using a Zeiss microscope (Oberkochen, Germany). MMP-2/-9 protein expression level was analyzed quantifying red fluorescence intensity in the ROI.

Elastin Imaging

Elastin layers were visualized using modified Verhoeff–Van Gieson stain (VVG) according to manufacturer's protocol (Abcam). The number of MLUs was counted in both thoracic and abdominal aortic segments. Elastin fragmentation was quantified in the histological images using elastin morphometric analysis (ImageJ). As previously described (Raaz et al., 2015a), each continuous set of pixels that formed a connected group was defined as an object. An elastin fragmentation index was defined as the ratio of the number of elastin objects to the area of elastin objects. The number of elastin objects was defined by the count of elastin objects within the media ROI. The area of elastin objects was equivalent to the total pixel count across all elastin objects within the media ROI.

Metalloproteinase *in situ* Zymography

In situ zymography was performed according to manufacturer's instructions. In brief, aortic sections were exposed to DQ gelatin (10 µg/ml; Invitrogen) and 1% agarose solution (ratio 1:10). Representative images were obtained after digestion of fluorescein-labeled gelatin by the endogenous gelatinases MMP-2 and MMP-9. MMP activity was quantified measuring the fluorescence intensity in the ROI.

RNA Isolation From Aortic Tissue

Animals were anesthetized, and aortic tissue was dissected. Tissue was snap-frozen and homogenized in TRIzol Reagent (Invitrogen, United States). After phase separation, total RNA was washed and eluted in Nuclease-Free Water (Ambion, United States).

Quantitative Real-Time PCR

To synthesize first-strand cDNA from mRNA, the SuperScript VILO cDNA Synthesis Kit (Invitrogen) was used. TaqMan qRT-PCR assay was used to quantitate mRNA levels. Specific oligonucleotide primers for *MMP-2* (NM_008610.2) and *MMP-9* (NM_013599.3) were obtained from Fisher Scientific, United States. Data are normalized to 18S and all fold changes were calculated using the ΔΔCt method.

Statistical Analyses

The data are shown as the mean ± SEM. Statistical analysis was performed using GraphPad Prism 6.0 (San Diego, CA, United States). Pressure-strain graphs of experimental groups were analyzed by calculating the AUC. Shapiro–Wilk normality test was applied to examine the normality of the data. One and two-way ANOVA with Holm–Sidak multiple comparison test was applied to compare the study groups after 10 and 40 days, respectively. Student's *t*-test was used to compare elastin baseline levels for the AS and TS. The level of significance was set to $p < 0.05$.

RESULTS

Nicotine Infusion Increases Overall Aortic Stiffness in Mice

We measured aortic PWV (from the LSA to the aortic bifurcation; **Supplementary Figure 1A**) as the clinical gold standard to globally assess aortic stiffness via ultrasound after 10 and 40 days of nicotine infusion via osmotic pump. As expected, we found significantly elevated serum cotinine levels in nicotine-infused mice after 10 and 40 days when compared to PBS-infused controls, indicating effective nicotine delivery (**Supplementary Figure 1B**). Mice that received nicotine infusion showed significantly elevated overall aortic stiffness (i.e., increased PWV) both 10 and 40 days after osmotic pump implantation compared to mice that received PBS infusion (**Figure 1A**). Additionally, aortic stiffness increased significantly from day 10 to day 40 (**Figure 1A**).

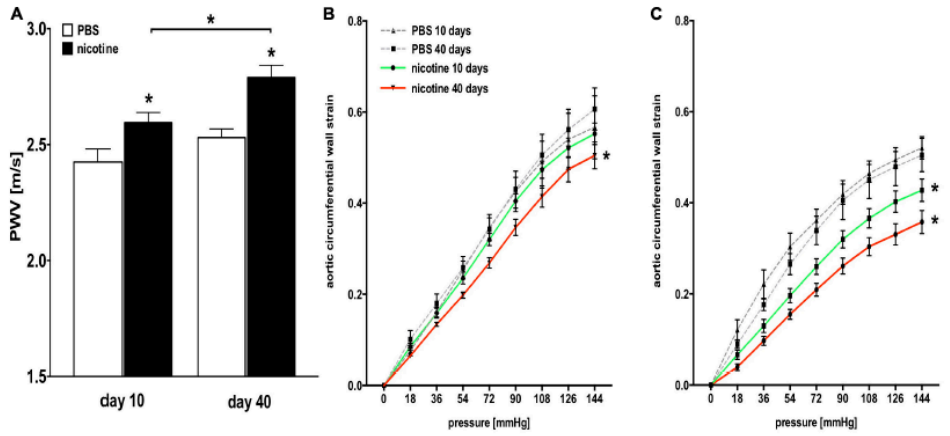

FIGURE 1 | Structural aortic stiffness is increased in nicotine-infused mice. **(A)** Pulse wave velocity (PWV) measurements in nicotine-treated and PBS control mice. (n = 4–6 mice/group); *$p < 0.05$ vs. PBS control or day 10 vs. day 40, respectively; values are mean ± SEM. **(B)** Passive pressure-strain curves derived from pressure myography of the thoracic aortic segment (TS) in nicotine-treated and PBS control mice 10 and 40 days after pump implantation. (n = 5–9 mice/group at day 10 and 4–7 mice/group at day 40); *$p < 0.05$ for area under the curve (AUC) vs. corresponding PBS control at day 10 and day 40, respectively; values are mean ± SEM. **(C)** Passive pressure-strain curves derived from pressure myography of the abdominal aortic segment (AS) in nicotine-treated and PBS control mice 10 and 40 days after pump implantation. (n = 5–9 mice/group at day 10 and 4–7 mice/group at day 40); *$p < 0.05$ for AUC vs. corresponding PBS control at day 10 and day 40, respectively; values are mean ± SEM. **(A–C)** Two-way ANOVA with Holm–Sidak's multiple comparison test.

Nicotine Infusion Induces Segmental Aortic Stiffness in Mice

We directly quantified the passive, structural stiffness of the aortic wall by performing aortic *ex vivo* mechanical testing using pressure myography. We verified that mice responded to nicotine infusion over time with increased aortic stiffness, both in the TS (**Figure 1B**) and AS (**Figure 1C**), as stiffness-related AUC decreased with nicotine infusion.

Given the distinct embryologic and structural differences between the thoracic and abdominal aorta, we next investigated whether nicotine exposure differentially affects those aortic segments. As such, we compared *ex vivo* mechanical stiffness of both segments under nicotine and control conditions.

Control mice receiving PBS infusion did not exhibit significant differences in aortic stiffness between the TS and AS, either at day 10 or at day 40 (**Figures 2A,C**), indicating homogenous aortic stiffness levels. In contrast, mice that received nicotine infusion developed disproportionately increased global aortic stiffness in the AS compared to the TS at 10 and 40 days after pump implantation (as indicated by increased AUC differential in the AS) and resulting in a stiffness gradient along the aorta (**Figures 2B,D**).

Elastin Architecture Is Disrupted in Nicotine-Treated Mice

To investigate the mechanisms leading to globally increased aortic stiffness as well as stiffness segmentation in nicotine-treated mice, we examined the aortic elastin structure. Elastin is a major component of the aortic wall, critically defining the passive mechanical properties (elasticity) of the vessel. We modified VVG staining (**Figures 3A–D**), and quantified elastin organization and damage as described previously (Raaz et al., 2015a).

Under basal (PBS) conditions we found well preserved elastin architecture in the thoracic and abdominal aortic media (**Figures 3A,B**). However, the number of elastin lamellae was higher in the TS vs. AS (**Figures 3A,B,E**).

Following 40 days of nicotine exposure, we detected significant elastin damage (thinning and fragmentation) in both the thoracic as well as the abdominal aorta (**Figures 3C,D,F**). However, there was no significant difference in the ratio of elastin fragmentation between the TS and AS.

Nicotine Treatment Increases Aortic MMP-2 and MMP-9 Expression and Elastolytic Activity

MMPs are enzymes involved in turnover and degradation of most extracellular matrix (ECM) proteins, including elastin. We therefore sought to further delineate their potential role in the development of nicotine-induced aortic stiffness.

First, we analyzed *MMP-2* and *MMP-9* expression via qRT-PCR and found that both genes were significantly upregulated in both the TS and AS at 40 days after nicotine pump implantation when compared to PBS controls (**Figures 4A,B**). On the protein level, this translated into marked upregulation of MMP-2 and MMP-9 protein expression as detected by increased red immunofluorescence in the media of aortic sections

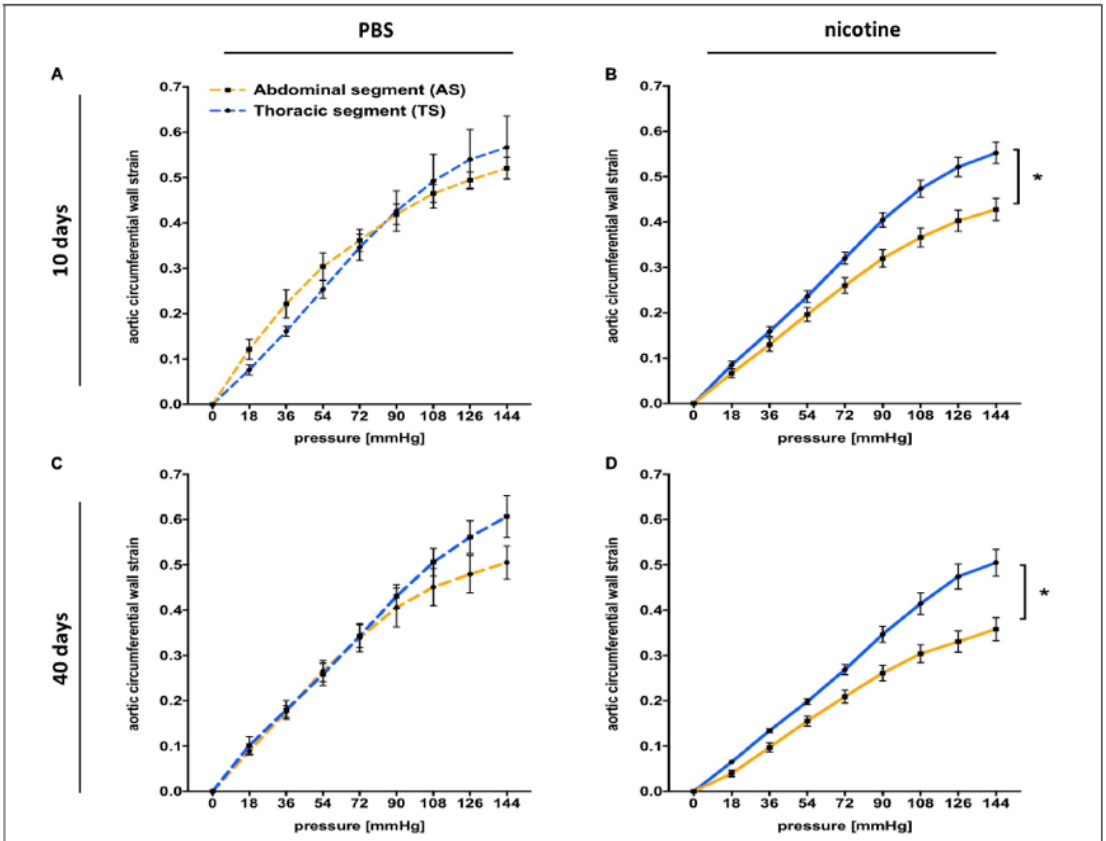

FIGURE 2 | Segmental aortic stiffness is increased after nicotine infusion. **(A)** Pressure myography indicates similar global stiffness between the thoracic (TS) and the abdominal (AS) aortic segment for PBS control mice 10 days after pump implantation [equal area under the curve (AUC)]. (n = 5 mice/group); values are mean ± SEM. **(B)** Pressure myography indicates a significant stiffness gradient (difference for AUC) between the TS and the AS in nicotine-treated mice 10 days after pump implantation (n = 9 mice/group); *p < 0.05 AS vs. TS; values are mean ± SEM. **(C)** Pressure myography indicates similar global stiffness between the TS and the AS for PBS control mice 40 days after pump implantation. (n = 4–5 mice/group) (equal AUC); values are mean ± SEM. **(D)** Pressure myography indicates a significant stiffness gradient (difference for AUC) between the TS and the AS for nicotine-treaded mice 40 days after pump implantation. (n = 6–7 mice/group); *p < 0.05; values are mean ± SEM. **(A–D)** Two-way ANOVA with Holm–Sidak's multiple comparison test.

(**Figures 4C–F**), again without particular differences between TS and AS.

In order to assess the functional impact of nicotine-triggered MMP induction, we performed *in situ* zymography in aortic sections. Aortic sections from nicotine-treated mice exhibited significantly higher elastolytic enzyme activity than PBS controls indicated by enhanced green–blue fluorescence (**Figures 4G,H**). Again, we detected no significant differences between the thoracic and abdominal aortic segments regarding this endpoint.

MMP-2/-9 Inhibition via SB-3CT Prevents Nicotine-Induced Aortic Stiffening

In a prophylactic approach, we next investigated whether MMP-2/-9 inhibition via SB-3CT was sufficient to prevent nicotine-induced aortic stiffness and stiffness segmentation. As before, we used PWV (**Figure 5A**) and *ex vivo* myograph measurements (**Figures 5B,C**) to quantify aortic stiffness 40 days after pump implantation and found that SB-3CT was sufficient to reduce overall and segmental aortic stiffness in nicotine-treated mice.

SB-3CT Ameliorates Nicotine-Induced Elastin Destruction and MMP Activity

Mechanistically, *in situ* zymography confirmed markedly reduced MMP activity in aortic sections taken from nicotine-treated mice with additional SB-3CT administration after 40 days of nicotine exposure. This was indicated by a significantly reduced green/blue fluorescence in aortic sections (**Figures 5D,E**). On a structural level, this translated into preserved elastin architecture as detected via modified VVG staining (**Figures 5F,G**).

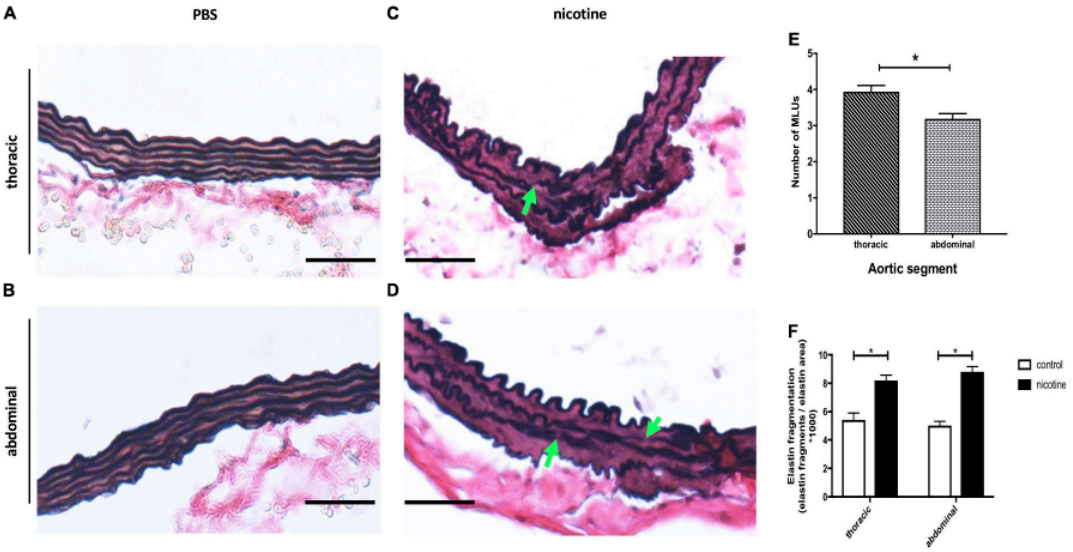

FIGURE 3 | Nicotine infusion induces aortic elastin fragmentation. **(A–D)** Representative images of thoracic **(A,C)** and abdominal **(B,D)** aortic sections taken from mice treated with PBS **(A,B)** or nicotine **(C,D)** and stained with modified Elastin Verhoeff's Van Gieson (VVG). Green arrows indicate locations of elastin fragmentation. Original magnification 200×, scale bar 100 μm. **(E)** Quantification of medial lamellar units (MLUs) of thoracic and abdominal aortic segments from PBS-treated control mice 40 days after pump implantation (the mean was calculated from 4 high-power fields/aorta, $n = 3$ different aortas per group). *$p < 0.05$ AS vs. TS, values are mean ± SEM; Student's t-test. **(F)** Elastin fragmentation index 40 days after pump implantation (the mean was calculated from 3 high-power fields/aorta, $n = 5$ different aortas per group). *$p < 0.05$ vs. respective PBS control; values are mean ± SEM. One-way ANOVA with Holm–Sidak's multiple comparison test.

DISCUSSION

This study provides evidence that chronic nicotine exposure, at concentrations similar to those experienced by ECIG users, promotes aortic stiffening, with enhanced impact on the abdominal aortic segment with regards to the time of onset and quantity. Mechanistically, nicotine infusion led to induction of MMP expression and activity, with associated elastin degradation in the aortic wall, reduction in elastic properties, and stiffening of the aortic segments. This process was effectively prevented with the administration of SB-3CT, a potent and competitive MMP-2/-9 inhibitor.

Nicotine has long been known to induce significant cardiovascular effects, including the release of catecholamines resulting in acute increase of blood pressure and heart rate, although long-term effects seem to be contrary (Leone, 2011; Morris et al., 2015). ECIGs and conventional tobacco cigarettes generate similar plasma levels of the nicotine metabolization product cotinine in humans (Flouris et al., 2013). This supports findings from Barua et al. who found plasma cotinine levels of 140 ng/ml in light and 286 ng/ml in heavy smokers, while a previous literature review suggested peak plasma cotinine levels of approximately 300 ng/ml for ECIG users after a number of free puffs (Barua et al., 2002; Marsot and Simon, 2016). Notably, this study reveals similar plasma cotinine levels for nicotine-treated mice suggesting valid transferability. Recently, it was reported that ECIG usage acutely increases arterial stiffness in healthy volunteers (Lundbäck et al., 2017). This finding leads to fundamental questions regarding the safety of ECIG usage—taking into consideration that arterial stiffness is a risk factor for a wide set of cardiovascular diseases (Lyle and Raaz, 2017). In the acute setting, arterial stiffness may increase passively as a function of rising blood pressure and then similarly normalize. In contrast, chronic arterial stiffness may arise out of (irreversibly) altered biomechanical properties of the arterial wall, resulting from sustained structural remodeling processes (Wolinsky and Glagov, 1964; Wagenseil and Mecham, 2009). In this regard, our ultrasound and pressure myography data, along with histochemical evidence, clearly indicate that nicotine exposure induces chronic structural stiffening of the aortic wall.

Elastin and collagen represent the major structural components of the arterial ECM that critically define vessel biomechanical characteristics. Elastic fibers are found in the medial layer of large elastic arteries, primarily the aorta. The fibers form a network in which each layer of elastic fibers is circumferentially surrounded by smooth muscle cells (SMCs) and collagen fibers forming a lamellar unit (Wagenseil and Mecham, 2012). As elastin fibers straighten with increasing pressure they become load-bearing (Clark and Glagov, 1985). This linear distension is limited by collagen fibers, protecting the vessel from rupture when the pressure exceeds normal physiological levels (Armentano et al., 1991). Within the standard physiologic blood pressure range, medial elastin degradation and fragmentation (mainly caused by enhanced MMP activity) may be the major

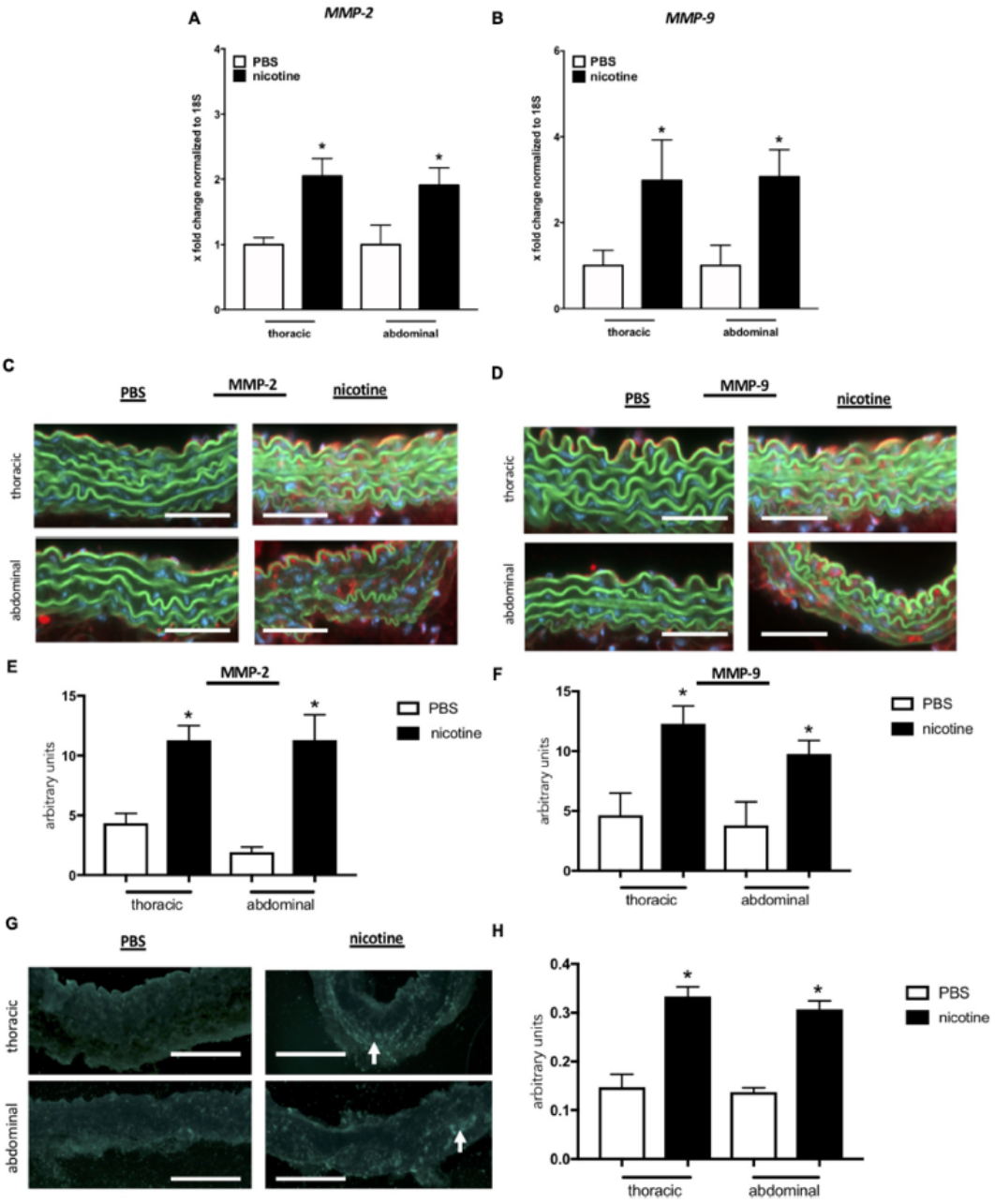

FIGURE 4 | Nicotine treatment induces MMP-2 and MMP-9 gene and protein expression resulting in increased MMP activity. **(A,B)** mRNA expression levels of MMP-2 and MMP-9 are upregulated in the thoracic (TS) and the abdominal aortic segment (AS) after nicotine treatment. (n = 5 mice/group); *$p < 0.05$ vs. respective PBS control; values are mean ± SEM. **(C,D)** Representative images of aortic sections stained for MMP-2 **(C)** and MMP-9 **(D)**. Strong red fluorescence (MMP-2/-9) indicates protein up-regulation in nicotine-treated mice aortae. Original magnification 200×, scale bar 100 μm. **(E,F)** Quantification of MMP-2 **(E)** and MMP-9 **(F)** protein expression level in the aortic wall based on red fluorescence in sections taken from AS and TS of nicotine-treated and PBS control mice 40 days after pump implantation (the mean was calculated from 3 high-power fields/aorta, n = 5 different aortas per group). *$p < 0.05$ vs. respective PBS control; values are mean ± SEM. **(G)** Representative images of aortic zymography of TS and the AS taken from nicotine-treated or PBS control mice. Green–blue fluorescence indicates regions of active MMPs (white arrows). Original magnification 200×, scale bar 100 μm. **(H)** Quantification of MMP activity based on green–blue fluorescence in zymography images taken from AS and TS of nicotine-treated and PBS control mice 40 days after pump implantation (the mean was calculated from 3 high-power fields/aorta, n = 5 different aortas per group). *$p < 0.05$ vs. respective PBS control; values are mean ± SEM. **(A,B,E,F,H)** One-way ANOVA with Holm–Sidak's multiple comparison test.

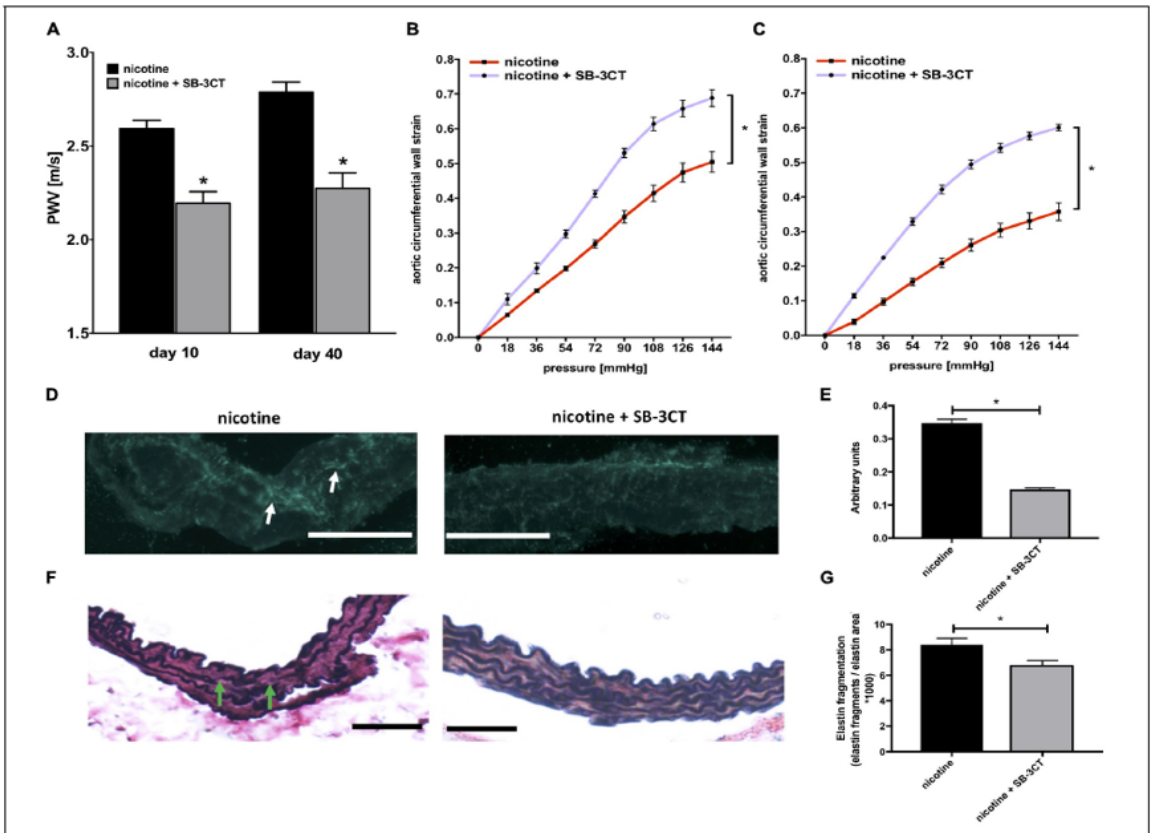

FIGURE 5 | MMP inhibition via SB-3CT prevents aortic wall remodeling and stiffening in nicotine-treated mice. **(A)** PWV for nicotine-treated mice ± additional SB-3CT administration (n = 4–8 mice/group); *$p < 0.05$ vs. nicotine; values are mean ± SEM. **(B,C)** Pressure-strain curves for the thoracic (TS) **(B)** and the abdominal **(C)** aortic segment (AS) from nicotine-infused mice ± SB-3CT administration 40 days after pump implantation (4–7 mice/group); *$p < 0.05$ area under the curve (AUC) nicotine vs. AUC nicotine + SB-3CT; values are mean ± SEM. **(D)** Representative images of aortic zymography of the TS taken from nicotine-treated ± SB-3CT administrated mice. Green–blue fluorescence indicates regions of active MMPs (white arrows). Original magnification 200×, scale bar 100 µm. **(E)** Quantification of MMP activity based on green–blue fluorescence intensity in zymography images taken from nicotine-treated ± SB-3CT administrated mice 40 days after pump implantation (the mean was calculated from 3 high-power fields/aorta, n = 5 different aortas per group); *$p < 0.05$ nicotine vs. nicotine + SB-3CT; values are mean ± SEM. **(F)** Representative images of thoracic aortic sections from nicotine ± SB-3CT-treated mice stained with Elastica van-Giesson (EvG). Green arrows indicate locations of elastin fragmentation. Original magnification 200×, scale bar 100 µm. **(G)** Elastin fragmentation index (the mean was calculated from 3 high-power fields/aorta, n = 5 different aortas per group). *$p < 0.05$ nicotine vs. nicotine + SB-3CT; values are mean ± SEM. **(E,G)** One-way ANOVA with Holm–Sidak's multiple comparison test.

factors behind early aortic stiffening (Murphy et al., 1991; Ishii and Asuwa, 1996; Lyle and Raaz, 2017). In this regard, we find that nicotine treatment induces significant damage to the aortic wall elastin network, resulting in increased structural arterial stiffness. Unfortunately, elastic fibers are almost exclusively assembled during tissue development, and then must function for the entire lifespan of the organism with low potential for repair (Wagenseil and Mecham, 2009). As such, elastin damage inflicted by chronic nicotine usage may be permanent—even after removal of the noxious trigger.

There are a number of MMPs with known elastolytic activity, including some with important roles in vascular remodeling (Perlstein and Lee, 2006; Jacob-Ferreira et al., 2010) MMP-2 (gelatinase A) is constitutively expressed by SMCs. MMP-9 (gelatinase B) can be produced by macrophages, fibroblasts, or SMCs with a secretory phenotype. Interestingly, high serum levels of MMP-2 and MMP-9 have been associated with increased arterial stiffness in healthy individuals, and patients with isolated systolic hypertension (Yasmin et al., 2005). Wang et al. (2012) found that AMP-activated protein kinase α2 showed increased nuclear co-localization with nicotine, upregulating MMP expression, and instigating the formation of AAA in genetically modified mice. Our data are in line with these findings, as they show upregulated aortic expression and activity

ACKNOWLEDGMENTS

The authors thank Tooba Khan for her excellent support during the study. MW also wants to express his gratitude to his family for their support and ongoing encouragement.

SUPPLEMENTARY MATERIAL

The Supplementary Material for this article can be found online at: https://www.frontiersin.org/articles/10.3389/fphys.2018.01459/full#supplementary-material

REFERENCES

Armentano, R. L., Levenson, J., Barra, J. G., Fischer, E. I., Breitbart, G. J., Pichel, R. H., et al. (1991). Assessment of elastin and collagen contribution to aortic elasticity in conscious dogs. *Am. J. Physiol.* 260, H1870–H1877. doi: 10.1152/ajpheart.1991.260.6.H1870

Arrazola, R. A., Singh, T., Corey, C. G., Husten, C. G., Neff, L. J., Apelberg, B. J., et al. (2015). Tobacco use among middle and high school students - United States, 2011-2014. *MMWR Morb. Mortal. Wkly. Rep.* 64, 381–385.

Barua, R. S., Ambrose, J. A., Eales-Reynolds, L.-J., DeVoe, M. C., Zervas, J. G., and Saha, D. C. (2002). Heavy and light cigarette smokers have similar dysfunction of endothelial vasoregulatory activity: an *in vivo* and *in vitro* correlation. *J. Am. Coll. Cardiol.* 5, 1758–1763. doi: 10.1016/S0735-1097(02)01859-4

Bunnell, R. E., Agaku, I. T., Arrazola, R. A., Apelberg, B. J., Caraballo, R. S., Corey, C. G., et al. (2015). Intentions to smoke cigarettes among never-smoking US middle and high school electronic cigarette users: National Youth Tobacco Survey, 2011-2013. *Nicotine Tob. Res.* 17, 228–235. doi: 10.1093/ntr/ntu166

Canistro, D., Vivarelli, F., Cirillo, S., Babot Marquillas, C., Buschini, A., Lazzaretti, M., et al. (2017). E-cigarettes induce toxicological effects that can raise the cancer risk. *Sci. Rep.* 7:2028. doi: 10.1038/s41598-017-02317-8

Carty, C. S., Soloway, P. D., Kayastha, S., Bauer, J., Marsan, B., Ricotta, J. J., et al. (1996). Nicotine and cotinine stimulate secretion of basic fibroblast growth factor and affect expression of matrix metalloproteinases in cultured human smooth muscle cells. *J. Vasc. Surg.* 24, 927–934. doi: 10.1016/S0741-5214(96)70038-1

Clark, J. M., and Glagov, S. (1985). Transmural organization of the arterial media 1985. The lamellar unit revisited. *Arteriosclerosis* 5, 19–34. doi: 10.1161/01.ATV.5.1.19

Collins, M. J., Bersi, M., Wilson, E., and Humphrey, J. D. (2011). Mechanical properties of suprarenal and infrarenal abdominal aorta: implications for mouse models of aneurysms. *Med. Eng. Phys.* 33, 1262–1269. doi: 10.1016/j.medengphy.2011.06.003

Dawkins, L. E., Kimber, C. F., Doig, M., Feyerabend, C., and Corcoran, O. (2016). Self-titration by experienced e-cigarette users: blood nicotine delivery and subjective effects. *Psychopharmacology* 233, 2933–2941. doi: 10.1007/s00213-016-4338-2

Dom, A. M., Buckley, A. W., Brown, K. C., Egleton, R. D., Marcelo, A. J., Proper, N. A., et al. (2011). The α7-nicotinic acetylcholine receptor and MMP-2/-9 pathway mediate the proangiogenic effect of nicotine in human retinal endothelial cells. *Invest. Ophthalmol. Vis. Sci.* 52, 4428–4438. doi: 10.1167/iovs.10-5461

Flouris, A. D., Chorti, M. S., Poulianiti, K. P., Jamurtas, A. Z., Kostikas, K., Tzatzarakis, M. N., et al. (2013). Acute impact of active and passive electronic cigarette smoking on serum cotinine and lung function. *Inhal. Toxicol.* 25, 91–101. doi: 10.3109/08958378.2012.758197

Goergen, C. J., Barr, K. N., Huynh, D. T., Eastham-Anderson, J. R., Choi, G., Hedehus, M., et al. (2010). In vivo quantification of murine aortic cyclic strain, motion, and curvature: implications for abdominal aortic aneurysm growth. *J. Magn. Reson. Imaging* 32, 847–858. doi: 10.1002/jmri.22331

Gravely, S., Fong, G., Cummings, K., Yan, M., Quah, A., Borland, R., et al. (2015). Correction: Gravely, S., et al. awareness, trial, and current use of electronic cigarettes in 10 countries: findings from the itc project. *Int. J. Environ. Res. Public Health* 12, 4631–4637. doi: 10.3390/ijerph111111691

Halloran, B. G., Davis, V. A., McManus, B. M., Lynch, T. G., and Baxter, B. T. (1995). Localization of aortic disease is associated with intrinsic differences in aortic structure. *J. Surg. Res.* 59, 17–22. doi: 10.1006/jsre.1995.1126

Hickson, S. S., Butlin, M., Graves, M., Taviani, V., Avolio, A. P., McEniery, C. M., et al. (2010). The relationship of age with regional aortic stiffness and diameter. *JACC Cardiovasc. Imaging* 3, 1247–1255. doi: 10.1016/j.jcmg.2010.09.016

Ishii, T., and Asuwa, N. (1996). Spiraled collagen in the major blood vessels. *Mod. Pathol.* 9, 843–848.

Jacob-Ferreira, A. L., Palei, A. C., Cau, S. B., Moreno, H., Martinez, M. L., Izidoro-Toledo, T. C., et al. (2010). Evidence for the involvement of matrix metalloproteinases in the cardiovascular effects produced by nicotine. *Eur. J. Pharmacol.* 627, 216–222. doi: 10.1016/j.ejphar.2009.10.057

Leone, A. (2011). Does smoking act as a friend or enemy of blood pressure? let release pandora's box. *Cardiol. Res. Pract.* 19:264894. doi: 10.4061/2011/264894

Lundbäck, M., Antoniewicz, L., Brynedal, A., and Bosson, J. (2017). "Acute effects of active e-cigarette inhalation on arterial stiffness," in *Proceedings of the 2017 Tobacco, Smok Control Heal Educ in Tobacco, Smoking Control and Health Education 50, OA1979*. (Lausanne: European Respiratory Society).

Lyle, A. N., and Raaz, U. (2017). Killing me unsoftly. *Arterioscler. Thromb. Vasc. Biol.* 37, e1–e11. doi: 10.1161/ATVBAHA.116.308563

Maegdefessel, L., Azuma, J., Toh, R., Deng, A., Merk, D. R., Raiesdana, A., et al. (2012). MicroRNA-21 blocks abdominal aortic aneurysm development and nicotine-augmented expansion. *Sci. Transl. Med.* 4:122ra22. doi: 10.1126/scitranslmed.3003441

Marsot, A., and Simon, N. (2016). Nicotine and cotinine levels with electronic cigarette. *Int. J. Toxicol.* 35, 179–185. doi: 10.1177/1091581815618935

McMillen, R. C., Gottlieb, M. A., Shaefer, R. M. W., Winickoff, J. P., and Klein, J. D. (2015). Trends in electronic cigarette use among U.S. adults: use is increasing in both smokers and nonsmokers. *Nicotine Tob. Res.* 17, 1195–1202. doi: 10.1093/ntr/ntu213

Morris, P. B., Ference, B. A., Jahangir, E., Feldman, D. N., Ryan, J. J., Bahrami, H., et al. (2015). Cardiovascular effects of exposure to cigarette smoke and electronic cigarettes: clinical perspectives from the prevention of cardiovascular disease section leadership council and early career councils of the american college of cardiology. *J. Am. Coll. Cardiol.* 66, 1378–1391. doi: 10.1016/j.jacc.2015.07.037

Murphy, G., Cockett, M. I., Ward, R. V., and Docherty, A. J. (1991). Matrix metalloproteinase degradation of elastin, type IV collagen and proteoglycan. A quantitative comparison of the activities of 95 kDa and 72 kDa gelatinases, stromelysins-1 and -2 and punctuated metalloproteinase (PUMP). *Biochem. J.* 277(Pt 1), 277–279.

O'Rourke, M. F. (2007). Arterial aging: pathophysiological principles. *Vasc. Med.* 12, 329–341. doi: 10.1177/1358863X07083392

Perlstein, T. S., and Lee, R. T. (2006). Smoking, metalloproteinases, and vascular disease. *Arterioscler. Thromb. Vasc. Biol.* 26, 250–256. doi: 10.1161/01.ATV.0000199268.27395.4f

Raaz, U., Schellinger, I. N., Chernogubova, E., Warnecke, C., Kayama, Y., Penov, K., et al. (2015a). Transcription factor runx2 promotes aortic fibrosis and stiffness in type 2 diabetes mellitus. *Circ. Res.* 117, 513–524. doi: 10.1161/CIRCRESAHA.115.306341

Raaz, U., Zollner, A. M., Schellinger, I. N., Toh, R., Nakagami, F., Brandt, M., et al. (2015b). Segmental aortic stiffening contributes to experimental abdominal aortic aneurysm development. *Circulation* 131, 1783–1795. doi: 10.1161/CIRCULATIONAHA

Talih, S., Balhas, Z., Eissenberg, T., Salman, R., Karaoghlanian, N., El Hellani, A., et al. (2015). Effects of user puff topography, device voltage, and liquid nicotine concentration on electronic cigarette nicotine yield: measurements and model predictions. *Nicotine Tob. Res.* 17, 150–157. doi: 10.1093/ntr/ntu174

Wagenseil, J. E., and Mecham, R. P. (2009). Vascular extracellular matrix and arterial mechanics. *Physiol. Rev.* 89, 957–989. doi: 10.1152/physrev.00041.2008

Wagenseil, J. E., and Mecham, R. P. (2012). Elastin in large artery stiffness and hypertension. *J Cardiovasc. Transl. Res.* 5, 264–273. doi: 10.1007/s12265-012-9349-8

Wang, S., Zhang, C., Zhang, M., Liang, B., Zhu, H., Lee, J., et al. (2012). Activation of AMP-activated protein kinase α2 by nicotine instigates formation of abdominal aortic aneurysms in mice in vivo. *Nat. Med.* 18, 902–910. doi: 10.1038/nm.2711

Wolinsky, H., and Glagov, S. (1964). structural basis for the static mechanical properties of the aortic media. *Circ. Res.* 14, 400–413. doi: 10.1161/01.RES.14.5.400

Wolinsky, H., and Glagov, S. (1969). Comparison of abdominal and thoracic aortic medial structure in mammals. Deviation of man from the usual pattern. *Circ. Res.* 25, 677–686. doi: 10.1161/01.RES.25.6.677

Yasmin, McEniery, C. M., Wallace, S., Dakham, Z., Pulsalkar, P., Pusalkar, P., et al. (2005). Matrix metalloproteinase-9 (MMP-9), MMP-2, and serum elastase activity are associated with systolic hypertension and arterial stiffness. *Arterioscler. Thromb. Vasc. Biol.* 25:372. doi: 10.1161/01.ATV.0000151373.33830.41

Zhang, J., Zhao, X., Vatner, D. E., McNulty, T., Bishop, S., Sun, Z., et al. (2016). Extracellular matrix disarray as a mechanism for greater abdominal versus thoracic aortic stiffness with aging in primates. *Arterioscler. Thromb. Vasc. Biol.* 36, 700–706. doi: 10.1161/ATVBAHA.115.306563

Conflict of Interest Statement: The authors declare that the research was conducted in the absence of any commercial or financial relationships that could be construed as a potential conflict of interest.

The reviewer CH and handling Editor declared their shared affiliation at the time of the review.

Article

Journal of Histochemistry & Cytochemistry 2019, Vol. 67(4) 267–274

DOI: 10.1369/0022155418814231
journals.sagepub.com/home/jhc
SAGE

An Automated Algorithm to Quantify Collagen Distribution in Aortic Wall

Dustin M. Nguyen, Markus U. Wagenhäuser, Dennis Mehrkens, Matti Adam, Philip S. Tsao, and Anand K. Ramasubramanian

Department of Chemical and Materials Engineering, San José State University, San José, CA (DMN, AKR); Division of Cardiovascular Medicine, Stanford University School of Medicine, Stanford, CA (MUW, PST); VA Palo Alto Health Care System, Palo Alto, CA (MUW, PST); and Department of Cardiovascular Medicine, University Heart Center and Cologne Cardiovascular Research Center, University of Cologne, Cologne, Germany (DM, MA)

Summary

Arterial diseases including abdominal aortic aneurysm and atherosclerosis are biomechanical diseases characterized by significant changes in the structure and strength of the vessel wall. It is now established that local variations in fibrillar collagen and elastin matrix turnover is critical to arterial stiffening and progression of the disease. The collagen content in the aortic wall has nominally been quantified by biochemical assays and immunohistochemical analysis as the total amount because of the difficulty in separating the media and adventitia. In this work, we have developed an algorithm for automatic quantification of layer-specific collagen content from bright-field and polarized microscopic images of histological sections of mouse aorta stained with Picrosirius red (PSR) stain. The images were processed sequentially including separation of layers, erosion, segregation of regions, binarization, and quantification of pixel intensities to obtain collagen content in the media and adventitia separately. We observed that the automated algorithm rapidly and accurately quantified collagen content from a wide range of image quality compared with manual measurements particularly when the medial and adventitial layers overlap. Together, our algorithm will be of significant impact in the rapid, reliable, and accurate analyses of collagen distribution in histological sections of connective tissues. (J Histochem Cytochem 67:267–274, 2019)

Keywords

AAA, histology, stiffening

Introduction

Aortic stiffness is an independent predictor of cardiovascular and cerebrovascular mortality and morbidity even after accounting for the classical risk factors.[1] Aortic stiffness increases not only in normal aging process but also in aortic diseases including aneurysm, dissection, and atherosclerosis. As aortic stiffness is one of the earliest detectable manifestations of the adverse functional changes in the blood vessel, evaluating the underlying structural changes is critical for detection and intervention of cardiovascular diseases.

The aortic wall is comprised of three layers of distinct composition and properties: intima, media, and adventitia. In healthy arteries, the intima is composed of a single layer of endothelial cells, a thin basal membrane, and a subendothelial layer composed of collagen fibrils; the media is composed of smooth muscle cells, a network of elastin, and collagen fibrils, which are separated by a few layers of circumferentially lamellar elastin sheets; and the adventitia is composed of thick bundles of collagen fibrils arranged in helical

Received for publication June 5, 2018; accepted October 29, 2018.

Corresponding Author:
Anand K. Ramasubramanian, Department of Chemical and Materials Engineering, San José State University, San José, CA 95112, USA.
E-mail: anand.ramasubramanian@sjsu.edu

structures and fibroblasts.[2] In healthy human aorta, the intimal, medial, and adventitial thickness is ~50 to 150 µm, 300 to 500 µm, and 500 to 1000 µm, respectively, and total thickness of 1 to 2 mm.[3,4] Aortic stiffness is mainly determined by the major extracellular matrix (ECM) components of the arterial wall, that is, collagen and elastin, and less so by cellular components.[5] The breakdown of elastin and fibrillar collagen is compensated by the deposition of uncoiled neo-collagen synthesized by the vascular smooth muscle cells (VSMC), which leads to the transfer of load to less compliant collagen. Thus, changes in collagen content can be important for the understanding of the etiology of increase in aortic stiffness.

Traditionally, the total collagen content of the aorta is estimated by either biochemical assay for hydroxyproline levels or by histological or immunohistochemical analysis of tissue sections.[6] Although these assays provide the total collagen content, changes in individual layers of the aorta is often of immense interest. In abdominal aortic aneurysms (AAA), spatial variations in the ECM distribution is correlated with segmental stiffening which in turn determines disease progression and severity.[7] The Picrosirius red (PSR) staining provides a convenient, inexpensive, fade-resistant, and reproducible staining of collagen in tissue sections, and is preferred over traditional trichrome stains. The PSR staining method relies on the elongated, anionic structure of the Sirius red dye molecule–binding parallel to cationic collagen fibers, thus enhancing the natural birefringence of collagen bundles.[8] The PSR staining technique has been widely used for qualitative or quantitative description of changes in collagen content, not only of the aorta but also of numerous other connective tissues including skin and myocardial scars wherein relative distribution between different regions of the tissue is of interest.[9,10] In this work, we describe an automated methodology to quantify collagen content separately in the medial and adventitial layers of mouse aortic sections from bright-field and polarized microscopy images. Combining information from these two microscopy techniques allows for rapid and reliable quantification of localized collagen content in histological sections.

Methods

Sample Processing

Murine aorta were explanted from C57BL/6J mice and incubated in 4% paraformaldehyde (PFA) at 4C for 2 hr. Thereafter, aorta were transferred to a new 4% PFA in PBS solution supplemented with 20% sucrose and incubated overnight at 4C. The next day, the aorta were cut in 1 cm pieces and rinsed quickly in cold PBS. Next, samples were embedded in Tissue Plus OCT compound (Fisher Scientific) and immediately frozen down. Samples were stored at –80C until further processing. Similar procedures were followed for processing, sectioning, and imaging of murine femoral and carotid arteries, and images were analyzed, similar to aortic sections, as described below.

Sample Sectioning

Materials were allowed to equilibrate to the chamber temperature of –20C for 10 min. After attaching samples to the circular cryostat block, the tissue blocks were sectioned at 7 µm using a cryostat (CM3050 S, Leica Biosystems Inc., Wetzlar, Germany), and mounted on SuperFrost Ultra Plus (Fisher Scientific) glass slides. Sections were incubated in ice-cold acetone for 4 min and stored at –80C until further processing.

Picrosirius Red Staining

Sections were thawed and allowed to equilibrate to room temperature for 10 min. Then, sections were fixed in ice-cold acetone for 4 min again and allowed to dry. PSR staining was performed using Picrosirius Red Stain Kit (catalog number: ab150681, Abcam) according to the manufacturer instructions. In short, PSR solution was applied to completely cover the tissue section and incubated for 60 min. Sections were rinsed twice in acetic acid and once in absolute ethanol (Fisher Scientific). Sections were dehydrated with two washes in absolute ethanol and mounted using synthetic resin (catalog number: 1900231, Fisher Scientific). Samples were stored at room temperature until imaging.

Image Acquisition

PSR-stained sections were visualized utilizing a Leica microscope (Leica DM4000B, Leica Biosystems Inc., USA) and a polarized filter (Leica ICT/Pol, Leica Biosystems Inc.). Images of different aortic segments were obtained using DISKUS (Version 5.0.6.277, Hilgers technisches Buero, Koenigswinter, Germany) and saved as a pairwise results objects (bright-field/polarized light) for further processing.

Image Selection

Complementary images obtained by bright-field microscopy and polarized light microscopy of the same histological section are necessary for quantification of collagen content. The section must have a contiguous

adventitia, which means that the red ring in the adventitia must be continuous with no breaks. The bright-field and polarized light images must also be aligned to properly use the bright-field image to distinguish between the adventitia and media. The lighting throughout the images must be relatively even to accurately discriminate between the background and the histological section. There must also be minimized debris on the histological slide to ensure the collagen is quantified accurately. Finally, the adventitia and media should not overlap as it may sometimes happen due improper processing.

Automated Analysis of Collagen Content Using MATLAB

Downloading and Running the Program. The program for automated collagen quantification can be found at https://git.io/vhsGV. The repository needs to be downloaded and extracted into the active MATLAB (MathWorks, Natick, MA) directory. The program was run within MATLAB by using the command "Automatic_Collagen_Quant_AAA_PSR." The graphical user interface (GUI) was then available for use to quantify the collagen using bright-field and polarized images.

The program needs complementary pairs of bright-field and polarized images to quantify the collagen of the tissue section. The program supports various image types such as .JPG, .IMG, and .TIFF, but it is highly recommended to use uncompressed .TIFF files to maintain the integrity of the image. The bright-field image is loaded by clicking the "Load Bright Field" button in the GUI and selecting the corresponding image. A preview of the image and its file name will appear in the GUI for verification. The polarized image is loaded by clicking the "Load Polarized" button in the GUI and selecting the corresponding image. A preview of the image and its file name will be displayed next to the preview of the bright-field image. At this point, the program can quantify collagen content by pressing the "Process" button. However, some extra steps may be necessary to properly process the images depending on the conditions for image acquisition or the output format. (1) If the bright-field and polarized images are not properly aligned, the "Offset" button must be toggled on and the amount of offset in pixels should be entered for the X-Offset and Y-Offset. (2) Depending on the resolution of the image, the size of the structural elements used to process the bright-field image may also need to be changed. This process is elaborated on further in the "Results" section. (3) The data can be expressed as the surface area of the image if the "Scale Bar" button is toggled on, and the length of the scale bar and its length are entered as input into the GUI.

Uploading the Image. The bright-field and polarized images were uploaded into MATLAB. The images should ideally be uncompressed .TIFF images, which are preferable to best preserve the quality of the images, although the program does allow for the uploading of other image format types.

Preprocessing of Images. The uploaded images are adjusted to an array of $m \times n \times 3$ to account for images that may be in RGBa space, which outputs images in an $m \times n \times 4$ array. The green channel of the bright-field image was isolated by selecting the second of the three layers of the image array which resulted in a grayscale image. The polarized image was converted into grayscale and the contrast of the image was improved. The conversion into grayscale was achieved using the MATLAB function, *rgb2gray*, which converts the RGB values to grayscale by performing a weighted sum of the red (R), green (G), and blue (B) components using the following formula: $0.2989 \times (R) + 0.5870 \times (G) + 0.1140 (B)$. Improving the contrast was accomplished using the *adapthisteq* MATLAB function, which uses contrast-limited adaptive histogram equalization (CLAHE) algorithm. The algorithm operates on small regions of the image, referred to as tiles, rather than the image as a whole. The contrast of each tile is enhanced using a contrast transform function, and the neighboring tiles are combined using bilinear interpolation to eliminate the artificially created boundaries between the tiles.

Processing the Bright-field Image

The grayscale image obtained from the green channel of the image was then adaptively binarized using the *imbinarize* function with a sensitivity of 0.3. The locally adaptive threshold in MATLAB utilizes Bradley's Method.[11] This sensitivity was chosen to sufficiently thin the portions associated with the media, that would later be removed through erosion and dilation techniques, and to preserve the integrity of the adventitia. Two structural elements in the form of a disk were created with diameters of four and two pixels. The two-pixel structural element was used for erosion and the four-pixel structural element was used for dilation. These two structural elements are set to be two and four pixels by default, but the sizes can be changed within the GUI to account for different resolutions. The binarized image was eroded, dilated, and eroded to remove the small fibers associated with the media, while preserving the integrity of the image. The *bwareaopen* function was used to remove small objects that were not associated with the tissue and to remove any possible residual debris. This was done by

determining the connected components throughout the image and their respective areas, and the connected components that were smaller than desired size were removed. By default, the program will remove any isolated components that are comprised of less than 600 pixels, but the threshold for the small objects can be changed within the GUI. The adventitia is now isolated with an empty center which will be used as the region of interest (ROI). The ROI was calculated by finding the center of the image and using the *graycon-nected* function to select all the pixels within the borders of the adventitia that are now contiguous after removing the excess debris in the previous step. A mask was created by duplicating the ROI and scaling it to 80% of its original size. This mask was used to delete any extraneous debris in ROI.

Processing the Polarized Image

The polarized image, now in grayscale, was binarized using Otsu's method by using *imbinarize* with global thresholding.[12] The ROI was then used to isolate the collagen associated with the media and the extra debris in the middle that may appear during binarization was removed using the mask.

Quantifying Collagen

The total collagen was quantified by counting the number of white pixels in the binarized polarized image. The white pixels that were within the ROI were counted as collagen within the media. These values were then used to determine the percent of collagen locally. If the scale bar measurements are available, the size of the scale bar and the actual length of the scale bar may be used in their respective fields in the GUI, allowing the program to compute the surface area covered by collagen.

Manual Analysis of Collagen Content Using Adobe Photoshop

Two operators were trained to trace the outlines between adventitia and media in the image slices. The operators were given the same set of 15 images and manually drew a line to represent the border between the adventitia and media in the polarized light images. The outlines were done in Adobe Photoshop by creating a layer over the image and drawing an outline around the inside of the heavily red portions of the image, representing the border between adventitia and media. The operators were also timed to determine the amount of time that was required to trace the outlines. These outlines were then used to produce ROIs that were imported into MATLAB for collagen quantification using the same methods as previously described. The localized percentage of collagen within the automatically generated ROI and manually created ROI were then compared along a scatter plot to determine if the two measurements were comparable.

Statistics

We obtained 20 image sets from various parts of the mouse aorta, and they were analyzed for total collagen content by either automated program or manual methods. The data sets were plotted against each other, and linear regression (GraphPad Prism) was used to compare the quality of the fit.

Results and Discussion

We created a GUI to quantify collagen content and distribution in histological sections obtained from murine aorta. The overall process flow that is built into the automated program and the GUI are shown in Fig. 1A and B, respectively. Each PSR-stained image set consists of two images, each obtained from bright-field and polarized light microscopy, and the program superimposes these two images to demarcate the media and adventitia, identify the inner and outer boundaries of the two regions, and from the residual intensities, calculate the collagen content in these regions.

The bright-field images of PSR-stained sections show a distinct rich red outer ring, and an orange-yellow inner ring (Fig. 2A). The outer red stain is from the adventitia, which has the highest amount of collagen, thus stains red. The orange-yellow in the bright-field image is from the media. However, there is still some collagen within this layer of the vessel wall, but it is not possible to see using only by bright-field microscopy. Polarized light microscopy, allows for the observation of the collagen that is present within the media (Fig. 2B). Collagen stained with PSR is birefringent under polarized light and there are changes in the birefringence colors that range from green, yellow, or red. Although the origins of the color were initially thought to be representative of collagen subtypes (I vs. III based on yellow-red vs. green), and the fiber thickness, it is now believed that the birefringence colors largely depend on the orientation of the collagen with respect to orientation of the polarized light.[13–15] Thus, polarized light microscopy in combination with PSR is most useful when used for quantification of the overall collagen content as the colors are easily differentiated from the black background.

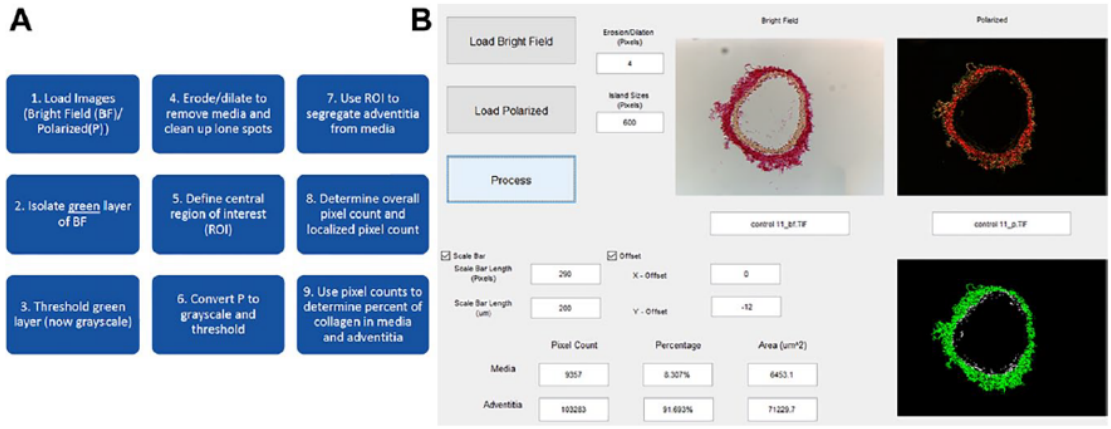

Figure 1. (A) A simplified flowchart outlining the steps taken within the program to quantify the collagen. (B) The graphical user interface of the program used for quantifying collagen content in media and adventitia.

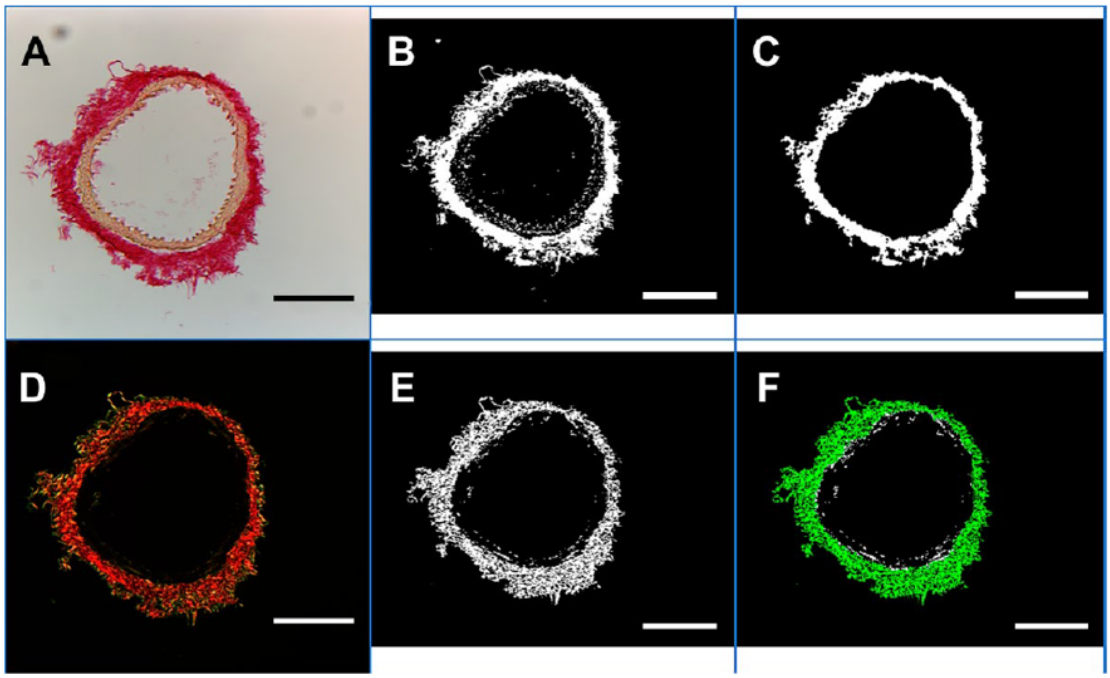

Figure 2. The original bright-field (A) and polarized light microscopy images (D); Grayscale representation of the green layer isolated from RGB composition and segmented from bright-field image (B), and from polarized image (E). (C) The segmented images from (B) were subjected to a cycle of erosion, dilation, and erosion to remove the pixel associated with the media while maintaining image integrity. Isolated islands were also removed to remove extraneous debris. (F) A visual representation of the polarized image separated by adventitia (green) and the media (white). The scale bar is 200 µm.

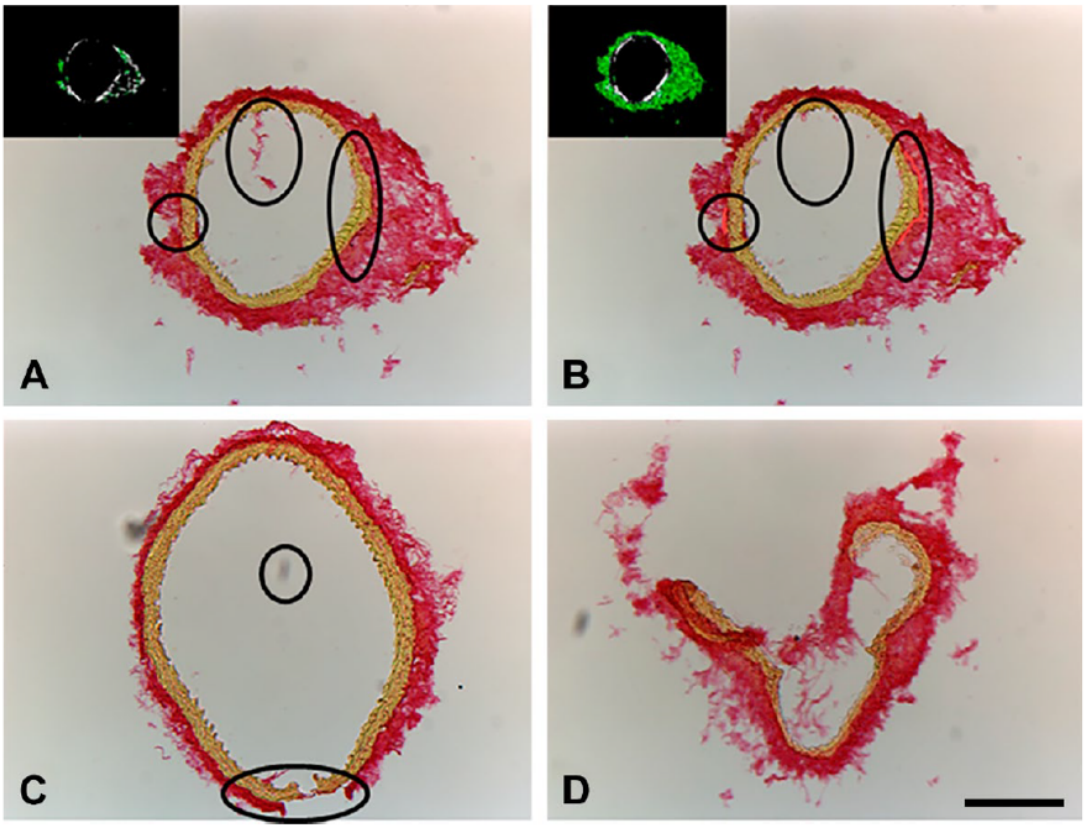

Figure 3. Sample images that require preprocessing. (A) A non-ideal image with small separations within the adventitia and excess debris and the program is not able to establish a proper ROI. (B) The non-ideal case with the excess debris removed and the adventitia bridged to produce a proper ROI for collagen quantification. (C) Another non-ideal image with corrections. (D) A non-salvageable image. Abbreviation: ROI, region of interest. The scale bar is 200 μm.

Processing of Ideal Cases

Image sets with perfect alignment of bright-field and polarized microscopy images, distinct adventitia and media, and proper lighting may be processed readily using the algorithm described in Fig. 1, and is shown stepwise in Fig. 2. First, the green channel from both bright-field and polarized microscopy images was isolated and converted into grayscale (Fig. 2C and D). The green channel was chosen because it allowed for the greatest contrast between adventitia and media when compared with the red and blue channels (Fig. S1). Once in grayscale, adaptive thresholding was performed on the bright-field image, as seen in Fig. 2C, and the thin fibers and debris were filtered out to establish the ROI, shown in Fig. 2D. Afterward, the polarized image was processed using a global threshold method (Fig. 2E), and the collagen was quantified using the ROI to establish the amounts of collagen in the media and adventitia (Fig. 2F). Finally, the results are displayed as the cross-sectional area containing collagen or as pixels positive for collagen content. We also followed similar image processing steps for bright-field and polarized images of PSR-stained sections of femoral and carotid arteries of mice. As shown in Figs. S2 and S3, respectively, our program successfully demarcates the media and adventitia without any noticeable overlap.

Processing of Non-ideal Cases

We observed that inherently most of the images were less than ideal, and required some extra processing steps (Fig. 3). These include non-contiguous adventitia, excessive debris in the sample, or misalignment between bright-field and polarized images. If these

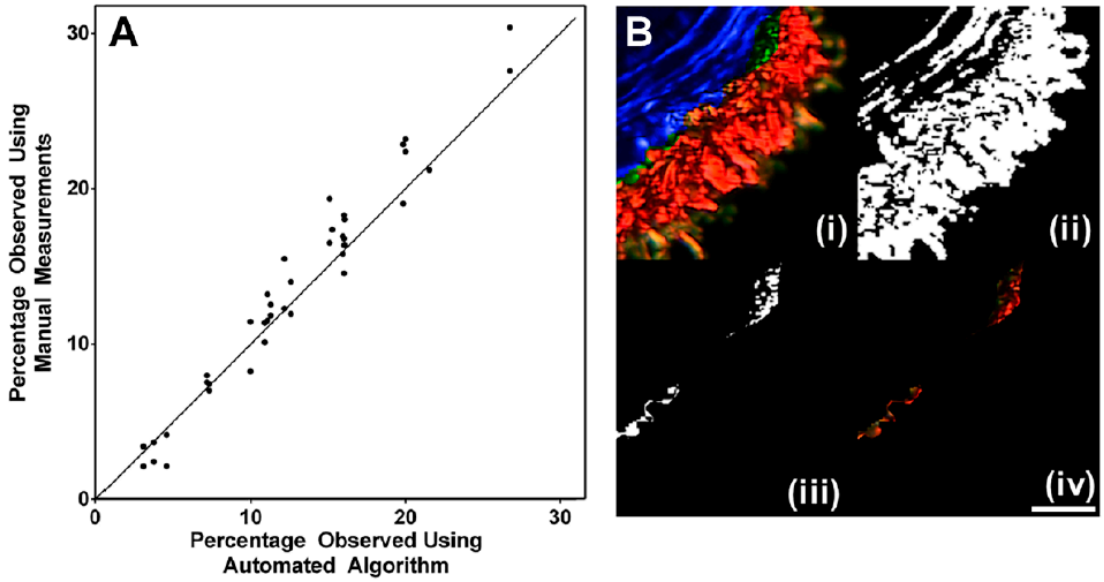

Figure 4. (A) Scatter plot demonstrating the similarity between manually defining the ROI and automatically defining the ROI with the program (n=20). The methods produced virtually identical results at lower collagen levels although the manual method overpredicted at higher collagen levels (R^2 = 0.94). (B) Accuracy of the automatic program versus manual tracing. (i) A subsection of a polarized image with the ROI generated by the automated program (blue) and by manual tracing (green); (ii) Binarized image; (iii) The extra pixels that were counted after global thresholding in manual measurement but not automated algorithm; (iv) The extra pixels were pixels that should be attributed to adventitia by showing the pixels were associated with red color. Abbreviation: ROI, region of interest. The scale bar is 100 μm.

images were processed as is, neither total collagen content nor regional distribution could be obtained (Fig. 3A, inset). Fortunately, these common issues can be easily fixed by a few corrective actions, either in Adobe Photoshop before uploading the images into the GUI or in the GUI itself. (1) The adventitia can be bridged to make it contiguous using Adobe Photoshop. We used the eyedropper tool to sample the color of the adventitia, and used the pencil tool set at 8 pixels to bridge any gaps within the adventitia. (2) In case of excessive debris in the sample, we used the clone stamp tool to mask the debris and preserve the integrity of the image to not have an effect on future segmentation. (3) We observed a consistent 12 pixel vertical offset between the bright-field and polarized images, probably due to physical reasons while switching the filters in the microscope. To nullify this offset, the value of the offset can be obtained by manual alignment of one set of images. This value may be entered in the GUI before processing by clicking the check box next to "Offset" in the GUI and feeding in the x and y offsets in their respective fields. Once corrected, the collagen content can be quantified using the automated program (Fig. 3B and inset, Fig. 3C). Despite these corrections, some images may not be salvageable because of poor quality such as excessive overlap of adventitia and media or complete loss of tissue integrity (Fig. 3D). However, if the media and adventitia are intact, the presence of extraneous tissue will not affect the quantification, and hence preprocessing is not necessary (Fig. S3).

After preprocessing as necessary, we compared the workflow and the results obtained from automated measurements with manual measurements using Adobe Photoshop (Fig. 4A). To obtain the pixel distribution in adventitia and media separately by manual measurement, a user took an average of 4 min per image to define the ROI without quantifying the collagen. The manually defined ROI was then imported into MATLAB to locally quantify the collagen. On the contrary, the program can process the images in a matter of seconds and offers consistent measurements between samples. After preprocessing, the non-ideal cases produced results identical to that of ideal cases. The results obtained from the automated algorithm were virtually identical to those obtained by manual measurements at lower collagen levels, although at higher collagen levels, the manual measurements consistently overpredicts the collagen distribution. The reason is that the

automated algorithm can work inherently much easier as the analysis is done on a pixel-by-pixel basis when compared with a human which is inherently much coarser, and this difference is exemplified in Fig. 4B. As the ROI is being defined by the stark contrast between the coloration in the layers, it is highly dependent on the ability to distinguish between the layers. When doing manual analysis, any number of factors can lead to inaccuracies such as the steadiness or fatigue of the hand, the accuracy and resolution of the mouse/trackpad itself, and the amount of time necessary to achieve the same kind of outline that is supplied by the program. In contrast, as the automated algorithm operates on a rigid set of rules, it is an ideal method for consistent demarcation between layers. For instance, in Fig. 4B, the number of pixels for the segment shown was determined to be 15,406 pixels out of the 219,375 pixels of the entire sample. The errors made using the manual method lead to an over-measurement of 565 pixels, shown in green.

In summary, we have developed an automated algorithm for efficient, reliable, and rapid estimation of collagen content in the various regions of the aortic sections. This algorithm will enable comprehensive analyses of localized matrix remodeling in aortic sections that are routinely processed for insights into the mechanisms and functional consequences. Furthermore, our algorithm may be easily adapted for the histopathological analysis of non-homogeneously distributed fibrosis typical of myocardial infarction and other connective tissue disorders.

Competing Interests

The author(s) declared no potential conflicts of interest with respect to the research, authorship, and/or publication of this article.

Author Contributions

DMN developed the algorithm and wrote the code, MUW, DM, and MA obtained and stained aortic sections, DMN, MUW, PST, and AKR designed the study, analyzed the data, and wrote the manuscript. All authors have read and approved the final manuscript.

Funding

The author(s) disclosed receipt of the following financial support for the research, authorship, and/or publication of this article: This work was supported by research grants from the National Institute of Health (R01 HL122939 and R56 HL135654) and the Department of Veterans Affairs (1I01BX002641-01A) to PST.

ORCID iD

Dustin M. Nguyen https://orcid.org/0000-0001-6715-4627

Literature Cited

1. Cavalcante JL, Lima JAC, Redheuil A, Al-Mallah MH. Aortic stiffness: current understanding and future directions. J Am Coll Cardiol. 2011;57(14):1511–22. doi:10.1016/j.jacc.2010.12.017.
2. Tsamis A, Krawiec JT, Vorp DA. Elastin and collagen fibre microstructure of the human aorta in ageing and disease: a review. J R Soc Interface. 2013;10(83):20121004. doi:10.1098/rsif.2012.1004.
3. Restrepo C, Strong JP, Guzmán MA, Tejada C. Geographic comparisons of diffuse intimal thickening of the aorta. Atherosclerosis. 1979;32:177–93.
4. Rosero EB, Peshock RM, Khera A, Clagett P, Lo H, Timaran CH. Sex, race, and age distributions of mean aortic wall thickness in a multiethnic population-based sample. J Vasc Surg. 2011;53:950–7.
5. Wagenseil JE, Mecham RP. Vascular extracellular matrix and arterial mechanics. Physiol Rev. 2009;89(3):957–89. doi:10.1152/physrev.00041.2008.
6. Coats WD, Whittaker P, Cheung DT, Currier JW, Han B, Faxon DP. Collagen content is significantly lower in restenotic versus nonrestenotic vessels after balloon angioplasty in the atherosclerotic rabbit model. Circulation. 1997;95:1293–300.
7. Raaz U, Zöllner AM, Schellinger IN, Toh R, Nakagami F, Brandt M, Emrich FC, Kayama Y, Eken S, Adam M, Maegdefessel L, Hertel T, Deng A, Jagger A, Buerke M, Dalman RL, Spin JM, Kuhl E, Tsao PS. Segmental aortic stiffening contributes to experimental abdominal aortic aneurysm development. Circulation. 2015;131:1783–95.
8. Wegner KA, Keikhosravi A, Eliceiri KW, Vezina CM. Fluorescence of picrosirius red multiplexed with immunohistochemistry for the quantitative assessment of collagen in tissue sections. J Histochem Cytochem. 2017;65(8):479–90.
9. Vogel B, Siebert H, Hofmann U. Determination of collagen content within picrosirius red stained paraffin-embedded tissue sections using fluorescence microscopy. MethodsX. 2015;2:124–34.
10. Street JM, Souza ACP, Alvarez-Prats A, Horino T, Hu X, Yuen PST, Star RA. Automated quantification of renal fibrosis with Sirius Red and polarization contrast microscopy. Physiol Rep. 2014;2(7):e12088.
11. Bradley D, Roth G. Adaptive thresholding using the integral image. J Graph Tools. 2007;12:13–21.
12. Otsu N. A Threshold selection method from gray-level histograms. IEEE Trans Syst Man Cybern. 1979;9(1):62–6. http://ieeexplore.ieee.org/document/4310076/.
13. Rich L, Whittaker P. Collagen and picrosirius red staining : a polarized light assessment of fibrillar hue and spatial distribution. Braz J Morphol Sci. 2005;22(2):97–104. http://jms.org.br/PDF/v22n2a06.pdf.
14. Coleman R. Picrosirius red staining revisited. Acta Histochem. 2011;113(3):231–3.
15. Lattouf R, Younes R, Lutomski D, Naaman N, Godeau G, Senni K, Changotade S. Picrosirius red staining: a useful tool to appraise collagen networks in normal and pathological tissues. J Histochem Cytochem. 2014;62(10):751–8.

Systemic Upregulation of IL-10 (Interleukin-10) Using a Nonimmunogenic Vector Reduces Growth and Rate of Dissecting Abdominal Aortic Aneurysm

Matti Adam,* Nigel Geoffrey Kooreman,* Ann Jagger, Markus U. Wagenhäuser, Dennis Mehrkens, Yongming Wang, Yosuke Kayama, Kensuke Toyama, Uwe Raaz, Isabel N. Schellinger, Lars Maegdefessel, Joshua M. Spin, Jaap F. Hamming, Paul H.A. Quax, Stephan Baldus, Joseph C. Wu, Philip S. Tsao

Objective—Recruitment of immunologic competent cells to the vessel wall is a crucial step in formation of abdominal aortic aneurysms (AAA). Innate immunity effectors (eg, macrophages), as well as mediators of adaptive immunity (eg, T cells), orchestrate a local vascular inflammatory response. IL-10 (interleukin-10) is an immune-regulatory cytokine with a crucial role in suppression of inflammatory processes. We hypothesized that an increase in systemic IL-10-levels would mitigate AAA progression.

Approach and Results—Using a single intravenous injection protocol, we transfected an IL-10 transcribing nonimmunogenic minicircle vector into the Ang II (angiotensin II)-ApoE$^{-/-}$ infusion mouse model of AAA. IL-10 minicircle transfection significantly reduced average aortic diameter measured via ultrasound at day 28 from 166.1±10.8% (control) to 131.0±5.8% (IL-10 transfected). Rates of dissecting AAA were reduced by IL-10 treatment, with an increase in freedom from dissecting AAA from 21.5% to 62.3%. Using flow cytometry of aortic tissue from minicircle IL-10-treated animals, we found a significantly higher percentage of CD4$^+$/CD25$^+$/Foxp3 (forkhead box P3)$^+$ regulatory T cells, with fewer CD8$^+$/GZMB$^+$ (granzyme B) cytotoxic T cells. Furthermore, isolated aortic macrophages produced less TNF-α (tumor necrosis factor-α), more IL-10, and were more likely to be MRC1 (mannose receptor, C type 1)–positive alternatively activated macrophages. These results concurred with gene expression analysis of lipopolysaccharide-stimulated and Ang II-primed human peripheral blood mononuclear cells.

Conclusions—Taken together, we provide an effective gene therapy approach to AAA in mice by enhancing antiinflammatory and dampening proinflammatory pathways through minicircle-induced augmentation of systemic IL-10 expression.

Visual Overview—An online visual overview is available for this article. (***Arterioscler Thromb Vasc Biol*. 2018;38:1796-1805. DOI: 10.1161/ATVBAHA.117.310672.)

Key Words: aneurysm ■ cytokines ■ interleukin ■ macrophages ■ mannose receptor ■ transfection

Human abdominal aortic aneurysm (AAA) is defined as a pathological dilatation that exceeds the normal diameter by 50% or that has an antero-posterior diameter of >30 mm. AAAs are a significant cause of morbidity and mortality in the United States and worldwide. The average incidence in Western civilizations is 0.4% to 0.67%.[1] Although mortality numbers are slowly decreasing because of better endovascular and open surgical repair techniques as well as better risk factor management,[2] AAAs still accounted for up to 10 000 deaths per year in the United States in 2014 or ≈3.1 deaths per 100 000 people.[3]

Infiltration of monocytes/macrophages, polymorphonuclear leukocytes, and T and B lymphocytes mark the early phases of aneurysm development.[4] With further progression, a variety of cytokines, leukotrienes, and immunoglobulins attract additional inflammatory cells and establish a local vascular inflammatory response. Matrix degeneration with disruption of local collagen and elastin follows, accompanied by smooth muscle cell apoptosis in the aortic media, and ultimately leading to AAA expansion and rupture.[5,6]

With vascular inflammation being one of the major initial hallmarks of AAA formation, mechanisms that dampen the immune response might be leveraged to prevent progressive tissue damage. IL-10 (interleukin-10) is a well-described antiinflammatory cytokine, with a crucial role in suppression of inflammatory processes in diseases, such as environmental

Received on: November 25, 2015; final version accepted on: April 26, 2018.

From the Division of Cardiovascular Medicine, Cardiovascular Institute, Stanford University School of Medicine, CA (M.A., N.G.K., A.J., M.U.W., Y.W., Y.K., K.T., U.R., I.N.S., L.M., J.M.S., J.C.W., P.S.T.); Department of Cardiovascular Medicine, Cologne Cardiovascular Research Center, University of Cologne, University Heart Center, Germany (M.A., D.M., S.B.); VA Palo Alto Health Care System, CA (M.A., A.J., M.U.W., Y.K., K.T., U.R., I.N.S., J.M.S., P.S.T.); Department of Vascular Surgery, Leiden University Medical Center, The Netherlands (N.G.K., J.F.H., P.H.A.Q.); Heart Center, Georg-August-University Göttingen, Germany (U.R., I.N.S.); and Department of Medicine, Karolinska Institutet, Stockholm, Sweden (L.M.).

*These authors contributed equally to this article.

The online-only Data Supplement is available with this article at https://www.ahajournals.org/journal/atvb/doi/suppl/10.1161/atvbaha.118.310672.

Correspondence to Philip S. Tsao, PhD, Veterans Affairs Palo Alto Health Care System, 3801 Miranda Ave, Palo Alto, CA 94304. E-mail ptsao@stanford.edu or philip.tsao@va.gov

Nonstandard Abbreviations and Acronyms	
AAA	abdominal aortic aneurysm
Ang II	angiotensin II
CTL	cytotoxic T cell
FOXP3	forkhead box P3
GFP	green fluorescent protein
GZMB	granzyme B
IL	interleukin
MMP	matrix metallopeptidase
MRC1	mannose receptor, C type 1
PBMC	peripheral blood mononuclear cell
PCR	polymerase chain reaction
TNF-α	tumor necrosis factor-α
T_{reg}	regulatory T cell

allergy, asthma, or inflammatory bowel disease. There is evidence that the immune-regulatory capacities of IL-10 might also be crucial in aneurysm development, as the IL-10–1082 A polymorphism (associated with lower IL-10 production[7]) is more common in patients with AAA,[8] and patients with this polymorphism are at an increased risk of developing AAA.[9] IL-10 plasma concentrations in patients with AAA are significantly decreased compared with matched patients with coronary artery disease.[10] Also, IL-10-knockout mice show increased susceptibility to Ang II (angiotensin II)-induced aortic aneurysm and aortic rupture.[11] To our knowledge, no studies have to-date been conducted utilizing transgenic IL-10 animals.

IL-10 treatment has already been successfully performed in inflammatory bowel disease and glomerulosclerosis in rodents. However, recent studies have encountered major pitfalls. Intravenous or intraperitoneal injections of recombinant IL-10 need to be performed close to the time point of disease induction, or be repeated daily, because of IL-10's short plasma half-life.[12–14] In humans, outcomes in the treatment of inflammatory bowel disease did not demonstrate efficacy.[15] Although disease-specific reasons for these limited results may exist, 1 major drawback is the lack of sufficient IL-10 bioavailability at the tissue of interest.[16]

To increase IL-10 bioavailability and to overcome IL-10 delivery issues, here we applied a nonviral minicircle transfection approach to the Ang II infusion-ApoE$^{-/-}$ AAA model.

Minicircles are episomal DNA vectors lacking a bacterial plasmid backbone. Because of their small size compared with standard plasmids, they display higher transfection efficiency and survival rate of the target cells. In addition, minicircle constructs sustain a higher expression rate of their harboring transgenes over a longer period of time. This, combined with their low immunogenicity, makes them intriguing vectors for gene therapy.[17–19]

Materials and Methods

The data that support the findings of this study are available from the corresponding author on reasonable request.

Mouse Model

B6.129P2-*Apoetm1Unc*/J male mice (ApoE$^{-/-}$) were transfected via intravenous injection of 25 µg minicircle into the retro-orbital venous plexus at a concentration of 25 µg/100 µL containing either a transgenic transcript for murine IL-10 or GFP (green fluorescent protein; control). Minicircle GFP was chosen as a control vector against minicircle IL-10 to adjust for the effects of actual translation of proteins from minicircle DNA to protein in transfected cells. Based on this approach, the experiment was performed as shown in Figure I in the online-only Data Supplement, showing that minicircle GFP did not alter aneurysm formation unexpectedly and randomly compared with Ang II+PBS treatment alone.

Seven days after transfection, aortic aneurysm formation was induced using continuous subcutaneous Ang II infusion. Osmotic pumps (model 2004, Alzet) containing either Ang II (1 µg/kg per minute; Sigma-Aldrich) or saline were implanted in ApoE$^{-/-}$ male mice (C57BL/6J background) as previously described.[20] Pump implantation occurred at 3 to 6 months of age (mean age, 168±7.6 days, total n=78), mice were age-matched before starting the experiment.

Suprarenal aortic diameter was followed via ultrasound measurements on a VisualSonics Vevo2100 for 28 days as previously described[21–23] and validated.[24] Diameter was assessed using the leading edge-to-leading edge method.[25] Lesions were classified as dissecting AAA if intramural hematoma was visible by ultrasound, by histology or at necropsy.

Bioluminescence imaging was performed with the Xenogen In Vivo Imaging System on days 1, 3, 9, and 15 after transfection. D-Luciferin (Promega) was administered intraperitoneally at a dose of 375 mg/kg of body weight.

Murine plasma was collected with a standardized method via mandibular vein and centrifuged at 15 minutes at 3000 rpm at 4°C. ELISA for IL-10 was performed according to the manufacturer's instructions (Quantikine ELISA Mouse IL-10 Immunoassay).

Construction and Amplification of Minicircle-IL-10 Plasmids

For minicircle amplification, a single colony *Escherichia coli* was grown at 37°C overnight and subsequently spun down. The pellet was redissolved with broth (pH 7.0) containing 1% L-(+)-arabinose and incubated at 30°C for 2 hours. Minicircle constructs were isolated from the culture using plasmid purification kits (Qiagen, Venlo, The Netherlands). Primers (cactagtcgcgcccggggag/gacccatgggggcccgcc) were used to polymerase chain reaction (PCR) minicircle DNA with attB/attP elements and obtain DNA fragment A. The cytomegalovirus promoter, multiple cloning site, and poly A elements were PCR-amplified from pcDNA3.1/zeo(+) (Invitrogen) with primers aattgcatgaagaatctgct/ctggttctttccgcctcaga to obtain DNA fragment B. Ligation of DNA fragment A and DNA fragment B resulted in vector C. The IL-10 coding sequence was synthesized and subcloned into the KpnI/XhoI site of vector C, resulting in pMC-IL10. For detailed methods, please see Huang et al[18] and Figure V in the online-only Data Supplement.

Similar minicircles bearing transcripts for GFP and firefly luciferase were used for control purposes.[26]

Tissue Harvesting

Mice were euthanized with an inhalation overdose of isoflurane (Vet One). Aortas were immediately flushed via the left ventricle with ice-cold PBS and then dissected from fat and connective tissue from the renal arteries to the diaphragm (via Microscope, Leica). Specimens were snap-frozen in liquid nitrogen and stored at −80°C.

Histological Staining

Histological staining after harvesting was performed in the correlating suprarenal region of the AAA. Using already evaluated techniques,[24] aortic tissue was cut in 7-µm-thick serial sections and subsequently stained with hematoxylin and eosin (Sigma-Aldrich) and Picrosirius red (Sigma-Aldrich) according to standard protocols. All histological analyses were obtained at room temperature using a Keyence BZ-9000 microscope with BZ2 Analyzer software.

a firefly luciferase reporter construct (minicircle-Luc). Minicircle-Luc was injected and subsequent bioluminescence imaging was performed at days 1, 3, 9, and 15. We found a noticeable increase in luciferase activity in regions corresponding to the lungs at 1 to 3 days after transfection, with increasing activity in the liver and kidney regions over the course of the first 9 days (Figure 1A). By 15 days after transfection, the luciferase signal had significantly dropped, indicating a considerable loss of activity (Figure 1B).

Ang II treatment began at day 7 after minicircle transfection, to ensure active vector expression during aneurysm induction. We also evaluated IL-10 plasma levels of mice at 7 and 14 days after injection with minicircle IL-10 or minicircle control, confirming expression and production of IL-10 in a similar fashion to minicircle-Luc. We found a significant increase in plasma IL-10 levels in minicircle IL-10-treated mice (versus matched controls) at day 7 after transfection (161.3±14.6 versus 55.5±15.4 pg/mL; $P<0.01$; n=5; Figure 1C). At day 14 after minicircle injection, no differences could be found for IL-10 expression in minicircle IL-10 versus minicircle control (46.8±13.4 versus 36.8±10.6 pg/mL; P=ns; n=4/5). To further evaluate the long-term effects of minicircle IL-10 injection on tissue levels of IL-10, expression in peripheral tissues were quantified with quantitative real time-PCR at day 28 after Ang II infusion. Here, IL-10 did not show significantly higher expression in aortic tissue, lung tissue, or hepatic tissue in comparison with minicircle control (Figure 1D). Interestingly, however, splenic IL-10 expression was significantly higher in minicircle IL-10 than in controls (2.52±0.5-fold increase versus minicircle control; $P<0.01$; n=10). This was accompanied by higher splenic Foxp3 expression at day 28 after Ang II (1.9±0.3-fold; $P<0.05$; n=10; Figure 1E) but not increased TNF levels.

Subcutaneous Ang II pump implantation at day 7 after transfection led to significant suprarenal aortic aneurysm formation in ApoE$^{-/-}$ mice as previously described,[20] with 78% of the mice having a diameter of >150% of baseline in the control group. Aneurysm formation was attenuated in mice that had been injected with minicircle IL-10, as only 10% of these animals had a diameter increase of ≥150% (average diameter, 166.1±10.8% in control versus 131.0±5.8% in IL-10 treated animals; $P<0.01$; n=9 versus 10; Figure 2A). Differences in diameter remained throughout the time course of aneurysm formation, starting at day 7 (Figure 2A). These findings were supported by H&E and Picrosirius Red stainings, which showed a relevant decrease in AAA diameter after minicircle IL-10 treatment (Figure 2B).

In the murine ApoE$^{-/-}$ Ang II infusion AAA model, aneurysm formation is typically driven by intramural hematoma or myointimal dissection of the aortic wall. Therefore, in addition to aneurysm size, the presence of a dissecting AAA is an important aspect of AAA formation.[28] In concert with the significantly decreased diameter after minicircle IL-10 treatment, we found improved dissecting AAA-free survival in animals transfected with the IL-10 vector (21.5% versus 62.3% at day 28 in Ang II versus Ang II minicircle-IL-10; P=0.01; n=41; Figure 2C).

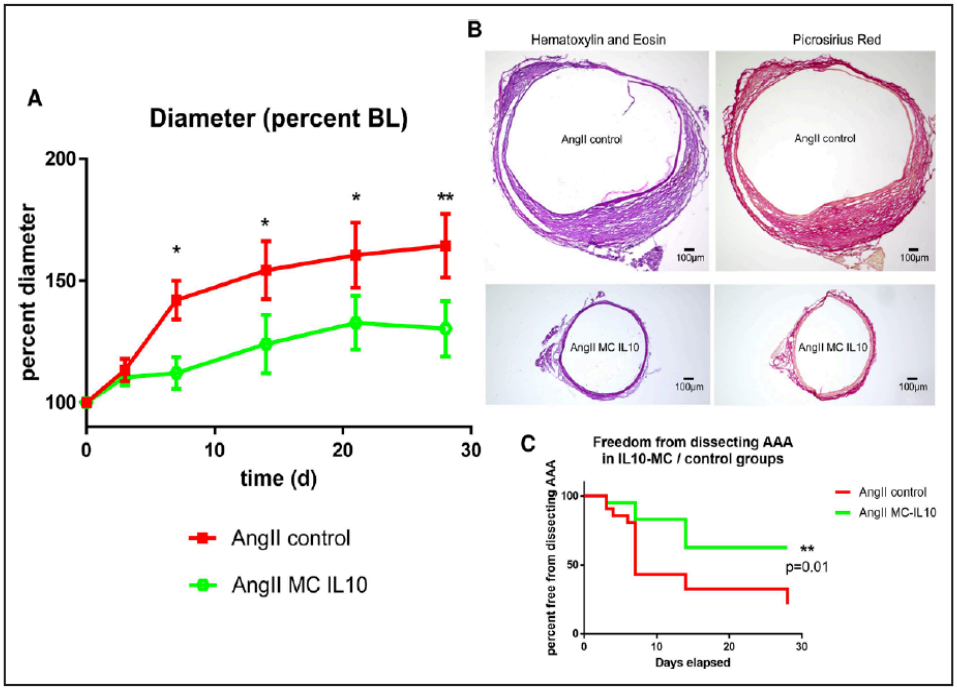

Figure 2. Aortic diameter and rate of dissecting abdominal aortic aneurysms (AAAs) after minicircle (MC) IL-10 (interleukin-10) transfection. Ultrasound measurements of ApoE$^{-/-}$ mice after subcutaneous infusion of Ang II (angiotensin II; 1 µg/kg per minute). **A**, Aortic diameter in percent of baseline diameter over a time course of 28 d; n=15 vs 15, *=P≤0.05, **=P≤0.01 vs Ang II MC control. **B**, Representative H&E and Picrosirius Red staining of suprarenal aortic sections harvested day 28 after Ang II infusion. **C**, Kaplan-Meier curve for freedom from dissecting AAA; n=15 vs 15, **P≤0.01 vs Ang II MC control.

Next, we evaluated the number and polarization of CD45+/CD3+ lymphocytes and F4/80+ macrophages in suprarenal aortic tissue 7 days after aneurysm induction via flow cytometry. Ang II minicircle IL-10–treated animals showed a significantly higher percentage of regulatory T cells (T_{reg} cells) than Ang II control or non–Ang II-treated animals (CD4+/CD25+/Foxp3+, 1.8±0.1% of CD45+/CD3+ versus 0.6±0.08% in Ang II control versus 0.7±0.05% in non–Ang II-treated animals; P<0.01 versus Ang II control and non-Ang II, n=5/6/5 per group; Figure 3A). In contrast, Ang II-control–treated animals had an increased percentage of cytotoxic T cells (CTL) compared with Ang II minicircle IL-10 or non–Ang II-treated mice (CD8+/GZMB+, 3.9±0.2% of CD45+/CD3+ versus 2.3±0.3% in Ang II control and 2.6±0.3% in non-Ang II; P<0.01 versus Ang II minicircle IL-10 and non-Ang II, n= 6/5/5 per group; Figure 3B). As a result, the T_{reg} cell to cytotoxic T-cell ratio (CD4+/CD25+/FOXP3+ per CD8+/GZMB+) was highly and significantly increased in the Ang II minicircle IL-10–treated animals (Figure 3C).

We did not find a significant difference in absolute cell number in aortic tissue (CD4+ or CD8+ or CD3+/CD45+ or F4/80+ cells of single cells) between the 3 experimental groups, indicating that there was a difference in cell polarization, rather than cell number (Figure II in the online-only Data Supplement).

Peripheral blood quantification did not reveal significant differences in T-cell polarization on T_{reg} and CTLs. CD4+ cells were significantly more present in peripheral blood in Ang II-treated animals, independent of minicircle IL-10 treatment (CD4+ of single cells, 2.2±0.3% in non–Ang II-treated animals versus 3.5±0.4% in Ang II control versus 3.7±0.4% in Ang II minicircle IL-10; P<0.01 versus non-Ang II, n=5/6/5 per group; Figure IIID in the online-only Data Supplement).

F4/80-positive macrophages in suprarenal aortic tissue were more prone to TNF-α production (38.6±5.3% of F4/80+ cells) without minicircle IL-10 application than after transfection with IL-10 (20.0±3% of F4/80+; P<0.05; n=4/5/4 per group; Figure 4A) and also showed decreased IL-10 signal (3.9±0.5% of F4/80+ cells versus 8.6±1.6% of F4/80+ cells; P<0.01 versus Ang II control; n=4/5/4 per group; Figure 4B). Notably, the increased TNF-α/IL-10 ratio in Ang II-treated control animals was reversed with IL-10 transfection (Figure 4C). Intriguingly, suprarenal aortic macrophages showed increased differentiation into the more antiinflammatory M2-like phenotype with minicircle IL-10 treatment (19.4±1.2% of MRC1+ over F4/80+ cells versus 11.6±1.9% in Ang II control; P<0.05 versus control; n=4/5/4 per group; Figure 4D).

To further investigate translational potential in human cells, we primed human PBMCs with Ang II or Ang II/IL-10 before stimulation with lipopolysaccharides and evaluated expression of inflammatory markers. There was a significant reduction in inflammatory gene expression with Ang II/IL-10 versus Ang II alone for all markers except *FOXP3* (0.07±0.01

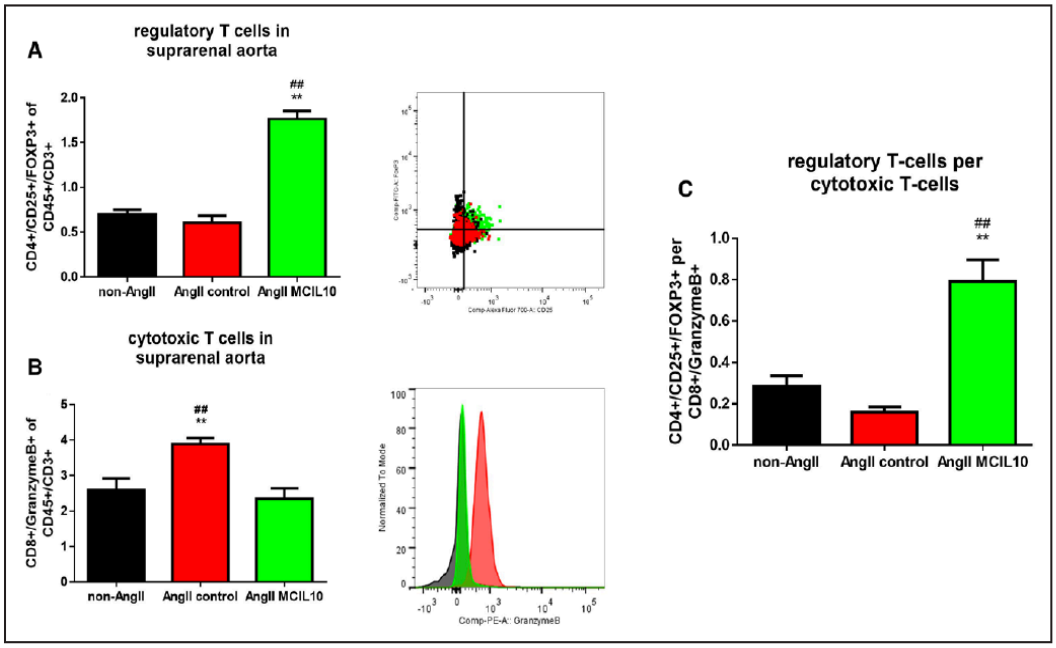

Figure 3. T-lymphocyte presence and differentiation in aortic tissue. At day 7 after aneurysm induction (day 14 after transfection with minicircle [MC]), aortic tissue was harvested, lysed, and analyzed via flow cytometry to characterize T-cell differentiation. **A** and **B** include representative flow cytometry graphs and histograms; n=4/5/4; n=5/6/5. **A**, Percentage of CD4+/CD25+/Foxp3 (forkhead box P3) of CD45+/CD3+ cells in untreated animals, Ang II (angiotensin II)-infused controls and Ang II-infused/MC-IL-10 (interleukin-10) transfected animals; **P≤0.01 vs Ang II, ##P≤0.01 vs untreated. **B**, Percentage of CD8+/GZMB+ (granzyme B) of CD45+/CD3+ cells; **P≤0.01 vs Ang II MC IL-10, ##P≤0.01 vs untreated. **C**, Ratio of CD4+/CD25+/Foxp3 over CD8+/GZMB+ cell (T_{reg} to cytotoxic T-cell ratio), **P≤0.01 vs Ang II, ##P≤0.01 vs untreated. MRC indicates mannose receptor, C type 1.

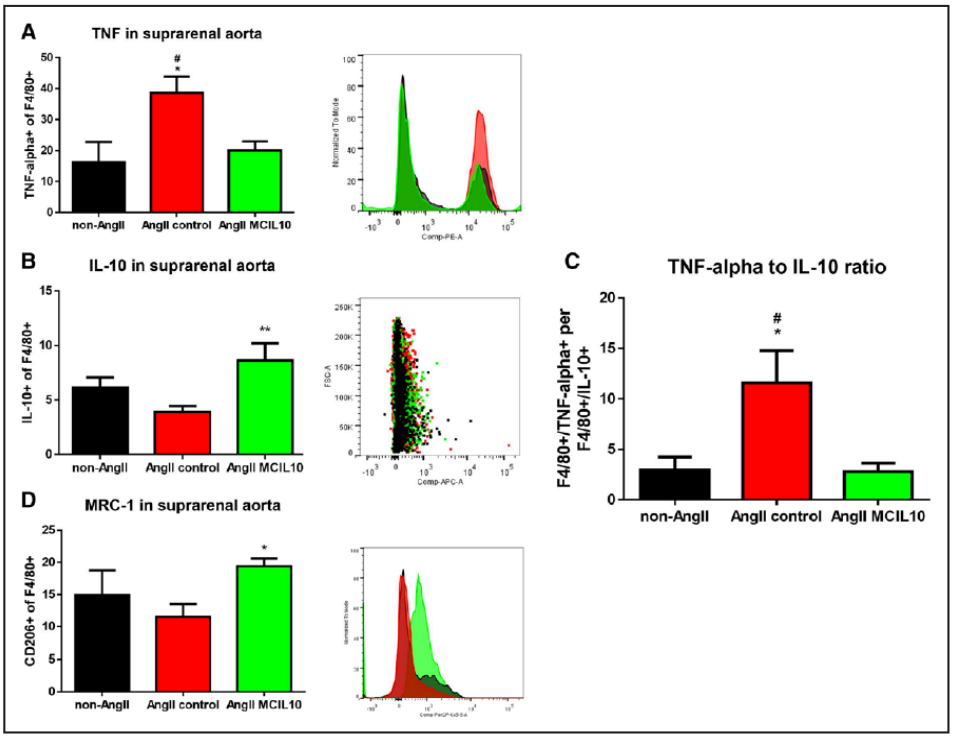

Figure 4. Macrophage presence and differentiation in aortic tissue. At day 7 after aneurysm induction (day 14 after transfection with minicircle [MC]), aortic tissue was harvested, lysed, and analyzed via flow cytometry to characterize macrophage differentiation markers. **A**, **B**, and **D** include representative flow cytometry graphs and histograms; n=4/5/4. **A**, Percentage of TNF-α (tumor necrosis factor-α)+ of F4/80⁺ cells in untreated, Ang II (angiotensin II)-infused, and Ang II-infused/MC-IL-10 (interleukin-10)-transfected animals; *P≤0.05 vs Ang II MC-IL-10, #P≤0.05 vs untreated. **B**, Percentage of IL-10⁺ of F4/80⁺ cells; **P≤0.01 vs Ang II. **C**, Ratio of TNF-α⁺ over IL-10⁺ cells; *P≤0.05 vs Ang II MC-IL-10, #P≤0.05 vs untreated. **D**, Percentage of MRC1 (mannose receptor, C type 1)+ of F4/80⁺ cells; *P≤0.05 vs Ang II.

versus 0.31±0.05 versus 0.19±0.04 relative expression versus GAPDH in cells not primed with Ang II versus Ang II primed cells versus Ang II/IL-10–treated cells; P=0.07 versus (+) Ang II, n=9/18/19; Figure 5A). *GZMB* expression was lower in Ang II/IL-10–treated cells (0.19±0.05 versus 0.2±0.02 versus 0.14±0.01 relative expression versus GAPDH in cells with (−) Ang II versus (+) Ang II versus (+) Ang II/IL-10; P<0.05 versus (+) Ang II, n=9/18/19; Figure 5B), resulting in no significant change of *FOXP3* to *GZMB* ratio in Ang II (+) versus Ang II (+)/IL-10 (0.47±0.1 versus 1.55±0.25 versus 1.48±0.3-fold, P=ns versus (+) Ang II, n=9/18/19; Figure 5C).

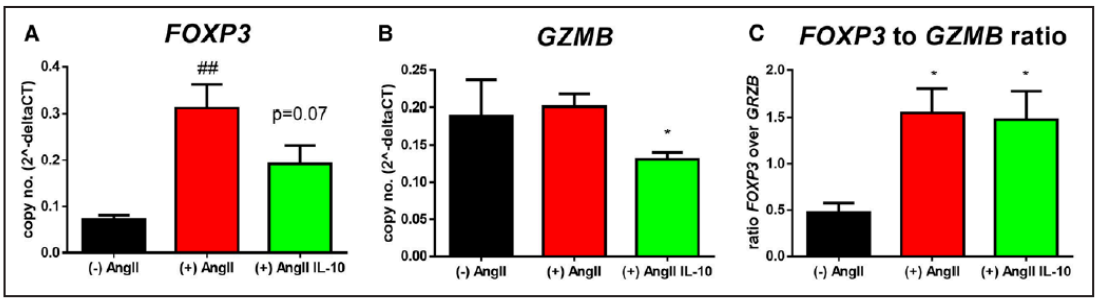

Figure 5. T-lymphocyte differentiation in human peripheral blood mononuclear cells (PBMCs) after Ang II (angiotensin II) priming and stimulation. Human PBMCs were isolated and primed with Ang II or Ang II/IL-10 (interleukin-10) for 24 h before cells were activated with lipopolysaccharides (24 h) to further evaluate gene expression of T-cell characterizing markers; n=9/18/19. **A**, Relative expression of FOXP3 (forkhead box P3) over GAPDH in unprimed, Ang II primed, and Ang II/IL-10 primed PBMCs; ##P≤0.01 vs untreated; P=0.07 in Ang II IL-10 vs Ang II. **B**, Relative expression of GZMB (granzyme B) in unprimed, Ang II, Ang II/IL-10 PBMCs; *P≤0.05 vs Ang II. **C**, Ratio (relative expression) of FOXP3 over GZMB; *P≤0.05 vs Ang II.

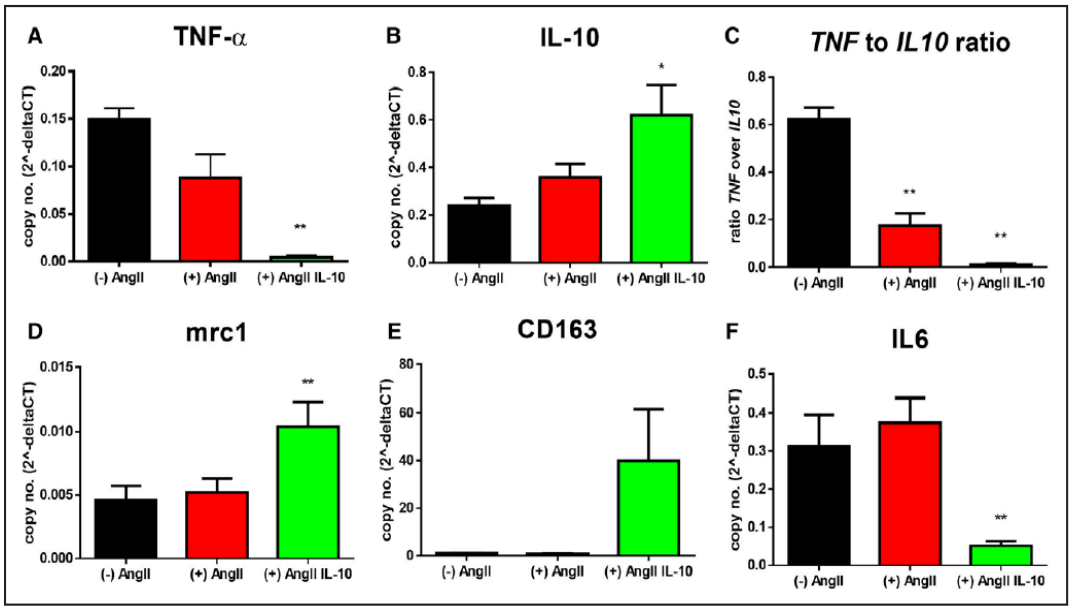

Figure 6. Macrophage differentiation in human peripheral blood mononuclear cells (PBMCs) after Ang II (angiotensin II) priming and stimulation. Human PBMCs were isolated and primed with Ang II or Ang II/IL-10 (interleukin-10) for 24 h before cells were activated with lipopolysaccharides (24 h) to further evaluate macrophage activation (n=9/18/19). **A**, Relative expression of TNF-α (tumor necrosis factor-α) over GAPDH in unprimed, Ang II primed, and Ang II/IL-10 primed PBMCs; ***P*≤0.01 vs Ang II. **B**, Relative expression of IL-10 in unprimed, Ang II, and Ang II/IL-10 PBMCs; **P*≤0.05 vs Ang II. **C**, Ratio (relative expression) of TNF over IL-10; ***P*≤0.01 vs Ang II, ##*P*≤0.01 vs unprimed. **D**, Relative expression of MRC1 (mannose receptor, C type 1) in unprimed, Ang II, and Ang II/IL-10 PBMCs; ***P*≤0.01 vs Ang II. **E**, Relative expression of CD163 in unprimed, Ang II, and Ang II/IL-10 PBMCs; ***P*≤0.01 vs Ang II. **F**, Relative expression of IL-6 in unprimed, Ang II, and Ang II/IL-10 PBMCs; ***P*≤0.01 vs Ang II.

Looking at macrophage markers revealed beneficial effects for (+) Ang II/IL-10 versus (+) Ang II alone. TNF-α (TNF) expression dropped significantly with minicircle IL-10 treatment (0.15±0.01 versus 0.09±0.03 versus 0.004±0.002; *P*<0.05 versus (+) Ang II, n=9/18/19; Figure 6A). IL-10 expression was increased in (+) Ang II/IL-10 (0.24±0.03 versus 0.36±0.06 versus 0.62±0.12; *P*<0.05 versus (+) Ang II, n=9/15/11; Figure 6B), resulting overall in a significantly decreased TNF-α-to-IL-10 ratio (0.62±0.05 versus 0.18±0.07 versus 0.01±0.01; *P*<0.01 versus (+) Ang II and versus (−) Ang II, n=6/14/11; Figure 6C). Markers of alternatively activated M2-macrophages, such as MRC1 (0.005±0.001 versus 0.005±0.001 versus 0.01±0.002; *P*<0.05 versus (+) Ang II, n=9/15/17; Figure 6D) and CD163 (1.04±0.16 versus 0.8±0.09 versus 39.92±21.79; *P*<0.01 versus (+) Ang II, n=9/18/11; Figure 6E), were significantly upregulated. Conversely, IL-6 expression was reduced in cells that were treated with IL-10 (0.32±0.08 versus 0.37±0.06 versus 0.05±0.01; *P*<0.01 versus (+) Ang II and versus (−) Ang II, n=6/15/14; Figure 6F).

Discussion

Here, we show that systemic transfection with a nonimmunogenic delivery method using IL-10 expressing minicircles is feasible and effective in a murine model of AAA disease. Plasma IL-10 levels were significantly increased at 1 week after transfection in ApoE$^{-/-}$ mice, and IL-10 induction significantly decreased aneurysm size and likelihood of suprarenal dissecting AAA formation. These beneficial effects on aneurysm development were accompanied by a significant increase in T_{reg} cells and a decrease in CTLs. Furthermore, local macrophages were more likely to differentiate into the alternatively activated M2-macrophages and express less TNF-α as well as more IL-10. Human PBMCs with IL-10 treatment after Ang II incubation showed ameliorated expression of differentiation markers GZMB, TNF-α, MRC1, CD163, and IL-6, indicating possible translational potential in the application of IL-10.

One major IL-10–induced antiinflammatory process in tissue is the induction of CD4$^+$CD25$^+$FOXP3$^+$$T_{reg}$ cells.[29] In general, their mechanism of action also involves production of IL-10 itself,[29,30] providing a self-amplifying feedback loop, which we also identified. The induction of a subset of more antiinflammatory macrophages by T_{reg} cells,[31] particularly the so-called deactivated M2c-macrophages which are thought to be important for tissue remodeling and matrix deposition, is also regulated by IL-10.[32,33] In AAA disease, M2-macrophages are present in the later phases of development[34] and are involved in healing and prevention of further AAA growth. By contrast, activation and clonal expansion of CD8$^+$ CTLs induces cell damage and apoptosis potentially worsening AAA disease, if not properly regulated.[35,36] Because IL-10 has been shown to contribute to CD8$^+$ CTL expansion under certain conditions, we monitored the CD8$^+$ GZMB$^+$ CTL amount in tissue and calculated the ratio of T_{reg}/CTL ratio to further characterize the impact of IL-10 on the T-cell population in the aortic wall.

Using the Ang II-induced AAA model, we observed that systemic overexpression of IL-10 via single timepoint minicircle transfection led to aortic cell polarization into T_{reg} cells and antiinflammatory M2-macrophages expressing MRC1. These changes in adaptive and innate immune cell differentiation were associated with a clear reduction in aneurysm formation. We did not find a significant change in $CD3^+$/$CD45^+$, $CD4^+$, $CD8^+$ or macrophage cell number in aortic tissue after minicircle injection. Therefore, our results suggest a polarization effect, rather than a recruitment. Considering the limited expression period of the minicircle-delivered plasmids of, at most, 2 weeks with regard to IL-10 plasma levels (when compared with the 4-week period of aneurysm development), it could be that this treatment might have sparked self-amplifying cascades and cell-cell interactions that maintain the antiinflammatory response. At 28 days after aneurysm induction, only splenic tissue showed increased expression of IL-10 (Figure 1D). This was accompanied by higher Foxp3 expression, possibly indicating pronounced T_{reg} polarization (Figure 1E). This is especially intriguing because flow cytometry analysis of spleens at day 7 after Ang II showed significantly fewer $CD4^+$ cells and a tendency toward fewer Foxp3-positive T_{reg} cells (Figure IVA and IVD in the online-only Data Supplement). This might indicate an initial mobilization of $CD4^+$ cells from the spleen in response to Ang II, a redistribution process to nonlymphoid tissue known to occur after recognition of certain antigens.[37] Subsequently, splenic IL-10 and Foxp3 expression might increase again over the next 3 weeks if minicircle IL-10 expression had successfully induced antiinflammatory processes in the aorta.

In patients with AAA, both the number and function of T_{reg} cells as well as the expression of FOXP3 are significantly decreased in peripheral blood,[38,39] suggesting that the lack of T_{reg} immunomodulation may accelerate AAA formation. Indeed, adoptive transfer of T_{reg} cells to Ang II-treated $ApoE^{-/-}$ mice reduced AAA incidence and severity in a dose-dependent manner.[40] Furthermore, direct treatment with T_{reg} cells decreased macrophage number and the expression of proinflammatory cytokines in local aortic tissue. After T_{reg} treatment in vitro, macrophages had a more pronounced M2-like phenotype, consistent with previous reports.[31,33] As such, the beneficial effects of T_{reg} cells are likely mediated via direct cell-cell contact as well as paracrine effects.

Yodoi et al[41] demonstrated that the expansion of $Foxp3^+$ T_{reg} cells by IL-2 complex treatment resulted in a marked decrease in the incidence and mortality of AAA, and that this effect could be reversed by genetic depletion of $Foxp3^+$ T_{reg} cells, further underlining the importance of T_{reg} cells in the prevention of aneurysm disease. Moreover, Zhou et al[39] further clarified the importance of IL-10 in mediating the beneficial effects of T_{reg} cells in AAA formation. Transfusion of T_{reg} cells from wild-type animals suppressed macrophage activation and reduced lesion macrophage and T-cell counts in the murine Ang II AAA model. However, this was not the case in mice that were infused with T_{reg} cells from $IL\text{-}10^{-/-}$ animals, suggesting that the presence of IL-10 is imperative for cell-cell interaction of T_{reg} cells with the surrounding tissue. IL-10 has also been shown to be a crucial regulator of inflammation-matrix interaction because T_{reg} cells from IL-10 competent mice suppress MMP-9 (matrix metallopeptidase 9) and MMP-13 activity more strongly than T_{reg} cells from $IL\text{-}10^{-/-}$ mice.[39] Notably, $IL\text{-}10^{-/-}$ mice show increased elastin degradation[11] and, T_{reg} treatment inhibits apoptosis of aortic wall cells in the Ang II-induced aneurysm model.[40] Our data support a critical role for the mediator IL-10 in prevention of AAA formation and suggest that a transient increase in IL-10 might be sufficient to induce a critical mass of antiinflammatory T_{reg} cells and regulatory macrophages at the site of lesion, thereby possibly decreasing AAA growth by positively modulating the inflammatory response, with potential downstream effects on extracellular matrix degradation and apoptosis via IL-10.

Recent work highlights the special considerations that need to be taken into account on the role of aortic dissection in the Ang II AAA model.[28,42] Inflammatory cell infiltration tends to localize to sites of aortic dissection.[43] It is thought that classical activation of macrophages induces vascular dissection, thereby promoting AAA formation at least in part by an IL-6–dependent mechanism.[44] Our work suggests that readjusting the macrophage activation cascades using IL-10 treatment suppresses IL-6 as well as TNF-α expression and promotes MRC1 and CD163 transcription. The IL-10–induced increase in T_{reg} cells and the shift from classical to alternatively activated macrophages in aortic tissue is therefore likely to be an important mechanism in the prevention of dissecting AAA. We assume that our antiinflammatory treatment primarily suppresses both micro- and macro-ruptures because these hemorrhagic events are thought to drive AAA growth in the Ang II-model. This is further underscored by the early separation of our AAA diameter and dissecting AAA-free survival curves (Figure 2A and 2B) at day 7 with a subsequently similar growth rate.

In PBMCs from healthy controls stimulated with Ang II, we observed minimal impact on inflammatory gene expression in the absence of IL-10 treatment. Our cells of interest, mainly monocytes/macrophages and T cells, all express receptors for Ang II[41,45,46] and should therefore be susceptible to Ang II priming. However, effects of Ang II on leukocytes seem to be context-sensitive[45,47] and are difficult to duplicate in vitro.[48] We acknowledge that our understanding of Ang II-induced effects on mononuclear cells is not complete; nevertheless, IL-10 treatment was beneficial after PBMCs were primed with Ang II, supporting our main hypothesis that IL-10 initiates an antiinflammatory and self-amplifying polarization toward T_{reg} cells and M2-macrophages.

There are limitations to our study. We applied the minicircle IL-10 vector systemically, once, and did not seek to control the site of expression nor the effect duration. It is possible that observed effects might be even stronger and display less off-target impact if a more specific approach to the vasculature or immune cells had been chosen.[49,50] In addition, we cannot definitively conclude whether systemic or local increases of IL-10 are more important to prevent AAA formation because the cellular changes we induced in aortic tissue were observed after systemic IL-10 delivery with an initial increase of plasma IL-10. With regard to clinical applicability and the known methodological shortcomings of cell-specific transfections, we deliberately chose this approach, intending to maintain translational potential and seeking to prove that minicircles are feasible nonimmunogenic vectors for the treatment of

AAAs in this mouse model. We did not seek to provide deeper mechanistic insights because the interaction of IL-10 with lymphocytes and myeloid cells has been extensively studied before. Although we do not provide hemodynamic data (such as blood pressure) in these animals, and therefore cannot exclude differences in minicircle-IL-10–treated versus non–minicircle-IL-10–treated animals, a recent publication suggests no prognostic value of hemodynamic markers on aneurysm growth.[51] Also, initial characterization of the model did not show any alteration in arterial blood pressure after Ang II infusion.[20] The recently published prevention of blood pressure increase by continuous IL-10 infusion has only been shown in combination with significantly higher doses of Ang II (90 ng/min) and vastly higher IL-10 levels (0.5 ng/min) when compared with our plasma IL-10 concentration.[52]

In summary, we provide evidence that a one-time application of an IL-10 transcribing minicircle vector successfully limits aneurysm formation in a mouse model of AAA while increasing regulatory T cells and alternatively activated macrophages in the aortic wall. IL-10 treatment of PBMCs partially recapitulated the antiinflammatory effects of IL-10, indicating possible translational potential in humans.

Acknowledgments

We thank Mark Kay, Stanford University, Stanford, CA, for kindly providing the technical background on the MC technology.

Sources of Funding

This work was supported by research grants from the National Institutes of Health (R01 HL105299 and R01 HL122939 to P.S. Tsao, R01 AI085575 and R01 HL093172 to J.C. Wu), the Department of Veterans Affairs (1I01BX002641-01A to P.S. Tsao), the Deutsche Forschungsgemeinschaft (AD 492/1-1 to M. Adam, WA 3583/2-1 to M.U. Wagenhäuser, RA 2179/1-1 to U. Raaz), the Boehringer Ingelheim Fonds and the International Scholarship for Medical Students, Medical School of the University Erlangen, Germany (both to I.N. Schellinger), the Banyu Fellowship Program by Banyu Life Science Foundation International (to K. Toyama), and the Stanford Cardiovascular Institute (to J.M. Spin).

Disclosures

None.

References

1. Nordon IM, Hinchliffe RJ, Loftus IM, Thompson MM. Pathophysiology and epidemiology of abdominal aortic aneurysms. *Nat Rev Cardiol*. 2011;8:92–102. doi: 10.1038/nrcardio.2010.180.
2. Schermerhorn ML, Bensley RP, Giles KA, Hurks R, O'malley AJ, Cotterill P, Chaikof E, Landon BE. Changes in abdominal aortic aneurysm rupture and short-term mortality, 1995-2008: a retrospective observational study. *Ann Surg*. 2012;256:651–658. doi: 10.1097/SLA.0b013e31826b4f91.
3. CDC. Centers for disease control and prevention, National Center for Health Statistics. Underlying cause of death 1999–2015 on CDC wonder online database, released December, 2016. Data are from the multiple cause of death files, 1999–2015, as compiled from data provided by the 57 vital statistics jurisdictions through the vital statistics cooperative program. October 4, 2017. http://wonder.Cdc.Gov/ucd-icd10.Html.
4. Thomas M, Gavrila D, McCormick ML, Miller FJ Jr, Daugherty A, Cassis LA, Dellsperger KC, Weintraub NL. Deletion of p47phox attenuates angiotensin II-induced abdominal aortic aneurysm formation in apolipoprotein E-deficient mice. *Circulation*. 2006;114:404–413. doi: 10.1161/CIRCULATIONAHA.105.607168.
5. Kunieda T, Minamino T, Nishi J, Tateno K, Oyama T, Katsuno T, Miyauchi H, Orimo M, Okada S, Takamura M, Nagai T, Kaneko S, Komuro I. Angiotensin II induces premature senescence of vascular smooth muscle cells and accelerates the development of atherosclerosis via a p21-dependent pathway. *Circulation*. 2006;114:953–960. doi: 10.1161/CIRCULATIONAHA.106.626606.
6. Ailawadi G, Moehle CW, Pei H, Walton SP, Yang Z, Kron IL, Lau CL, Owens GK. Smooth muscle phenotypic modulation is an early event in aortic aneurysms. *J Thorac Cardiovasc Surg*. 2009;138:1392–1399. doi: 10.1016/j.jtcvs.2009.07.075.
7. Turner DM, Williams DM, Sankaran D, Lazarus M, Sinnott PJ, Hutchinson IV. An investigation of polymorphism in the interleukin-10 gene promoter. *Eur J Immunogenet*. 1997;24:1–8.
8. Bown MJ, Lloyd GM, Sandford RM, Thompson JR, London NJ, Samani NJ, Sayers RD. The interleukin-10-1082 'A' allele and abdominal aortic aneurysms. *J Vasc Surg*. 2007;46:687–693. doi: 10.1016/j.jvs.2007.06.025.
9. McColgan P, Peck GE, Greenhalgh RM, Sharma P. The genetics of abdominal aortic aneurysms: a comprehensive meta-analysis involving eight candidate genes in over 16,700 patients. *Int Surg*. 2009;94:350–358.
10. Kadoglou NP, Papadakis I, Moulakakis KG, Ikonomidis I, Alepaki M, Moustardas P, Lampropoulos S, Karakitsos P, Lekakis J, Liapis CD. Arterial stiffness and novel biomarkers in patients with abdominal aortic aneurysms. *Regul Pept*. 2012;179:50–54. doi: 10.1016/j.regpep.2012.08.014.
11. Ait-Oufella H, Wang Y, Herbin O, Bourcier S, Potteaux S, Joffre J, Loyer X, Ponnuswamy P, Esposito B, Dalloz M, Laurans L, Tedgui A, Mallat Z. Natural regulatory T cells limit angiotensin II-induced aneurysm formation and rupture in mice. *Arterioscler Thromb Vasc Biol*. 2013;33:2374–2379. doi: 10.1161/ATVBAHA.113.301280.
12. Grool TA, van Dullemen H, Meenan J, Koster F, ten Kate FJ, Lebeaut A, Tytgat GN, van Deventer SJ. Anti-inflammatory effect of interleukin-10 in rabbit immune complex-induced colitis. *Scand J Gastroenterol*. 1998;33:754–758.
13. Rachmawati H, Beljaars L, Reker-Smit C, Bakker HI, Van Loenen-Weemaes AM, Lub-De Hooge MN, Poelstra K. Intravenous administration of recombinant human IL-10 suppresses the development of anti-thy 1-induced glomerulosclerosis in rats. *PDA J Pharm Sci Technol*. 2011;65:116–130.
14. Duchmann R, Schmitt E, Knolle P, Meyer zum Büschenfelde KH, Neurath M. Tolerance towards resident intestinal flora in mice is abrogated in experimental colitis and restored by treatment with interleukin-10 or antibodies to interleukin-12. *Eur J Immunol*. 1996;26:934–938. doi: 10.1002/eji.1830260432.
15. Buruiana FE, Sola I, Alonso-Coello P. Recombinant human interleukin 10 for induction of remission in Crohn's disease. *Cochrane Database Syst Rev*. 2010;11:CD005109.
16. Marlow GJ, van Gent D, Ferguson LR. Why interleukin-10 supplementation does not work in Crohn's disease patients. *World J Gastroenterol*. 2013;19:3931–3941. doi: 10.3748/wjg.v19.i25.3931.
17. Chen ZY, Riu E, He CY, Xu H, Kay MA. Silencing of episomal transgene expression in liver by plasmid bacterial backbone DNA is independent of CpG methylation. *Mol Ther*. 2008;16:548–556. doi: 10.1038/sj.mt.6300399.
18. Huang M, Chen Z, Hu S, Jia F, Li Z, Hoyt G, Robbins RC, Kay MA, Wu JC. Novel minicircle vector for gene therapy in murine myocardial infarction. *Circulation*. 2009;120(11 suppl):S230–S237. doi: 10.1161/CIRCULATIONAHA.108.841155.
19. Lijkwan MA, Hellingman AA, Bos EJ, van der Bogt KE, Huang M, Kooreman NG, de Vries MR, Peters HA, Robbins RC, Hamming JF, Quax PH, Wu JC. Short hairpin RNA gene silencing of prolyl hydroxylase-2 with a minicircle vector improves neovascularization of hindlimb ischemia. *Hum Gene Ther*. 2014;25:41–49. doi: 10.1089/hum.2013.110.
20. Daugherty A, Manning MW, Cassis LA. Angiotensin II promotes atherosclerotic lesions and aneurysms in apolipoprotein E-deficient mice. *J Clin Invest*. 2000;105:1605–1612. doi: 10.1172/JCI7818.
21. Maegdefessel L, Azuma J, Toh R, Deng A, Merk DR, Raiesdana A, Leeper NJ, Raaz U, Schoelmerich AM, McConnell MV, Dalman RL, Spin JM, Tsao PS. MicroRNA-21 blocks abdominal aortic aneurysm development and nicotine-augmented expansion. *Sci Transl Med*. 2012;4:122ra22. doi: 10.1126/scitranslmed.3003441.
22. Maegdefessel L, Azuma J, Toh R, Merk DR, Deng A, Chin JT, Raaz U, Schoelmerich AM, Raiesdana A, Leeper NJ, McConnell MV, Dalman RL, Spin JM, Tsao PS. Inhibition of microRNA-29b reduces murine abdominal aortic aneurysm development. *J Clin Invest*. 2012;122:497–506. doi: 10.1172/JCI61598.
23. Maegdefessel L, Spin JM, Raaz U, et al. miR-24 limits aortic vascular inflammation and murine abdominal aneurysm development. *Nat Commun*. 2014;5:5214. doi: 10.1038/ncomms6214.

24. Azuma J, Maegdefessel L, Kitagawa T, Dalman RL, McConnell MV, Tsao PS. Assessment of elastase-induced murine abdominal aortic aneurysms: comparison of ultrasound imaging with in situ video microscopy. *J Biomed Biotechnol*. 2011;2011:252141. doi: 10.1155/2011/252141.
25. Gürtelschmid M, Björck M, Wanhainen A. Comparison of three ultrasound methods of measuring the diameter of the abdominal aorta. *Br J Surg*. 2014;101:633–636. doi: 10.1002/bjs.9463.
26. Jia F, Wilson KD, Sun N, Gupta DM, Huang M, Li Z, Panetta NJ, Chen ZY, Robbins RC, Kay MA, Longaker MT, Wu JC. A nonviral minicircle vector for deriving human iPS cells. *Nat Methods*. 2010;7:197–199. doi: 10.1038/nmeth.1426.
27. Motulsky HJ, Brown RE. Detecting outliers when fitting data with nonlinear regression - a new method based on robust nonlinear regression and the false discovery rate. *BMC Bioinformatics*. 2006;7:123. doi: 10.1186/1471-2105-7-123.
28. Trachet B, Fraga-Silva RA, Piersigilli A, Tedgui A, Sordet-Dessimoz J, Astolfo A, Van der Donckt C, Modregger P, Stampanoni MF, Segers P, Stergiopulos N. Dissecting abdominal aortic aneurysm in Ang II-infused mice: suprarenal branch ruptures and apparent luminal dilatation. *Cardiovasc Res*. 2015;105:213–222. doi: 10.1093/cvr/cvu257.
29. Saraiva M, O'Garra A. The regulation of IL-10 production by immune cells. *Nat Rev Immunol*. 2010;10:170–181. doi: 10.1038/nri2711.
30. Steinke JW, Lawrence MG. T-cell biology in immunotherapy. *Ann Allergy Asthma Immunol*. 2014;112:195–199. doi: 10.1016/j.anai.2013.12.020.
31. Tiemessen MM, Jagger AL, Evans HG, van Herwijnen MJC, John S, Taams LS. CD4+CD25+FOXp3+ regulatory T cells induce alternative activation of human monocytes/macrophages. *Proc Natl Acad Sci USA*. 2007;104:19446–19451.
32. Martinez FO, Gordon S. The M1 and M2 paradigm of macrophage activation: time for reassessment. *F1000Prime Rep*. 2014;6:13. doi: 10.12703/P6-13.
33. Liu G, Ma H, Qiu L, Li L, Cao Y, Ma J, Zhao Y. Phenotypic and functional switch of macrophages induced by regulatory CD4+CD25+ T cells in mice. *Immunol Cell Biol*. 2011;89:130–142. doi: 10.1038/icb.2010.70.
34. Rateri DL, Howatt DA, Moorleghen JJ, Charnigo R, Cassis LA, Daugherty A. Prolonged infusion of angiotensin II in apoE(-/-) mice promotes macrophage recruitment with continued expansion of abdominal aortic aneurysm. *Am J Pathol*. 2011;179:1542–1548. doi: 10.va1016/j.ajpath.2011.05.049.
35. Lindeman JH, Abdul-Hussien H, van Bockel JH, Wolterbeek R, Kleemann R. Clinical trial of doxycycline for matrix metalloproteinase-9 inhibition in patients with an abdominal aneurysm: doxycycline selectively depletes aortic wall neutrophils and cytotoxic T cells. *Circulation*. 2009;119:2209–2216. doi: 10.1161/CIRCULATIONAHA.108.806505.
36. Henderson EL, Geng YJ, Sukhova GK, Whittemore AD, Knox J, Libby P. Death of smooth muscle cells and expression of mediators of apoptosis by T lymphocytes in human abdominal aortic aneurysms. *Circulation*. 1999;99:96–104.
37. Bronte V, Pittet MJ. The spleen in local and systemic regulation of immunity. *Immunity*. 2013;39:806–818. doi: 10.1016/j.immuni.2013.10.010.
38. Yin M, Zhang J, Wang Y, Wang S, Böckler D, Duan Z, Xin S. Deficient CD4+CD25+ T regulatory cell function in patients with abdominal aortic aneurysms. *Arterioscler Thromb Vasc Biol*. 2010;30:1825–1831. doi: 10.1161/ATVBAHA.109.200303.
39. Zhou Y, Wu W, Lindholt JS, Sukhova GK, Libby P, Yu X, Shi GP. Regulatory T cells in human and angiotensin II-induced mouse abdominal aortic aneurysms. *Cardiovasc Res*. 2015;107:98–107. doi: 10.1093/cvr/cvv119.
40. Meng X, Yang J, Zhang K, An G, Kong J, Jiang F, Zhang Y, Zhang C. Regulatory T cells prevent angiotensin II-induced abdominal aortic aneurysm in apolipoprotein E knockout mice. *Hypertension*. 2014;64:875–882. doi: 10.1161/HYPERTENSIONAHA.114.03950.
41. Yodoi K, Yamashita T, Sasaki N, Kasahara K, Emoto T, Matsumoto T, Kita T, Sasaki Y, Mizoguchi T, Sparwasser T, Hirata K. Foxp3+ regulatory T cells play a protective role in angiotensin II-induced aortic aneurysm formation in mice. *Hypertension*. 2015;65:889–895. doi: 10.1161/HYPERTENSIONAHA.114.04934.
42. Saraff K, Babamusta F, Cassis LA, Daugherty A. Aortic dissection precedes formation of aneurysms and atherosclerosis in angiotensin II-infused, apolipoprotein E-deficient mice. *Arterioscler Thromb Vasc Biol*. 2003;23:1621–1626. doi: 10.1161/01.ATV.0000085631.76095.64.
43. Cao RY, Amand T, Ford MD, Piomelli U, Funk CD. The murine angiotensin II-induced abdominal aortic aneurysm model: rupture risk and inflammatory progression patterns. *Front Pharmacol*. 2010;1:9. doi: 10.3389/fphar.2010.00009.
44. Tieu BC, Lee C, Sun H, Lejeune W, Recinos A III, Ju X, Spratt H, Guo DC, Milewicz D, Tilton RG, Brasier AR. An adventitial IL-6/MCP1 amplification loop accelerates macrophage-mediated vascular inflammation leading to aortic dissection in mice. *J Clin Invest*. 2009;119:3637–3651. doi: 10.1172/JCI38308.
45. Yanagitani Y, Rakugi H, Okamura A, Moriguchi K, Takiuchi S, Ohishi M, Suzuki K, Higaki J, Ogihara T. Angiotensin II type 1 receptor-mediated peroxide production in human macrophages. *Hypertension*. 1999;33(1 pt 2):335–339.
46. Crowley SD, Song YS, Sprung G, Griffiths R, Sparks M, Yan M, Burchette JL, Howell DN, Lin EE, Okeiyi B, Stegbauer J, Yang Y, Tharaux PL, Ruiz P. A role for angiotensin II type 1 receptors on bone marrow-derived cells in the pathogenesis of angiotensin II-dependent hypertension. *Hypertension*. 2010;55:99–108. doi: 10.1161/HYPERTENSIONAHA.109.144964.
47. Crowley SD, Frey CW, Gould SK, Griffiths R, Ruiz P, Burchette JL, Howell DN, Makhanova N, Yan M, Kim HS, Tharaux PL, Coffman TM. Stimulation of lymphocyte responses by angiotensin II promotes kidney injury in hypertension. *Am J Physiol Renal Physiol*. 2008;295:F515–F524. doi: 10.1152/ajprenal.00527.2007.
48. Keidar S, Heinrich R, Kaplan M, Hayek T, Aviram M. Angiotensin II administration to atherosclerotic mice increases macrophage uptake of oxidized ldl: a possible role for interleukin-6. *Arterioscler Thromb Vasc Biol*. 2001;21:1464–1469.
49. Mayer CR, Geis NA, Katus HA, Bekeredjian R. Ultrasound targeted microbubble destruction for drug and gene delivery. *Expert Opin Drug Deliv*. 2008;5:1121–1138. doi: 10.1517/17425247.5.10.1121.
50. Sapet C, Laurent N, Bertosio E, Bertuzzi M, Sicard F. Targeted transfection of cells/tissue in vivo. *Protoc Exch*. June 8, 2012. doi:10.1038/protex.2012.025. https://www.nature.com/protocolexchange/protocols/2410#/.
51. Prins PA, Hill MF, Airey D, Nwosu S, Perati PR, Tavori H, F Linton M, Kon V, Fazio S, Sampson UK. Angiotensin-induced abdominal aortic aneurysms in hypercholesterolemic mice: role of serum cholesterol and temporal effects of exposure. *PLoS One*. 2014;9:e84517. doi: 10.1371/journal.pone.0084517.
52. Lima VV, Zemse SM, Chiao CW, Bomfim GF, Tostes RC, Clinton Webb R, Giachini FR. Interleukin-10 limits increased blood pressure and vascular RhoA/Rho-kinase signaling in angiotensin II-infused mice. *Life Sci*. 2016;145:137–143. doi: 10.1016/j.lfs.2015.12.009.

Highlights

- Application of a nonviral, nonimmunogenic vector (minicircle) to systemically overexpress IL-10 (interleukin-10) is feasible in mice and increases plasma IL-10 significantly 7 days after injection.
- After minicircle IL-10 injection, aneurysm growth and size as well as rate of dissecting abdominal aortic aneurysm decreased in a murine abdominal aortic aneurysm model (angiotensin II [Ang II]-ApoE$^{-/-}$ infusion).
- These relevant effects were accompanied by higher amounts of beneficial T_{reg} cells and alternatively activated, antiinflammatory macrophages in local aortic tissue. Furthermore, local proinflammatory immune response was dampened with lower TNF-α (tumor necrosis factor-α) production and fewer cytotoxic T cells.
- Human peripheral blood mononuclear cells with IL-10 treatment after Ang II incubation show ameliorated expression of differentiation markers GZMB (granzyme B), TNF-α, MRC1 (mannose receptor, C type 1), CD163, and IL-6, indicating possible translational potential in the application of IL-10.

4.2. Physiologische Wundheilung/Wundheilungsstörungen

4.2.1. Zitationen

Wagenhäuser MU, Duran M, Dueppers P, Witte M, Schelzig H, Oberhuber A. *Preliminary results of transcutaneous oxygen pressure measurement as effective monitoring for conservative therapy in peripheral occlusive disease.* Ital J Vasc Endovasc Surg. 2015; 22(4):163-70.

Wagenhäuser MU, Mulorz J, Ibing W, Simon F, Spin JM, Schelzig H, Oberhuber A. *Oxidized (non)-regenerated cellulose affects fundamental cellular processes of wound healing.* Sci Rep. 2016;25;6:32238.

Wagenhäuser MU, Garabet W, van Bonn M, Ibing W, Mulorz J, Yea RH, Spin JM, Dimopoulos C, Oberhuber A, Schelzig H, Simon F. *Time-dependent effects of cellulose and gelatin-based hemostats on cellular processes of wound healing*. Arch Med Sci. 2020; doi:10.5114/aoms.2020.92830.

4.2.2. Spezifische Fragestellung/Methodik

Die physiologische postoperative Wundheilung besitzt für alle medizinischen Fachdisziplinen, insbesondere für die Gefässchirurgie, große Bedeutung[90]. Wenn der physiologische Prozess der Wundheilung gestört wird, kann sich eine chronische Wunde entwickeln, was mit immensen Kosten für das Gesundheitssystem verbunden ist. So werden ca. 2% des EU-weiten Gesundheitsetats gebunden, und zwischen 12 und 38 Milliarden US Dollar jährlich für chirurgische Wundheilungsstörungen bereitgestellt[91,92].
Die physiologische Wundheilung kann durch verschiedene externe Noxen sowie Begleiterkrankungen gestört werden. Zu den wesentlichsten Komorbiditäten, die eine postoperative Wundheilungsstörung begünstigen, zählen ein Diabetes mellitus, Fettleibigkeit, sowie eine Malnutrition[93–95]; zu den exogenen Noxen das Rauchen von Tabakzigaretten und die chronische Einnahme von Steroiden[96,97]. Ischämisch bedingte Wunden im Rahmen einer fortgeschrittenen pAVK treten gehäuft bei über 70-jährigen männlichen Rauchern auf[98].
Hämostyptika werden zur lokalen Blutungskontrolle für diverse klinische Zwecke eingesetzt[99]. Zellulose, ein lineares Homopolymer aus aneinandergereihten Hydroglykose-Einheiten mit primären und sekundären Hydroxylgruppen, findet in der Medizin historisch Anwendung[100,101]. Jedoch erkannten erst die amerikanischen Forscher Frantz und Clarke, dass die Begasung einer Baumwollmullbinde mit Nitrogendioxid ein

für den menschlichen Organismus resorbierbares und zugleich blutungsstillendes Material erzeugt[100]. Durch Oxidation entstehen Carboxygruppen. Die entstandene Glukoronsäure bildet den Hauptbestandteil von oxidierter Zellulose, die je nach Organisationsgrad der Fasern in regenerierter (ORC = oxidierte regenerierte Zellulose) oder nicht regenerierter (ONRC = oxidierte nicht regenerierte Zellulose) Form vorliegen kann[102]. Der menschliche Körper kann Zellulose-basierte Hämostyptika (CBH), wie ORC und ONRC innerhalb von 1-2 Wochen durch Hydrolyse glykosidischer Bindung resorbieren[103].

Neben ORC und ONRC sind auch Gelatine-basierte Hämostyptika (GBH) verbreitet, die in verschiedenen Applikationsformen und in Verbindung mit anderen Materialien im medizinischen Alltag genutzt werden[104–106]. GBH sind porcinen Ursprungs und werden zur Generierung eines Hydrochlorids durch partielle Hydrolyse aus Kollagen gewonnen[107]. Da Gelatine das bis zu 40-fache seines Gewichts absorbieren kann, besitzt es ein enormes Expansionsvermögen. Die signifikante Volumenzunahme ist ein wesentliches Charakteristikum[108]. Seit seiner Einführung in den 1940er Jahren sind nur geringfügige Modifikationen am Ausgangsmaterial vorgenommen worden, so dass Gelatine bis heute in seiner Ursprungsform fortbesteht[109].

CBH und GBH haben viele Gemeinsamkeiten in Hinblick auf Praktikabilität und Funktionalität[110]. Obwohl die Materialien schon länger als lokale Hämostyptika Verwendung finden, sind ihre Auswirkungen für die postoperative Wundheilung bisher nur wenig erforscht. Die Fragestellung gewinnt weiter an Relevanz, da die Materialien häufig *in-situ* belassen werden und somit unmittelbar Einfluss auf lokale, das Geweberemodeling steuernde Signalprozesse in den beteiligten Zellen, insbesondere stromalen Fibroblasten, nehmen können. Es sollte geklärt werden, ob die Hämostyptika wesentliche zelluläre Prozesse der physiologischen Wundheilung und damit des Geweberemodelings wie Zellproliferation bzw.-vitalität, -migration und Kontraktion der EZM beeinflussen. Aufgrund der oft nur begrenzten Applikationszeit während operativen Eingriffen sollte weiterhin untersucht werden, ob mögliche Effekte von der Expositionszeit abhängig sind.

Für die Experimente wurden humane stromale Fibroblasten verwendet. Die verschiedenen Hämostyptika (ORC = Tabotamp, Johnson & Johnson Medical GmbH,

Ethicon Deutschland, Norderstedt, Deutschland, ONRC = ResorbaCell, Resorba Medical GmbH, Nürnberg, Deutschland, GELA = GELITA TUFT-IT, Gelita Medical GmbH, Eberbach, Deutschland) wurden im Überstand exponiert. Die zellulären Zielparameter wurden in *in-vitro* Experimenten untersucht. Der pH-Wert Verlauf im Überstand wurde während des Degradationsprozesses der Hämostyptika gemessen. Die Zellvitalität wurde durch kommerzielle „Assays" bestimmt. Die Fähigkeit, zweier Fibroblastenfraktionen unter Hämostytikaexposition über einen vordefinierten Spalt zu migrieren, wurde durch „live-cell imaging" analysiert. Die Kontraktion der EZM wurde anhand einer Oberflächenberechnung von Kollagen Typ I Matrixgelen bestimmt und im zeitlichen Verlauf ausgewertet. Die Veränderung von Zytokinspiegeln während Hämostytikaexposition, die mit dem Geweberemodeling in Verbindung stehen und die zuvor genannten zellulären Funktionen regulieren, wurden durch Enzyme-linked Immunosorbent Assay (ELISA) quantifiziert.

Neben postoperativen Wundheilungsstörungen spielen ähnliche Prozesse des Geweberemoedelings bei ischämisch bedingten Wunden eine entscheidende Rolle[111]. Der ungestörte und organsierte Ablauf dieser Prozesse hängt entscheidend von einem ausreichenden Sauerstoffangebot ab[112]. An einer Patientenkohorte mit fortgeschrittener pAVK soll abgeschätzt werden, ob eine Infusionstherapie mit Prostaglandin E1 bzw. eine CT gesteuerte lumbale Sympathikolyse (CTLS) zu einer Verbesserung des lokalen Sauerstoffangebots und des damit einhergehenden Geweberemodeling führt. Das Sauerstoffangebot in der lokalen Mikrozirkulation soll durch die Messung der transkutanen Sauerstoffspannung (TcPO2) mit Hilfe der E5250 Sensoren des TCM 400 (Radiometer Medical ApS, Bronshoj, Dänemark) beurteilt werden. Die TcPO2 soll sowohl in direkter Umgebung der ischämisch bedingten Wunde (distaler Messpunkt, DMP) als auch 15-20 cm proximal davon (proximaler Messpunkt, PMP) bestimmt werden. Eine Normalisierung der Werte soll gegen die herznahe TcPO2 erfolgen und aus dem gebildeten Quotienten soll der regionale Perfusionsindex (RPI) bestimmt werden.

4.2.3. Synopsis der Ergebnisse/Diskussion

ORC und ONRC führen während des Degradationsprozesses zu einer ausgeprägten Azidose. Bereits nach wenigen Minuten kommt es zu einem starken Abfall des pH-

Wertes. Wird der pH-Wert nicht in 0,9%-iger NaCl, sondern im Zellkulturmedium bestimmt, so ist eine stärkere Azidose während der ONRC verglichen mit der ORC Degradation zu beobachten.

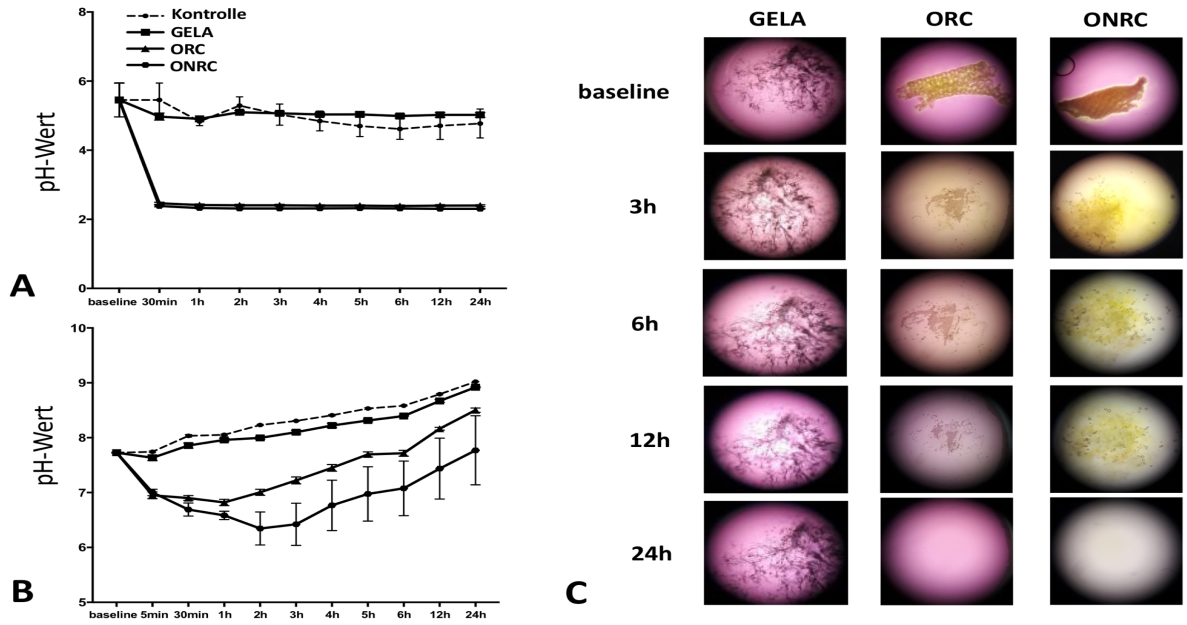

Abbildung 10: Verlauf des pH-Wertes während der Degradation von Hämostyptika. A: pH-Wert Verlauf während der Degradation verschiedener Hämostyptika in 0,9%-iger NaCl Lösung. Oxidierte regenerierte Zellulose (ORC) und oxidierte nicht regenerierte Zellulose (ONRC) bedingen einen starken Abfall des pH-Wertes innerhalb der ersten halben Stunde, während GELA (Gelatine-basiertes Hämostyptikum; GBH) den pH-Wert im Vergleich zu Kontrollen nicht ändert. **B:** pH-Wert Verlauf während der Degradation verschiedener Hämostyptika in Zellkulturmedium. Während der ersten Stunden zeigen ORC und ONRC einen unterschiedlichen pH-Wert Verlauf mit einem verzögerten Anstieg des pH-Wertes für ORC. **C:** Morphologische Dokumentation der Degradation von ORC, ONRC und GELA. GELA zeigt eine intakte Materialintegrität nach 24 Stunden, während ORC und ONRC bereits vollständig degradiert sind. Modifiziert aus Wagenhäuser et al. *Time-dependent effects of cellulose and gelatin-based hemostats on cellular processes of wound healing.* Arch Med Sci. doi:10.5114/aoms.2020.92830 (2020). (Mit freundlicher Genehmigung von Termedia, lizenziert, CC-BY Creative Commons attribution license (CC-BY, version 4.0 http://creativecommons.org/licenses/by/4.0/)

Insbesondere innerhalb der ersten Stunden nach Beginn des Experiments ist eine unterschiedliche Entwicklung des pH-Wertes im Überstand unter ORC und ONRC Exposition zu beobachten. Während ONRC innerhalb dieses Zeitrahmens den pH-Wert weiter erniedrigt, reicht die Pufferkapazität des Zellkulturmediums aus, um den pH-Wert unter ORC Exposition zu stabilisieren bzw. bereits tendenziell zu erhöhen. Im weiteren Fortgang kommt es zu einer ähnlichen tendenziellen Veränderung des pH-Wertes für beide Hämostyptika, jedoch verbleibt der pH-Wert während des gesamten Beobachtungszeitraumes über 24 Stunden unter ONRC verglichen mit ORC Exposition erniedrigt ***(Abbildung 10A und B)***. Diese Erkenntnisse könnten auf der größeren

Oberfläche von ONRC Hämostyptika beruhen, die zudem eine weniger organisierten Faserstruktur besitzen. Aufgrund der größeren Oberfläche könnte es zu einer gesteigerten Freisetzung von H^+-Ionen pro Zeiteinheit kommen, was den unterschiedlichen Verlauf des pH-Wertes teilweise erklären könnte[113].

Gleiches gilt nicht für GELA, das während des gesamten Untersuchungszeitraumes zu keiner wesentlichen Änderung des pH-Wertes verglichen mit den Kontrollen führt ***(Abbildung 10A und B)***. Diese Neutralität scheint Grundlage für die fehlende anti-bakterielle Eigenschaft von GELA zu sein. Dies stellt für einige wenige klinische Anwendungen einen Nachteil dar[114]. Zugleich besitzen GBH eine deutliche längere Degradationszeit, was eigene morphologische Beobachtungen stützt, die eine nur minimale Degradation von GELA innerhalb von 24 Stunden fanden[103] (***Abbildung 10C***).

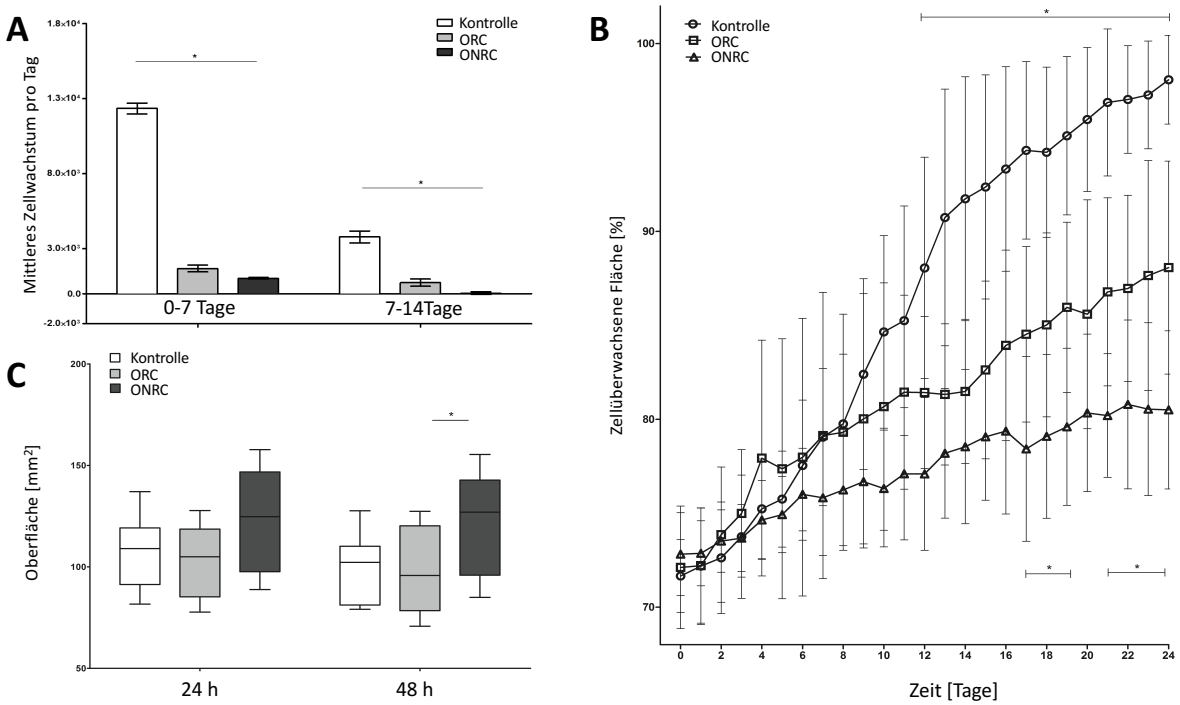

Abbildung 11: Proliferation, Migration und Kontraktion der extrazellulären Matrix (EZM) bei Exposition mit zellulose-basierten Hämostyptika (CBH). A: Verminderte Proliferation stromaler Fibroblasten unter kontinuierlicher CBH Exposition. Oxidierter nicht-regenerierter Zellulose (ONRC) hemmt die Fibroblastenproliferation stärker als oxidierte regenerierte Zellulose (ORC) während der ersten und zweiten Woche. **B:** Verminderte Fibroblastenmigration über 24 Stunden unter kontinuierlicher CBH Exposition. ONRC führt zu einer stärkeren Hemmung als ORC. **C:** Geringere Kollagenmatrixkontraktion unter ONRC verglichen zu ORC Exposition nach 2 Tagen. *p<.05 One-way ANOVA und multipler t-test mit Bonferroni Korrektur für normal verteilte Daten und Kruskal-Wallis Test mit Dunn's post Test, sowie Mann–Whitney U Test für nicht normal verteilte Daten. Modifiziert aus Wagenhäuser, M. U. et al. *Oxidized (non)-regenerated cellulose affects fundamental cellular processes of wound healing.* Sci Rep. Aug 25;6:32238 (2016). (Mit freundlicher Genehmigung der Nature Publishing Group, lizenziert, CC-BY Creative Commons attribution license (CC-BY, version 4.0 http://creativecommons.org/licenses/by/4.0/).

ORC und ONRC wirken sich unterschiedlich auf zelluläre Funktionen aus, die das Geweberemodeling unmittelbar beeinflussen und für die physiologische Wundheilung in unterschiedlichen Phasen wesentlich sind. So inhibiert ONRC die Zellproliferation und -migration stärker als ORC. Auch die Kontraktion der EZM ist unter ONRC signifikant stärker supprimiert als unter ORC Exposition, die keinen Einfluss auf die Kontraktion und die damit verbundene Differenzierung von Fibroblasten in Myofibroblasten zeigt[115] (***Abbildung 11A-C***).

Die inhibitorischen Effekte von ORC und ONRC auf die Proliferation von stromalen Fibroblasten scheinen durch die Azidose während des Degradationsprozesses ausreichend erklärbar zu sein[116]. Allerdings wurden in Tierexperimenten davon abweichende Beobachtungen mit einer erhöhten epidermalen Proliferationsrate und einem gesteigerten Geweberemodeling während der Exposition mit CBH beschrieben[117,118]. Die Beobachtungen erfolgten an epidermalen Keratinozyten. Die Ergebnisse an stromalen Fibroblasten erscheinen für die schichtenübergreifende postoperative Wundheilung von höherer Relevanz, da diese Zellart in tieferen subdermalen Gewebeschichten lokalisiert ist. Weiterhin besteht eine hohe Heterogenität innerhalb der einzelnen Subpopulationen von Fibroblasten in der Haut, was die abweichenden Ergebnisse ebenfalls teilweise erklären könnte[119].

Kontroverse Ergebnisse wurden für die Auswirkungen von ORC und/oder ONRC auf die Zellmigrationsfähigkeit *in-vivo* beschrieben. Es wurden sowohl fördernde als auch inhibierende Beobachtungen gemacht. Diese führten dementsprechend auch zu einer schnelleren Reifung des Granulationsgewebes als auch zum genauen Gegenteil[120,121]. Für eine abschließende Beurteilung erscheinen humane randomisierte Studien unerlässlich.

Interessanterweise scheinen die beschriebenen Beobachtungen kausal nicht ausschließlich auf Veränderungen des pH-Wertes zu beruhen. Eine experimentelle Adjustierung des pH-Wertes in den Kontrollgruppen auf Werte, vergleichbar denen während des ORC und ONRC Degradationsprozesses, zeigte weiterhin eine signifikante Inhibierung der Zellproliferation, -migration in den Expositionsgruppen. Die Kontraktion der extrazellulären Matrix war nur in der ONRC Expositionsgruppe verringert (***Abbildung 12A-D***). Für die pH-Wert unabhängigen Effekte könnten fibrinöse hydrolytische

Endprodukte verantwortlich sein, die während des Degradationsprozesses entstehen[122,123]. Die Veränderung bzw. Verringerung dieser Produkte könnte ein bedeutendes Ziel zukünftiger Bestrebungen zur Materialverbesserung sein.

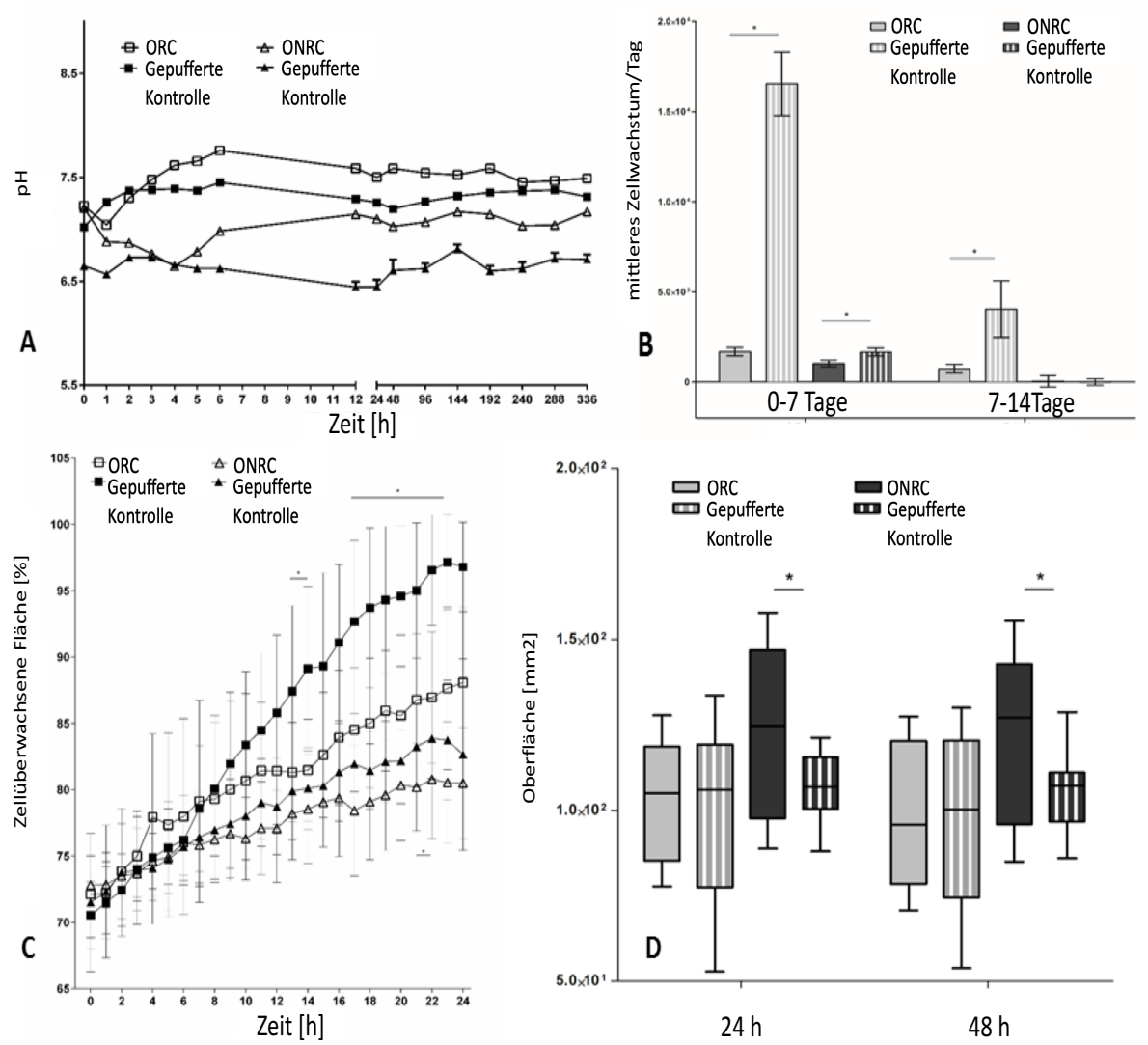

Abbildung 12: Vergleich zellulärer Subprozesse unter Exposition mit Zellulose-basierten Hämostyptika (CBH) und pH-Wert adjustierten (gepufferten) Zellkulturmedien (Kontrolle). A Verlauf des pH-Wertes von Zellulose-basierten Hämostyptika (CBH) und gepufferten Kontrollmedien: ORC (medium pH 7.0) und ONRC (medium pH 6.6). Eine Abweichung von 10% zu jedem Auswertungszeitpunkt zwischen den Versuchsgruppen und den gepufferten Kontrollen wurde akzeptiert. **B:** Verminderte Fibroblastenproliferation unter ORC und ONRC Exposition während der ersten Woche verglichen mit gepufferten Kontrollmedien. **C:** Verminderte Fibroblastenmigration unter ORC und ONRC Exposition verglichen mit gepufferten Kontrollmedien. **D:** Verminderte Matrixkontraktionsfähigkeit bzw. größere Oberfläche eines Kollagen I Matrixgels unter ONRC Exposition nach 24h und 48 h verglichen mit gepufferten Kontrollen. *p<.05 Kotroll- vs. ORC- vs. ONRC exponierten Gruppen bzw. ORC- und ONRC exponierten Gruppen und gepufferten Kontrollmedien. Mann-Whitney U Test. Modifiziert aus Wagenhäuser, M. U. et al. *Oxidized (non)-regenerated cellulose affects fundamental cellular processes of wound healing.* Sci Rep. Aug 25;6:32238 (2016). (Mit freundlicher Genehmigung der Nature Publishing Group, lizenziert, CC-BY Creative Commons attribution license (CC-BY, version 4.0 http://creativecommons.org/licenses/by/4.0/)

Es bleibt ungewiss, ob solche Modifikationen zu einer Verminderung Geweberemodeling-assoziierter inhibitorischer zellulärer Effekte führen, die sich positiv auf die physiologische postoperative Wundheilung auswirken.

Betrachtet man detailliert den Einfluss der Expositionszeit (kurz: 5-10 min, mittel: 30 min, lang: 60 min und kontinuierlich: 24 h) von ORC, ONRC und GELA auf die metabolische Aktivität und die Migrationsfähigkeit von stromalen Fibroblasten, so zeigte sich, dass bereits kurze Expositionszeiten zu einer transienten Reduktion der Zellviabilität führen. Je länger hierbei die Expositionszeit, desto länger ist die Reduktion der Zellviabilität zu den jeweiligen Nachbeobachtungszeitpunkten. Von Bedeutung ist hier, dass GELA unabhängig von der Expositionszeit zu keiner Verminderung der Zellviabilität führte. Die Erkenntnisse scheinen durch die lokalen pH-Wert Veränderungen während des Degradationsprozesses erklärbar, da eine direkte Assoziation der Zellviabilität und des lokalen pH-Wertes bei Verwendung gingivaler Fibroblasten berichtet wurde[124]. Ähnliche Beobachtungen wurden auch für andere Zelltypen beschrieben, was die Azidose während der Degradation von ORC und ONRC kausal für die Beobachtungen erscheinen lässt[125] (***Abbildung 13A und B)***.

Im Gegensatz zu der Zellviabilität ist die Migrationsfähigkeit erst durch längere Expositionszeiten von ORC und ONRC und zu späteren Nachbeobachtungszeitpunkten reduziert (***Abbildung 13C und D)***. Eine „verzögerte“ oder „verschleppte“ Zellreaktion ist plausibel, was eine Signaltransduktion mit zwischengeschalteter Proteinsynthese nahelegt. Eine von der degradationsbedingten Azidose unabhängige Signaltransduktion erscheint möglich. In dieser Hinsicht könnte die Aktivierung der „mitogen-activated protein kinase“ (MAPK) ein interessanter intrazellulärer Signaltransduktionsweg sein, da die Aktivität dieser Kinase eine direkte Regulation der Zellmigration bedingt[126]. TGF-β aktiviert diese Kinase über ein nicht kanonisches nicht Smad-abhängiges „Signaling“, das über die Aktivierung des „extracellular-signal-regulated kinase“ (ERK)/MAPK Signaltransduktionswegs agiert[126]. TGF-β ist als wesentlicher Regulator der Zellmigration von großer Bedeutung und besitzt für die physiologische Wundheilung hohe Relevanz[127]. CBH, wie ORC und ONRC führen zu einem reduzierten intrazellulären Proteinlevel von TGF-β, während GBH (GELA) keine Änderungen bedingt (***Abbildung 13E***).

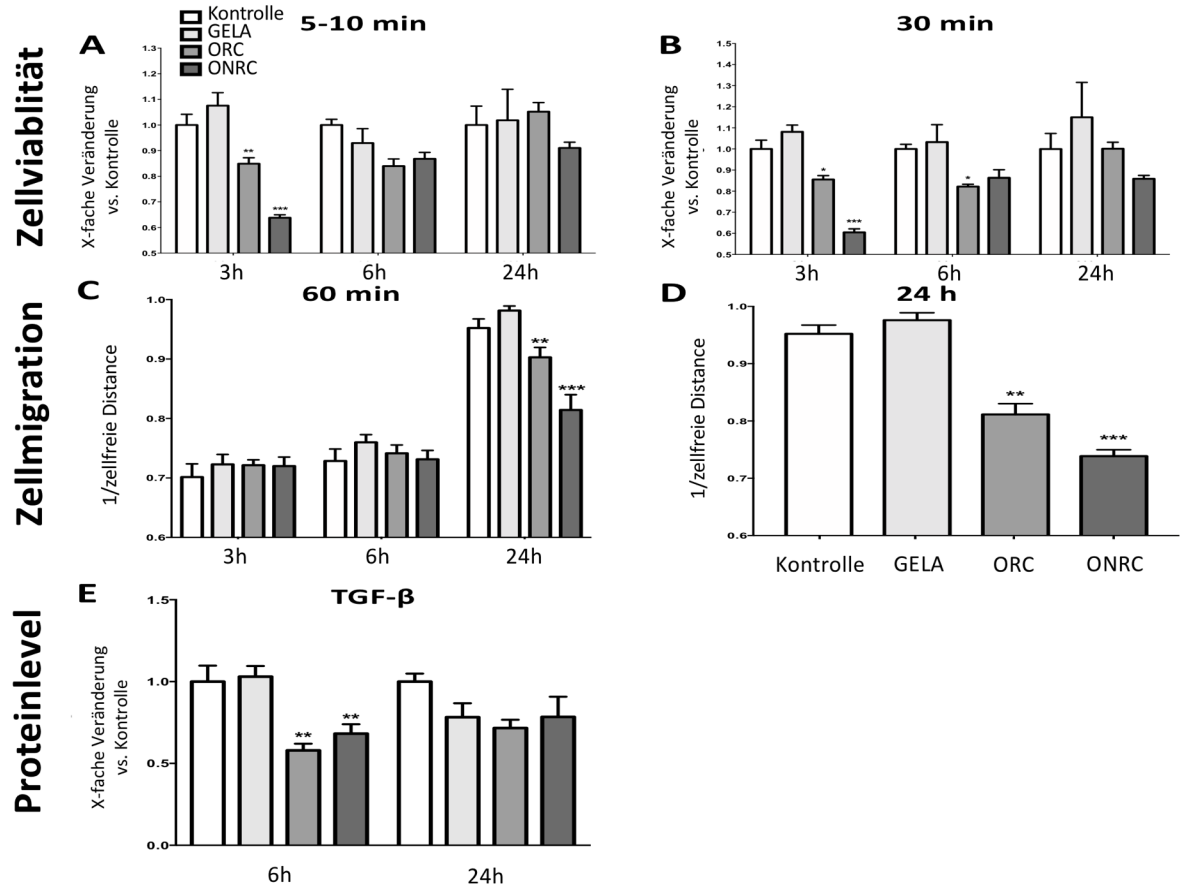

Abbildung 13: Applikationszeit basierte Effekte auf Zellvitalität, Zellmigrationsfähigkeit und „transforming growth factor-β" (TGF-β) Proteinlevel unter Gelatine- (GBH) und Zellulose-basierten Hämostyptika (CBH). A: 3-(4,5-Dimethylthiazol-2-yl)-2,5-diphenyltetrazoliumbromid (MTT)-Assay nach 5-10 min ORC, ONRC und GELA Exposition. ORC und ONRC reduzieren die Zellvitalität nach 3 Stunden Nachbeobachtungszeit. GELA verändert die Zellvitalität nicht. **B:** MTT-Assay nach 30 min Hämostyptika Exposition. ORC und/oder ONRC reduzieren die Zellvitalität nach 6 Stunden Nachbeobachtungszeit. GELA hat keinen Einfluss auf die Zellvitalität. **C:** Zellmigration nach 60 min Hämostyptika Exposition. ORC und ONRC reduzieren die Zellmigrationsfähigkeit von stromalen Fibroblasten nach 24 h Nachbeobachtungszeit. GELA verändert die Zellmigrationsfähigkeit nicht. **D:** Zellmigration nach 24 h kontinuierlicher Hämostyptika Exposition. ORC und ONRC reduzieren die Zellmigrationsfähigkeit von stromalen Fibroblasten. GELA hat keinen Einfluss auf die Zellmigration. **E:** Intrazelluläre TGF-β Proteinlevels nach 6 und 24 h kontinuierlicher Hämostyptika Exposition. ORC und ONRC reduzieren die TGF-β Proteinlevel nach 6 h, GELA hat keinen Einfluss auf den TGF-β Proteinlevel. *p<.05 vs. Kontrolle ** vs. Kontrolle und GELA *** vs. Kontrolle, GELA und ORC. 2-way ANOVA mit 2-stage step-up Methode nach Benjamini, Krieger and Yekutieli. Modifiziert aus Wagenhäuser et al. *Time-dependent effects of cellulose and gelatin-based hemostats on cellular processes of wound healing.* Arch Med Sci. doi:10.5114/aoms.2020.92830 (2020). (Mit freundlicher Genehmigung von Termedia, lizenziert, CC-BY Creative Commons attribution license (CC-BY, version 4.0 http://creativecommons.org/licenses/by/4.0/)

Aufgrund der aufgeführten Zusammenhänge erscheint eine ursächliche Verbindung zwischen dem reduzierten TGF-β Proteinniveau unter ORC und ONRC Exposition und der reduzierten Migrationsfähigkeit stromaler Fibroblasten über den zuvor beschriebenen Signaltransduktionsweg wahrscheinlich[126]. Folglich verspricht die experimentelle

Aktivierung dieses Signaltransduktionswegs therapeutisches Potential, da so einer reduzierten Migrationsfähigkeit entgegengewirkt werden könnte. Da GELA nach keiner der o.g. Expositionszeiten zu einer Einschränkung der Zellviabilität und/oder -migration führte, erscheint die Verwendung von GBH in Bezug auf diese Endpunkte vorteilhaft gegenüber CBH.

Eine optimale Sauerstoffversorgung ist nicht nur für die postoperative Wundheilung, sondern auch für ischämisch bedingte Wunden bei pAVK Patienten unerlässlich. Für die Therapie dieser Wunden stehen in fortgeschritten Stadien neben endovaskulären und operativen auch konservative Therapieansätze zur Verfügung. Diese haben eine Erhöhung des lokalen Sauerstoffangebots durch Verbesserung der Mikrozirkulation zum Ziel. Die physiologische Wundheilung soll durch eine Verbesserung des Geweberemodelings erreicht werden.

Prostanoide verbessern die Heilungstendenz von chronischen Wunden, indem sie neben einer Vasodilatation die Aktivierung, Adhäsion und Aggregation von Thrombozyten reduzieren und zeitgleich die fibrinolytische Aktivität steigern. Außerdem begrenzen sie die Leukozytenaktivität und besitzen für das Endothel protektive Eigenschaften[128–132]. Die Steigerung des lokalen Sauerstoffangebots im Wundgebiet, die auch durch eine CTLS erreicht werden soll, verbessert die Heilungstendenz ischämischer Wunden[133]. Um die Effektivität dieser Therapien abschätzen zu können, kann die TcPO2 im Wundgebiet durch die E5250 Sensoren des TCM 400 gemessen werden (***Abbildung 14A und B***).

In einem Patientenkollektiv mit fortgeschrittener pAVK (Durchschnittsalter von 64 ± 11 Jahren, Rutherford V/VI, Einschlusszeitraum 1. Juni 2013 bis 31. Juni 2014) wurden die TcPO2 unter Prostaglandin E1 Infusionstherapie ± ergänzender CTLS an zwei peripheren Lokalisationen (PMP und DMP) bestimmt. Außerdem wurde die TcPO2 herznah gemessen.

Eine Erhöhung des RPI, der sich durch Normalisierung der herznahen TcPO2 Werte errechnet, konnte nur am PMP beobachtet werden. In unmittelbarer Umgebung der ischämischen Wunde (DMP) konnte keine Erhöhung der TcPO2 Werte bzw. des RPI gefunden werden. Hier könnte eine subliminale Inflammation in unmittelbarer Wundumgebung zu einem lokal gesteigerten Blutfluss in dem eigentlich ischämischen Gewebe geführt haben, so dass vaskuläre Adaptationsmöglichkeiten begrenzt und

dementsprechend keine Veränderung bzw. Reduktion des TcPO2 zu erwarten ist[111]. Folglich würde auch eine funktionelle Erhöhung des Sauerstoffangebots nicht zu einer Erhöhung der messbaren Sauerstoffspannung in unmittelbarer Wundumgebung führen und ein effektives Monitoring in dieser Lokalisation erschweren ***(Abbildung 14C und D***). Ableitend erscheint der regionale Perfusionsindex aussagekräftiger als die alleinige Bestimmung der absoluten TcPO2. Eine zusätzliche CTLS führte zu keiner Zunahme der TcPO2 bzw. des RPI.

Zusammenfasend kann durch konservative rheologische Infusionstherapie mit Prostaglandin E1 eine Erhöhung des RPI erreicht werden, was eine Verbesserung des lokalen Sauerstoffangebots bzw. des Geweberemodelings nahelegt.

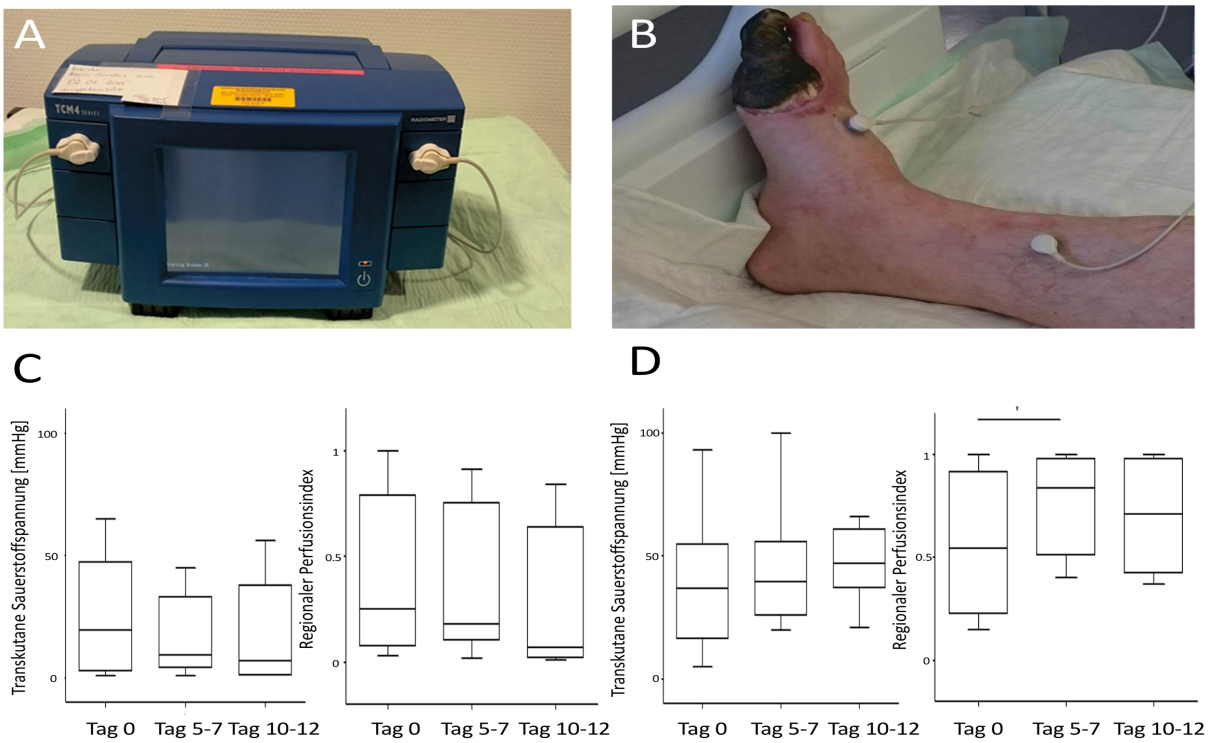

Abbildung 14: Die transkutanen Sauerstoffspannung (TcPO2) und der regionalen Perfusionsindex (RPI) unter Prostaglandin E1 Infusionstherapie und bei CT-gesteuerte lumbale Symapthikolyse (CTLS). A: Die E5250 Sensoren des TCM 400, (Radiometer Medical ApS, Bronshoj, Dänemark) wurden zur Bestimmung der TcPO2 im Gewebe verwendet. **B:** Die Sensoren wurden 15-20 cm oberhalb der Wunde (proximaler Messpunkt, PMP) und in direkter Wundumgebung (distaler Messpunkt, DMP) angebracht. Ein weiterer Sensor wurde thorakal herznah angebracht. Der Quotient aus dem herznahen Messpunkt und peripheren Messpunkten wurde zur Bestimmung des RPI verwendet. Eine Equilibrierung von 15-20 Minuten wurde abgewartet. **C und D:** TcPO2 und RPI am DMP **(C)** und am PMP (**D).** Der RPI ist nur für den PMP unter Prostaglandin E1 Infusionstherapie erhöht. *p<.05 Wilcoxon matched paired test. Modifiziert aus Wagenhäuser MU et al. *Preliminary results of transcutaneous oxygen pressure measurement as effective monitoring for conservative therapy in peripheral occlusive disease*. Ital J Vasc Endovasc Surg. 22(4):163-170 (2015). (Mit freundlicher Genehmigung des Edizioni Minerva Medica Verlags).

4.2.4. Zusammenfassung/Ausblick

Die physiologische Wundheilung postoperativer und chronischer Wunden beruht auf einem funktionalen Zusammenspiel verschiedener Teilaspekte des Geweberemodelings während der einzelnen Wundheilungsphasen. Ist dieses gestört, resultieren Wundheilungsstörungen oder chronische Wunden mit immenser sozioökonomischer Relevanz.

Eine mögliche Noxe, die zu einer dysfunktionalen postoperativen Wundheilung führen könnte, sind Hämostyptika. Diese werden im gefäßchirurgischen Alltag häufig verwendet. CBH führen während der Degradation zu einer signifikanten Azidose und reduzieren die Proliferations- und Migrationsfähigkeit stromaler Fibroblasten. Außerdem schränken sie die Kontraktionsfähigkeit der extrazellulären Matrix ein. Innerhalb der CBH Gruppe sind die Effekte unter ONRC stärker ausgeprägt als unter ORC Exposition. Die Beobachtungen sind dabei nicht ausschließlich durch die lokale Azidose zu erklären. Auch kurze Applikationszeiten, wie im chirurgischen Alltag üblich, führen zu ähnlichen Effekten. GBH zeigen auch bei kurzen Expositionszeiten keine Auswirkungen auf die zuvor genannten zellulären Subprozesse der physiologischen Wundheilung. Es bleibt abzuwarten, ob die monozellulären Beobachtungen auch in einem *in-vivo* System zu einer gestörten Wundheilung führen. Sollten zukünftige Ergebnisse dies nahelegen, so könnte ein relevantes Verbesserungspotential in Materialmodifikationen, die zu weniger oder anderen fibrösen Endprodukten im Rahmen des Degradationsprozesses führen, liegen.

Eine Infusionstherapie mit Prostaglandin E1 steigert das lokale Sauerstoffangebot bei ischämisch bedingten Wunden. Dies kann durch eine Erhöhung der TcPO2 und des RPI an einem Messpunkt 15-20 cm proximal der Wunde abgeleitet werden. Aufgrund der Verbesserung des Sauerstoffangebots ist von einem verbesserten, für die Abheilung chronischer Wunden unerlässlichen, Geweberemodeling auszugehen.

SCIENTIFIC REPORTS

OPEN

Oxidized (non)-regenerated cellulose affects fundamental cellular processes of wound healing

Received: 22 April 2016
Accepted: 03 August 2016
Published: 25 August 2016

M. U. Wagenhäuser[1,2], J. Mulorz[1], W. Ibing[1], F. Simon[1], J. M. Spin[2], H. Schelzig[1] & A. Oberhuber[1]

In this study we investigated how hemostats such as oxidized regenerated cellulose (ORC, TABOTAMP) and oxidized non-regenerated cellulose (ONRC, RESORBA CELL) influence local cellular behavior and contraction of the extracellular matrix (ECM). Human stromal fibroblasts were inoculated *in vitro* with ORC and ONRC. Cell proliferation was assayed over time, and migration was evaluated by Live Cell imaging microscopy. Fibroblasts grown in collagen-gels were treated with ORC or ONRC, and ECM contraction was measured utilizing a contraction assay. An absolute pH decline was observed with both ORC and ONRC after 1 hour. Mean daily cell proliferation, migration and matrix contraction were more strongly inhibited by ONRC when compared with ORC ($p < 0.05$). When control media was pH-lowered to match the lower pH values typically seen with ORC and ONRC, significant differences in cell proliferation and migration were still observed between ONRC and ORC ($p < 0.05$). However, in these pH conditions, inhibition of matrix contraction was only significant for ONRC ($p < 0.05$). We find that ORC and ONRC inhibit fibroblast proliferation, migration and matrix contraction, and stronger inhibition of these essential cellular processes of wound healing were observed for ONRC when compared with ORC. These results will require further validation in future *in vivo* experiments to clarify the clinical implications for hemostat use in post-surgical wound healing.

Vascular surgery patients are at elevated risk to develop superficial and deep incisional surgical site infections, with increased morbidity leading to prolonged hospital stays. These complications are common, with an overall risk of 3–44%, leading to enormous costs for health systems[1–3]. Thus accelerated, or at least normalized, surgical wound healing in these patients would be greatly beneficial[4,5].

Wound healing is hierarchically regulated based on an interplay between cellular, humoral and molecular mechanisms, and begins immediately after wounding[6]. The process is often subdivided into 3 independent phases, which partially overlap[7]. Initially there is an inflammatory phase, during which pro-inflammatory cytokines are released, leading to the recruitment of pro-inflammatory cells[8,9]. In this milieu, keratinocytes and fibroblast begin to proliferate within 3–4 days, establishing a collagen-rich granulation tissue[10]. After the proliferation phase, remodeling slowly transforms the granulation tissue into robust scar tissue. This final process can continue for years[8,10].

Chemical hemostats are often used by surgeons for local bleeding control after performing vascular anastomoses. Although, newer materials such as plasma-derived thrombin and fibrinogen have shown satisfying results, cellulose-based hemostats are still commonly used, as they are highly cost-effective[11]. Cellulose is a homopolysaccharide which is created through polymerization of glucopyranose through β-glucosidic bonds[12]. The manufacturing process differs slightly between oxidized regenerated cellulose (ORC), in which organized fibers are formed prior to oxidation, and oxidized non-regenerated cellulose (ONRC). Oxidation of cellulose is typically performed using dinitrogen tetroxide[13]. The primary component of oxidized cellulose is polyuronic acid, which is rapidly processed by glycosidases using β-elimination *in vivo*; however non-oxidized hydroxyl groups remain as a fibrous component which require phagocytosis by macrophages prior to hydrolysis[14]. However, the effect of *in situ* remaining hemostats on the postoperative wound healing process is poorly investigated so far.

[1]Department of Vascular and Endovascular Surgery, University Hospital Düsseldorf, Moorenstraße 5, 40225 Düsseldorf, Germany. [2]Division of Cardiovascular Medicine, Stanford University School of Medicine, Stanford University, Stanford, CA 94305, USA. Correspondence and requests for materials should be addressed to W.M.U. (email: markus.wagenhaeuser@med.uni-duesseldorf.de)

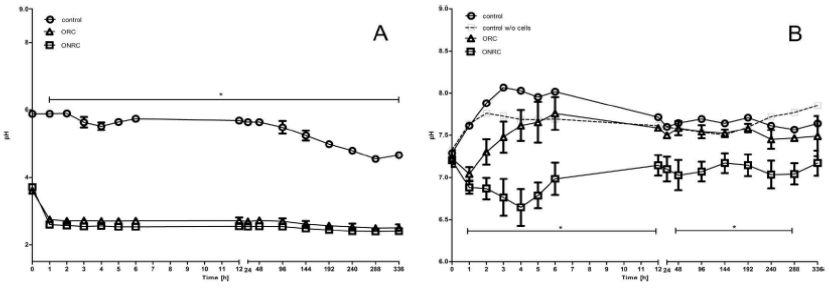

Figure 1. pH-value time course. (**A**) Absolute pH value of normal saline (NaCl 0,9%) during ORC and ONRC exposition. Decline in pH value occurred during the first hour before equilibration. No difference in total pH value decline between ORC and ONRC. (**B**) pH values of cell culture medium (without w/o cells) in a human fibroblast cell culture. Both hemostats had lower pH values compared to controls (*$p < 0.05$ between 1–5 h and at 240 h). ONRC showed lower pH value throughout the investigation period compared to ORC (*$p < 0.05$; one-way ANOVA with Bonferroni post test). $n = 12$.

The objective of this study is to compare an ONRC-based hemostat (RESORBA CELL, Resorba, Nuremberg, Germany) with an ORC-based hemostat (TABOTAMP, Norderstedt, Germany) regarding their effects on fundamental processes of deep incisional wound healing (DIWH), including cell proliferation and migration, and contraction of the extracellular matrix (ECM).

Results

Postoperative wound healing is highly dependent on the interaction between different cell lines; however, fibroblasts seem to be of particular relevance for DIWH. For that reason, human fibroblasts were used for analyzing key cellular sub-processes. As degradation of ORC and ONRC initially consists of hydrolysis with release of acidic groups, we investigated the pH-value time course for both hemostats.

A significant decline in absolute pH was observed for ONRC and ORC compared to controls. Over the first hour there was a significant pH drop with both hemostats in normal saline. After 1-hour absolute pH value remained constantly at approximately 2.5 for ONRC and ORC (Fig. 1A) ($p < 0.05$). The results showed a significant lower pH value for ONRC throughout the whole investigation period ($p < 0.05$). We observed opposite tendencies in pH value trend between 1–4 hours, as ONRC continued to lower the local pH, while ORC followed the pH value trend of controls and exhibited a gradual increase (Fig. 1B).

We also found that mean daily proliferation of fibroblasts was lower during the first week for ONRC (1.0×10^3 Δcells/day $\pm$ 180 Δcells/day) and ORC (1.6×10^3 Δcells/day $\pm$ 790 Δcells/day) as well as for the second week (ONRC: 32 $\pm$ 320 Δcells/day; ORC: 730 $\pm$ 840 Δcells/day) when compared to controls ($1.2 \times 10^4 \pm 1.3 \times 10^3$ Δcells/day: $3.8 \times 10^3 \pm 1.4 \times 10^3$ Δcells/day) ($p < 0.05$). Overall, ONRC displayed lower mean daily cell proliferation compared to ORC over both weeks ($p < 0.05$). There was near-total inhibition of cell proliferation within the second week for ONRC, whereas proliferation remained similar for ORC over the full duration (Fig. 2).

Cell migration is essential for functional DIWH. We found that both hemostats inhibited cell migration compared to controls. Throughout the investigation period, cell migration was more strongly inhibited by ONRC compared to ORC. Differences between the hemostats were statistically significant for the periods between 17–19 hours and between 21–24 hours ($p < 0.05$). After 24 h, coverage of the inter-chamber gap was 98.1% $\pm$ 2.3% for controls, and 88.1% $\pm$ 5.7% and 80.5% $\pm$ 4.2% for ORC and ONRC respectively (Fig. 3).

Contraction of the ECM is also indispensable for development of mature scar tissue. Our contraction assay results illustrate that nearly all observed contraction in matrix surface area occurred within the first 24 hours. Surface area of ORC matrices decreased ~25% $\pm$ 8.9%, within 24 hours, and ~16% $\pm$ 10.1% for ONRC. Thus, ONRC (24 h: 123 $mm^2 \pm 24.3$ mm^2; 48 h: 127 $mm^2 \pm 24$ mm^2) matrices showed a greater surface area after 24 and 48 hours compared to ORC (24 h: 103.9 $mm^2 \pm 17.9$ mm^2; 48 h: 98.6 $mm^2 \pm 20.2$ mm^2) and controls (24 h: 107.4 $mm^2 \pm 18$ mm^2; 48 h: 99.7 $mm^2 \pm 17$ mm^2) ($p < 0.05$). Differences between ORC and controls were not significant at either time point (Fig. 4).

To investigate hemostat-based effects that might be due solely to acidosis/pH changes, we used low pH-media, imitating the values achieved during the hemostat time-course (Fig. 5A). The low-pH control media was set initially at pH 7.0 for ORC ("medium pH 7.0") and at pH 6.6 for ONRC ("medium pH 6.6") as per the initial pH value measurements (Fig. 1B). Again cell proliferation was decreased for both ONRC and ORC within the first week compared to low-pH-media controls (medium pH 6.6: 1.6×10^3 Δcells/day $\pm$ 220 Δcells/day; medium pH 7.0: 1.6×10^4 Δcells/day $\pm$ 1.7×10^3 Δcells/day) ($p < .05$). During the second week, this effect could only be seen for ORC (ORC: 730 $\pm$ 840 Δcells/day; medium pH 7.0: 4.0×10^3 Δcells/day $\pm$ 1.6×10^3 Δcells/day) ($p < 0.05$) (Fig. 5B). Cell migration studies revealed that ORNC and ORC displayed enhanced inhibition of migration compared to low-pH-media controls, and the difference was accentuated after 6 hours in both study groups. Results were statistically significant between 13–14 and 17–23 hours for ORC and between 21–22 hours for ONRC ($p < 0.05$). After 24 h, controls with medium pH 7.0 showed 96.8% $\pm$ 3.4% cell coverage of the inter-chamber

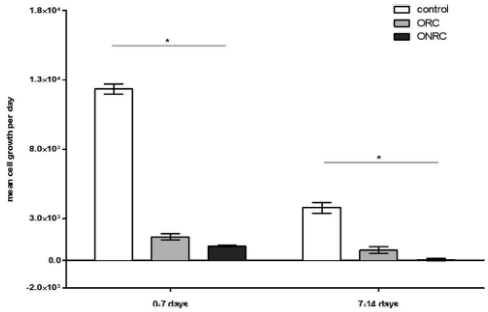

Figure 2. Mean cell growth rate. Mean cell growth rate was determined using WST-1 assay. Total cell number was measured at day 7 and 14. Mean cell growth rate per day was calculated for the first and second week separately. Significant inhibition of cell proliferation for ORC and ONRC, stronger inhibition for ONRC compared to ORC for both investigation periods. (*$p < 0.05$; Kruskal-Wallis test with Dunn's post test). $n = 12$.

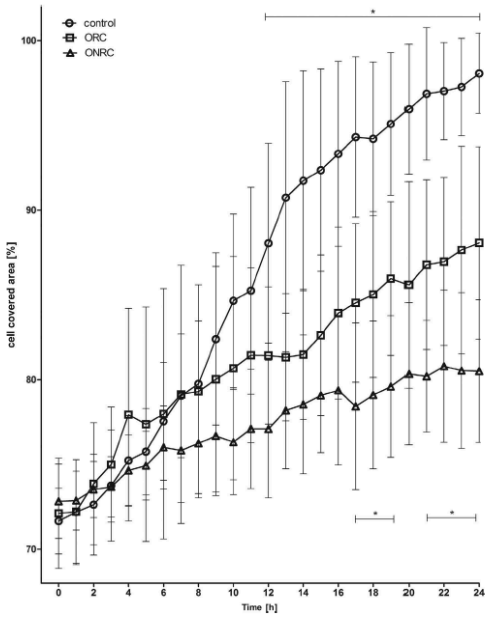

Figure 3. Cell migration. Shown is the cell covered area between two cell fractions using a cell migration assay. Inhibition of cell migration for ORC and ONRC. ONRC showed slower cell migration compared to ORC (*$p < 0.05$; one-way ANOVA with Bonferroni post test; significant difference between all study groups; — significant difference between both hemostats and controls). $n = 12$.

space, while controls with medium pH 6.6 showed 82.7 ± 7.2% coverage (Fig. 5C). Matrix contraction studies identified no differences for ORC compared to low-pH controls at 24 hours (ORC: 103.9 $mm^2 \pm 17.9\ mm^2$; medium pH 7.0: 104.6 $mm^2 \pm 24.9\ mm^2$) or 48 hours (ORC: 97.6 $mm^2 \pm 20.2\ mm^2$; medium pH 7.0: 103.2 $mm^2 \pm 24.7\ mm^2$). In contrast, there was significant inhibition of contraction for ONRC compared to low-pH controls at 24 hours (ONRC: 125 $mm^2 \pm 24.3\ mm^2$; medium pH 6.6: 107.1 $mm^2 \pm 9.3\ mm^2$) ($p < 0.05$), and near-significance at 48 hours (ONRC: 128.5 $mm^2 \pm 24\ mm^2$; medium pH 6.6: 107.6 $mm^2 \pm 11.4\ mm^2$) ($p = 0.052$) (Fig. 5D).

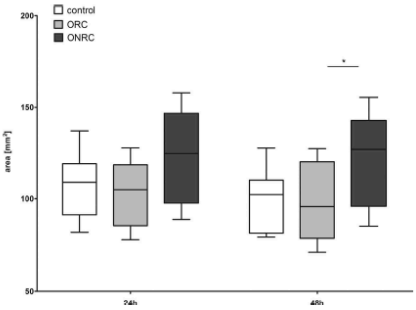

Figure 4. Contraction of the extracellular matrix. Shown is the surface area of 1%-collagen matrices after 24 and 48 hours. While ORC showed no differences compared to controls at both time points, ONRC demonstrated weaker matrix contraction compared to ORC (*$p < 0.05$; Kruskal-Wallis test with Dunn's post test). $n = 12$.

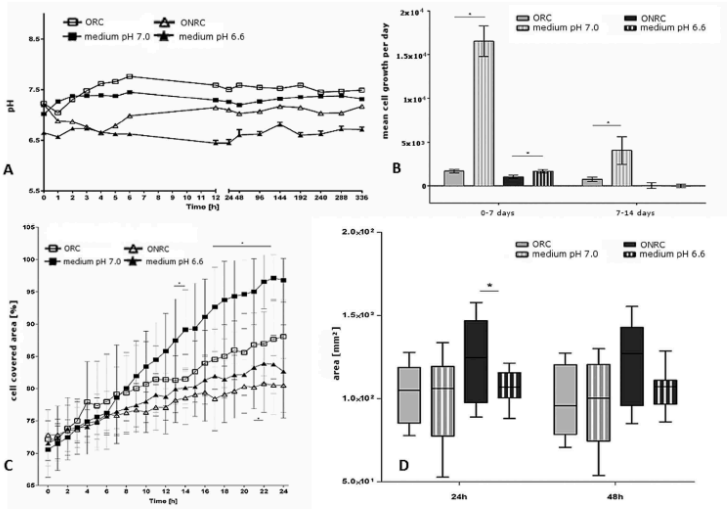

Figure 5. pH value, mean cell growth, cell migration and matrix contraction compared to pH-lowered cell media. (**A**) pH value of fibroblast cultures with pH-lowered control media compared to ORC and ONRC. A difference in pH of 10% for each measuring point was accepted for experiments. (**B**) Shown is the mean cell growth rate for the first and second week. Inhibition of cell proliferation for ORC and ONRC compared to pH-lowered controls in the first week, for ORC for the second week (*$p < 0.05$; Mann-Whitney U test). $n = 12$. (**C**) Cell migration for ORC and ONRC compared to pH-lowered controls as percentage of a cell covered area between two cell fractions. Inhibition of cell migration for ORC and ONRC compared to controls (*$p < 0.05$; multiple t-test with Bonferroni correction). $n = 12$. (**D**) Contraction of the extracellular matrix for ORC and ONRC compared to pH-lowered controls. ORC showed almost no difference at both measuring points compared to pH-lowered controls, whereas ONRC outlined inhibited matrix contraction. (*$p < 0.05$; Mann-Whitney U test). $n = 12$.

Discussion

Cellulose-based hemostats are known for high clinical convenience, as they are storable at room temperature and can be quickly deployed or removed. The macroscopic appearance of RESORBA CELL is more frayed at the edges, and overall more flexible compared to TABOTAMP. These agents are primarily used for small amounts of bleeding[15–17]. Lewis *et al.* describe superior hemostasis for ONRC, with equivalent bactericidal effectiveness when compared to ORC[13]. Both materials have already proven beneficial antibacterial effects even against antibiotic resistant microorganisms such as VRE, MRSA[13,18]. Little is known regarding how ORC and ONRC influence

DIWH. Therefore, we investigated the effects of ONRC and ORC on fibroblast cell proliferation, migration, and ECM contraction after hemostat degradation *in vitro* to clarify their potential impact in impaired DIWH.

As degradation of both hemostats results in a release of acidic groups, we investigated the effect of ORC and ONRC on the pH value over time. In the absence of cells and cell culture media, there was a sudden drop in pH value within the first hour for both hemostats. After this initial decline, no further changes in pH were noted; however, we later observed a marginally lower pH for ONRC. Next, we modeled the pH values observed in humans *in vivo* in the presence of fibroblasts utilizing cell cultures. ONRC showed lower pH values in cell culture throughout the investigation period. The hemostats showed opposite effects on pH value, particularly in the time period between 1–4 hours. Within this time frame, ONRC continued to lower the pH value whereas ORC showed an increase in pH value, similar to non-hemostat controls. Two different hypotheses might explain this behavior. The observed effect could be based on the greater surface area of the frayed fibers found in ONRC. This might lead to an increased release of acidic-groups per time unit, exceeding the buffering capacity of the culture media and lowering the pH value[13]. We suspect the differences seen between fibroblast cell cultures and normal saline experiments may be due in part to the logarithmic nature of the pH scale. Chemical buffers in culture media tend to hold the pH value more towards the middle of the scale, where changes in [H+] would have less impact on the pH value than at the end of the scale. Evaluation of this theory will require that material input and surface area be tightly controlled in future experiments. One possible approach to this would be to normalize the hemostat input to its density and pestle the hemostats thereafter. In this way, the release of acidic groups and changes in pH value could be investigated independently from the different working surfaces of both hemostats.

Another possible explanation of the divergence in pH value in cell culture media of fibroblast cultures between the hemostats might be that alterations occur in the cellular function of fibroblasts, meaning the fibroblasts themselves might acidify the environment. *In vivo* degradation of cellulose-based hemostats was studied by Pierce *et al.* and Dimitrijevich *et al.*, who showed that beyond enzymatic degradation there is a fibrous component of hemostats which requires phagocytosis by macrophages for complete clearance[14,19]. We believe that these fibrous components might alter cell function, leading fibroblasts to release acid or more likely to apoptose. The vicious cycle of acidosis causing increased apoptosis leading to further acidic group release has been described previously, and might explain our findings[20]. Future experiments would benefit from investigations of the effects of these hemostats and the associated pH phenomena on fibroblast apoptosis. As we only observed the pH effect for ONRC, we suspect it might be ONRC specific.

In this study we also modulated the pH value to investigate whether hemostats themselves, rather than the associated changes in pH value could be responsible for the effects of both hemostats on cell proliferation, migration and matrix contraction. To investigate this, we elected to lower the pH value of the controls rather than adding buffer to the hemostat samples, as total depletion of buffer capacity due to massive acidic group release over a short time might also occur *in vivo*. For that reason, this approach might better mimic *in vivo* conditions. More importantly, depletion of buffer capacity might even be essential to the findings we observed. For example, fibrous degradation components might have variable influences at different pH values.

Fibroblast function is crucial for several aspects of healthy post-surgical wound healing. Overcoming the spatial defects through generation of cell-rich tissue is aided by adequate cell proliferation. We therefore studied the influence of ONRC and ORC on cell proliferation, and demonstrated that both hemostats inhibited fibroblast proliferation compared to controls. This effect was larger for ONRC compared to ORC. Froehlich *et al.* described reduced fibroblast proliferation at lower pH values, as there is a greater tendency towards contact-inhibition and decreased sensitivity to growth stimulation once confluent[21]. Our low-pH culture media experiments suggest that effects of both hemostats on fibroblast proliferation are independent of their impact on pH alone. Akyol *et al.* and Liu *et al.* investigated the effect of ORC on fibroblast proliferation in animal models. Both authors described either no significant effect or even enhanced remodeling of the extracellular matrix, which they conclude resulted from increased cell proliferation[22,23]. It should be emphasized that these authors focused on either epithelial or mucosal wound healing reactions, which are somewhat different processes from this study. Epithelium and mucosa have high regenerative capacity, with a high basal proliferation rate, and multiple cell-cell interactions. This structure is histologically different from the way fibroblasts are organized in connective tissue, which seems to be the most relevant tissue in DIWH. Fibroblasts in different tissues might also react differently to external stimuli, as Varkey *et al.* demonstrated for fibroblast sub-populations within the skin[24]. Our studies focus on stromal fibroblasts, which appear to play a central role in DIWH. Clearly, the use of fibroblasts alone is not a perfect model to mimic *in vivo* conditions, where wound healing depends on multicellular interactions. Nevertheless, our results regarding hemostats and fibroblast proliferation stand in clear contrast to some published findings.

Fibroblast migration is also crucial for DIWH, helping to develop bands of connective tissue and establish immature granulation tissue. The current literature provides variable results with regard to the influence of hemostats on cell migration. Hart *et al.* found that wounds in diabetic animals treated with ORC/collagen sponges demonstrated significantly accelerated wound closure when compared to control wounds in similar animals. Histological analysis of the wound tissues suggested that using ORC/collagen sponges enhanced the formation and maturation of granulation tissue as a result of increased cell migration[25]. Rassu *et al.* showed that using ORC in oncoplastic breast surgery could promote dermal fibroblast proliferation and cell migration which resulted in beneficial effects for adjustment of the shape[26]. In contrast, Krishnan *et al.* described ORC as detrimental to wound healing *in vivo,* and uncovered no advantageous effects for ORC on cell proliferation and migration[27]. Notably, these *in vivo* results have limited applicability to our study. Their authors found that the prevention of postoperative hematoma led to increased cell proliferation, a process we did not investigate. Rather we concentrated on the direct inter-dependency between hemostats and cellular function. Moreover, the above authors used diabetic mice to study wound healing with cellulose hemostats. In that model, the antibacterial effect of hemostats might have outweighed the potential inhibiting effects on wound healing. Our study found that cell migration was inhibited *in vitro* for ORC and ONRC compared to controls. This effect remains after buffering controls to

similar pH values produced by hemostats. Therefore, we suggest that there exists a material-based negative effect on fibroblast cell migration, which is more evident for ONRC compared to ORC.

A balanced level of wound contraction is essential for optimal healing. Fibroblasts promote wound contraction, through activation of signaling pathways promoting a shift from fibroblast to myofibroblast[28]. We found that ONRC inhibit matrix contraction, whereas we could not observe a difference between ORC and controls. These results suggest that ONRC in particular might be responsible for inhibition of matrix contraction, and again the findings appear independent of acidosis resulting from hydrolysis. They might be dependent on fibrous compounds, which we believe may differ significantly between ORC and ONRC, leading to prolongation of clearance. Such compounds may also differ in their resistance towards contraction forces, resulting in inhibited matrix contraction. It appears likely that ONRC-specific fibrous hydrolysis end-products suppress matrix contraction more than ORC derived end-products.

In conclusion, both ORC and ONRC inhibit fibroblast proliferation, and migration. These effects do not exclusively depend on acidosis, suggesting that material-specific compounds such as fibrous hydrolysis end-products are responsible. Further, ONRC inhibits matrix contraction, unlike ORC. ONRC may more strongly inhibit essential cellular sub-processes, which are fundamentally important for functional wound healing. However, these findings will require further validation using *in vivo* models before their clinical impact can be assessed.

Methods

Hemostats. Employed hemostats included RESORBA CELL (oxidized non-regenerated cellulose -ONRC) and TABOTAMP (oxidized regenerated cellulose - ORC).

Cell culture. Human stromal fibroblasts were purchased from PromoCell (Heidelberg, Germany) and propagated using Dulbecco's Modified Eagle Medium (Biochrom, Berlin, Germany) supplemented with 20% fetal bovine calf serum (FBS-Superior, Biochrom Berlin, Germany), and 10 Units/ml Penicillin/0,1 mg/ml Streptomycin (PAN Biotech). Conditions included 37 °C, CO_2 5%, with medium changes every second to third day. Medium changes were suspended during subsequent experiments – detailed below. Cells were subcultured at 80–90% confluence, using 0.05% trypsin/0.02% ethylenediaminetetraacetic acid (EDTA) (PAN Biotech, Aidenbach, Germany). Morphological cell assessment was performed using phase-contrast microscopy (Olympus CKX41, Olympus, Germany).

pH value measurement. ONRC (RESORBA CELL) and ORC (TABOTAMP) hemostats were sliced into 1 × 1 cm sections using a sterile scissor (Aesculap AG, Tuttlingen, Germany). Sections were placed in normal saline (NaCl 0.9%) to study whether there was a difference in the acidifying behavior of the hemostats. To better imitate *in vivo* conditions, fibroblasts were seeded into 12-well plates (Greiner Bio-One, Solingen, Germany) and sections were placed in culture medium (total volume: 3 ml). The pH-value was measured at baseline and hourly for the first 1–6 hours, with further measurements being performed at 12 h, 48 h, 96 h, 144 h, 192 h, 240 h, 288 h and 336 h using a pH meter (FiveEasy™Profi-Kit 20 ATC, MettlerToledo, Gießen, Germany).

Cell proliferation. As described above, hemostat sections were placed in the medium of fibroblasts (4×10^3) seeded in 12-well plates (Greiner Bio-One, Solingen, Germany). After 7 and 14 days, total cell number was measured using the WST-1 proliferation assay (Roche Life Scientific; Penzberg, Germany) according to the manufacturer's instructions. Briefly, all culture media was removed and replaced by 450 µl of fresh medium, supplemented with 50 µl of WST-1 reagent. After incubation for 2 h, the supernatant was mixed at 500 rpm for 3 min using an orbital shaker (IK-Schüttler MTS4, IKA-Werke GmbH, Staufen, Germany). An aliquot of 100 µl of the supernatant was measured at 450 nm by microplate reader (Victor X4, PelkinElmer, Massachusetts, USA). Mean daily proliferation was calculated using the difference in total cell number between measuring points divided by days of cultivation.

Matrix contraction. Fibroblasts at 10×10^6 cells/ml were seeded in a collagen I matrix (5 mg/ml rat tail collagen 1, ibidi GmbH, Planegg, Germany). The concentration of collagen I in the matrix was set to 1.5 mg/ml. During gelation, the mixture was pipetted into 24-well plates (Greiner Bio-One, Solingen, Germany) and supplemented with culture medium to a final volume of 300 µl. Mixtures were then placed in a cell culture incubator (HERAcell240, Heraeus, Hanau, Germany) for 30 minutes. 1 × 1 cm hemostat slices were placed in the supernatant and an additional 2 ml of culture medium were added.

After 24 h, the adherent matrices were gently detached using a sterile spatula and photographed (ChemiDoc MP Imaging System, Bio Rad-Laboratories, Hercules, California, USA). Matrices were placed in the incubator for 48 h, with images obtained at 24 and 48 h. Matrix surface area was calculated using Axio Vision 40 × 64 V 4.9.1.0. (Carl Zeiss Microscopy GmbH, Jena, Germany).

Cell migration. Fibroblasts ($3{,}5 \times 10^3$) suspended in a volume of 70 µl were placed in both chambers of a µ- dish insert (ibidi GmbH, Planegg, Germany) and incubated (37 °C, 5% CO_2) for 24 h. The insert was removed using a sterile tweezer (Aesculap AG, Tuttlingen, Germany) and 1 × 1 cm hemostat slices together with 3 ml of culture medium were added. The µ- dishes were placed under a live-cell-imaging microscope (JuLI Br, NanoEnTek, Seoul, Korea) for 24 h, taking 1 picture per hour and documented the gap between the two cell fractions. Picture analysis was performed using Wound Healing Image Analysis, WimScratch (ibidi GmbH, Planegg, Germany).

Hemostat-based pH effects. In order to identify the cellular effects resulting from post-degradation hemostat end-products, we lowered the pH of cell culture medium of controls to the pH value of ONRC (medium pH 6.6) or ORC (medium pH 7.0). We imitated pH values obtained over time, matching values for the experiments described above for each measuring point independently, utilizing a 5N HCL solution (Merck, Grafing, Germany). Differences in pH value of less than 10% for each measuring point were considered acceptable.

Statistical analysis. The data are shown as the mean ± SD. Statistical analysis was performed using GraphPad Prism 6.0 (San Diego CA, USA). Kolmogorov–Smirnov test was used to test for the normality of data. One way ANOVA and multiple t-test with Bonferroni correction was used to compare differences between ORC, ONRC and controls (ORC, ONRC and buffered controls) in a time course for normally distributed data. Kruskal-Wallis test with Dunn's post test and Mann–Whitney U test were applied for not normally distributed data. The level of significance was set to $p < 0.05$.

References

1. Ploeg, A. J., Lardenoye, J.-W. P., Peeters, M.-P. F. M. V., Hamming, J. F. & Breslau, P. J. Wound complications at the groin after peripheral arterial surgery sparing the lymphatic tissue: a double-blind randomized clinical trial. *Am. J. Surg.* **197,** 747–751 (2009).
2. Lawlor, D. K. *et al.* The role of platelet-rich plasma in inguinal wound healing in vascular surgery patients. *Vasc Endovasc. Surg* **45,** 241–245 (2011).
3. Exton, R. J. & Galland, R. B. Major groin complications following the use of synthetic grafts. *Eur. J. Vasc. Endovasc. Surg.* **34,** 188–190 (2007).
4. Jeschke, M. G., Sandmann, G., Schubert, T. & Klein, D. Effect of oxidized regenerated cellulose/collagen matrix on dermal and epidermal healing and growth factors in an acute wound. *Wound Repair Regen.* **13,** 324–331 (2005).
5. Hillenbrand, M., Taeger, C. D., Al-Muharrami, A., Arkudas, A. & Horch, R. E. Vakuum-Instillation zur Therapie chronisch infizierter Wunden. *Gefässchirurgie* **20,** 365–369 (2015).
6. Reinke, J. M. & Sorg, H. Wound repair and regeneration. *Eur. Surg. Res.* **49,** 35–43 (2012).
7. Singer, A. J. & Clark, R. a. F. Cutaneous Wound Healing. *N. Engl. J. Med.* **341,** 738–746 (1999).
8. Schäfer, M. & Werner, S. Cancer as an overhealing wound: an old hypothesis revisited. *Nat. Rev. Mol. Cell Biol.* **9,** 628–638 (2008).
9. Werner, S. & Grose, R. Regulation of wound healing by growth factors and cytokines. *Physiol. Rev.* **83,** 835–870 (2003).
10. Baum, C. L. & Arpey, C. J. Normal cutaneous wound healing: clinical correlation with cellular and molecular events. *Dermatol. Surg.* **31,** 674–686; discussion 686 (2005).
11. Gupta, N. *et al.* Randomized trial of a dry-powder, fibrin sealant in vascular procedures. *J. Vasc. Surg.* **62,** 1288–1295 (2015).
12. Pierce A., Wilson, D. & Wiebkin, O. Surgicel: macrophage processing of the fibrous component. *Int. J. Oral Maxillofac. Surg.* **16,** 338–345 (1987).
13. Lewis, K. M. *et al.* Comparison of regenerated and non-regenerated oxidized cellulose hemostatic agents. *Eur. Surg.-Acta Chir. Austriaca* **45,** 213–220 (2013).
14. Dan Dimitrijevich, S. *et al. In vivo* degradation of oxidized, regenerated cellulose. *Carbohydr. Res.* **198,** 331–341 (1990).
15. Keshavarzi, S., MacDougall, M., Lulic, D., Kasasbeh, A. & Levy, M. Clinical experience with the surgicel family of absorbable hemostats (oxidized regenerated cellulose) in neurosurgical applications: a review. *Wounds a Compend. Clin. Res. Pract.* **25,** 160–167 (2013).
16. Spotnitz, W. D. & Burks, S. Hemostats, sealants, and adhesives III: a new update as well as cost and regulatory considerations for components of the surgical toolbox. *Transfusion* **52,** 2243–2255 (2012).
17. Spotnitz, W. D. & Burks, S. Hemostats, sealants, and adhesives: components of the surgical toolbox. *Transfusion* **48,** 1502–1516 (2008).
18. Spangler, D. *et al. In vitro* antimicrobial activity of oxidized regenerated cellulose against antibiotic-resistant microorganisms. *Surg. Infect.* (*Larchmt*). **4,** 255–262 (2003).
19. Pierce, A. M., Wiebkin, O. W. & Wilson, D. F. Surgicel: its fate following implantation. *J. Oral Pathol.* **13,** 661–670 (1984).
20. Guerra, R. R., Kriazhev, L., Hernandez-Blazquez, F. J. & Bateman, A. Progranulin is a stress-response factor in fibroblasts subjected to hypoxia and acidosis. *Growth Factors* **25,** 280–285 (2007).
21. Froehlich, J. E. & Anastassiades, T. P. Role of pH in fibroblast proliferation. *J. Cell. Physiol.* **84,** 253–260 (1974).
22. Akyol, N. & Akpolat, N. Effects of intraoperative oxidated regenerated cellulose on wound healing reaction after glaucoma filtration surgery: a comparative study with Interceed and Surgicel. *Indian J. Ophthalmol.* **56,** 109–114 (2008).
23. Liu, S.-A. *et al.* Effect of oxidized regenerated cellulose on the healing of pharyngeal wound: an experimental animal study. *J. Chin. Med. Assoc.* **75,** 176–182 (2012).
24. Varkey, M., Ding, J. & Tredget, E. E. Fibrotic remodeling of tissue-engineered skin with deep dermal fibroblasts is reduced by keratinocytes. *Tissue Eng. Part A* **20,** 716–727 (2014).
25. Hart, J. *et al.* The role of oxidised regenerated cellulose/collagen in wound repair: effects *in vitro* on fibroblast biology and *in vivo* in a model of compromised healing. *Int. J. Biochem. Cell Biol.* **34,** 1557–1570 (2002).
26. Rassu, P. C., Serventi, A., Giaminardi, E., Ferrero, I. & Tava, P. Use of oxidized and regenerated cellulose polymer in oncoplastic breast surgery. *Ann. Ital. Chir.* **84** (2013).
27. Krishnan, L. K., Mohanty, M., Umashankar, P. R. & Lal, A. V. Comparative evaluation of absorbable hemostats: advantages of fibrin-based sheets. *Biomaterials* **25,** 5557–5563 (2004).
28. Ibrahim, M. M. *et al.* Myofibroblasts contribute to but are not necessary for wound contraction. *Lab. Invest.* **95,** 1429–1438 (2015).

Acknowledgements

This work was supported by a research grant from the Deutsche Forschungsgemeinschaft (WA 3583/2-1 to MU Wagenhäuser).

Author Contributions

W.M. and M.J. planned the experiments and drafted the manuscript. W.M. participated in study conception and design, wrote the main manuscript text and prepared the figures. W.M. contributed to data analysis and interpretation. W.M. also performed the statistical analysis. M.J. participated in data collection and carried out experiments. M.J. contributed to data analysis and helped writing the methods section of the manuscript. M.J. also helped with statistical analysis. I.W. contributed to establish different assays and participated in the design of the study. I.W. also contributed to data interpretation and data collection. S.J. revised the data critically and helped with data interpretation and analysis. S.J. performed language editing of the manuscript. S.F. and S.H. conceived of the study, contributed to the study conception and design and revised the data critically. S.F. helped with the statistical analysis and participated in data interpretation and analysis. O.A. contributed to the study conception and design. O.A. also participated in coordinating several experiments and helped to interpret the data. O.A. also revised the data critically. O.A. and M.W. have the overall responsibility of the manuscript. All authors have read and finally approved the manuscript.

Additional Information

Competing financial interests: The authors declare no competing financial interests.

How to cite this article: Wagenhäuser, M. U. *et al.* Oxidized (non)-regenerated cellulose affects fundamental cellular processes of wound healing. *Sci. Rep.* **6**, 32238; doi: 10.1038/srep32238 (2016).

Clinical research

Time-dependent effects of cellulose and gelatin-based hemostats on cellular processes of wound healing

Markus U. Wagenhäuser[1], Waseem Garabet[1], Mia van Bonn[1], Wiebke Ibing[1], Joscha Mulorz[1,2], Yae Hyun Rhee[1], Joshua M. Spin[2], Christos Dimopoulos[1], Alexander Oberhuber[1], Hubert Schelzig[1], Florian Simon[1]

[1]Department of Vascular and Endovascular Surgery, Heinrich-Heine University Düsseldorf, Düsseldorf, Germany
[2]Stanford Cardiovascular Institute, Stanford University School of Medicine, Stanford, CA, USA

Submitted: 13 March 2019
Accepted: 21 July 2019

Arch Med Sci
DOI: https://doi.org/10.5114/aoms.2020.92830

Corresponding author:
Dr. Markus Udo Wagenhäuser
Department of Vascular and Endovascular Surgery
Heinrich-Heine University Düsseldorf
Moorenstrasse 5
40225, Düsseldorf, Germany
E-mail: markus.wagenhaeuser@freenet.de

Abstract

Introduction: Oxidized regenerated cellulose-based (ORC – TABOTAMP), oxidized non-regenerated cellulose-based (ONRC – RESORBA CELL), and gelatin-based (GELA – GELITA TUFT-IT) hemostats are commonly used in surgery. However, their impact on the wound healing process remains largely unexplored. We here assess time-dependent effects of exposure to these hemostats on fibroblast-related wound healing processes.
Material and methods: Hemostats were applied to fibroblast cell cultures for 5–10 (short-), 30 and 60 min (intermediate-) and 24 h (long-term). Representative images of the hemostat degradation process were obtained, and the pH value was measured. Cell viability, apoptosis and migration were analyzed after the above exposure times at 3, 6 and 24 h follow-up. Protein levels for tumor necrosis factor α (TNF-α) and transforming-growth factor β (TGF-β) were assessed.
Results: ORC and ONRC reduced pH values during degradation, while GELA proved to be pH-neutral. Hemostat structural integrity was prolonged for GELA (vs. ORC and ONRC). TGF-β and TNF-α levels were reduced for ORC and ONRC (vs. GELA and control) ($p < 0.05$). Further, exposure of ORC and ONRC for longer than 5-10 min reduced cell viability vs. GELA and control at 3 h post-exposure ($p < 0.05$). Similarly, cell migration was impaired with ORC and ONRC exposure longer than 60 min at 24 h follow-up ($p < 0.05$).
Conclusions: Short-term exposure to ORC and ONRC impairs relevant wound healing-related processes in fibroblasts, and alters protein levels of key mediating cytokines. GELA does not show similar effects. We conclude that GELA may be preferred over ORC and ONRC over short-, intermediate- and long-term exposures. Future validation of the clinical relevance is warranted.

Key words: hemostats, wound healing, fibroblast, exposure, cell migration, cell proliferation, gelatin, cellulose, cytokine.

Introduction

Hemostats are commonly used to control suture-hole and minor parenchymatous bleeding in all fields of surgery. As such, a wide range of materials has been introduced [1, 2]. Among these, cellulose-based hemostats (CBH) and gelatin-based hemostats (GBH) are well estab-

lished and have revealed similar practicality and functionality [3–5].

Originating from polymerized glucopyranose, oxidized cellulose is fabricated in a multi-step process, generating polyuronic acid as the main structural compound through the oxidation of cellulose fibers [6]. This process makes the materials biodegradable by the human body through β-elimination and enzymatic degradation [7]. In contrast to non-regenerated cellulose, the regenerated form consists of continuous fibers with a more defined ultrastructure [8].

Gelatin is a well-established hemostatic agent and was first introduced in the 1940s. Gelatin is generated by acid partial hydrolysis from porcine-derived collagen, forming a hydrocolloid [9]. Since the implementation of the first GBH, minimal product evolution has occurred [10]. Gelatin foams can expand up to 200% and are capable of absorbing as much as 40 times their weight, which can limit their practicality in specific clinical settings [11].

Given that these hemostats are often left at the application side following hemostasis or may only be applied for short time, it is important to consider the impact of different exposure times on the local wound healing process.

Wound healing is a complex sequence of inflammation, proliferation and matrix remodeling involving various cell types [12–14]. Of these, activated fibroblasts play a pivotal role, as they synthesize an early-stage collagen-rich matrix and then differentiate to myofibroblasts to create a wound-closing tensile force [14, 15]. Therefore, fibroblast proliferation and migration are imperative to ensure physiological wound healing after surgery [16].

There is controversy as to whether hemostats interfere with post-surgical wound healing, with some evidence showing that degradation end-products might interfere with cellular sub-processes [17,18]. As the application time of hemostats during surgery might vary from several minutes, up to weeks in those cases in which the material is left *in situ*, this study explores how the application time of oxidized regenerated cellulose-based (ORC), oxidized non-regenerated cellulose-based (ONRC) and GBH (GELA) alters fibroblast migration, metabolic activity and apoptosis. Further, this study analyzes changes in pH values over a 24 h time course and explores alterations of key mediating cytokines which are essential for physiological wound healing.

Material and methods

Hemostats

RESORBA CELL (RESORBA Medical GmbH, Nuremberg, Germany) (ONRC), TABOTAMP (Ethicon, Norderstedt, Germany) (ORC) and GELITA TUFT-IT (GELITA Medical, Eberbach Germany) (GELA) were used in this study. Hemostats were applied to the supernatant of fibroblast cell cultures for 5–10 minutes (min) (short-term), 30 and 60 min (intermediate-term) and continuously for 24 hours (h) (long-term).

Cell culture

Human stromal fibroblasts (PromoCell GmbH, Heidelberg, Germany) were cultivated in Dulbecco's Modified Eagle Media (DMEM) (Biochrom GmbH, Berlin, Germany) supplemented with 20% fetal bovine calf serum (Biochrom Berlin, Germany) and 10 U/ml Penicillin/Streptomycin (PAN Biotech GmbH, Aidenbach, Germany). Fibroblasts were cultured at 37°C and CO_2 5% (HERAcell240, Heraeus, Hanau, Germany) with regular media exchange. At 90% confluence, cells were sub-cultured using 0.05% trypsin/0.02% ethylenediaminetetraacetic acid (EDTA) (PAN Biotech GmbH, Aidenbach, Germany). Passages 3 to 9 were used for experiments. Morphological cell assessment was performed using phase-contrast microscopy (Olympus CKX41, Olympus, Shinjuku, Japan).

Hemostat degradation and pH value measurement

To visualize the degradation process, hemostat sections (1 × 1 cm) were placed in 3 ml of physiological saline solution (NaCl 0.9%) (B. Braun Melsungen AG, Melsungen, Germany) or fibroblast culture media (Invitrogen/Thermo Fisher Scientific, Waltham MA USA) for 24 h. The pH value was measured at baseline, after 5, 30 and 60 min, and then hourly for the first 6 h, with additional measurements at 12 and 24 h using a pH meter (FiveEasy Profi-Kit 20 ATC, MetlerToledo, Gießen, Germany). Representative images at given time points were taken using a Discovery.V8 SteREO microscope (Carl Zeiss, Oberkochen, Germany) and/or Olympus XC10 Camera (Olympus, Shinjuku, Japan) at 30× magnification.

Enzyme-linked immunosorbent assay

Enzyme-linked immunosorbent assay (ELISA) for TGF-β (DY 240) and TNF-α (DY 210) were performed on fibroblast lysates according to the manufacturer's instructions (R&D Systems, Minnesota, USA). Briefly, fibroblast cell cultures were exposed to hemostats for the stated exposure times. Next, hemostats and cell culture media were removed, and fibroblast cell cultures washed 3 times with ice-cold phosphate-buffered saline (dPBS, Invitrogen/Thermo Fisher Scientific, Waltham MA USA). Next, cell lysates were generated using RIPA buffer supplemented

with protease inhibitor cocktail (Sigma-Aldrich, Taufkirchen, Germany). Protein concentration was measured utilizing BCA-Assay (Pierce/Thermo Fisher Scientific, Waltham MA USA). Optical density was measured using a microplate reader (Victor X4, Perkin Elmer, Massachusetts, USA) with wavelengths 450 nm/570 nm.

Cell metabolic activity

Fibroblasts (1×10^5 cells/well) were seeded into a 24-well plate (Greiner Bio-One, Solingen, Germany). Hemostats were sliced into 0.5 × 0.5 cm pieces to ensure constant material input and added to the supernatant. Fibroblast cell cultures were exposed to hemostats for the stated exposure times. Thereafter, cell culture media were replaced to equal volumes. Cell metabolic activity was measured using MTT (3-(4,5-dimethylthiazol-2-yl)-2,5-diphenyltetrazolium bromide) proliferation assay (Carl Roth GmbH & Co, Karlsruhe, Germany) according to the manufacturer's instructions at baseline and after 3, 6 and 24 h of incubation. Cell culture medium was replaced with 400 µl of a 1 : 9 mixture of MTT stock solution at 5 mg/ml in dPBS (Carl Roth GmbH & Co, Karlsruhe, Germany) and culture medium. After 2 h of incubation, cells were lysed using 200 µl of 2-Propanol. Measurements were performed at a wavelength of 570 nm using a microplate reader (Victor X4, Perkin Elmer, Massachusetts, USA).

Cell migration

Suspended fibroblasts were added to both chambers of a µ-dish insert (ibidi GmbH, Planegg, Germany) and incubated for 24 h. After cell attachment, the insert was removed, and fresh culture medium was added. Hemostats were sliced into 1 × 1 cm pieces and transferred to the supernatant for 5–10, 30 and 60 min, and 24 h. After exposure, slices were removed, and culture medium was exchanged at the same volume. Representative images were taken at baseline and after 3, 6 and 24 h using a light microscope (JuLI Br, NanoEnTek, Seoul, Korea). The analysis of the images was performed using TScratch (2008, T. Gebäck and M. Schulz, ETH Zürich).

Apoptosis assay

Fibroblast apoptosis was studied using a caspase-3/7 assay following the manufacturer's instructions (Promega, Mannheim, Germany). In short, fibroblasts were exposed to hemostats for the stated exposure times, and 100 µl of Luciferase-Mix was added. Then, the mix was incubated at room temperature for 1 h. Luciferase activity was measured using a microplate reader (Victor X4 (PerkinElmer, Massachusetts, USA).

Statistical analysis

Data are presented as mean ± SEM. Analysis was performed using GraphPad Prism 6.0 (San Diego CA, USA). Iglewicz and Hoaglin's two-sided robust test was used to identify outliers and the modified *z*-score was set to 3.5. The Kolmogorov-Smirnov test was used to test for normality and 2-way ANOVA with 2-stage step-up method of Benjamini, Krieger and Yekutieli was used to test for significance. The significance level was set to $p < 0.05$.

Results

Throughout the 24 h observation period, ORC and ONRC induced lower pH values when compared to GELA and the control. ONRC more strongly acidified cell culture medium when compared to ORC (Figures 1 A, B). Specifically, both ORC and ONRC reduced pH values within 30 min in physiological saline, while GELA showed no effect on pH value when compared to control. Notably, beyond 30 min after application of ORC and ONRC the pH value stabilized (Figure 1 A). Evaluating pH values in cell culture medium, which contains substantial buffering capacity, we found that both ORC and ONRC again caused acidosis, albeit milder when compared to effects in saline. Again, GELA did not change pH values when compared to the control. After two hours of exposure, pH values started trending towards an alkaline milieu for all groups due to lower atmospheric carbon dioxide concentration (vs. incubator), suggesting no further release of acidic groups (Figure 1 B). When studying the degradation process at a macroscopic level, we observed other differences between the three hemostats. Faster degradation of ONRC compared to ORC was found after 3 h, while minimal residual material was observed after 24 h for both ORC and ONRC. Changes in pH values for both ORC and ONRC were reflected in the marked color changes of the cell culture medium. Notably GELA did not appear to degrade over time, and showed prolonged structural integrity over a 24 h time period (Figure 1 C).

Next, we analyzed protein levels of TGF-β and TNF-α in response to hemostat exposure, given that they are key mediators for physiologic wound healing. We found that 6 h of hemostat exposure decreased TGF-β levels for ORC and ONRC significantly when compared to GELA and/or control, but this effect was not sustained to the level of statistical significance after 24 h (Figure 2 A). In contrast, TNF-α levels were decreased with ONRC exposure after 6 h and for both ORC and ONRC after 24 h of exposure (Figure 2 B). Notably, GELA did not significantly alter TGF-β or TNF-α levels at any time point (Figures 2 A, B).

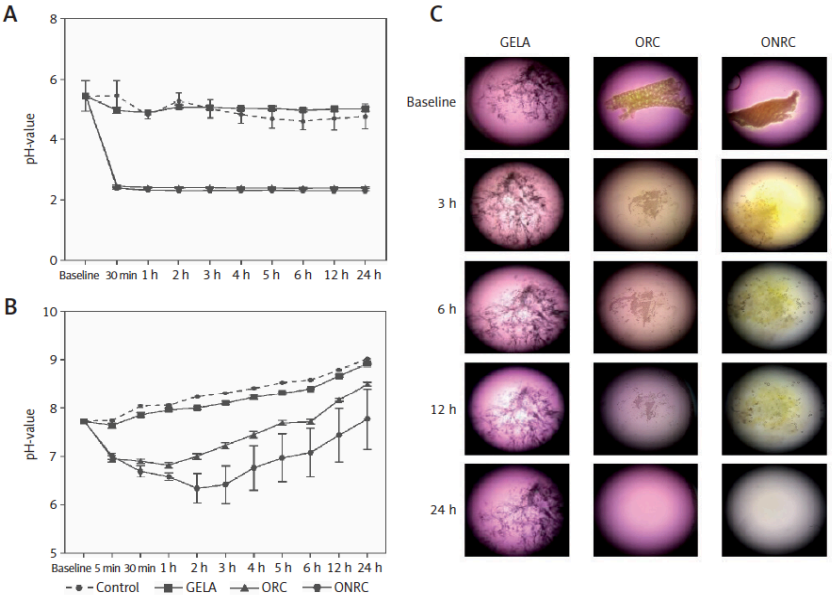

Figure 1. pH values and hemostat degradation. **A, B** – pH values over a 24 hour time course for GELA, ORC and ONRC in saline (**A**) and cell culture medium (**B**). Recognize the immediate drop in pH value for ORC and ONRC. ONRC creates a lower pH value during the investigation period in cell culture medium vs. ORC and GELA. GELA mimicked pH values of controls in saline and cell culture medium (n = 6 samples/time point). **C** – Representative light microscopy images of GELA, ORC and ONRC after 3, 6, 12, and 24 hours (h) in cell culture medium. GELA was dyed with blue ink for visualization. Note the color change of the medium indicating change in pH value. Also note the structural integrity of GELA after 24 h vs. completely degraded ORC and ONRC. Original magnification: 30× (n = 6)

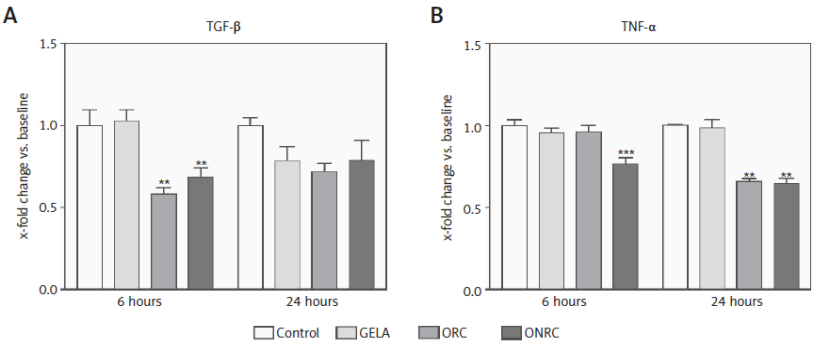

Figure 2. Cytokine protein levels. Fibroblast cell cultures were exposed to hemostats for 6 and 24 hours (h). Protein levels of TGF-β (**A**) and TNF-α (**B**) were analyzed from cell lysates. ORC and ONRC reduced TGF-β levels after 6 h, while protein levels normalized after 24 h of exposure (**A**). ONRC reduced TNF-α levels after 6 and 24 h, while ORC reduced TNF-α levels after 24 h (**B**). No differential regulation vs. control was observed for GELA (**A** and **B**). $^{**}p < 0.05$ ORC and/or ONRC vs. control and GELA; $^{***}p < 0.05$ ONRC vs. control, GELA and ORC. Two-way ANOVA with 2-stage step-up method of Benjamini, Krieger and Yekutieli was applied (q = 0.05, n = 4–5 samples/time point)

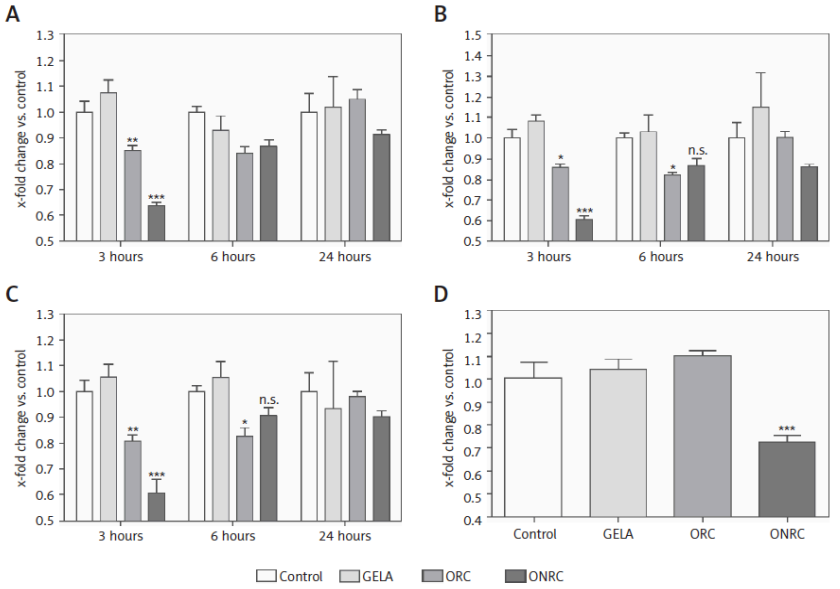

Figure 3. MTT-cellular metabolic activity assay for fibroblast cell cultures with different hemostat exposure times. Data are normalized to controls. Human stromal fibroblasts were exposed to hemostats placed in their medium for 5–10 (**A**), 30 (**B**), or 60 minutes (min) (**C**) or continuously over 24 hours (h) (**D**). Cell metabolic activity was analyzed using an MTT assay after 3, 6 and 24 h. Reduced cellular metabolism was observed for both ORC and ONRC (vs. GELA and controls) at 5–10 and 60 min of hemostat exposure after 3 h (**A** and **C**). ONRC showed reduced cellular metabolism vs. control, GELA and ORC after 5–10, 30 and 60 min hemostat exposure after 3 h (**A–C**). This effect was maintained with continuous hemostat exposure for 24 h (**D**). Two-way ANOVA with 2-stage step-up method of Benjamini, Krieger and Yekutieli was applied (q = 0.05). No difference in cellular metabolism was found for GELA vs. control at any given exposure time. *$p < 0.05$ ORC vs. GELA; **$p < 0.05$ ORC vs. control and GELA; ***$p < 0.05$ ONRC vs. control, GELA and ORC (n = 8–12/group)

We then evaluated how different exposure times interfere with metabolic activity and migration of fibroblasts. Fibroblasts were exposed to hemostats for short- (5–10 min), intermediate- (30 and 60 min) and long-term (24 h) periods. We observed significantly reduced signal intensity during short- and intermediate-term exposure with ONRC after 3 h and with ORC after 3 h and 6 h follow-up when compared to GELA and/or control. At 24 h follow-up of the short- and intermediate-term exposures, no differences between the study groups were observed, suggesting a transient reduction of metabolic activity during ONRC and ORC exposure (Figure 3 A–C). Notably, only ONRC reduced metabolic fibroblast activity after continuous exposure for 24 h (Figure 3 D), while no changes were observed during GELA exposure at any exposure time for any follow-up time point when compared to controls (Figures 3 A–D).

Analyzing fibroblast migration over a pre-defined gap/area between two cell fractions, we found that none of the hemostats interfered with migration after short-term exposure (Figure 4 A). In comparison, intermediate- and/or long-term exposure with ORC and/or ONRC inhibited fibroblast migration at 24 h follow-up, although shorter follow-up time points revealed no effects (Figures 4 B–D). Notably, ONRC more strongly inhibited cell migration when compared to ORC for the aforementioned exposure times (Figures 4 B, C), while GELA had no impact on fibroblast migration during any given exposure period or follow-up time point (Figures 4 A–D).

We found no relevant cell apoptosis differences in response to exposure with either ORC, ONRC or GELA vs. control (Suppl. Figure 1).

Discussion

In this study we investigated the impact of different exposure times of CBH (ORC and ONRC) and GBH (GELA) on wound healing. Short-term exposure to CBH reduced cellular metabolic activity, while long-term exposure impaired cell migration.

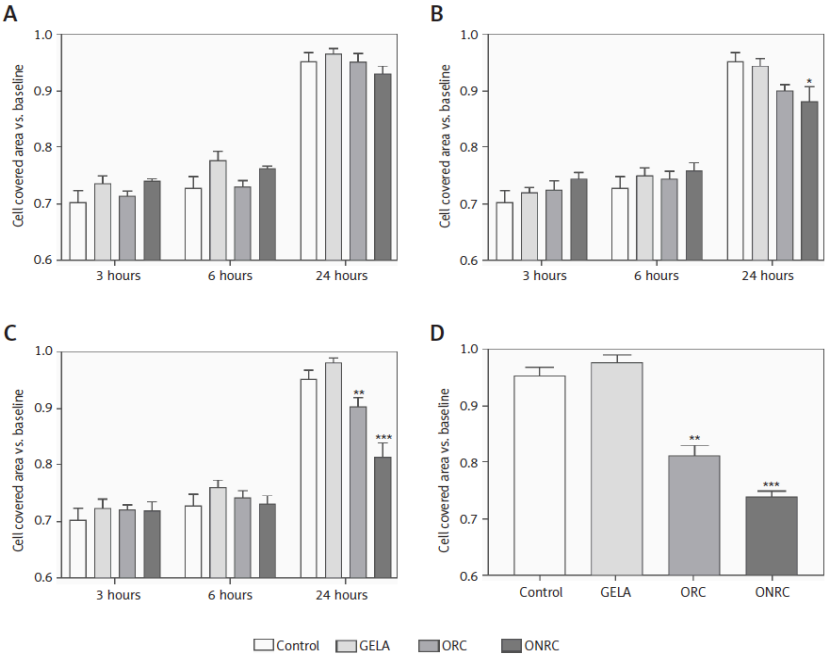

Fig. 4. Fibroblast migration time course after different exposure times to hemostats. Human stromal fibroblasts were placed in both chambers of a µ-dish insert. After removal of the µ-dish insert the area between the cell fractions was measured at baseline. Hemostats were applied to the cell culture medium for 5–10 (**A**), 30 (**B**), or 60 minutes (min) (**C**) or continuously over 24 hours (h) (**D**). The area between the two cell fractions was measured after 3, 6 and 24 h from representative images. Impaired cell migration was observed for ORC/ONRC vs. GELA/control and for ORC vs. ONRC for 60 min and 24 h of exposure (**C** and **D**). *$p < 0.05$ vs. control; **$p < 0.05$ vs. control and GELA; ***$p < 0.05$ vs. control, GELA and ORC. Two-way ANOVA with 2-stage step-up method of Benjamini, Krieger and Yekutieli was applied ($q = 0.05$, $n = 5–7$/experimental group)

None of these unfavorable effects were observed during GBH exposure. Coincidently, CBH also acidified the local environment and altered protein levels of TGF-β and TNF-α, both key mediators of physiological wound healing [19].

Hemostats provide conformability and convenient handling, leading to these materials being integrated into daily surgical routine. As of today, there are multiple different products available, characterized by material-specific attributes. There is long-standing clinical experience with CBH and GBH, with both providing effective hemostasis and biodegradability. Despite many similarities, their mode of action differs [20, 21]. In particular, ORC and ONRC are thought to directly promote platelet activation and aggregation, forming a gel-like clot, while GBH is considered to anchor fibrinogen on the nano-rough material surface while simultaneously enhancing capillary effects [8, 22, 23]. Aside their different mode of action, hemostatic agent costs were 28–56% lower for CBH compared with other adjunctive hemostats, suggesting a major impact on overall treatment costs [24]. Indeed, current purchasing costs for GBH (GELA) appear to be higher compared with CBH (TABOTAMP > RESORBA CELL).

Our results suggest that CBH release acid groups during degradation, while GBH is pH neutral. For that reason, it might be expected that GBH lacks the anti-bacterial properties of CBH [25]. Since both CBH and GBH are bio-absorbable, they may change essential cellular wound healing processes at the site of application. Given that the application time of hemostats during surgery may or may not be limited to several minutes, we explored the impact of short-, intermediate- and long-term exposure of CBH and GBH on relevant cellular processes for physiological wound healing.

Our group and others have previously demonstrated that CBH (ORC and/or ONRC) materials cause rapid local acidosis during degradation due

to the absence of buffer-acting serum components [26, 27]. Consistent with previous findings, this study found that ONRC caused the strongest decline of pH values during degradation, as frayed and less condensed fibers form a larger surface area, leading to more rapid release of acidic groups [27]. In contrast, GELA proved to be pH neutral and maintained prolonged structural integrity over 24 h. Our findings seem plausible, since reported time frames for complete degradation *in vivo* vary from 14 days up to 5 weeks for CBH, while the same process may take as long as 4-6 weeks for GBH and may be accelerated und standardized in *in vitro* conditions [28–30].

Lan *et al.* demonstrated that local acidosis can reduce cell metabolic activity, adhesion capacity and protein synthesis in cultured human gingival fibroblasts and described these effects as being reversible when pH values are re-adjusted to physiological conditions [31]. Similar observations have been reported for different cell types when exposed to an extracellular acidic milieu [32, 33]. The findings of the present study reveal that short-term exposure to ORC and/or ONRC significantly reduces cell metabolic activity at 3 h post-exposure, while intermediate-term and long-term exposure reduced metabolic activity at 6 h and/or 24 h, respectively. Our results do suggest that the reduction of metabolic activity for short- and intermediate-term exposure times with CBH is transient. However, GBH does not interfere with cell metabolic activity at all. Since metabolic activity is imperative for the initiation of physiological wound healing, including recruitment of various cell types and the formation of a provisional wound matrix, we conclude that GBH might be preferable when compared with CBH with regard to this endpoint [12, 34].

Along with proliferation, cell migration is crucial during the proliferative phase of physiological wound healing, as it enables the formation of granulation tissue at the side of injury [35]. Our results suggest that intermediate-term and long-term exposure to CBH impairs the migratory activity of fibroblasts at 24 h post-exposure. An association with local acidosis seems likely, since Kruse *et al.* demonstrated that acidic extracellular environments can impair fibroblast migration [36]. Transferring this functional finding to a cell signaling level, there is evidence that extracellular acidosis beyond the physiological range may activate mitogen-activated protein kinase (MAPK) signaling, which has shown to be involved in the regulation of cell migration [37, 38]. Given this, future experiments using targeting of MAPK signaling could help to validate our *in vitro* findings. For now, we again conclude that GBH might be preferred over CBH with regard to preserving fibroblast migration.

Of interest, our data suggest that some differences in functional findings may not devolve solely from acidosis, which is known to occur during CBH degradation. Our group recently found that CBH degradation end products might also cause functional alterations in migration and proliferation in fibroblasts as well as matrix contraction after exposure for 1–2 weeks [27]. Some of the phenotypic findings might have resulted from marked changes in wound healing-relevant cytokine levels. TGF-β signaling is involved in cardiovascular and pulmonary diseases [39, 40]. Denton *et al.* emphasized the significance of TGF-β for physiological wound healing using a mouse model of type II TGFbeta receptor (TbetaRII) deletion in fibroblasts [41]. The present study suggests that, in contrast to GBH, CBH can reduce TGF-β protein levels in fibroblasts. Of interest, non-canonical intracellular TGF-β signaling might link reduced TGF-β levels upon CBH exposure to impaired fibroblast migration. In particular, it has been demonstrated that non-Smad depended signaling is able to activate the Erk MAPK pathway, which in turn interferes with cell migration [38]. Since our findings reveal delayed impaired fibroblast migration during intermediate- and long-term CBH exposure at late follow-up time points, the authors propose that evolutionarily conserved canonical TGF-β-induced Smad-signaling with interposed protein might also be critical for the findings of the present study [42–44]. Notably, short-term acidosis, such as that caused by CBH exposure, has shown to be sufficient to induce TGF-β-induced signaling [37].

Apart from TGF-β, the importance of TNF-α for physiological wound healing has been elucidated in various studies, as it promotes inflammatory leukocyte recruitment into the wounded tissues and enhances fibroblast proliferation/growth both *in vitro* and *in vivo* [45–48]. Our results indicate that CBHs can reduce intracellular TNF-α protein levels after 6 h and 24 h exposure. As a side point, these reductions in TNF-α levels might have contributed to reduced metabolic activity, which in turn serves as an indirect marker for the proliferative capacity of fibroblasts. Although reduced TNF-α levels in an acidic environment upon CBH exposure might seem contradictory at first glance, Riemann *et al.* also found that exposing rat kidney fibroblasts to acidic cell culture medium decreases TNF-α levels [37]. Further, since TGF-β is pivotal for the control of cell proliferation simultaneously decreased levels of TNF-α and TGF-β might have also substantially contributed to the observed impaired metabolic activity, linking the varying cytokine levels during CBH and GBH exposure to our functional findings [49, 50].

Our study has several limitations. First, we studied the effects of hemostat exposure in a mono-

cellular *in vitro* model using stromal fibroblasts, which does not sufficiently mimic wound healing *in vivo,* as several different interacting cell types are involved. Further, the regulation of cell migration and metabolic activity through TGF-β and/or TNF-α has not been directly addressed using pathway inhibitors. Thus, a direct association between the altered cytokine levels and functional findings remains hypothetical. Lastly, it is unclear to what extent our findings are of clinical relevance, as neither experimental animal models nor human trials were part of this study.

In conclusion, this study found that ORC and ONRC (CBH) in contrast to GELA (GBH) impair essential cellular processes of physiological wound healing *in vitro* in fibroblasts even after short-term exposure. Decreased protein levels of TGF-β and TNF-α in response to ORC and ONRC exposure suggest that these effects may be cytokine-related. We conclude that GELA (GBH) might be more beneficial for physiological wound healing after surgery, although verification of the clinical relevance of these findings is required.

Acknowledgments

The study was supported by a Research Grant from Deutsche Gesellschaft für Gefässchirurgie und Gefässmedizin to MU Wagenhäuser.

Conflict of interest

All authors who are affiliated with the Department of Vascular and Endovascular Surgery, Heinrich-Heine University Düsseldorf, Germany and Alexander Oberhuber participated in the "GELITA Medical Gelatin Hemostat Postmarket Registry" (Registry-ID: 2016116001).

References

1. Baumann P, Schumacher H, Hüsing J, Luntz S, Knaebel HP. A randomized, controlled, prospective trial to evaluate the haemostatic effect of Lyostypt versus Surgicel in arterial bypass anastomosis: "COBBANA" trial. Trials 2009; 10: 91.
2. Sawada T, Nishizawa H, Nishio E, Kadowaki M. Postoperative adhesion prevention with an oxidized regenerated cellulose adhesion barrier in infertile women. J Reprod Med 2000; 45: 387-9.
3. Zoucas E, Göransson G, Bengmark S. Comparative evaluation of local hemostatic agents in experimental liver trauma: a study in the rat. J Surg Res 1984; 37: 145-50.
4. Coln D, Horton J, Ogden ME, Buja LM. Evaluation of hemostatic agents in experimental splenic lacerations. Am J Surg 1983; 145: 256-9.
5. Chvapil M, Owen JA, DeYoung DW. A standardized animal model for evaluation of hemostatic effectiveness of various materials. J Trauma 1983; 23: 1042-7.
6. Dimitrijevich SD, Tatarko M, Gracy RW, et al. In vivo degradation of oxidized, regenerated cellulose. Carbohydr Res 1990; 198: 331-41.
7. Pierce AM, Wiebkin OW, Wilson DF. Surgicel: its fate following implantation. J Oral Pathol 1984; 13: 661-70.
8. Martina B, Kateřina K, Miloslava R, Jan G, Ruta M. Oxycellulose: Significant characteristics in relation to its pharmaceutical and medical applications. Adv Polym Technol 2009; 28: 199-208.
9. Vyas KS, Saha SP. Comparison of hemostatic agents used in vascular surgery. Expert Opin Biol Ther 2013; 13: 1663-72.
10. Sundaram CP, Keenan AC. Evolution of hemostatic agents in surgical practice. Indian J Urol 2010; 26: 374-8.
11. Echave M, Oyagüez I, Casado MA. Use of Floseal®, a human gelatine-thrombin matrix sealant, in surgery: a systematic review. BMC Surg 2014; 14: 111.
12. Reinke JM, Sorg H. Wound repair and regeneration. Eur Surg Res 2012; 49: 35-43.
13. Schäfer M, Werner S. Cancer as an overhealing wound: an old hypothesis revisited. Nat Rev Mol Cell Biol 2008; 9: 628-38.
14. Baum CL, Arpey CJ. Normal cutaneous wound healing: clinical correlation with cellular and molecular events. Dermatol Surg 2005; 31: 674-86.
15. Grinnell F. Fibroblasts, myofibroblasts, and wound contraction. J Cell Biol 1994; 124: 401-4.
16. Bainbridge P. Wound healing and the role of fibroblasts. J Wound Care 2013; 22: 407-8, 410-12.
17. Jeschke MG, Sandmann G, Schubert T, Klein D. Effect of oxidized regenerated cellulose/collagen matrix on dermal and epidermal healing and growth factors in an acute wound. Wound Repair Regen 2005; 13: 324-31.
18. Cullen B, Watt PW, Lundqvist C, et al. The role of oxidised regenerated cellulose/collagen in chronic wound repair and its potential mechanism of action. Int J Biochem Cell Biol 2002; 34: 1544-56.
19. Behm B, Babilas P, Landthaler M, Schreml S. Cytokines, chemokines and growth factors in wound healing. J Eur Acad Dermatol Venereol 2012; 26: 812-20.
20. Hutchinson RW, George K, Johns D, Craven L, Zhang G, Shnoda P. Hemostatic efficacy and tissue reaction of oxidized regenerated cellulose hemostats. Cellulose 2013; 20: 537-45.
21. Wolkow N, Jakobiec FA, Yoon MK. Gelatin-based hemostatic agents: histopathologic differences. Ophthal Plast Reconstr Surg 2018; 34: 452-5.
22. Krízová P, Másová L, Suttnar J, et al. The influence of intrinsic coagulation pathway on blood platelets activation by oxidized cellulose. J Biomed Mater Res A 2007; 82: 274-80.
23. Hajosch R, Suckfuell M, Oesser S, Ahlers M, Flechsenhar K, Schlosshauer B. A novel gelatin sponge for accelerated hemostasis. J Biomed Mater Res B Appl Biomater 2010; 94: 372-9.
24. Martyn D, Meckley LM, Miyasato G, et al. Variation in hospital resource use and cost among surgical procedures using topical absorbable hemostats. Clinicoecon Outcomes Res 2015; 7: 567-74.
25. Spangler D, Rothenburger S, Nguyen K, Jampani H, Weiss S, Bhende S. In vitro antimicrobial activity of oxidized regenerated cellulose against antibiotic-resistant microorganisms. Surg Infect (Larchmt) 2003; 4: 255-62.
26. Dimitrijevich SD, Tatarko M, Gracy RW, Linsky CB, Olsen C. Biodegradation of oxidized regenerated cellulose. Carbohydr Res 1990; 195: 247-56.
27. Wagenhäuser MU, Mulorz J, Ibing W, et al. Oxidized (non)-regenerated cellulose affects fundamental cellular processes of wound healing. Sci Rep 2016; 6: 32238.

28. Charlesworth TM, Agthe P, Moores A, Anderson DM. The use of haemostatic gelatin sponges in veterinary surgery. J Small Anim Pract 2012; 53: 51-6.
29. Weaver FA, Hood DB, Zatina M, Messina L, Badduke B. Gelatin-thrombin-based hemostatic sealant for intraoperative bleeding in vascular surgery. Ann Vasc Surg 2002; 16: 286-93.
30. Chiara O, Cimbanassi S, Bellanova G, et al. A systematic review on the use of topical hemostats in trauma and emergency surgery. BMC Surg 2002; 16: 286-93.
31. Lan WC, Lan WH, Chan CP, Hsieh CC, Chang MC, Jeng JH. The effects of extracellular citric acid acidosis on the viability, cellular adhesion capacity and protein synthesis of cultured human gingival fibroblasts. Aust Dent J 1999; 44: 123-30.
32. Lecocq J, Dambly C. A bacterial RNA polymerase mutant that renders lambda growth independent of the N and cro functions at 42 degrees C. Mol Gen Genet 1976; 145: 53-64.
33. Huang S, He P, Xu D, et al. Acidic stress induces apoptosis and inhibits angiogenesis in human bone marrow-derived endothelial progenitor cells. Oncol Lett 2017; 14: 5695-702.
34. Robson MC, Steed DL, Franz MG. Wound healing: biologic features and approaches to maximize healing trajectories. Curr Probl Surg 2001; 38: 72-140.
35. Kirsner RS, Eaglstein WH. The wound healing process. Dermatol Clin 1993; 11: 629-40.
36. Kruse CR, Singh M, Targosinski S, et al. The effect of pH on cell viability, cell migration, cell proliferation, wound closure, and wound reepithelialization: In vitro and in vivo study. Wound Repair Regen 2017; 25: 260-9.
37. Riemann A, Ihling A, Thomas J, Schneider B, Thews O, Gekle M. Acidic environment activates inflammatory programs in fibroblasts via a cAMP-MAPK pathway. Biochim Biophys Acta 2015; 1853: 299-307.
38. Huang C, Jacobson K, Schaller MD. MAP kinases and cell migration. J Cell Sci 2004; 117 (Pt 20): 4619-28.
39. Shao S, Fang H, Duan L, et al. Lysyl hydroxylase 3 increases collagen deposition and promotes pulmonary fibrosis by activating TGFβ1/Smad3 and Wnt/β-catenin pathways. Arch Med Sci 2018; 24: 8592-601.
40. Kulach A, Dabek J, Wilczok T, Gasior Z. Changes in transforming growth factor β; and its receptors' mRNA expression in monocytes from patients with acute coronary syndromes. Arch Med Sci 2010; 6: 526-32.
41. Denton CP, Khan K, Hoyles RK, et al. Inducible lineage-specific deletion of TbetaRII in fibroblasts defines a pivotal regulatory role during adult skin wound healing. J Invest Dermatol 2009; 129: 194-204.
42. Simeone DM, Zhang L, Graziano K, et al. Smad4 mediates activation of mitogen-activated protein kinases by TGF-beta in pancreatic acinar cells. Am J Physiol Cell Physiol 2001; 281: C311-9.
43. Olsson N, Piek E, Sundström M, ten Dijke P, Nilsson G. Transforming growth factor-beta-mediated mast cell migration depends on mitogen-activated protein kinase activity. Cell Signal 2001; 13: 483-90.
44. Zhang YE. Non-Smad pathways in TGF-beta signaling. Cell Res 2009; 19: 128-39.
45. Mast BA, Schultz GS. Interactions of cytokines, growth factors, and proteases in acute and chronic wounds. Wound Repair Regen 1996; 4: 411-20.
46. Liu JY, Brass DM, Hoyle GW, Brody AR. TNF-alpha receptor knockout mice are protected from the fibroproliferative effects of inhaled asbestos fibers. Am J Pathol 1998; 153: 1839-47.
47. Ortiz LA, Lasky J, Hamilton RF, et al. Expression of TNF and the necessity of TNF receptors in bleomycin-induced lung injury in mice. Exp Lung Res 1998; 24: 721-43.
48. Battegay EJ, Raines EW, Colbert T, Ross R: TNF-alpha stimulation of fibroblast proliferation. Dependence on platelet-derived growth factor (PDGF) secretion and alteration of PDGF receptor expression. J Immunol 1995; 154: 6040-7.
49. Huang SS, Huang JS. TGF-beta control of cell proliferation. J Cell Biochem 2005; 96: 447-62.
50. Clark RA, McCoy GA, Folkvord JM, McPherson JM. TGF-beta 1 stimulates cultured human fibroblasts to proliferate and produce tissue-like fibroplasia: a fibronectin matrix-dependent event. J Cell Physiol 1997; 170: 69-80.

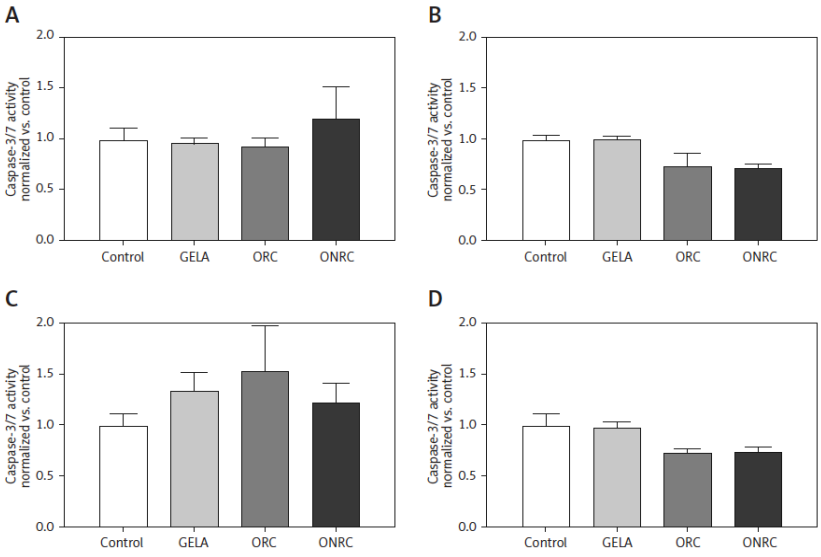

Suppl. Fig. 1. Fibroblast caspase-3/7 activity after different exposure times to hemostats. Human stromal fibroblasts were exposed to hemostats placed in their medium for 5–10 (**A**), 30 (**B**), or 60 minutes (min) (**C**) or continuously over 24 hours (h) (**D**). Caspase-3 and -7 activity was analyzed as an indirect measurement for apoptosis. None of the applied hemostats caused significant apoptosis at the given exposure times (**A–D**). Two-way ANOVA with 2-stage step-up method of Benjamini, Krieger and Yekutieli was applied (q = 0.05, *n* = 5–7/experimental group)

ORIGINAL ARTICLES

J VASC ENDOVASC SURG 2015;22:163-70

Preliminary results of transcutaneous oxygen pressure measurement as effective monitoring for conservative therapy in peripheral occlusive disease

M. U. WAGENHÄUSER, M. DURAN, P. DUEPPERS, M. WITTE, H. SCHELZIG, A. OBERHUBER

Department of Vascular and Endovascular Surgery University Hospital Düsseldorf, Düsseldorf, Germany

Aim. **Lower limb peripheral arterial occlusive disease (PAOD) is an increasing problem in Western countries. In critical limb ischaemia (CLI) amputation rate and mortality is high. If an operative or interventional approach is not feasible, conservative options remain. We questioned whether lumbar sympatholysis and prostaglandin E1 infusion therapy influence transcutaneous oxygen pressure (TcPO2) to evaluate short-term effectiveness of these therapies.**

Methods. **Fourteen people with an average age of 64±11 years, suffering from PAOD Rutherford stage V and VI, and treated from June 1, 2013 to June 31, 2014, were included in the study. TcPO2 levels were measured at 3 different time points during prostaglandin E1 infusion therapy. Electrodes were placed at a proximal (PMP) and a distal (DMP) measuring point on the affected legs. A Regional Perfusion Index (RPI) was calculated separately for both measuring points to consider the partial pressure of oxygen in systemic arterial blood. If patients underwent lumbar sympathicolysis (LS) between two time points, TcPO2 levels were compared to those without this therapy in the interval. Statistical analysis was performed using the Mann–Whitney U test and P<0.05 was considered statistically significant.**

Results. **Data before therapy was as follows; PMP: 37.5±24.9 mmHg (RPI 0.56±0.34); DMP: 26.8±24.5 mmHg (RPI 0.43±0.38). 5-7 days during therapy; PMP: 44.2±21.7 mmHg (RPI 0.77±0.23; P<0.05); DMP: 17.6±15.9 mmHg (RPI 0.37±0.35). 10-12 days during therapy; PMP: 44.9±15.1 mmHg (RPI 0.69±0.26) DMP: 20±22.1 mmHg (RPI 0.28±0.32). Comparing the intervals with (w) and without (wo) LS, the differences in TcPO2 levels and RPI were as follows: PMP (w): -1.38 mmHg±35.14 (RPI 0.06±0.43); DMP (w): -2 mmHg±16 (RPI -12±0.26); PMP (wo): 1.83 mmHg±30.07 (RPI: 0.03±0.37); DMP (wo): -5 mmHg±20 (RPI -0.04±0.34). 12 of 14 patients presented with raised C-reactive protein (CRP) levels, 3.8 (mg/dL)±6.1 on admission.**

Conclusion. **Data leads to the conclusion that the RPI is more accurate than the absolute TcpO2 levels. A measuring point about 10 cm proximal to the lesion could be more effective as TcpO2 levels next to the lesion may be overestimated due to hyperperfusion caused by local infection. Data suggests that LS may not have an influence on TcPO2 levels.**

KEY WORDS: Blood gas monitoring, transcutaneous - Arterial occlusive diseases - Therapy - Alprostadil - Infusions, intravenous.

Lower limb peripheral arterial occlusive disease (PAOD) represents a huge problem in Western Countries.[1] The cost for health care systems are alarming.[2] Critical limb ischemia (CLI) is defined as the presence of ischemic rest pain requiring analgesia for more than two weeks, or either ulceration or gangrene of the lower extremity with an ankle systolic blood pressure <50 mmHg and/or toe systolic pressure <30 mm Hg.[3] One-year mortality rate of patients with CLI is approximately 25%, 2-year mortality rate is 45%, respectively and increases up to 45% if patients have undergone amputation.[4-7] There are patients for whom interventional or surgical approaches are not feasible.[8] Here, prostanoids

Corresponding author: M. U. Wagenhäuser, Department of Vascular and Endovascular Surgery, Moorenstrasse 5, 40225 Düsseldorf, Germany. E-mail: markus.wagenhaeuser@med.uni-duesseldorf.de

have shown to be effective in promoting the healing of skin lesions, and reducing the risk of amputations as their pharmacologic actions include inhibition of activation, adhesion and aggregation of platelets, vasodilatation, vascular endothelial cytoprotection, inhibition of leucocyte activation, and antithrombotic and profibrinolytic activities.[9-13] Another therapeutic option in patients with CLI is CT-guided lumbar sympathicolysis (LS), which has already demonstrated its effectiveness and might even be advantageously combined with intravenous prostaglandin E1 infusion therapy.[14] A measurable parameter to confirm the success of these therapies might be the transcutaneous oxygen pressure (TcPO2).

For this reason, we analysed the TcPO2 levels of patients with CLI during prostaglandin E1 infusion therapy and LS, to determine the short-term effectiveness of intravenous prostaglandin E1 infusion therapy and LS. In this observational study we monitored the TcPO2 levels of patients before and during intravenous prostaglandin E1 infusion therapy at two different measuring points to investigate whether measuring point locations influence TcPO2 levels. Some patients also underwent LS during infusion therapy, and we investigated whether this intervention may have additional effects on TcPO2 levels.

Materials and methods

Data collection

Data collection was performed as a preliminary observational study in the context of a modified protocol of the routinely conducted TcPO2 measurements as quality control during intravenous prostaglandin E1 infusion therapy. The study was approved by the local ethic committee and any informed consent from human subjects was obtained as required.

The study included the legs of 14 people with an average age of 64±11 years suffering from advanced PAOD Rutherford stage V and VI, and treated from June 1 2013 to June 31 2014. PAOD was caused by atherosclerosis in 13 patients, 1 patient suffered from Buerger's disease. Patient characteristics and data from their hospital stay was analysed from archived medical records. All patients underwent open operation and/or interventions prior to intravenous prostaglandin E1 infusion therapy. Reviewing the medical records of the patient cohort 5 years prior to admission, 10 patients underwent interventional therapy with percutaneous transluminal angioplasty, 7 patients underwent open surgery, respectively. Thus, 3 patients underwent both therapies. Table I gives an overview of comorbidities and previous interventions/open surgery. Within the investigation period all measurements were performed consecutively.

Inclusion criteria

Patients had to be at least 18 years old. All patients included were known in the department for at least 5 years and were seen by senior physicians in our outpatient department prior to therapy. We included patients who suffered from advanced PAOD Rutherford stage V and VI. Chronic ulceration had to persist for at least 6 weeks prior to presentation. Site and kind of ulcer are outlined in Table I. Based on their medical history, current vascular status and general condition, endovascular and operative approaches to improve peripheral blood supply were not feasible. Exclusion criteria for peripheral bypass surgery were as follows: lack of available peripheral arterial outflow based on angiography; high perioperative risk and poor general condition. Reasons for not revascularizing interventionally were documented failure of the latest interventional revascularization attempt, inauspicious success due to a disseminated pattern of disease with technical unsuitability for angioplasty and missing consent to interventional therapy. The decision about admission for prostaglandin E1 infusion therapy was taken by senior physicians in our outpatient department. Patients had to agree with elective hospital admission and intravenous prostaglandin E1 infusion therapy over a period of at least 12 days. LS was possible on some patients as additional treatment during infusion therapy. Thus, the last LS had to be at least 6 months previous, and patients needed to agree to this therapy prior to treatment.

Measuring protocol

TcPO2 levels were recorded at 3 different time points using the Radiometer Medical ApS (Brønshøj, Denmark); before therapy, 5-7 days after therapy started, and 10-12 days after therapy started. Calibration of the transcutaneous sensors was performed according to manufacturer guidelines. Where necessary, skin was prepared with alcohol and hair was shaved before starting the measuring protocol. The

TABLE I.—*Characteristics of the patient cohort.*

		Frequency (%)
Gender		
	Male	28 (93)
	Female	2 (7)
	Male	1 (7)
	Feee	
	Female	13 (92)
Risk factors		
	Hypertension	12 (86)
	Coronary heart disease	9 (64)
	Diabetes mellitus	4 (29)
	Smoking	12 (86)
	Adipositas (BMI>30 kg/m²)	1 (7)
Medical history (PAOD)		
	Preceded interventional therapy	10 (71)
	Iliacal femoral	2 (14)
	Femoral	2 (14)
	Crural	6 (43)
	Preceded open surgery	9 (64)
	Desobliteration femoral	3
	Infragenicular bypass	4
Site and kind of ulcer		
	Site of ulcer	
	Distal foot	7 (50)
	Heel	4 (29)
	Lower leg	3 (21)
	Kind of ulcer	
	Arterial ulcer	13 (93)
	Ulcer mixtum	1 (7)
Clinical presentation		
	Concomitant infection	12 (86)
	No concomitant infection	2 (14)

first sensor attachment to the subject's anterior chest was placed at the midclavicular line approximately 5 cm below the clavicle in a non-bony area. Areas of injury on the skin surface, such as hematomas, were avoided. The second sensor was placed at the distal measuring point (DMP) directly proximal to the lesion at the lower extremity and a third electrode was placed at the proximal measuring point (PMP) 15-20 cm proximal to the second sensor. An equilibration time of 10 to 15 minutes preceded the reading so as to gain stabilized values. Before repositioning of the sensors, recalibration was performed and new double-layer membranes were applied to the sensor. All patients rested in the supine position throughout the measuring protocol to guarantee replicable conditions. Figure 1 illustrates the Radiometer and the sensor positioning. The Regional Perfusion Index (RPI) was calculated to consider partial pressures of oxygen in systemic arterial blood for the DMP and the PMP separately, using the following formula: TcPO2 DMP (PMP)/TcPO2 chest. The differences in TcPO2 levels and RPIs were also analysed separately for the DMP and the PMP. To determine whether LS might have additional effects on TcPO2 levels, the cohort was divided into patients with LS (wLS) and patients who did not undergo this therapy (woLS) in the interval between two measuring points.

Statistical analysis

Graph Pad Prism® Version 5.01 was used to plot graphs and perform analyses. A Wilcoxon matched pairs test was performed to compare TcPO2 levels at the different measuring points. A Mann-Whitney U test was performed to compare the differences in TcPO2 levels and RPIs between the measuring points for patients wLS and woLS in the interval. $P<0.05$ was considered statistically significant.

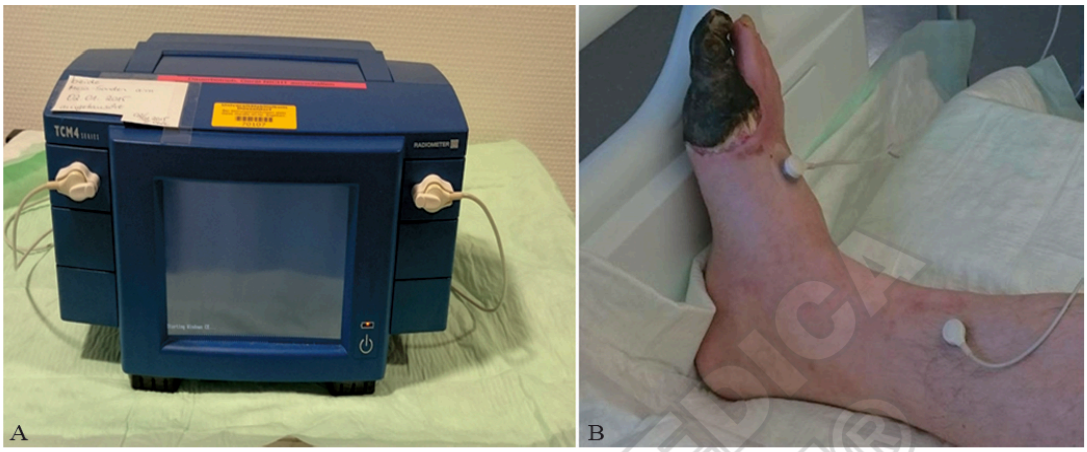

Figure 1.—Radiometer and sensor positioning. A: The Radiometer Medical ApS (Brønshøj, Denmark), used for measuring transcutaneous oxygen pressure (TcPO2). B: The sensor positions used in this study. The first sensor was placed next to the lesion. The second sensor was placed at a distance of 15-20 cm proximal to the lesion. To normalize transcutaneous oxygen pressure by calculating the regional perfusion index a third electrode was placed at the midclavicular line approximately 5 cm below the clavicle in a non-bony area to consider partial pressures of oxygen in systemic arterial blood.

Results

We analyzed the legs of 14 PAOD Rutherford stage V and VI patients altogether. Their mean age was 64±11 years. The cohort consisted of 13 men and 1 woman. 12/14 patients presented on admission with raised C-reactive protein (CRP) levels. Although we started with antibiotics according to the current resistogram, CRP levels before therapy were 3.8 mg/dL±6.1, at day 5-7 4.3 mg/dL±3.9 and at day 10-12 3.5mg/dL±3.5. No other infection focus, such as the urinary or the respiratory tract, was present in any patient on admission.

During prostaglandin E1 infusion therapy 1 major amputation (7%) had to be performed. Thus, no minor amputations were necessary and no heart disease symptoms occurred. However, one patient required emergency surgery during the infusion therapy due to acute ischemia. In this case an attempt with the creation of a femoropedal bypass and local distal desobliteration was performed. We used autologous vein as bypass graft. In due course, 2 days after operative revascularisation an occlusion occurred, and major amputation was necessary.

Data for TcPO2 levels at the three measuring time point were as follows: day 0 37.5±24.9 mmHg for the PMP and 26.8±24.5 mmHg for the DMP; day 5-7 - 44.2±21.7 mmHg for the PMP (P=0.63 *vs.* day 0) and 17.6±15.9 mmHg for the DMP (P=0.05 *vs.* day 0); day 10-12 - 44.9±15.1 mmHg for the PMP (P=0.76 *vs.* day 5-7; P=0.15 *vs.* day 0) and 20±22.1 mmHg (P=0.86 *vs.* day 5-7; P=0.43 *vs.* day 0) for the DMP.

Data for RPI was as follows: day 0 - 0.56±0.34 for the PMP and 0.43±0.38 for the DMP; day 5-7 - 0.77±0.23 for the PMP (P=0.02 *vs.* day 0) and 0.37±0.35 for the DMP (P=0.38 *vs.* day 0); Day 10-12 - 0.69±0.26 for the PMP (P=0.37 *vs.* day 5-7; P=0.19 *vs.* day 0) and 0.28±0.32 for the DMP (P=0.11 *vs.* day 5-7; P=0.52 *vs.* day 0). Figure 2 summarizes these results and illustrates them for TcPO2 levels and RPIs separately.

Altogether, LS was performed at 8 intervals between 2 measuring points (2 between day 0 and day 5-7 and 6 between day 5-7 and day 10-12). Comparing the difference in TcPO2 levels on patients wLS and woLS between two measuring points, data for the PMP was as follows: woLS - 1.83 mmHg±30.01 (RPI 0.03±0.37); wLS - -1.38 mmHg±35.14 P=0.52 (RPI 0.06±0.43 P=0.6). Data for the DMP was as follows: woLS - -5 mmHg±20 (RPI -0.04±0.34); wLS - -2 mmHg±16 P=0.76 (RPI -0.12±0.26 P=0.47). Results are illustrated in Figure 3.

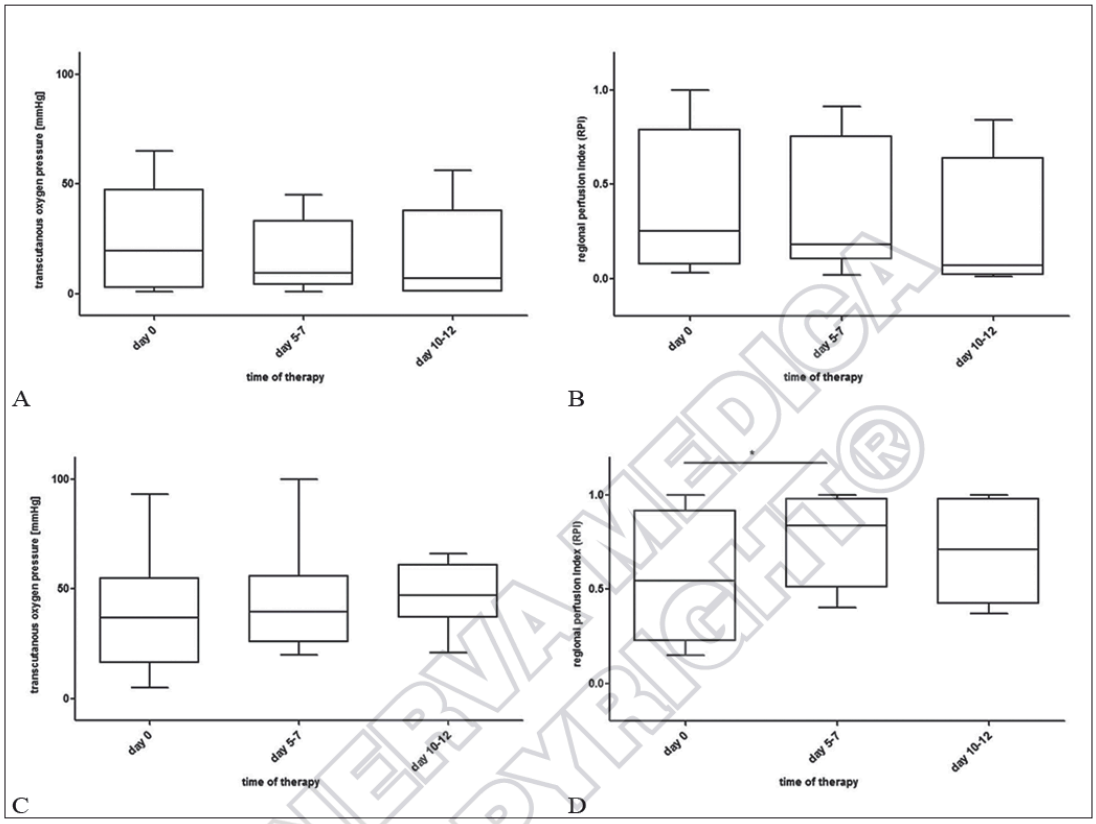

Figure 2.—Transcutaneous oxygen pressure (TcPO2 levels) and regional perfusion index (RPI) during conservative prostaglandin E 1 infusion therapy in Rutherford stage V and VI. TcPO2 levels and RPI are illustrated at different times during therapy. Results are presented separately for the distal (A+B) and proximal (C+D) measuring points. Day 0 and day 5-7: N.=15; day 10-12: N.=12; P<0.05 (Wilcoxon matched pairs test).

Discussion

After the exhaustion of angiographic-interventional and surgical measures in advanced PAOD, limited therapeutic options remain; however, this situation is rare and therefore patient cohorts are small. Prostaglandin E1 has been shown to have a positive impact on rest-pain relief and ulcer healing in CLI as it affects platelet activation and blood clotting, causes a reduction of free radicals and cytokine production and lowers the expression of intercellular adhesion molecules.[15-20] LS proved its clinical benefit in PAOD with an increase in peripheral circulation that persisted even after 6 months.[21] To quantify the beneficial short-term effects of both therapies, we used a Radiometer to record TcPO2 levels and questioned whether sensor positioning in relation to the lesion influences TcPO2 levels.

Measurements of TcPO2 levels have been used in neonates as an indicator of arterial pressure of oxygen but their field of application has increased ever since.[22] Andrews *et al*. reported that this method could help to predict amputation site healing in patients with ischemic wounds,[23] and Deng *et al*. showed that it might be a valuable diagnostic tool for peripheral neuropathy in Type 2 diabetes pa-

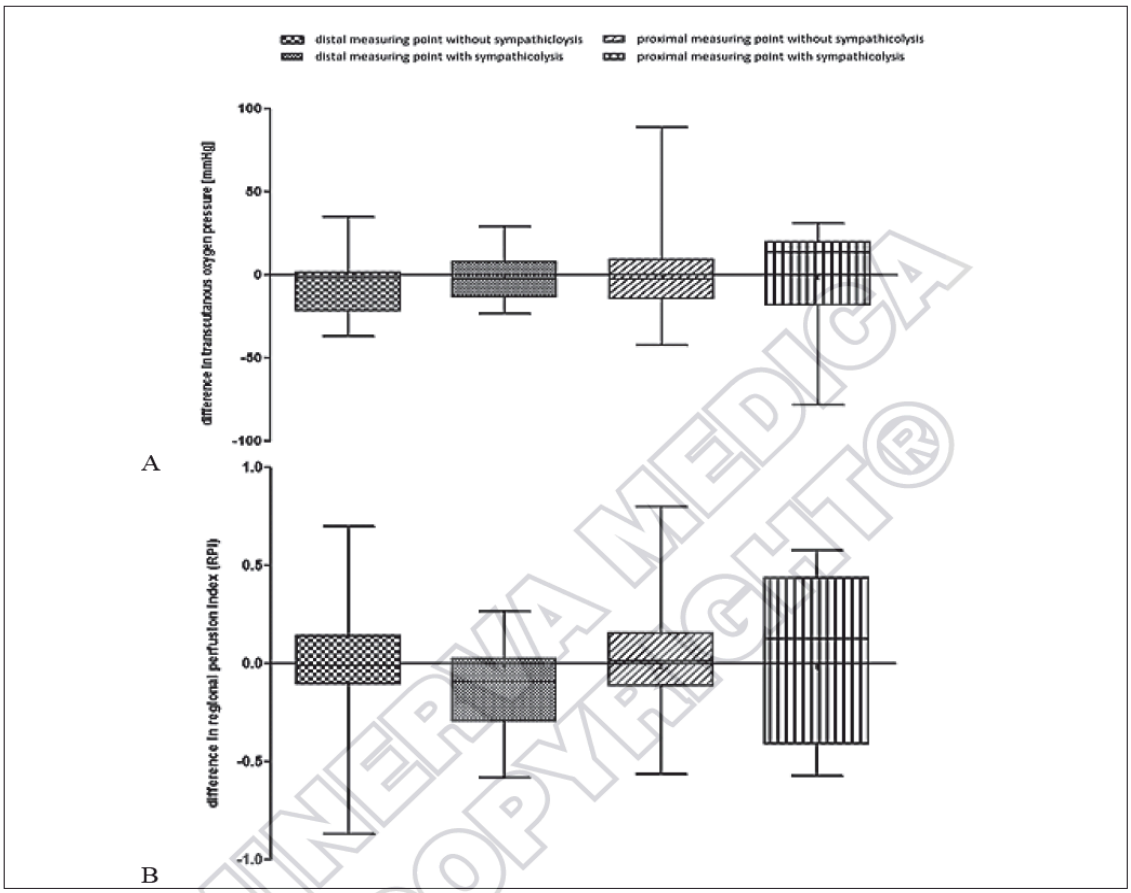

Figure 3.—Differences in transcutaneous oxygen pressure (TcPO2 levels) and regional perfusion index (RPI) between intervals with and without lumbar sympathicolysis (LS). Results are shown for the distal and proximal measuring points. Data is presented as differences in TcPO2 levels and RPI concerning the intervals with (N.=8) and without (N.=18) LS separately. Results were not statistically significant (Mann-Whitney U test).

tients.[24] Wherever used, the basic approach of this non-invasive diagnostic tool is the physiologic assessment of the local microcirculatory status. In the present preliminary observational study it could be demonstrated that its application might be useful as a monitoring tool for conservative therapy in advanced PAOD.

Interestingly, the sensor positioned next to the lesion in PAOD Rutherford stage V and VI showed a decline in TcPO2 levels during therapy, whereas contrary results were observed for a sensor positioned 10 cm proximal to the lesion. The increase was significant during the first week of therapy. To particularly investigate the effect of LS on TcPO2 levels we compared intervals with and without this additional therapy. The beneficial effect of LS could be seen for the PMP, as the DMP again showed contrary results. Here, the results did not reach statistical significance. What comprehensible explanation might there be for contrary data on the PMP and the

DMP, which is even more significant if using the RPI rather than absolute TcPO2 levels?

As most of the patients showed raised levels of inflammatory markers and infection foci different from ulcer could be excluded, we assumed a concomitant infection emanating from ulceration. According to Conheim`s classification there are alterations in the vascular system due to infections. Hence, vasodilatation starts at the arteriole level and progresses to the capillary level and therefore increases local blood flows. The resulting increased local oxygen supply might have led to high TcPO2 levels in the direct surroundings of the ulcer.[25-26] For that reason, these vascular inflammatory changes might be partly responsible for the disproportional high TcPO2 levels at the DMP before and at the beginning of the therapy in this study. After admission all patients received antibiotics to treat local infection. Although inflammatory markers did not decline remarkably during antibiotic therapy, we assumed that concomitant infections were treated effectively. As a consequence antibiotic therapy might counteract above described inflammatory vascular changes, resulting in a vasoconstriction and normalization of the microcirculatory situation. Thus, the disproportional high local oxygen supply would have reduced. This hypothesis might at least partly explain the reduction of TcPO2 levels at the DMP due to antibiotic therapy.

Interestingly, there are other factors which might influence TcPO2 levels and could therefore, at least partly, be responsible for the divergent observations at the measuring points in this study. Falstie-Jensen *et al*. demonstrated that TcPO2 levels differ at various locations on the body, ascribing this effect to the thickness of the epidermis.[27] It cannot be expected that this effect influenced data in this study as data was not normalized to the thickness of the epidermis; however the authors believe that the impact might be low. Rodriguez *et al*. could demonstrate that hypothermia also affects TcPO2 levels,[28] however, the effect is limited and the authors performed experiments in the same room, where it should be presumed that temperature did not differ remarkably between different measurements.

We believe that a sensor positioning 10 cm proximal to the lesion might deliver more reliable results as TcPO2 levels increase during therapy. This senor position might therefore be more reliable for quantification of short-term benefits of both therapies. As the minority of patients with PAOD Rutherford stage V and VI are not feasible for revascularization it is difficult to achieve sufficient statistical power. However, we would suggest using this sensor position for monitoring in future studies, even though these results are preliminary due to the small study cohort and must to be verified with greater statistical power.

Conclusions

This preliminary study demonstrates that measurements of TcPO2 levels during prostaglandin E1 infusion therapy occasionally combined with LS in PAOD Rutherford stage V and VI could be used effectively to monitor short-term effects, if a sensor position at some distance to the lesion is used. As the power of this study is limited, we will verify these results on a larger study cohort to correlate objective measuring data with clinical outcomes.

References

1. Daskalopoulou SS, Pathmarajah M, Kakkos SK, Daskalopoulos ME, Holloway P, Mikhailidis DP *et al.* Association between ankle-brachial index and risk factor profile in patients newly diagnosed with intermittent claudication. Circ J 2008;72:441-8.
2. Mundet X, Pou A, Piquer N, Sanmartin MI, Tarruella M, Gimbert R *et al*. Prevalence and incidence of chronic complications and mortality in a cohort of type 2 diabetic patients in Spain. Prim Care Diabetes 2008;2:135-40.
3. Second European Consensus Document on chronic critical leg ischemia. Circulation 1991,84:IV1-26.
4. Criqui MH, Langer RD, Fronek A, Feigelson HS, Klauber MR, McCann TJ, *et al.* Mortality over a period of 10 years in patients with peripheral arterial disease. N Engl J Med 1992;326:381-6.
5. Luther M. The influence of arterial reconstructive surgery on the outcome of critical leg ischaemia. Eur J Vasc Surg 1994;8:682-9.
6. Ebskov B. Relative mortality and long term survival for the non-diabetic lower limb amputee with vascular insufficiency. Prosthet Orthot Int 1999;23:209-16.
7. Thomas AR, Raats JW, Lensvelt MM, de Groot HG, Veen EJ, van der Laan L. Conservative treatment in selected patients with severe critical limb ischemia. World J Surg [Epub ahead of print April 17, 2015].
8. O'Hare AM, Bertenthal D, Sidawy AN, Shlipak MG, Sen S, Chren MM. Renal insufficiency and use of revascularization among a national cohort of men with advanced lower extremity peripheral arterial disease. Clin J Am Soc Nephrol 2006;1:297-304.
9. Balzer K, Bechara G, Bisler H, Clevert HD, Diehm C, Heisig G *et al.* Reduction of ischaemic rest pain in advanced peripheral arterial occlusive disease. A double blind placebo controlled trial with iloprost. Int Angiol 1991;10:229-32.
10. Brock FE, Abri O, Baitsch G, Bechara G, Beck K, Corovic D *et al*. Iloprost in the treatment of ischemic tissue lesions in diabetics. Results of a placebo-controlled multicenter study with a stable prostacyclin derivative. Schweiz Med Wochenschr 1990;120:1477-82 [Article in German].

11. Norgren L, Alwmark A, Angqvist KA, Hedberg B, Bergqvist D, Takolander R *et al*. A stable prostacyclin analogue (iloprost) in the treatment of ischaemic ulcers of the lower limb. A Scandinavian-Polish placebo controlled, randomised multicenter study. Eur J Vasc Surg 1990;4:463-7.
12. Trubestein G, Ludwig M, Diehm C, Gruss JD, Horsch S. Prostaglandin E1 in stage III and IV arterial occlusive diseases. results of a multicenter study. Dtsch Med Wochenschr 1987, 112(24):955-959 [Article in German].
13. Reiter M, Bucek RA, Stumpflen A, Minar E. Prostanoids for intermittent claudication. Cochrane Database Syst Rev 2004:CD000986.
14. Petronella P, Freda F, Nunziata L, Antropoli M, Manganiello A, Cutolo PP,*et al.* Prostaglandin E1 versus lumbar sympathectomy in the treatment of peripheral arterial occlusive disease: randomised study of 86 patients. Nutr Metab Cardiovasc Dis 2004;14:186-92.
15. Brodszky V, Farkas K, Jarai Z, Landi A, Pecsvarady Z, Baji P *et al.* Effectiveness of prostanoids in patients with critical leg ischemia. Orv Hetil 2011;152:2047-55 [Article in Hungarian].
16. de Donato G, Gussoni G, de Donato G, Cao P, Setacci C, Pratesi C *et al*. Acute limb ischemia in elderly patients: can iloprost be useful as an adjuvant to surgery? Results from the ILAILL study. Eur J Vasc Endovasc Surg 2007;34:194-8.
17. Grant SM, Goa KL. Iloprost. A review of its pharmacodynamic and pharmacokinetic properties, and therapeutic potential in peripheral vascular disease, myocardial ischaemia and extracorporeal circulation procedures. Drugs 1992;43:889-924.
18. Mazzone A, Faggioli P, Cusa C, Stefanin C, Rondena M, Morelli B. Effects of iloprost on adhesion molecules and F1 + 2 in peripheral ischemia. Eur J Clin Invest 2002;32:882-8.
19. Della Bella S, Molteni M, Mascagni B, Zulian C, Compasso S, Scorza R. Cytokine production in scleroderma patients: effects of therapy with either iloprost or nifedipine. Clin Exp Rheumatol 1997;15:135-41.
20. Creutzig A, Lehmacher W, Elze M. Meta-analysis of randomised controlled prostaglandin E1 studies in peripheral arterial occlusive disease stages III and IV. Vasa 2004;33:137-44.
21. Nickel J, Brinckmann W, Andresen R. Ambulatory, CT-assisted lumbar sympathicolysis in patients with severe peripheral artery disease: influence on peripheral blood flow and clinical outcome. Zentralbl Chir 2008;133:349-54 [Article in German].
22. Huch R, Huch A, Lubbers DW. Transcutaneous measurement of blood Po2 (tcPo2) -- Method and application in perinatal medicine. J Perinat Med 1973;1:183-91.
23. Andrews KL, Boon AJ, Dib M, LiedL DA, Yacyshyn A, Yacyshyn V. The use of elevation and dependency to enhance the predictive value of transcutaneous oxygen pressure measurements in the assessment of foot amputation healing. PM R 2010;2:829-34.
24. Deng W, Dong X, Zhang Y, Jiang Y, Lu D, Wu Q *et al.* Transcutaneous oxygen pressure (TcPO(2)): a novel diagnostic tool for peripheral neuropathy in type 2 diabetes patients. Diabetes Res Clin Pract 2014;105:336-43.
25. Pober JS, Cotran RS. The role of endothelial cells in inflammation. Transplantation 1990;50:537-44.
26. Conheim J. Über Entzündung und Eiterung. Arch Path Anat Physiol 1867, 40:1-79 [Article in German].
27. Falstie-Jensen N, Spaun E, Brochner-Mortensen J, Falstie-Jensen S. The influence of epidermal thickness on transcutaneous oxygen pressure measurements in normal persons. Scand J Clin Lab Invest 1988;48:519-23.
28. Rodriguez P, Lellouche F, Aboab J, Buisson CB, Brochard L. Transcutaneous arterial carbon dioxide pressure monitoring in critically ill adult patients. Intensive Care Med 2006;32:309-12.

Conflicts of interest.—The authors certify that there is no conflict of interest with any financial organization regarding the material discussed in the manuscript.

Received on March 4, 2015.
Accepted for publication on June 4, 2015.

4.3. Post-thrombotisches Syndrom (PTS)

4.3.1. Zitationen

Wagenhäuser MU, Sadat H, Dueppers P, Meyer-Janiszewski YK, Spin JM, Schelzig H, Duran M. *Open surgery for iliofemoral deep vein thrombosis with temporary arteriovenous fistula remains valuable.* Phlebology. 2018;33(9):600-609.

Wagenhäuser MU, Dimopoulos C, Antakyali K, Meyer-Janiszewski YK, Mulorz J, Ibing W, Ertas N, Spin JM, Schelzig H, Duran M. *Clinical outcomes after direct and indirect surgical venous thrombectomy for inferior vena cava thrombosis.* J Vasc Surg Venous Lymphat Disord. 2019;7(3):333-343.e2.

4.3.2. Spezifische Fragestellung/Methodik

Das PTS ist eine häufige und belastende Komplikation nach einer TVT und beruht kausal auf dysfunktionalem Geweberemodeling der Venenklappen/-wand in betroffenen Segmenten[134]. Die resultierende obstruktiv-fibrotische Widerstandserhöhung im Ausflusstrakt und der damit verbundene insuffiziente Venenklappenschluss führen zu einer venösen Hypertension und bedingen eine Druckübertragung auf das Kapillarbett. Der gesteigerte Kapillardruck erzwingt eine Transsudation von Flüssigkeit und größeren Molekülen, die zur Ausbildung von chronischen Ödemen und schließlich zur Gewebehypoxie mit Ulzerationen führen[56–58]. Dies entspricht einem PTS in schwerer Ausprägung.

Es existieren multiple Faktoren, die zur Entwicklung eines PTS nach einer TVT führen können. So konnte gezeigt werden, dass ein „body-mass index“ (BMI) > 30, eine vorbestehende venöse Insuffizienz sowie ein hohes Lebensalter die Auftretenswahrscheinlichkeit deutlich erhöhen[135–137]. Ein weiterer wesentlichster Prädiktor ist die Lokalisation der TVT. So ist das Risiko ein PTS im Langzeitverlauf zu entwickeln bei einer proximalen Thrombose (Ilikalvenen und/oder der V. femoralis communis), aufgrund fehlender Möglichkeiten der Kollateralisierung gegenüber peripheren Thrombosen (z.B. Thrombose einer Unterschenkelvene) deutlich erhöht[138].

Neben einer Antikoagulation, die zu einer Reduktion der Inzidenz eines PTS nach TVT führt, bestehen additive Maßnahmen einer frühen Thrombusentfernung und Rekanalisation. Diese Ansätze beabsichtigen, die Auftretenswahrscheinlichkeit eines PTS weiter zu reduzieren[139].

Eine dieser Möglichkeiten ist die systemische Thrombolyse, die jedoch ein signifikantes Blutungsrisikos birgt[140]. Demgegenüber erscheint eine lokale Thrombolyse über einen minimal-invasiv eingelegten Katheter im Rahmen einer „catheter-directed thrombolysis“ (CDT) oder eine „pharmacomechanical CDT“ (PCDT) mit zusätzlich mechanischer Disruption des Thrombus sicherer.

Eine weitere, wenngleich im endovaskulären Zeitalter weniger beachtete Alternative, ist die offen-chirurgische Thrombektomie. Die chirurgische Entfernung des Thrombus wird traditionell mit der Anlage einer temporären arterio-venösen Fistel (AV-Fistel) kombiniert, um eine frühe erneute Thrombose betroffener Segmenten zu verhindern[141]. Interessanterweise zeigten auch jüngere Beobachtungen einen den endovaskulären Therapieansätzen mindestens vergleichbaren Therapieerfolg[142]. Prospektive randomisierte Studien, die offene und endovaskuläre Therapieansätze mit einem rein konservativen Vorgehen vergleichen, fehlen bisher.

Es sollte die Effektivität der offen chirurgischen Thrombektomie in Bezug auf Geweberemodeling-assoziierte Zielgrößen, wie die Entwicklung des PTS und die HRQOL untersucht werden. Daher wurden Patienten, die zwischen dem 1. Januar 2004 und 31. Dezember 2015 bzw. zwischen dem 1. Januar 1982 und 31. Dezember 2013 in der Klinik für Gefäß- und Endovaskularchiurgie des Uniklinikums Düsseldorf aufgrund einer iliofemoralen Thrombose (IFDVT) oder einer Thrombose der V. cava inferior (IVCT) offen chirurgisch behandelt wurden, systematisch nachuntersucht.

Patienten mit einer IFDVT und/oder einer IVCT wurden außerdem zu einer detaillierten phlebologischen Nachuntersuchung (DPFE) in der Gefäßambulanz eingeladen, um den venösen Status sowie das Ausmaß bzw. die Schwere eines potentiell vorhandenen PTS durch Sonographie bzw. Erhebung des Villalta score und der „clinical, etiological, anatomical, and pathophysiological“ (CEAP) Klassifikation beurteilen zu können. Mit Hilfe einer Kaplan-Maier-Schätzung wurden darüber hinaus die Überlebens- und/oder Offenheitsraten sowie das Auftreten bzw. die Abstinenz eines PTS im Nachuntersuchungszeitraum abgeschätzt. Außerdem wurden die Patienten gebeten, einen Fragebogen (SF-36) zur Bestimmung der HRQOL auszufüllen, um die gesundheitsbezogene Lebensqualität mit der deutschen Normalbevölkerung zu

vergleichen. Der standardisierte Fragebogen erlaubt, die HRQOL während der vergangenen vier Wochen in 8 Subskalen getrennt voneinander zu bewerten.

4.3.3. Synopsis der Ergebnisse/Diskussion

Tiefe iliofemorale Thrombose (IFDVT)

Es wurden 146 Patienten mit IFDVT im Untersuchungszeitraum behandelt. Eine vollständige medizinische Dokumentation lag für 48 Patienten vor, 26 Patienten folgten der Einladung einer DPFE in der Gefäßambulanz.

Eine Assoziation zwischen der Entwicklung eines PTS und den etablierten Risikofaktoren einer IFDVT und/oder allgemeinen Patientencharakteristika konnte nicht gefunden werden (***Tabelle 1***). Während des Nachuntersuchungszeitraumes traten drei Todesfälle auf. Zwei Patienten (4%) starben an einem Myokardinfarkt, ein Patient (2%) starb an einer Aortendissektion. Es ergaben sich keine prozedural-assoziierten Todesfälle.

Tabelle 1. Patientencharakteristika und Risikofaktoren[a]

	Durchschnitt/ Häufigkeitsverteilung (%)	SEM	Assoziation mit Offenheit *p Wert*	Assoziation mit PTS *p Wert*
Alter	*49*	±2.8	.991	.857
Körpergewicht (kg)	76	±2.5	1.000	.360
Grösse (cm)	172	±1.6	.998	.373
BMI	25	±4	.998	.341
Geschlecht, m/w	11 (42%)/15 (58%)			
betroffenes Bein rechts/links/beide	5 (19%)/18 (69%) /3 (12%)			

	Häufigkeitsverteilung	Prozent	Assoziation mit Offenheit *p Wert*	Assoziation mit PTS *p* value
Fettleibigkeit	2/26	8	.54	.54
Immobilisation	9/26	35	.55	.55
Rauchen	1/26	4	.22	.22
Maligne Erkrkankung	4/26	15	.95	.95
Hyperlipidämie	3/26	12	.77	.77

BMI: body mass index; PTS: post-thrombotisches Syndrom; SEM: Standardfehler des Mittelwerts: kg: Kilogramm; cm: Zentimeter

[a] Die Daten sind als Durchschnittswerte und SEM bzw. als Häufigkeitsverteilung mit absoluter Prozentangabe angegeben. Eine logistische Regressionsanalyse für kontinuierliche Variablen bzw. ein Chi-Quadrat Test mit Yate's Korrektur für dichotome Variablen wurden verwendet, um eine Assoziation mit der Offenheit bzw. dem Auftreten eines PTS nach venöser Thrombektomie zu prüfen. Modifiziert nach Wagenhäuser MU et al. Open surgery for iliofemoral deep vein thrombosis with temporary arteriovenous fistula remains valuable. Phlebology. Oct;33(9):600-609 (2018). (Mit freundlicher Genehmigung von SAGE Publications im Rahmen der „re-use and archiving policies").

Die ein-Jahresüberlebensrate lag bei 93±4%, die acht-Jahresüberlebensrate bei 91±5%. Die primäre Offenheitsrate lag bei 89±5% nach einem und bei 81±7% nach acht Jahren. Die sekundäre Offenheitsrate lag bei 97±3% nach acht Jahren. Nach fünf Jahren waren

100%, nach acht Jahren waren 80±12% der Patienten frei von einem PTS (***Abbildung 15***).

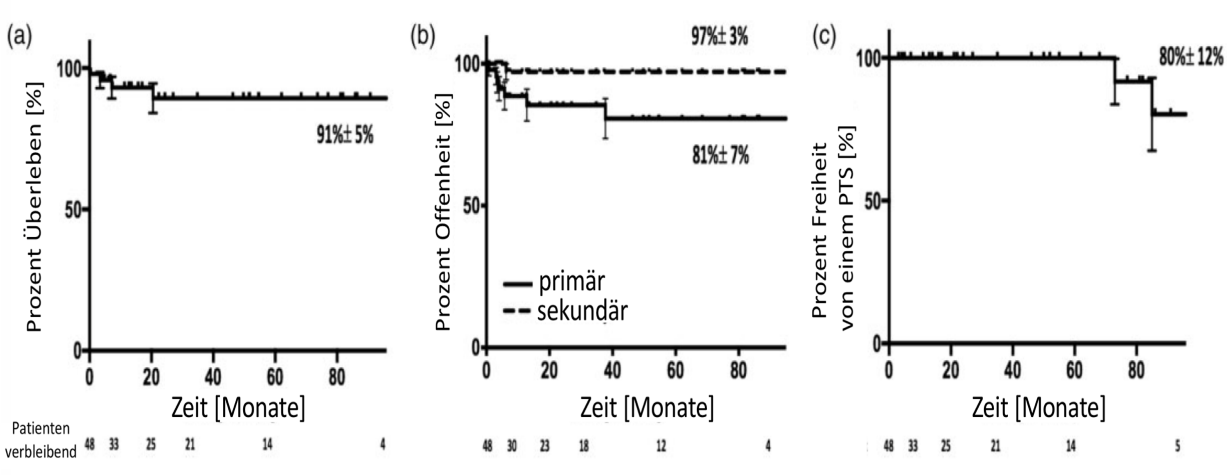

Abbildung 15: Überleben, Offenheit und Freiheit von einem post-thrombotischen Syndrom nach offen chirurgischer Thrombektomie. (a): Kaplan-Meier-Schätzung der Überlebensrate nach offen chirurgischer Thrombektomie. Gezeigt ist die acht-Jahresüberlebensrate. **(b):** Kaplan-Meier-Schätzung der Offenheit nach offen chirurgischer Thrombektomie. Gezeigt sind die primäre und sekundäre Offenheitsrate nach acht Jahren. **(c):** Kaplan-Meier-Schätzung der Freiheit von einem post-thrombotischen Syndrom (PTS). Gezeigt ist die Freiheitsrate nach acht Jahren. Modifiziert nach Wagenhäuser MU et al. *Open surgery for iliofemoral deep vein thrombosis with temporary arteriovenous fistula remains valuable.* Phlebology. Oct;33(9):600-609 (2018). (Mit freundlicher Genehmigung von SAGE Publications im Rahmen der „re-use and archiving policies“).

Tabelle 2. PTS Klassifikationen.[a]

C-Kategorie der CEAP Klassifikation

Klasse 0	Klasse 1	Klasse 2	Klasse 3	Klasse 4	Klasse 5	Klasse 6
13/26	5/26	2/26	2/26	2/26	1/26	1/26
50%	19.2%	7.7%	7.7%	7.7%	3.8%	3.8%
Villalta score						
	kein 0–5 Punkte	mild 5–9 Punkte	mittel 10–14 Punkte	schwer 15 Punkte	–	–
	23/26	1/26	0/26	2/26		
	88.5%	3.8%	–	7.7%		

CEAP: clinical, etiological, anatomical, and pathophysiological classification.

[a] Die Patienten wurden während einer detaillierten phlebologischen Nachuntersuchung (DPFE) untersucht und eine Einstufung gemäß der CEAP Klassifikation vorgenommen bzw. der Villalata score erhoben. Die Ergebnisse sind als Häufigkeitsverteilung mit Prozentangaben dargestellt. Modifiziert nach Wagenhäuser MU et al. Open surgery for iliofemoral deep vein thrombosis with temporary arteriovenous fistula remains valuable. Phlebology. Oct;33(9):600-609 (2018) (Mit freundlicher Genehmigung von SAGE Publications im Rahmen der „re-use and archiving policies“).

Wird keine Kaplan-Meier-Schätzung, sondern eine Bestimmung dieser Zielgröße für das Patientenkollektiv während der DPFE vorgenommen, so zeigt sich eine Rate von 11,5% bei Anwendung des Villalta Scores und von 23% bei Anwendung der C-Kategorie (≥ Klasse 3) der CEAP Klassifikation (***Tabelle 2***).

Um die Schwere eines PTS zu quantifizieren, wird aktuell die Verwendung des Villalta Scores empfohlen[134]. Es existieren Studien, die die Wahrscheinlichkeit einer PTS Entwicklung zwischen 24-53% nach konservativem Vorgehen mit durchgehender Antikoagulation nach zwei-drei Jahren berichten[143–145]. Die CDT und/oder die PCDT sind moderne endovaskuläre Verfahren zur frühen Beseitigung des Thrombus aus der venösen Strombahn. Sie konnten das Auftreten eines moderat-schweren PTS gegenüber einem konservativen Vorgehen verringern, wenngleich die Ergebnisse in prospektiv randomisierten Studien nicht einheitlich sind. Während zum einen von einem Vorteil der CDT gegenüber einem rein konservativen Vorgehen berichtet wird, konnte Gleiches nicht für die PCDT nachgewiesen werden[146,147]. Im Rahmen einer CDT erscheint eine verbesserte Exposition der Plasminogen-Bindungsstellen im Thrombus durch Ultraschallunterstützung zunächst vielversprechend, jedoch ergab sich in einer randomisierten Studie keine Verbesserung ultraschall-assoziierter Parameter und des Patientenoutcomes[148,149]. Eine Meta-Analyse aus drei randomisierten und drei nicht-randomisierten Studien resümierte einen Vorteil der CDT gegenüber der reinen Antikoagulation in Hinblick auf die PTS Inzidenz[150]. Abschließend bleibt demnach nicht geklärt, ob thrombusbeseitigende Maßnahmen einer alleinigen Antikoagulation bezüglich der PTS Entwicklung durch Verringerung der venösen Obstruktion und Erhöhung der Venenklappenkompetenz im Langzeitverlauf tatsächlich überlegen sind. In diesem Zusammenhang sollte auch eine uneinheitliche Verwendung verschiedener PTS Klassifikationen beachtet werden, so dass Vergleiche und Generalisierungen auch aus diesem Grund, schwierig erscheinen. Basierend auf eigenen Ergebnissen erscheint die Wahrscheinlichkeit einer PTS Entwicklung nach offen chirurgischer Thrombektomie modernen interventionellen Ansätzen vergleichbar. Dies entspricht auch Beobachtungen anderer Autoren in der aktuellen Literatur[141]. Bei der Wahl eines geeigneten Therapieverfahrens gilt es in der Güterabwägung mögliche Blutungskomplikationen und die Invasivität einer Behandlung mit zu berücksichtigen[151].

Zusammenfassend ist die offen chirurgische Thrombektomie mit temporärer Anlage einer AV-Fistel im Vergleich mit endovaskulären Ansätzen sicher. Die PTS Inzidenz im Langzeitverlauf ist vergleichbar mit endovaskulären Therapiealternativen. Aufgrund der größeren Invasivität und möglichen prozeduralen Komplikationen verbleibt die offen chirurgische Thrombektomie eine Therapiealternative für selektierte Patienten mit absoluter Kontraindikation zur Lyse und frischer deszendierender IFDVT. Auch bei jungen Patienten mit frischer IFDVT und/oder Phlegmasia coerulea dolens, sowie bei Schwangeren erscheint die offen chirurgische Thrombektomie weiterhin wertvoll[152,153].

Thrombose der Vena cava inferior (IVCT)

Eine isolierte IVCT ist sehr selten und wird zumeist von einer IFDVT begleitet. Das Auftreten von PTS Symptomen wird nach einer IVCT mit bis zu 90%, die Entwicklung eines schweren PTS mit Ulzerationen mit bis zu 15% angegeben[154].

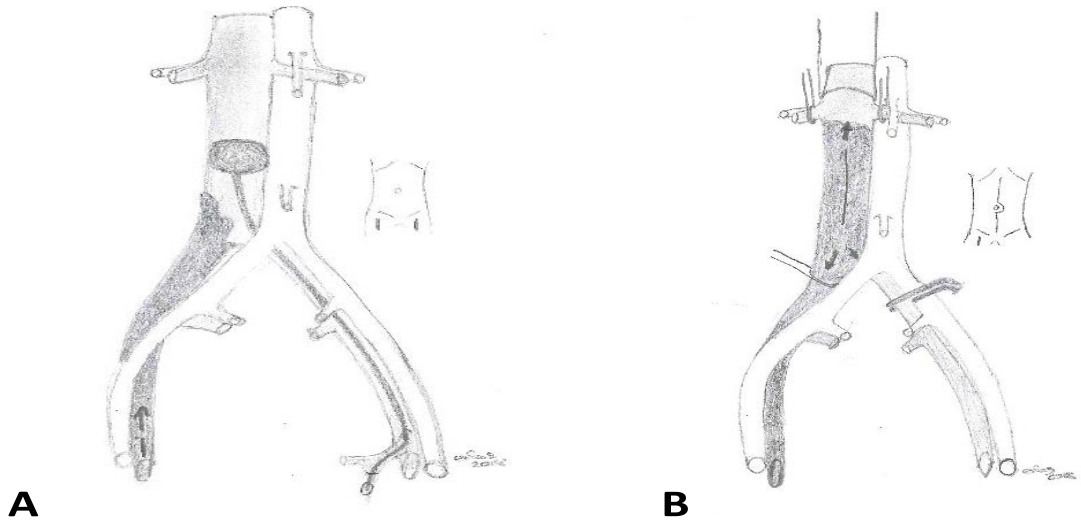

Abbildung 16: Offen chirurgische Therapiealternativen bei einer Thrombose der Vena cava inferior (IVCT). **A:** indirekte transfemorale venöse Thrombektomie (iTFVT). ICVT mit Thrombose der rechten Beckenachse, sowie den Oberschenkelvenen. Beidseitige inguinale Inzision mit Präparation aller relevanten Strukturen. Ein Okklusionsballon wird über die linke Femoralvene proximal der IVCT platziert und geblockt. Nun wird der Thrombus durch Thrombektomiemanöver über die rechte Femoralvene entfernt. Das finale Thrombektomiemanöver erfolgt durch Rückzug des Okklusionsballons über die linke Femoralvene. **B:** direkte offene venöse cavale Thrombektomie (dOVT). Extensive Thrombose der Vena cava bis knapp distal der Nierenvenen. Die Aorta und die Vena cava inferior werden durch mediane Laparatomie exponiert und dargestellt. Der Rückfluss aus den Nierenvenen und der rechten Beckenvene wird durch „Vesse Loops" kontrolliert. Die nicht betroffene Beckenvene wird abgeklemmt. Die Vena cava inferior wird venotomiert. Anschließend werden ante- und retrograde Thrombektomiemanöver mit dem Fogarty-Katheter durchgeführt. Aus Wagenhäuser, M. U. et al. *Clinical outcomes after direct and indirect surgical venous thrombectomy for inferior vena cava thrombosis.* J Vasc Surg Venous Lymphat Disord. May;7(3):333-343.e2 (2019). (Mit freundlicher Genehmigung des Elsevier Verlags im Rahmen der „author rights for suscription articles").

Im Untersuchungszeitrum wurden 180 Patienten mit IVCT identifiziert. Für 152 Patienten lag eine vollständige medizinische Dokumentation vor. Die Patienten wurden entweder durch indirekte transfemorale venöse Thrombektomie (iTFVT) (n=73), direkte offene venöse cavale Thrombektomie (n=35) oder durch eine Kombination der beiden Verfahren versorgt (n=44) (***Abbildung 16***). Nach offen chirurgischer Thrombektomie wurde, analog dem Vorgehen bei IFDVT, eine inguinale AV-Fistel für 3 Monate angelegt.
Die etablierten Risikofaktoren einer IVCT und/oder allgemeine Patientencharakteristika zeigten keine Assoziation mit dem Patientenüberleben, der Offenheit nach chirurgischer Thrombektomie oder der Auftretenswahrscheinlichkeit eines PTS (***Abbildung 17***).

	Patientenkollektiv (N = 152)			phlebologische Nachuntersuchung
Characteristika	**iTFVT (n = 73)**	**dOVT (n = 35)**	**kombiniert (n = 44)**	**(n = 38)**
Alter/ Jahre		42.4 ± 1.4		42.9 ± 2.8
	44.8 ± 2.1	44.8 ± 3	36.5 ± 2.3	
Krankenhausaufenthalt, Tage		12.8 ± 1		10.4 ± 0.7
	12.1 ± 1.7	15.8 ± 2.3	11.8 ± 0.9	
Geschlecht	M: 76/152 (50); F: 76/152 (50)			M: 19/38 (50) F: 19/38 (50)
	M: 33/73 (45.2) F: 40/73 (54.8)	M: 19/35 (54.3) F: 16/35 (45.7)	M: 24/44 (54.5) F: 20/44 (45.5)	
Lungenembolie vor Operation		59/152 (38.8)		17/38 (44.7)
	22/73 (30.1)	14/35 (40)	23/44 (52.3)	
Simultan betroffenes Bein	r: 36/152 (23.7); l: 66/152 (43.4); b: 50/152 (32.9)			r: 9/38 (23.7) l: 20/38 (52.6) b: 9/38 (23.7)
	r: 19/73 (26) l: 38/73 (52) b: 16/73 (22)	r: 9/35 (25.7) l: 14/35 (40) b: 11/35 (31.4)	r: 8/44 (18.2) l: 13/44 (29.5) b: 23/44 (52.3)	
AV-Fistel	ss: 110/152 (72.4); bs: 42/152 (27.6)			ss: 27/38 (71.1) bs: 11/38 (28.9)
	ss: 62/73 (84.9) bs: 11/73 (15.1)	ss: 23/35 (65.7) bs: 12/35 (34.3)	ss: 25/44 (56.8) bs: 19/44 (43.2)	
Antikoagulation, Monate		37.7 ± 6.1		48.2 ± 11.9
	69.4 ± 8.1	32.7 ± 11.6	50 ± 13.6	

	Patientenkollektiv (N = 152)					
				Log Regression		phlebologische Nachuntersuchung
Risikofaktoren	**iTFVT (n = 73)**	**dOVT (n = 35)**	**kombiniert (n = 44)**	**Sterblichkeit**	**Offneheit**	**(n = 38)**
Fettleibigkeit		19/152 (12.5)				
	8/73 (11)	4/35 (11.4)	7/44 (15.9)	.92	.39	6/38 (15.8)
Immobilisation		97/152 (63.8)				
	48/73 (65.8)	21/35 (60)	28/44 (63.6)	.75	.43	23/38 (60.5)
Rauchen		30/152 (19.7)				
	16/73 (21.9)	4/35 (11.4)	10/44 (22.7)	.51	.17	10/38 (26.3)
Malignom		23/152 (15.1)				
	11/73 (15.1)	7/35 (20)	5/44 (11.4)	.58	.41	3/38 (7.9)

l, links; r, rechts; b, beidseitig,; ss, einseitig; bs, beidseitig

Abbildung 17: Patientencharakteristika und Risikofaktoren bei Thrombose der Vena cava inferior (IVCT). Die Patientencharakteristika sind für alle Subgruppen dargestellt (indirekte transfemorale venöse Thrombektomie (iTFVT), direkte offene venöse cavale Thrombektomie (dOVT), Kombination der beiden Verfahren (kombiniert). Die Anlage einer AV-Fistel erfolgte auf der Seite der thrombosierten Beckenvenen für 3 Monate. Eine logistische Regressionsanalyse (Hosmer -Lemeshow Test) wurde zur Identifikation einer Assoziation zwischen Risikofaktoren und dem Patientenüberleben, der Offenheitsrate und der Entwicklung eines PTS verwendet. Die Daten sind als Mittelwert ± SEM oder als Häufigkeitsverteilung (%) dargestellt. Modifiziert aus Wagenhäuser, M. U. et al. *Clinical outcomes after direct and indirect surgical venous thrombectomy for inferior vena cava thrombosis.* J Vasc Surg Venous Lymphat Disord. May;7(3):333-343.e2 (2019). (Mit freundlicher Genehmigung des Elsevier Verlags im Rahmen der „author rights for suscription articles“).

Innerhalb des Untersuchungszeitraumes kam es zu 15 Todesfällen. Sechs Patienten erlitten einen Herzinfarkt, fünf Patienten starben an den Folgen einer malignen Erkrankung, drei Patienten verstarben an einer Lungenentzündung und ein Patient verstarb an Blutungen aufgrund einer Leberzirrhose.

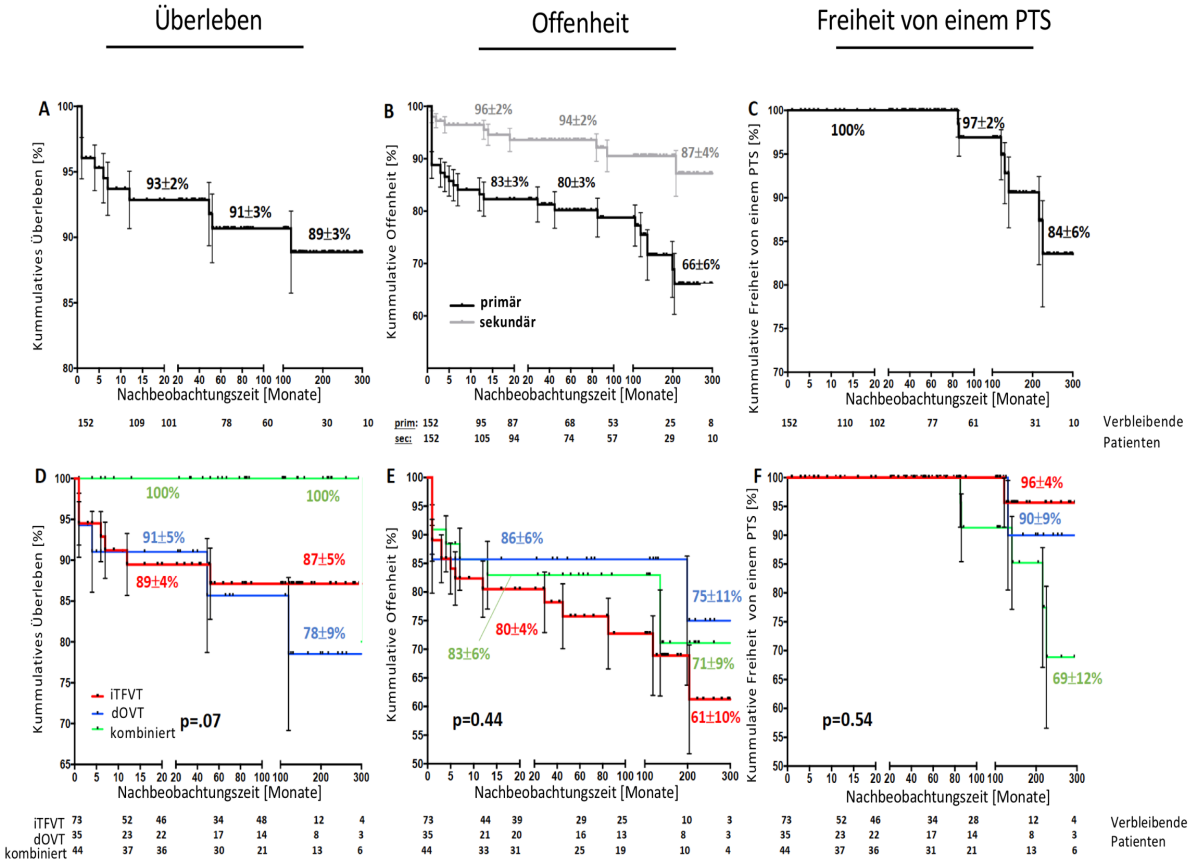

Abbildung 18: Überleben, Offenheit und Freiheit von einem PTS nach offen chirurgischer Thrombektomie bei Thrombose der Vena cava inferior (IVCT). A: Kaplan-Meier-Schätzung des Patientenüberlebens des Gesamtkollektivs nach offen chirurgischer Therapie bei IVCT. **B:** Kaplan-Meier-Schätzung der primären und sekundären Offenheitsrate des Gesamtkollektivs nach offen chirurgischer Therapie bei IVCT. **C:** Kaplan-Meier-Schätzung der Freiheit von einem post-thrombotischen Syndrom (PTS) des Gesamtkollektivs nach offen chirurgischer Therapie bei IVCT. **D:** Subgruppen-spezifische (indirekter transfemoraler venöser Thrombektomie (iTFVT), direkter offener venöser cavalen Thrombektomie (dOVT), Kombination aus beiden Verfahren (kombiniert)) Kaplan-Meier-Schätzung des Patientenüberlebens bei IVCT. **E:** Subgruppen-spezifische Kaplan-Meier-Schätzung der primären Offenheit bei IVCT. **F:** Subgruppen-spezifische Kaplan-Meier-Schätzung der Freiheit von einem PTS bei IVCT. Die dargestellten p-Werte sind durch Log-rank (Mantel-Cox) Test berechnet worden. Modifiziert aus Wagenhäuser, M. U. et al. *Clinical outcomes after direct and indirect surgical venous thrombectomy for inferior vena cava* thrombosis. J Vasc Surg Venous Lymphat Disord. May;7(3):333-343.e2 (2019). (Mit freundlicher Genehmigung des Elsevier Verlags im Rahmen der „author rights for suscription articles“).

Die ein-Jahresüberlebensrate betrug für das Gesamtkollektiv nach offen chirurgischer Thrombektomie 93±2%, die fünf-Jahresüberlebensrate betrug 91±3%. Nach 25 Jahren lebten noch 87±5% der Patientin in der iTFVT Gruppe, 78±9% in der iOVT und 100% der

Patienten mit kombiniertem Eingriff. Die Offenheitsrate des Gesamtkollektivs lag bei 83±3% nach einem und bei 80±3% nach fünf Jahren. Die sekundäre Offenheit betrug 96±2% nach einem und 94±6% nach fünf Jahren.

Nach 5 Jahren trat bei keinem der nachverfolgten Patienten ein PTS auf. Nach 25 Jahren waren 84±6% frei von einem PTS. In der spezifischen Analyse der Subgruppen betrug die Freiheit von einem PTS nach 25 Jahren 96±4% in der iTFVT Gruppe, 90±9% in der dOVT Gruppe und 69±12% in der Gruppe mit kombiniertem Eingriff (***Abbildung 18***).

Die Freiheit von einem PTS nach offen chirurgischer venöser Thrombektomie lag nach 25 Jahren bei 84%. Um die Effektivität des offen chirurgischen Vorgehens mit modernen endovaskulären Therapieansätzen vergleichen zu können, sind prospektive randomisierte Studien unerlässlich. Diese existieren für dieses Krankheitsbild bisher jedoch nicht. Daher muss auf retrospektive Studien zurückgegriffen werden. Das Auftreten eines PTS lag unter Therapie durch PTCD nach 3 Jahren bei 25%[155]. Vergleichbare Daten für eine reine CDT existieren bisher nur für eine IFDVT. Hier liegen die PTS Rate bei ca. 41% nach 2 Jahren Nachbeobachtungszeit[147].

Die offen chirurgische Therapie hat ähnlich den endovaskulären Verfahren eine komplette und frühe Entfernung des Thrombus mit daraus folgender Reduktion des Geweberemodelings an Venenklappen und -wand zum Ziel. Auf der Grundlage der erhobenen Daten erscheint das Verfahren in Bezug auf dieses Therapieziel ähnlich effektiv. Sollte eine offen chirurgische Thrombektomie zur Anwendung kommen, ist die Wahl der Methode vom Ausmaß der IVCT abhängig. Interessanterweise erscheint die Wahrscheinlichkeit einer PTS Entwicklung nicht methodenspezifisch.

Im Vergleich zu offen chirurgischen Ansätzen sind endovaskuläre Verfahren mit spezifischen prozeduralen Komplikationen verbunden, zu denen Lungenarterienembolien (LAE), intrakranielle Blutungen und das akute Nierenversagen zählen[156]. Um diese Komplikationen frühzeitig zu erkennen, wird eine kontinuierliche intensivmedizinische Überwachung gefordert, was zu einem erhöhten Patientendiskomfort führt[156]. Eigene Ergebnisse zeigen, dass schwerwiegende Komplikationen (Clavien-Dindo $\geq$ 3) bei offen chirurgischen Ansätzen selten sind und die Dauer der Hospitalisierung 12,8 Tage beträgt. Außerdem ist ein Aufenthalt auf der Intensivstation nicht notwendig, wenngleich das Verfahren invasiver ist.

Health-related quality of life (HRQOL)

Durch das Geweberemodeling wird nach einer TVT der Widerstand im venösen Abflussgebiet erhöht. Dies kann langfristig zur Ausbildung eines PTS führen, welches mit einer signifikanten Morbidität verbunden ist[157]. Um die HRQOL abzuschätzen, wurde ein SF-36 Fragebogen verwendet und mit der deutschen Normalbevölkerung verglichen.

		Vitalität	Körperliche Funktionsfähigkeit	Körperliche Schmerzen	Allgemeine Gesundheitswahrnehmung	Körperliche Rollenfunktion	Soziale Funktionsfähigkeit	Emotionale Rollenfunktion	Psychisches Wohlbefinden
Iliofemorale tiefe Venenthrombose	Durchschnitt	75.5 n=22	63.6 n=22	76.2 n=22	61.4 n=22	54.3 n=22	77.8 n=22	69.7 n=22	64.9 n=22
	SEM	0.4	0.6	0.5	0.4	0.4	0.4	0.5	0.3
Unterschied zur deutschen Normalbevölkerung	Differenz Durchschnitt	8.07	16.92	.88	4.69	7.44	9.83	18.05	7.89
	SEM Differenz	5.12	7.41	5.62	4.79	4.33	4.17	6.23	4.04
Analyse	Levene-Test	<.05	<.05	.58	.38	<.77	<.05	<.05	.33
	p-value Student's T-test	.12	*<.05	.88	.34	.10	*<.05	*<.05	.64

		Vitalität	Körperliche Funktionsfähigkeit	Körperliche Schmerzen	Allgemeine Gesundheitswahrnehmung	Körperliche Rollenfunktion	Soziale Funktionsfähigkeit	Emotionale Rollenfunktion	Psychisches Wohlbefinden
Thrombose der Vena Cava Inferior	Durchschnitt	74.1	79.5	71.9	62.3	58.1	80.5	83.3	72.8
	SEM	4.0	5.0	4.2	3.0	2.9	3.2	4.5	2.7
Unterschied zur deutschen Normalbevölkerung	Differenz Durchschnitt	83.6	80.3	77.2	66.0	61.8	87.7	87.7	72.8
	SEM Differenz	9.5	0.8	5.3	3.7	3.7	7.2	4.4	0
Analyse	Levene-Test	0.16	0.97	0.84	0.77	0.42	<.05	0.11	0.31
	p-value Student's T-test	*<.05	0.84	0.21	0.22	0.22	*<.05	0.34	0.99

Abbildung 19: SF-36 basierte gesundheitsbezogene Lebensqualität (HRQOL) im Vergleich zur deutschen Normalbevölkerung nach einer iliofemoralen Thrombose (IFDVT) und Thrombose der Vena cava inferior (IVCT). Dargestellt sind die Ergebnisse der 8 Subskalen eines SF-36 (Kurzfassung) für Patienten nach offen chirurgischer Thrombektomie bei IFDVT oder IVCT. Neben der körperlichen Funktionsfähigkeit ist insbesondere die soziale Funktionsfähigkeit stark gegenüber der deutschen Allgemeinbevölkerung eingeschränkt. SEM: Standardfehler des Mittelwerts. Modifiziert nach Wagenhäuser MU et al. *Open surgery for iliofemoral deep vein thrombosis with temporary arteriovenous fistula remains valuable.* Phlebology. Oct;33(9):600-609 (2018) und Wagenhäuser, M. U. et al. *Clinical outcomes after direct and indirect surgical venous thrombectomy for inferior vena cava thrombosis.* J Vasc Surg Venous Lymphat Disord. May;7(3):333-343.e2 (2019). (Mit freundlicher Genehmigung von SAGE Publications im Rahmen der „re-use and archiving policies" und des Elsevier Verlags im Rahmen der „author rights for suscription articles").

Es zeigte sich, dass insbesondere die soziale Rollenfunktion nach venöser Thrombektomie bei IFDVT und bei IVCT signifikant reduziert war. Es besteht ein

wissenschaftlicher Konsens, dass ein moderates bis schweres PTS die HRQOL der betroffenen Patienten stark beeinträchtigt[157,158]. Jedoch scheint auch die Angst bei noch nicht manifesten PTS vor sozialer Stigmatisierung aufgrund potentiell drohender offener sezernierender Wunden von hoher Relevanz. Dies wird durch hohe nummerische Unterschiede in der Subskala der sozialen Funktionsfähigkeit im Vergleich zur Allgemeinbevölkerung nahegelegt (**Abbildung 19**). Diese Beobachtung unterstreicht die enorme Bedeutung effektiver Therapien zur Verringerung eines dysfunktionalen Geweberemodelings der Venenklappen sowie -wand. Nur so kann den Patienten die Angst vor sozialer Ausgrenzung genommen werden.

4.3.4. Zusammenfassung/Ausblick

Die offen chirurgische venöse Thrombektomie ist ein invasives Verfahren, das zu einer frühen und sicheren Entfernung des okkludierenden Thrombus bei IFDVT und IVCT führt. Die prozeduralen Komplikationsraten sind gering und das Auftreten eines PTS im Langzeitverlauf scheint günstig beeinflussbar. Mechanistisch ist die frühzeitige Beseitigung des okkludierenden Thrombus, der substantiell für das dysfunktionale Geweberemodeling und die Entstehung eines PTS mitverantwortlich ist, vielversprechend. Allerdings konnten diese kausalen Überlegungen in prospektiv-randomisierten Studien aufgrund teils unterschiedlicher Ergebnisse nicht abschließend verifiziert oder widerlegt werden.

Moderne weniger invasive endovaskuläre Ansätze verfolgen gleichfalls die frühzeitige Beseitigung des okkludierenden Thrombus in der venösen Strombahn, erzeugen jedoch ein geringeres Trauma. Prospektive randomisierte Studien, die eine Überlegenheit der minimal-invasiv, endovaskulären Therapien gegenüber dem offen-chirurgischen Vorgehen in Hinblick auf die PTS Entwicklung und/oder HRQOL untersuchen, stehen weiterhin aus.

Abschließend verbleibt die offen chirurgische Thrombektomie heute aufgrund ihrer Invasivität eine Therapiealternative in selektierten Patienten und in Notfallsituationen. Die frühe Beseitigung des Thrombus und Rekanalisierung der venösen Strombahn scheint den endovaskulären Therapien vergleichbare Ergebnisse in Hinblick auf die PTS Inzidenz im Langzeitverlauf erzielen zu können.

Original Article

Phlebology

Phlebology
0(0) 1–10

DOI: 10.1177/0268355517736437
journals.sagepub.com/home/phl
SAGE

Open surgery for iliofemoral deep vein thrombosis with temporary arteriovenous fistula remains valuable

Markus U Wagenhäuser[1,2], Hellai Sadat[1], Philip Dueppers[1], Yvonne K Meyer-Janiszewski[1], Joshua M Spin[2], Hubert Schelzig[1] and Mansur Duran[1]

Abstract

Objective: We assessed outcomes of open surgical venous thrombectomy with temporary arteriovenous fistula, and the procedure's effect on health-related quality of life.

Method: We retrospectively analyzed 48 (26 at long-term) patient medical records. Mortality rates, patency, and risk of post-thrombotic syndrome were analyzed using Kaplan–Meier estimation. The association between risk factors/coagulation disorders and patency/post-thrombotic syndrome along with patient health-related quality of life at long-term was analyzed employing various statistical methods.

Results: Patient one-year survival rate was 93 ± 4% and primary one-year patency rate was 89 ± 5% (secondary one-year patency rate 97 ± 3%). Freedom from post-thrombotic syndrome after eight years was 80 ± 12% (post-thrombotic syndrome rate 20 ± 12%). Health-related quality of life was impaired vs. normative data in the physical and social subscales, and in the mental component score ($p < .05$).

Conclusions: Open surgical venous thrombectomy appears safe compared with literature-reported outcomes in similar patients using alternative approaches. Iliofemoral deep vein thrombosis impairs physical, social, and mental health-related quality of life.

Keywords

Deep vein thrombosis, post-thrombotic syndrome, surgery, duplex ultrasound, quality of life assessment

Introduction

Iliofemoral deep vein thrombosis (DVT) has an incidence of about 0.1% in Western Europe.[1] Its socioeconomic impact is often underestimated, as long-term complications are frequent and can be devastating. Although DVT itself is not life-threatening in most cases, resultant post-thrombotic syndrome (PTS) can severely impair quality of life with symptoms including leg pain, swelling, altered skin pigmentation, and leg ulcers.[2–4]

Hereditary coagulation disorders often increase the risk of developing DVT.[5] Thrombophilic disorders can be divided into loss-of-coagulation-inhibitor disorders and gain-of-coagulation function disorders.[6] The best studied gain-of-function disorder associated with an increased risk of iliofemoral DVT is Factor V Leiden (FVL) thrombophilia. Loss-of-inhibitor disorders include deficiencies of antithrombin III (ATIII), protein C or protein S and have been shown to increase the risk of DVT.[5]

The current understanding of DVT pathogenesis suggests that the early thrombus creates an inflammatory environment that recruits immune cells to the vein wall, leading to destruction of the extracellular matrix (ECM).[7] The subsequent increase in outflow resistance due to vein wall fibrotic remodeling results in venous

[1]Department of Vascular and Endovascular Surgery, University Hospital of Düsseldorf, Düsseldorf, Germany
[2]Division of Cardiovascular Medicine, Stanford University School of Medicine, Stanford, CA, USA

Corresponding author:
Markus U Wagenhäuser, Department of Vascular and Endovascular Surgery, University Hospital of Düsseldorf, Moorenstrasse.5, 40225 Düsseldorf, Germany.
Email: markus.wagenhaeuser@med.uni-duesseldorf.de

hypertension.[8–10] Outward filtration through the capillaries causes edema and can ultimately lead to venous ulcers. Therefore, treatment strategies typically focus on prevention of long-term PTS.[11–13] As early thrombus removal appears to be critical in preventing PTS, particularly in young and active patients, the Society of Vascular Surgeons (SVS) and the American Venous Forum recommend using catheter-directed thrombectomy (CDT) with or without pharmaco-mechanical thrombolytic therapy (PMT) as first line treatment. Alternatively, open surgical venous thrombectomy (VT) has also been shown to decrease the risk of developing PTS, venous reflux, and venous obstruction.[14,15] When there are contraindications or failure of thrombolysis, open surgical VT remains a valid alternative.[16,17] One approach to surgical VT includes the creation of a temporary arteriovenous fistula (AVF) to augment blood flow and prevent early recurrent thrombosis. This study analyzed clinical outcomes after open surgical VT with a temporary arteriovenous fistula (AVF) as treatment for iliofemoral DVT.

Methods

Data collection

The investigation period was between 1 January 2004 and 31 December 2015. Patients' archived medical records of in-hospital stays and regular follow-up examinations were analyzed along with data from a detailed phlebologic follow-up examination.

Surgery

All patients presented through the University Hospital Düsseldorf emergency room. Upon admission, patients underwent compression duplex ultrasound (CDU) analysis to confirm iliofemoral DVT. To verify the diagnosis and exclude a concomitant inferior vena cava (IVC) thrombosis or iliac vein (IV) compression syndrome, we performed a computed tomography (CT) scan in 38/44 patients (6 patients did not give informed consent for the scan). Patients received compression therapy after admission, and were screened for coagulation disorders before anticoagulation was started.

All patients gave informed consent prior to surgery. A standard operative procedure for inguinal VT was performed in all cases. A longitudinal inguinal incision was used to expose the femoral veins and arteries. The femoral vein was identified and clamped over the proposed entry site. After a longitudinal venotomy, antegrade VT was performed using Fogarty maneuvers. We used valve-preserving techniques involving manual compression of the leg augmented by elastic bandages (Esmarch bandages) to support distal clot removal. When no sufficient backflow could be obtained, sequential retrograde thrombectomy was performed, accepting partial valve destruction. At the time of VT, the positive end-expiratory pressure was increased by 15 mm Hg to prevent pulmonary embolism (PE). There was no IVC filter implantation. Appropriate venous backflow confirmed the success of the procedure, and the venotomy was closed using running sutures without resultant stenosis.

To prevent recurrent thrombosis, all patients received an AVF to increase blood flow over the critical three-month post-op period. The same-limb saphenous vein was used to create an AVF between the femoral vein and artery, and pulsatile fistula flow was confirmed using continuous-wave Doppler. The AVF was ligated during a second in-hospital stay three months after surgery.

Prior to discharge, all patients received a second CDU to exclude recurrent thrombosis and, if needed, a confirmatory CT scan. Anticoagulants were administered for at least six months to all patients after open VT. For warfarin, patients' INR levels were measured after surgery and prior to discharge to confirm effective anticoagulation (target range 2–3). D-dimer was tested during the first and second in-hospital stay within one week after surgery. The patients were transferred to the Institute of Hemostasis and Transfusion Medicine, where further strategic anticoagulation management was defined based on tests for coagulation disorders. Elevated D-dimer levels and additional risk factors such as smoking, contraception, and obesity were factored in when considering the duration of anticoagulation and lifelong anticoagulation was suggested to all FVL patients. Three months after surgery, the AVF was ligated during a second hospital admission using the same inguinal approach.

Compression therapy was started immediately after admission and continued after surgery with custom-made compression stockings with a pressure range of 23 to 32 mm Hg. Compression therapy was suggested for three months.

Inclusion and exclusion criteria

Inclusion criteria were as follows: >18 years of age; confirmed iliofemoral DVT using CDU or CT scans. Exclusion criteria were as follows: pregnancy, prior DVT, concomitant DVT elsewhere, prior endovascular therapy with a percutaneous inguinal approach on the affected leg, poor general condition, symptoms for more than a week (8 days), and a lack of consent after the risk–benefit assessment.

Detailed phlebologic follow-up examination

Included patients were contacted and invited to our outpatient department for a detailed phlebologic follow-up examination. On presentation, a clinical examination was performed to evaluate actual vein functional status and score PTS symptoms using the Villalata score and the clinical, etiological, anatomical, and pathophysiological (CEAP) classification. The examiners were not involved in further data processing or analysis.

CDU was used to examine venous function. The IVs, the common femoral vein (CFV), femoral vein (FV), deep femoral vein (DFV), popliteal vein (PV), posterior tibial vein (PTV), anterior tibial vein (ATV), fibular veins (FV), great saphenous vein (GSV), and small saphenous vein (SSV) on both legs were analyzed.

Patients also completed self-assessment SF-36 questionnaires over a period of four weeks (2nd version, Hogrefe Verlag GmbH & Co. KG, Goettingen, Germany) after giving informed consent. Eight independent health scores (physical functioning, physical role functioning, bodily pain, general health perceptions, social role functioning, vitality, emotional role functioning, and mental health) were used to create component summary scores (Physical Component Summary (PCS) and Mental Component Summary (MCS)).[18,19] The patient cohort was compared to German normative data based on a survey in 1994 for the same health and component summary scores as the patient cohort.

Statistical analysis

Categorical data are presented as a frequency distribution with percentages. Continuous data are presented as the means ± standard errors of the means. Kaplan–Maier estimator was used to calculate survival, patency, and PTS rates. We used logistic regression analysis (Hosmer–Lemeshow Test) for continuous independent variables (basic demographics), and Chi-square testing with Yates continuity correction for dichotomous independent variables (risk factors/coagulation disorders), to determine variable association with patency or PTS in the long-term. Levene's test was used to verify homogeneity of variances for SF-36 subgroups, and Student's or Welch t-test was applied accordingly to compare subscale scores. Statistical analysis was performed using SPSS version 22.0 and GraphPad Prism 7, a p value < 0.05 was considered to be statistically significant.

Results

Study setup/admission data

We identified a total of 142 patients who were treated using open surgery for DVT at our department within the investigation period. Of those, 84 patients were excluded due to concomitant IVC thrombosis, IVC agenesis, or pregnancy, and an additional 10 excluded for meeting other criteria (Figure 1). Symptoms upon admission had been present for an average of 6.8 ± 0.6 days. Data from CDU and CT scans identified 23 isolated thromboses of the iliofemoral trunk and 25 of the ilio-femoral-popliteal segment together.

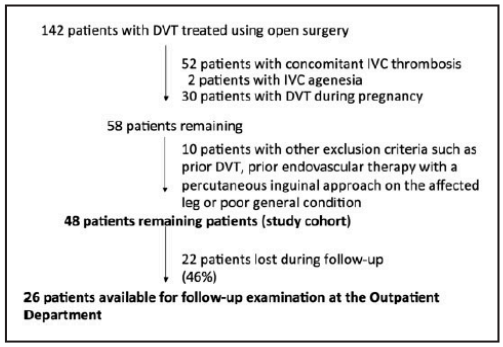

Figure 1. Patient recruitment and dropouts. Totally 142 patients were identified who underwent open surgical VT for iliofemoral DVT between 1 January 2004 and 31 December 2015. Of all, 94 patients were initially excluded. Another 10 patients were excluded due to other criteria. Of all, 48 patients remained for retrospective analysis and 26 patients were available for a detailed phlebologic follow-up examination (22 patients were lost to follow-up).
DVT: deep vein thrombosis; VT: venous thrombectomy; IVC: inferior vena cava.

May–Thurner syndrome

From the CT scans, we identified three patients with IV stenosis at presentation (two cases in the left common iliac vein (CIV) and one in the left external iliac vein (EIV)). The two patients who exhibited compression of the left CIV due to May–Thurner syndrome (compression from crossover of the right iliac artery) (MTS) (2/48, 4.1%) received subsequent endovascular stent implantation. The compression of the left EIV in the other patient resulted from prior radiation therapy due to rectal cancer, and stenosis was treated using a vein patch with peri-venous polytetrafluoroethylene (PTFE) coating. All three patients presented with a patent iliofemoral trunk at the follow-up examination.

Recurrent thrombosis/Revision surgery

The immediate procedural success rate of open surgical VT was 100%. We observed a total of seven cases with eventual recurrent thrombosis requiring revision

surgery. There were six cases of recurrent thrombosis that formed in the same leg as the first thrombosis, whereas one case affected the opposite leg. All cases of recurrent thrombosis formed in the CFV and IVs (iliofemoral trunk). The diagnosis was confirmed using CDU in all seven patients. Of those seven patients, five patients developed a recurrent thrombosis within the three-month time frame of augmented blood-flow via the AVF. Of those, three patients had a patent AVF and two patients an occluded AVF at the time of revision surgery. In the latter two patients AVF salvage was not possible, and creation of a new AVF was necessary. For revision surgery with re-thrombectomy the same surgical approach described above was performed. Of note, none of the seven patients with recurrent thrombosis suffered from an IV stenosis.

There were six technically successful revision surgeries (5 re-thrombectomy, 1 crossover ilio-iliac bypass) and one failed attempt at re-thrombectomy. We observed one patient with multiple recurrent thromboses after successful revision surgery. Surgery-related complications requiring revision surgery included hematoma (1/48, 2%) and impaired wound healing (2/48, 4%).

Survival/patency

During the follow-up, three deaths occurred. Of these, two (4%) were due to myocardial infarction and one (2%) was due to aortic dissection. No procedure-related deaths occurred. There was no new diagnosis of carcinoma during the follow-up. The Kaplan–Meier analysis illustrates a one-year survival rate of $93 \pm 4\%$ ($91 \pm 5\%$ after eight years) (Figure 2(a)). The primary one-year patency rate was $89 \pm 5\%$ ($81 \pm 7\%$ after eight years) and secondary one-year (and eight-year) patency rate was $97 \pm 3\%$ (Figure 2(b)). Freedom from PTS was 100% after five years and $80 \pm 12\%$ after eight years (PTS rate of $20 \pm 12\%$ respectively) (Figure 2(c)).

Long-term follow-up

Of the original 48 patients, we managed to obtain long-term data for 26 patients, who came back for a detailed follow-up examination. The mean follow-up time at examination was 63 ± 6 months. Of these 26 patients, 22 patients completed a SF-36 questionnaire for health-related quality of life (HRQoL) assessment.

Basic patient demographic data indicated there were more females, and more cases of iliofemoral DVT in the left leg. Immobilization (9/26, 35%) was the most common risk factor. The logistic regression analyses and Chi-square test analyses (with Yate's correction for continuity) revealed no correlation between patient characteristics or risk factors and patency or PTS at long-term (Table 1).

The data illustrate that FVL was the most common coagulation disorder in this patient cohort (8/26, 31%). Chi-square test analysis revealed that no coagulation disorder was associated/correlated with patency or PTS at long-term (Table 2). In addition to the 26 follow-up patients, we obtained information about anticoagulation after discharge from the hospital of an additional four patients from archived medical records. Of those 30 total patients, eight patients stopped anticoagulants after six months, eight patients stopped after one year, and four patients stopped within 1–3

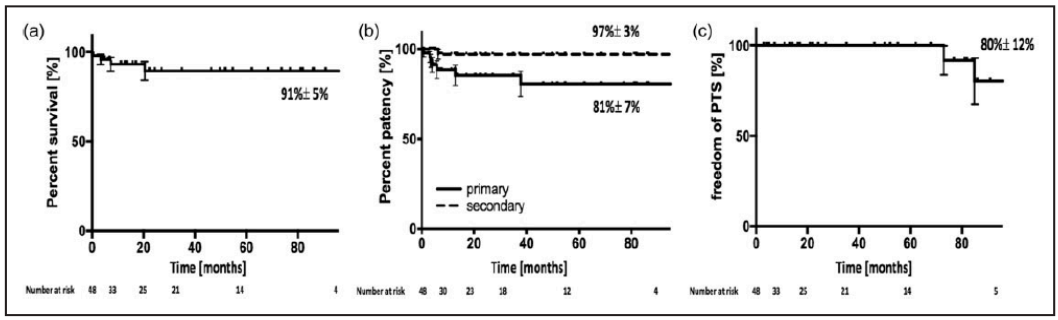

Figure 2. Mortality, patency rate, and freedom from PTS rates (X-axes were cut with 96 months/eight years). (a) Kaplan–Meier estimation for overall survival rate of patients with iliofemoral DVT with VT. Data are presented as percentage of survival primary operation. Eight-year survival rate is shown. (b) Kaplan–Meier estimation for primary and secondary patency rate in patients with iliofemoral DVT with open surgical VT. Eight-year patency rates are shown. (c) Kaplan–Meier estimation for freedom from PTS rate in patients with iliofemoral DVT with open surgical VT. Eight-year freedom from PTS rate is shown.
DVT: deep vein thrombosis; PTS: post-thrombotic syndrome; VT: venous thrombectomy.

Table 1. Patient characteristics and risk factors at long-term follow-up.[a]

Characteristics				
	Average/frequency distribution (%)	SEM	Association with patency *p* value	Association with PTS *p* value
Age	49	±2.8	.991	.857
Body weight (kg)	76	±2.5	1.000	.360
Body height (cm)	172	±1.6	.998	.373
BMI	25	±4	.998	.341
Gender, m/w	11 (42%)/15 (58%)	–	–	–
Affected leg right/left/both	5 (19%)/18 (69%) /3 (12%)	–	–	–
Risk factors				
	Frequency distribution	Percentage	Association with patency *p* value	Association with PTS *p* value
Obesity	2/26	8	.54	.54
Immobilisation	9/26	35	.55	.55
Smoking	1/26	4	.22	.22
Carcinoma	4/26	15	.95	.95
Hyperlipoproteinemia	3/26	12	.77	.77

BMI: body mass index; PTS: post-thrombotic syndrome.
[a]Data are presented as means with standard errors, or frequency distribution with percentages. A logistic regression analysis (Hosmer–Lemeshow test, continuous variables) and Chi-square test with Yate's correction for continuity (dichotomous variables) were employed to analyze whether patient characteristics/risk factors were associated with patency rate or PTS at long-term follow-up ($n = 26$).

Table 2. Coagulation disorders.[a]

Coagulation disorders	Frequency distribution	Percentage	Association with patency *p* value	Association with PTS *p* value
APC resistance	4/26	15%	.95	.95
Prothrombin mutation	1/26	4%	.22	.22
ATIII deficiency	0/26	0%	–	–
MTHFR mutation	2/26	8%	.60	.60
Antiphospholipid antibody	0/26	0%	–	–
Protein C deficiency	0/26	0%	–	–
Protein S deficiency	1/26	4%	.22	.22
Factor VII deficiency	1/26	4%	.22	.22
Factor V Leiden thrombophilia	8/26	31%	.57	.44
Elevated factor VIII level	1/26	4%	.22	.22
Hyperfibrinogenemia	1/26	4%	.22	.22
Homocysteinemia	0/26	0%	–	

APC: activated protein C; ATIII: antithrombin III; MTHFR: methylene tetrahydrofolate reductase; PTS: post-thrombotic syndrome.
[a]Patients were screened for coagulation disorders upon admission before anticoagulation was started. Data are presented as frequency distribution with percentages. Chi-square test with Yate's correction for continuity was employed to analyze the association between coagulation disorders and patency/PTS at long-term ($n = 26$).

years. Life-long anticoagulant treatment was recommended for all 11 patients with FVL thrombophilia. Notably, one patient with FVL thrombophilia refused life-long anticoagulation and stopped after six months.

In a detailed phlebologic CDU, the affected leg and the contralateral leg were examined and their venous function was evaluated. We observed reflux in the GSV of the affected leg in 5/26 (19%) patients (contralateral

Table 3. Patient clinical classification.[a]

CEAP classification						
Class 0	Class 1	Class 2	Class 3	Class 4	Class 5	Class 6
13/26	5/26	2/26	2/26	2/26	1/26	1/26
50%	19.2%	7.7%	7.7%	7.7%	3.8%	3.8%
Villalta score						
	None	Mild	Moderate	Severe	–	–
	0–5 points	5–9 points	10–14 points	15 points		
	23/26	1/26	0/26	2/26		
	88.5%	3.8%	–	7.7%		

CEAP: clinical, etiological, anatomical, and pathophysiological classification.
[a]Patients were examined at a detailed phlebologic follow-up examination. Data are presented as frequency distribution with percentages. The CEAP classification and Villalta score were calculated based on clinical findings.

2/26 (8%)). Notably, we observed 2/26 (8.3%) occlusions in the CFV/IVs (iliofemoral trunk) and 3/26 (12%) occlusions in the FV (Supplementary Table 1).

After CDU, the patients were asked to score the severity of their symptoms. Based on the results, we classified the patients according to the CEAP classification and Villalta score subgroups. When categorizing the patients according to the CEAP classification, we identified 13/26 (50%) patients with no clinical signs of venous disease (C0), 5/26 (19.2%) patients with telangiectasia only (C1), 2/26 (8%) patients with varicose veins (C2), 2/26 (8%) patients with edema (C3), and 2/26 (8%) patients with lipodermatosclerosis but no ulcers (C4). Healed or open ulcers (C5 and C6) were present in 2/26 (8%) patients. According to the Villalta score system, we observed 3/26 (12%) patients with PTS (1/26 (4%) patient had moderate PTS, and 2/26 (8%) patients had severe PTS). For the three affected patients, PTS was diagnosed 6, 7, and 8.5 years after surgical VT (Table 3).

The three patients with PTS included two females and one male. All three cases exhibited a thrombosis of the ilio-femoral-popliteal segment on admission. One patient had a smoking history of >20 pack years, suffered from an active carcinoma and had had a previous PE. One female was on oral contraception at the time of thrombosis. Revision surgery was necessary in one patient (female), however the AVF appeared patent during revision surgery. Besides this one recurrent thrombosis, there were no postoperative in-hospital complications. All patients were on oral coagulation at the time of detailed follow-up examination. Notably, two of the three patients suffered from FVL and of those two, one also had activated protein C (APC) resistance. We observed superficial venous reflux in all three patients.

HRQoL was measured using a 36-item health survey. The biggest differences between the patient cohort and German normative data in mean scores were identified for physical and social/emotional functioning/role subscales and the mental component score (MCS) ($p < .05$). However, we did not observe differences in regard to the physical component score (PCS) ($p = 0.56$) (Table 4).

Discussion

Iliofemoral DVT is a common disease with an enormous impact on the healthcare system. PTS is a long-term complication and results in 50% higher per-patient cost than DVT without PTS.[20] This study analyzed patients who received open surgical VT with a temporary AVF.

In the present study, we found an eight-year survival rate of 91% and a primary one-year patency rate of 89%. Freedom from PTS after eight years was 80% (PTS rate 20%). We observed that 4.2% of all cases suffered from MTS, however six patients refused to undergo a CT scan, so for those patients no reliable data are available. We observed FVL to be the most common coagulation disorder among the study cohort, and that patients' mental and physical HRQoL are affected long-term.

Given that 77% of iliofemoral DVT affected the left iliofemoral axis, it is likely that underlying MTS was a prevalent pathology. According to the current literature, MTS is diagnosed in about 2–5% of patients undergoing evaluation for venous disorders of the lower extremities, however Xue et al. reported it in up to 37% of affected patients among a study cohort of DVT.[21–23] Whenever MTS is confirmed, patients should receive additional endovascular stent implantation in the CIV, as this approach is critical to prevent PTS and immediate re-thrombosis. In this regard, we suggest that all patients with iliofemoral DVT consider further imaging, preferably using CT

Table 4. SF-36 scores.[a]

	Physical functioning	Role physical	Bodily pain	General health perceptions	Energy/ vitality	Social functioning	Role emotional	Mental health	Physical component score (PCS)	Mental component score (MCS)
Iliofemoral DVT										
Mean score	75.5	63.6	76.2	61.4	54.3	77.8	69.7	64.9	47.7	43.1
SEM	0.4	0.6	0.5	0.4	0.4	0.4	0.5	0.3	0.2	0.2
German normative data										
Mean score	83.6	80.3	77.2	66.0	61.8	87.7	87.7	72.8	49.2	51.0
Mean difference	8.1	16.7	1	4.6	7.5	9.9	18	7.9	1.5	7.9
Analysis										
Levene test	<.05	<.05	.58	.38	<.77	<.05	<.05	.33	.26	<.05
p value *t*-test	.12	<.05*	.88	.34	.10	<.05*	<.05*	.64	.56	<.05*

DVT: deep vein thrombosis; SEM: standard error mean.
[a]Scores for the 8 domains of Medical Outcomes Study 36-item Short Form (SF-36) and for the 2 summary scales (physical and mental component) for patients after open surgical VT with temporary AV fistula. All subscale and summary scale scores were lower in the study cohort when compared to German normative data. Scores were analyzed for homogeneity of variances (Levene test) and Student's/Welch *t*-test was employed accordingly to compare mean score (n = 22).

scanning, to reliably examine the IVs in detail. As Forauer et al. has previously demonstrated, intravascular ultrasound (IVUS) imaging might be a useful adjunct in the diagnosis and endovascular management of MTS, as it does not use ionizing radiation.[24] However, this approach might be limited to larger centers which access to and experience with this imaging technique.

FVL has been described as a major risk factor for recurrent thrombosis[25,26] and was the most common coagulation disorder in the present study. Published guidelines dictate that the first DVT should be treated with a course of low molecular weight heparin (LMWH) or intravenous unfractionated heparin. Warfarin is started concurrently with LMWH (except during pregnancy) and monitored with the international normalized ratio (INR) (target INR of 2.5).[27] Generally, heterozygous FVL mutation is not an indication for long-term anticoagulation, however it has been demonstrated that therapeutic anticoagulation decreases the risk of PTS long-term.[28,29] As surgical VT is invasive and partially destroys venous valves, the authors believe that it might be optimal for the FVL subgroup to receive chronic anticoagulation, given the high risk of recurrent thrombosis after surgical VT. As open surgical VT is only performed at experienced centers, and available data about patient outcome are rare, chronic anticoagulation for FVL patients should be considered on an individual center-basis rather than as a general suggestion, as there is no evidence for patient benefit in the currently available literature.

It has been reported previously that patency rates after open surgical VT are as high as 62–77%.[30,31] Patency rates in our study were slightly better. Whether the temporary AVF might contribute to this finding is unclear, since we surprisingly observed three cases of recurrent thrombosis with a patent AVF. In this context, Comerota et al. suggest that PTS development is related to residual thrombus.[32] The only current reliable imaging to exclude residual thrombus is a second CT scan after surgical VT, as this complication can be missed by planar imaging techniques such as intraoperative phlebography of the IVs. Given recent improvements in CT imaging as regards radiation dose reduction, it would again seem reasonable to suggest routine CT scanning after open surgical VT as a standard approach to prevent PTS.

To diagnose PTS and to quantify its severity, the Villalta score and the CEAP classification are typically used. Notably, the CEAP classification does not consider the severity of PTS, and has no agreed-upon cutoff, suggesting that this classification may not be suitable for diagnosis. For these reasons, the Subcommittee on Control of Anticoagulation of the International Society on Thrombosis and Hemostasis has suggested that the Villalta score is the most appropriate classification system.[33] There are several studies that report PTS rates being as high as 24–53% using medical treatment (anticoagulation) after 2–3 years.[2,34,35] While these studies described similar patient characteristics, some used the CEAP classification to diagnose PTS. As we report a slightly lower overall PTS long-term rate, patients might benefit from open surgical VT with temporary AVF when compared to anticoagulation therapy alone. Plate et al. have demonstrated that surgical VT with a temporary AVF improves venous patency and reduces PTS sequelae even after a 10-year follow-up.[36] Stain et al. further found that proximal DVT is the strongest risk factor to develop PTS (odds ratio (OR) 2.1, 95%

confidence interval (CI) 1.3–3.7), suggesting that early clot removal is beneficial.[37]

Other important therapeutic approaches with early clot removal have gained prominence in the last decade, including systemic, catheter-directed (CDT), and pharmaco-mechanical catheter-directed thrombolysis (PCDT). Two clinical trials reported a significant reduction in the relative risk (RR) of PTS when CDT or PCDT was used when compared with anticoagulation alone.[38,39] A meta-analysis by Casey et al. found that surgical VT also led to a reduction in the RR of PTS development (vs. anticoagulation) and that surgical VT decreases the incidence of PTS and venous reflux, whereas CDT decreases the incidence of PTS and venous obstruction.[40] While the less invasive approaches seem to deliver appropriate patient outcomes, surgical VT may remain valuable, particularly for patients who are not eligible for CDT or PCDT because of high bleeding risk or other contraindications.[41]

Various studies have analyzed the impact of PTS on patient HRQoL. Kumar et al. used the generic PedsQL 4.0 and reported a significant impact of moderate to severe PTS on HRQoL.[42] Broholm et al. investigated patients with iliofemoral DVT and CDT and suggested that venous reflux and occluded veins were the factors with the greatest influence on patient HRQoL.[43] Kahn et al. demonstrated that PTS had a significant impact on disease-specific quality of life, which generic quality-of-life measures might not sufficiently capture.[44] Moreover, they reported that patient-based quality-of-life measures correlated well with physician-assessed PTS. The results of the current study seem to be in line with previous findings, with impaired HRQoL occurring after iliofemoral DVT with surgical VT. Notably, our results suggest that patient mental and physical health are affected unequally, tilting towards stronger mental impairment. Since our patient cohort was younger on average, it is possible that the fear of developing severe PTS with visible ulcers that could lead to social exclusion and stigmatization might exceed perceived physical limitations. Given the limited number of patients, we could not compare between subgroups regarding patent and non-patent vein status. Likely for the same reason, we did not find a correlation between HRQoL and the severity of PTS, although such a correlation seems self-evident.

Limitations of this study include the small sample size of 26 patients available for detailed follow-up, as 22 patients were lost. Given that 26/48 (54%) agreed to present for a follow-up examination, this low patient number at follow-up could also affect the validity of the conclusions. For that reason, real patency or occlusion rates might be different than reported. Although missing post-surgical imaging might be a potential confounding factor, reported patency rates seem satisfactory.

The retrospective nature of this study might have led to biased measurements of patient outcomes and compromised our conclusions. Future multicenter studies are necessary for adequate patient recruitment to perform a comparative epidemiological statistical analysis and to verify our results.

In summary, PTS is a major complication after iliofemoral DVT and suggests that a multidisciplinary approach is mandatory. Open surgical VT with a temporary AVF appears to be a safe and reasonable treatment option in terms of patient outcomes in the long-term.

Declaration of Conflicting Interests

The author(s) declared no potential conflicts of interest with respect to the research, authorship, and/or publication of this article.

Funding

The author(s) received no financial support for the research, authorship, and/or publication of this article.

Ethical approval

This study protocol was approved by the Institutional Review Board of the University of Düsseldorf (4313). All patients provided written informed consent before participation.

Guarantor

MW.

Author contributions

MUW, HSa, YKMJ, and MD drafted the paper. MUW and MD designed the protocol. HSa collected and analyzed the data. MD supervised the design of the trial. MUW, HSa, and MD contributed to the figure design. JMS, HSa, YKMJ, PD, and HSsch contributed to data analysis and revised the manuscript critically for important intellectual content. JMS, MUW, HSa, and PD helped with formatting and editing of the manuscript. MUW, HSa, PD, and HSsch made substantial contribution to conception of the study and helped to procure the medical records. MUW and MD were the main investigators. MUW, HSa, YKMJ, and PD helped with statistical analysis and interpretation. All authors participated in study execution and finally approved the manuscript.

Acknowledgment

We would like to thank Firat Antakyali for his assistance during the follow-up examinations.

References

1. White RH. The epidemiology of venous thromboembolism. *Circulation* 2003; 107: 4I–8.

2. Prandoni P, Lensing AW, Cogo A, et al. The long-term clinical course of acute deep venous thrombosis. *Ann Intern Med* 1996; 125: 1–7.
3. Kahn SR and Ginsberg JS. The post-thrombotic syndrome: current knowledge, controversies, and directions for future research. *Blood Rev* 2002; 16: 155–165.
4. Utne KK, Tavoly M, Wik HS, et al. Health-related quality of life after deep vein thrombosis. *Springerplus* 2016; 5: 1278.
5. Cushman M. Epidemiology and risk factors for venous thrombosis. *Semin Hematol* 2007; 44: 62–69.
6. Crowther MA and Kelton JG. Congenital thrombophilic states associated with venous thrombosis: a qualitative overview and proposed classification system. *Ann Intern Med* 2003; 138: 128–134.
7. Wakefield TW, Strieter RM, Wilke CA, et al. Venous thrombosis-associated inflammation and attenuation with neutralizing antibodies to cytokines and adhesion molecules. *Arterioscler Thromb Vasc Biol* 1995; 15: 258–268.
8. Deroo S, Deatrick KB and Henke PK. The vessel wall: a forgotten player in post thrombotic syndrome. *Thromb Haemost* 2010; 104: 681–692.
9. Phillips LJ and Sarkar R. Molecular characterization of post-thrombotic syndrome. *J Vasc Surg* 2007; 45: A116–A122.
10. Jalaie H, Schleimer K, Barbati ME, et al. Interventional treatment of postthrombotic syndrome. Gefasschirurgie Zeitschrift Fur Vaskulare Und Endovaskulare Chir. Organ Der Dtsch. Und Der Osterr. *Gesellschaft Fur Gefasschirurgie Unter Mitarbeit Der Schweizerischen Gesellschaft Fur Gefasschirurgie* n.d; 21: 37–44.
11. Kurtoglu M, Koksoy C, Hasan E, et al. Long-term efficacy and safety of once-daily enoxaparin plus warfarin for the outpatient ambulatory treatment of lower-limb deep vein thrombosis in the TROMBOTEK trial. *J Vasc Surg* 2010; 52: 1262–1270.
12. Dueppers P, Grabitz K, Li Y, et al. Surgical management of iliofemoral vein thrombosis during pregnancy and the puerperium. *J Vasc Surg Venous Lymphat Disord* 2016; 4: 392–399.
13. Kniemeyer HW, Grabitz K, Buhl R, et al. Surgical treatment of septic deep venous thrombosis. *Surgery* 1995; 118: 49–53.
14. Meissner MH, Gloviczki P, Comerota AJ, et al. Society for Vascular Surgery, American Venous Forum, early thrombus removal strategies for acute deep venous thrombosis: Clinical Practice Guidelines of the Society for Vascular Surgery and the American Venous Forum. *J Vasc Surg* 2012; 55: 1449–1462.
15. Casey ET, Murad MH, Zumaeta-Garcia M, et al. Treatment of acute iliofemoral deep vein thrombosis. *J Vasc Surg* 2012; 55: 1463–1473.
16. Mousa AY and Broce M. Catheter-directed thrombolysis versus full anticoagulation alone in treating proximal iliofemoral deep venous thrombosis. *Vascular* 2017; 25: 111–112.
17. Eklof B, Arfvidsson B, Kistner RL, et al. Indications for surgical treatment of iliofemoral vein thrombosis. *Hematol Oncol Clin North Am* 2000; 14: 471–482.
18. McHorney CA, Ware JE, Lu JF, et al. The MOS 36-item Short-Form Health Survey (SF-36): III. Tests of data quality, scaling assumptions, and reliability across diverse patient groups. *Med Care* 1994; 32: 40–66.
19. Lyons RA, Perry HM and Littlepage BN. Evidence for the validity of the Short-form 36 Questionnaire (SF-36) in an elderly population. *Age Ageing* 1994; 23: 182–184.
20. Guanella R, Ducruet T, Johri M, et al. Economic burden and cost determinants of deep vein thrombosis during 2 years following diagnosis: a prospective evaluation. *J Thromb Haemost* 2011; 9: 2397–2405.
21. Hsu W-H, Chang T-C, Tsai T-C, et al. Managing May–Thurner syndrome: a review focusing on evolving treatment modalities. *J Exp Clin Med* 2012; 4: 265–269.
22. Taheri SA, Williams J, Powell S, et al. Iliocaval compression syndrome. *Am J Surg* 1987; 154: 169–172.
23. Xue G-H, Huang X-Z, Ye M, et al. Catheter-directed thrombolysis and stenting in the treatment of iliac vein compression syndrome with acute iliofemoral deep vein thrombosis: outcome and follow-up. *Surgery* 2014; 28: 957–963.
24. Forauer AR, Gemmete JJ, Dasika NL, et al. Intravascular ultrasound in the diagnosis and treatment of iliac vein compression (May–Thurner) syndrome. *J Vasc Interv Radiol* 2002; 13: 523–527.
25. Lijfering WM, Middeldorp S, Veeger NJGM, et al. Risk of recurrent venous thrombosis in homozygous carriers and double heterozygous carriers of factor v leiden and prothrombin G20210A. *Circulation* 2010; 121: 1706–1712.
26. De Stefano V, Chiusolo P, Paciaroni K, et al. Epidemiology of factor V Leiden: clinical implications. *Semin Thromb Hemost* 1998; 24: 367–379.
27. Kearon C, Kahn SR, Agnelli G, et al. Antithrombotic therapy for venous thromboembolic disease: American College of Chest Physicians Evidence-Based Clinical Practice Guidelines (8th Edition). *Chest* 2008; 133: 454S–545S.
28. Chitsike RS, Rodger MA, Kovacs MJ, et al. Risk of postthrombotic syndrome after subtherapeutic warfarin anticoagulation for a first unprovoked deep vein thrombosis: results from the REVERSE study. *J Thromb Haemost* 2012; 10: 2039–2044.
29. Stain M, Schönauer V, Minar E, et al. The post-thrombotic syndrome: risk factors and impact on the course of thrombotic disease. *J Thromb Haemost* 2005; 3: 2671–2676.
30. Puggioni A, Kistner RL, Eklof B, et al. Surgical disobliteration of postthrombotic deep veins – endophlebectomy – is feasible. *J Vasc Surg* 2004; 39: 1048–1052.
31. Jost CJ, Gloviczki P, Cherry KJ, et al. Surgical reconstruction of iliofemoral veins and the inferior vena cava for nonmalignant occlusive disease. *J Vasc Surg* 2001; 33: 320–328.
32. Comerota AJ, Grewal N, Martinez JT, et al. Postthrombotic morbidity correlates with residual thrombus following catheter-directed thrombolysis for iliofemoral deep vein thrombosis. *J Vasc Surg* 2012; 55: 768–773.

33. Kahn SR, Partsch H, Vedantham S, et al. Subcommittee on Control of Anticoagulation of the Scientific and Standardization Committee of the International Society on Thrombosis and Haemostasis, Definition of post-thrombotic syndrome of the leg for use in clinical investigations: a recommendation for standardization. *J Thromb Haemost* 2009; 7: 879–883.
34. Kahn SR, Shrier I, Julian JA, et al. Determinants and time course of the postthrombotic syndrome after acute deep venous thrombosis. *Ann Intern Med* 2008; 149: 698–707.
35. Stein PD, Matta F and Yaekoub AY. Incidence of vena cava thrombosis in the United States. *Am J Cardiol* 2008; 102: 927–929.
36. Plate G, Eklöf B, Norgren L, et al. Venous thrombectomy for iliofemoral vein thrombosis – 10-year results of a prospective randomised study. *Eur J Vasc Endovasc Surg* 1997; 14: 367–374.
37. Stain M, Schönauer V, Minar E, et al. The post-thrombotic syndrome: risk factors and impact on the course of thrombotic disease. *J Thromb Haemost* 2005; 3: 2671–2676.
38. Enden T, Haig Y, Kløw N-E, et al.; CaVenT Study Group. Long-term outcome after additional catheter-directed thrombolysis versus standard treatment for acute iliofemoral deep vein thrombosis (the CaVenT study): a randomised controlled trial. *Lancet* 2012; 379: 31–38.
39. Sharifi M, Bay C, Mehdipour M, et al.; TORPEDO Investigators. Thrombus Obliteration by Rapid Percutaneous Endovenous Intervention in Deep Venous Occlusion (TORPEDO) trial: midterm results. *J Endovasc Ther* 2012; 19: 273–280.
40. Casey ET, Murad MH, Zumaeta-Garcia M, et al. Treatment of acute iliofemoral deep vein thrombosis. *J Vasc Surg* 2012; 55: 1463–1473.
41. Kahn SR, Comerota AJ, Cushman M, et al.; American Heart Association Council on Peripheral Vascular Disease, Council on Clinical Cardiology, and Council on Cardiovascular and Stroke Nursing. The postthrombotic syndrome: evidence-based prevention, diagnosis, and treatment strategies. *Circulation* 2014; 130: 1636–1661.
42. Kumar R, Rodriguez V, Matsumoto JMS, et al. Health-related quality of life in children and young adults with post-thrombotic syndrome: results from a cross-sectional study. *Pediatr Blood Cancer* 2014; 61: 546–551.
43. Broholm R, Sillesen H, Damsgaard MT, et al. Postthrombotic syndrome and quality of life in patients with iliofemoral venous thrombosis treated with catheter-directed thrombolysis. *J Vasc Surg* 2011; 54: 18S–25S.
44. Kahn SR, Hirsch A and Shrier I. Effect of postthrombotic syndrome on health-related quality of life after deep venous thrombosis. *Arch Intern Med* 2002; 162: 1144–1148.

Clinical outcomes after direct and indirect surgical venous thrombectomy for inferior vena cava thrombosis

Markus U. Wagenhäuser, MD,[a] Christos Dimopoulos, MD,[a] Kamile Antakyali, MD,[a] Yvonne K. Meyer-Janiszewski, MD,[a] Joscha Mulorz, MD,[a,b] Wiebke Ibing, PhD,[a] Neslihan Ertas, MD,[a] Joshua M. Spin, MD, PhD,[c] Hubert Schelzig, MD,[a] *and* Mansur Duran, MD,[a] *Düsseldorf, Germany; and Stanford, Calif*

ABSTRACT

Objective: Inferior vena cava thrombosis is rare, but patients are at high risk for development of a post-thrombotic syndrome (PTS) in the long term. Surgical approaches include indirect transfemoral venous thrombectomy (iTFVT) and direct open venous thrombectomy (dOVT). This study reports patient outcomes after iTFVT and dOVT for inferior vena cava thrombosis covering a 25-year follow-up period.

Methods: The study period was from January 1, 1982, to December 31, 2013. Data were retrieved from archived medical records, and patients were invited for a detailed phlebologic follow-up examination (DPFE). Health-related quality of life was assessed with the 36-Item Short Form Health Survey questionnaire. Patient survival, patency rates, and freedom from PTS were calculated using Kaplan-Meier estimation with log-rank testing. The χ^2 test with Yates continuity correction and logistic regression analysis were applied to identify associations between risk factors or coagulation disorders, mortality, and PTS.

Results: Complete medical records were available for 152 patients. Patients' 5-year survival was 91% ± 3%, and 5-year primary and secondary patency rates were 80% ± 3% and 94% ± 2%. Freedom from PTS after 25 years was 84% ± 6%. No differences for patient survival, patency rates, or freedom from PTS were identified between iTFVT, dOVT, and a combination of both procedures. Antithrombin III deficiency was the most common coagulation disorder, and patients' physical function and social function were impaired compared with those found in German normative data ($P < .05$). No risk factor or coagulation disorder was associated with survival or PTS.

Conclusions: Open surgical venous thrombectomy is safe and delivers satisfying short- and long-term outcomes compared with endovascular approaches. It remains valuable for patients who are not eligible for other interventional therapies. (J Vasc Surg: Venous and Lym Dis 2019;7:333-43.)

Keywords: Iliofemoral; Deep venous thrombosis; Surgery; Post-thrombotic syndrome

Inferior vena cava (IVC) thrombosis (IVCT) is an underrated but severe problem. The diagnosis is challenging, given the heterogeneous clinical symptoms. Isolated IVCT is extremely rare and frequently accompanied by a concomitant deep venous thrombosis (DVT). DVT of the limb has an annual incidence as high as 48 to 122 per 100,000.[1,2] Of these patients, 2.6% to 4% might suffer from IVCT, which significantly affects patients' long-term morbidity and mortality.[3-5] Notably, patients with congenital IVC abnormalities are at higher risk for development of an IVCT.[6-8]

From the Department of Vascular and Endovascular Surgery, Heinrich-Heine University, Düsseldorf[a]; and the Stanford Cardiovascular Institute[b] and Division of Cardiovascular Medicine,[c] Stanford University School of Medicine, Stanford.

Author conflict of interest: none.

Additional material for this article may be found online at www.jvsvenous.org.

Correspondence: Christos Dimopoulos, MD, Department of Vascular and Endovascular Surgery, Heinrich-Heine University, Moorenstrasse 5, 40225 Düsseldorf, Germany (e-mail: christos.dimopoulos@med.uni-duesseldorf.de).

The editors and reviewers of this article have no relevant financial relationships to disclose per the Journal policy that requires reviewers to decline review of any manuscript for which they may have a conflict of interest.

2213-333X

https://doi.org/10.1016/j.jvsv.2018.11.005

Patients who do not receive appropriate treatment have a 90% risk for development of a post-thrombotic syndrome (PTS) after IVCT, and up to 15% may develop severe PTS with chronic leg ulcers.[9] PTS severely impairs patients' health-related quality of life (HRQOL) and has immense economic impact on the health care system.[9]

Patients with IVCT often describe symptoms similar to those that occur with an isolated DVT, such as leg heaviness, pain, swelling, and cramping. Although symptoms can be nonspecific or clinically silent, timely diagnosis is crucial to prevent severe life-threatening complications, such as pulmonary embolism (PE) or clot migration into the renal veins.[10]

Compression duplex ultrasound (CDU) is the modality of choice to confirm the clinical suspicion of an IVCT; however, computed tomography (CT) or magnetic resonance imaging scans may be required. After the diagnosis is established, immediate effective anticoagulation and appropriate compression therapy are obligatory. Despite a growing number of minimally invasive treatment options that have become increasingly feasible and broadly available during the last decades, open surgical venous thrombectomy remains a potential alternative.[11]

Open surgical venous thrombectomy with formation of an arteriovenous fistula (AVF) to temporarily augment venous blood flow is challenging and risky as procedure-related factors, such as passing a catheter through the IVCT or IVCT manipulations, may lead to potentially fatal PE.[12] Open surgical venous thrombectomy typically ensures complete and visually verifiable clot removal while significantly reducing the risk for development of PTS at long term. However, modern approaches, such as catheter-directed thrombolysis (CDT), have been claimed to be equally efficient in restoring venous patency.[13,14]

This study retroactively investigated patient mortality, patency, and freedom from PTS after indirect transfemoral venous thrombectomy (iTFVT) and direct open venous thrombectomy (dOVT) with temporary AVF for IVCT. It further analyzes the risk for development of long-term PTS and evaluates patients' HRQOL.

ARTICLE HIGHLIGHTS

- **Type of Research:** Single-center retrospective cohort study
- **Key Findings:** In a cohort of 152 patients who had open surgical thrombectomy for acute inferior vena cava thrombosis during a 32-year period, 5-year survival and secondary patency were 91% and 94%, respectively. Freedom from post-thrombotic syndrome after 25 years was 84%. Direct and indirect venous thrombectomy delivered similar outcomes.
- **Take Home Message:** Open surgical approaches may be considered for those patients with inferior vena cava thrombosis who are not candidates for endovascular treatment.

METHODS

Data collection. We reviewed our department's database and identified patients with IVCT starting from January 1, 1982, to December 31, 2013. Next, we included all patients who underwent open surgical venous thrombectomy as a first-line therapeutic approach. All relevant clinical information was extracted from archived medical records for patients' in-hospital stays and later outpatient department visits. The study was approved by the Ethic Committee of the Medical Faculty at the University Hospital Düsseldorf.

Surgery. CDU was used as first-line imaging to determine the extent of DVT and to aid in the diagnosis of an IVCT. Next, patients received a CT scan to confirm the diagnosis of IVCT, which was followed by recommendation of the appropriate direct or indirect surgical approach. On admission, patients received compression stockings along with intravenous administration of unfractionated heparin once the diagnosis was confirmed. Historically, once endovascular approaches had become a feasible alternative, patients were informed about the different therapeutic approaches. All cases were discussed among the senior surgeons of the department, considering severity of clinical symptoms and the patient's age. All cases underwent internal review, with consideration of the amount of IVC thrombus burden and lumen occlusion; the odds of successfully passing the IVCT with an occlusion catheter using a transfemoral approach followed by indirect thrombectomy were evaluated against the risk for PE. After thorough risk-benefit assessment, patients with disproportionate risk for thrombus mobilization with resultant PE (with use of iTFVT) were advised to undergo an open direct abdominal approach to improve the patient's safety. All patients gave their informed consent for the suggested surgical approaches. All procedures were performed by senior surgeons of the Department of Vascular and Endovascular Surgery at the University Hospital Düsseldorf. Patients received either iTFVT (n = 73) or dOVT (n = 35). In cases during which iTFVT or dOVT led to incomplete thrombus removal, both procedures were combined (n = 44; Supplementary Fig, online only).

iTFVT. All relevant veins were exposed using a longitudinal inguinal incision. Next, an entry-side segment in the femoral vein was identified, and a longitudinal venotomy was performed. The same approach was used on the contralateral side. Through the contralateral approach, an occlusion balloon catheter was advanced and placed proximal to the IVCT to prevent PE. Next, multiple venous thrombectomy maneuvers were performed on the thrombosed side using balloon catheters of increasing diameters to ensure complete thrombus removal (Fogarty maneuvers). To prevent PE, the positive end-expiratory pressure was temporarily raised to 15 mm Hg at the time of venous thrombectomy, and patients were kept in the supine anti-Trendelenburg position. Procedural success was confirmed by appropriate venous backflow. Thereafter, thrombectomy maneuvers were performed retrograde to remove the thrombus from the lower limb veins, guaranteeing appropriate backflow through the deep femoral vein. Manual compressions or Esmarch bandages were applied to augment complete clot removal. Sufficient backflow confirmed procedural success, and the venotomy was closed with running sutures. Before closure of the venotomy of the contralateral side, the occlusion balloon was used to perform a final Fogarty maneuver to remove mobilized residual thrombus (Supplementary Fig, *A*, online only).

dOVT through laparotomy. Briefly, median laparotomy was performed to open the abdominal cavity and to expose the IVC. Next, the proximal end of the thrombus was identified and the IVC was clamped. An entry-side

segment was identified, and a longitudinal IVC venotomy was performed. The thrombus was carefully removed. Multiple retrograde venous thrombectomy maneuvers were performed as described before, augmented with manual compression or Esmarch bandages. Again, procedural success was confirmed by sufficient backflow. Finally, IVC venotomy and midline laparotomy closure was performed (Supplementary Fig, *B*, online only).

Whenever there was suspicion of residual thrombus by either approach, the procedures were combined successively within the same operation. To reduce the risk for development of recurrent thrombosis during the critical postoperative 3-month period, an inguinal AVF was established to augment blood flow after either procedure, on whichever side was affected by iliac vein thrombosis. Whenever possible, we used a distal side branch of the superficial femoral artery and established the AVF at the most distal possible location. Next, we confirmed pulsatile fistula flow using continuous-wave Doppler.

All patients received a CDU examination before discharge to confirm patent veins. CDU or CT scans were used to diagnose recurrent thrombosis after surgery whenever clinical symptoms occurred.

Patients were transferred to the Department of Hemostasis and Transfusion Medicine for anticoagulation management, where the individual risk for recurrent thrombosis was assessed, considering the original thrombus burden, presence of anticoagulation disorders, and general risk factors. Whereas patients in the 1990s were advised to undergo prolonged anticoagulation, this time frame was reduced to 12 months starting with the new millennium. Novel oral anticoagulant drugs began to replace warfarin starting around 2014, after safety concerns had been dispelled.

Follow-up. The AVF was ligated 3 months after primary surgery during a second in-hospital stay. During that in-hospital stay, all patients received a CDU examination together with a CT scan to exclude recurrent thrombosis before AVF ligation. Further follow-up CDU scans were suggested at 6 and 12 months after primary surgery in our outpatient department. Thereafter, patients were transferred to collaborating general practitioners for annual CDU follow-up.

Inclusion and exclusion criteria. Patients had to be at least 18 years old and diagnosed with IVCT using CT scans. All patients had to undergo a clinical examination and to give informed consent before operation. The exclusion criteria were as follows: pregnancy, prior DVT, prior endovascular therapy with a percutaneous inguinal approach on the affected leg, poor general condition, absent consent after the risk-benefit assessment, and impossibility of establishing an inguinal AVF because of access site inaccessibility at presurgery evaluation.

Detailed phlebologic follow-up examination (DPFE) and HRQOL. Contact information was available for 90 patients. These patients were contacted and invited to our outpatient department for a DPFE. Together with a written invitation, patients were mailed a 36-Item Short Form Health Survey (SF-36) questionnaire and asked to send it back. At examination, patients were assessed on the severity of PTS symptoms along with a detailed examination of lower limb veins for occlusion and reflux using CDU. We used the Clinical, Etiology, Anatomy, and Pathophysiology (CEAP) classification and Villalta score to objectively categorize patients according to PTS severity.

The self-assessment-based SF-36 questionnaires gathered during a 4-week period (second version) were used to score eight independent health domains (physical functioning, physical role functioning, bodily pain, general health perceptions, social role functioning, vitality, emotional role functioning, and mental health). Component summary scores (physical component summary and mental component summary) were calculated from independent health scores.

Statistical analysis. Categorical data are presented as frequency distribution with percentages, continuous data as mean ± standard errors of mean. The Kaplan-Meier estimator was used to estimate patency, survival, and PTS rates using the latest available clinical information. The log-rank (Mantel-Cox) test was used to test for significance between subgroups. We used logistic regression analysis or χ^2 testing with Yates continuity correction to identify the association between risk factors or coagulation disorders and PTS or mortality. Statistical analysis was performed using GraphPad Prism 7 (GraphPad Software Inc, La Jolla, Calif) and SPSS 25.0 software (IBM Corp, Armonk, NY). A P value $<.05$ was considered statistically significant.

RESULTS

Recruitment of patients and basic demographics. We identified 180 patients who underwent open surgical venous thrombectomy for IVCT from January 1, 1982, through December 31, 2013. Complete clinical data were available for 152 patients. There were 38 patients who accepted the invitation to attend a DPFE in the outpatient department and filed SF-36 questionnaires; another 10 SF-36 questionnaires were filed by mail (Fig 1). In our study cohort, we identified four patients (3%) who required stent implantation in the left iliac vein for diagnosed May-Thurner syndrome on initial CT scans. These four patients were lost to follow-up at 7, 35, 52, and 112 months, respectively. None of these patients needed revision surgery because of stent complications or occlusions.

The mean age was 42.3 ± 1.4 years for the study cohort (n = 152) and 42.9 ± 2.8 years for patients at the DPFE

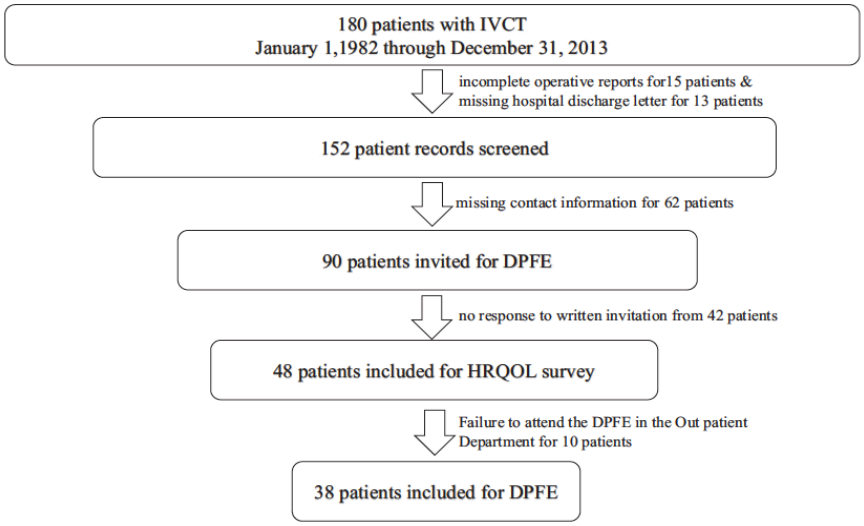

Fig 1. Patient recruitment and dropouts. We identified 180 patients with inferior vena cava thrombosis (*IVCT*) from January 1, 1982, through December 31, 2013, who underwent treatment at the University Hospital Düsseldorf. Of these, 90 patients were excluded because of incomplete clinical records; 90 patients were invited to attend a detailed phlebologic follow-up examination (*DPFE*) at the outpatient department. Patients also filed a 36-Item Short Form Health Survey (SF-36) questionnaire for assessment of health-related quality of life (*HRQOL*). Ultimately, 38 patients presented for the DPFE, and 48 patients returned the SF-36 questionnaire.

(n = 38). Mean follow-up time was 98.1 ± 8.5 months and 145.3 ± 15 at DPFE (143.5 ± 10.2 months for HRQOL). There was no sex preference. The left iliac-femoral veins were more frequently coaffected. The IVCT frequently extended to the lower extremity veins. Extension to the affected leg included 99.3% iliac, 77.63% femoral, and 33.55% popliteal veins. Logistic regression analysis revealed no association between risk factors and patient mortality or patency rates after open surgical venous thrombectomy. Patients received anticoagulation for a mean of 37.7 ± 6.1 months. Surgical subgroup-specific patient characteristics and risk factor distribution were similar to those of the total study cohort (Table I).

Mortality, patency, and freedom from PTS rates. Patient mortality, patency, and freedom from PTS rates were calculated using Kaplan-Meier estimation. During the follow-up period, 15 deaths occurred, none of them procedure related. Six patients died of a heart attack, three patients of lung cancer, two patients of colon cancer, three patients of pneumonia, and one patient of liver cirrhosis with visceral bleeding. Patients' 1- and 5-year survival rates were 93% ± 2% and 91% ± 3% after open surgical venous thrombectomy for IVCT (Fig 2, *A*). Subgroup-specific survival at 1 year (Fig 2, *B*) was as follows: iTFVT, 89% ± 4%; dOVT, 91% ± 5%; and combined, 100%. Subgroup-specific survival at 25 years (Fig 2, *B*) was as follows: iTFVT, 87% ± 5%; dOVT, 78% ± 9%; and combined, 100%. Patients' 1- and 5-year primary patency rates were 83% ± 3% and 80% ± 3%, and secondary 1- and 5-year patency rates were 96% ± 2% and 94% ± 2%, respectively (Fig 2, *C*). Subgroup-specific primary patency rates at 1 year (Fig 2, *D*) were as follows: iTFVT, 80% ± 4%; dOVT, 86% ± 6%; and combined, 83% ± 6%. Patients' 1- and 5-year freedom from PTS rates were both 100%, whereas 9 and 25 years later, they were 97% ± 2% and 84% ± 6%, respectively (Fig 2, *E*). Subgroup-specific 25-year freedom from PTS rates (Fig 2, *F*) were as follows: iTFVT, 96% ± 4%; dOVT, 90% ± 9%; and combined, 69% ± 12%.

Postsurgery complications. Overall postsurgery complications occurred in 46 of 152 (30%) patients. Complications were subclassified according to the Clavien-Dindo classification. Analyzing the complete patient cohort, the different surgical subgroups, and the patients who presented for DPFE, the distribution of complications was similar (Table II). Notably, there were no grade IVb complications (multiorgan dysfunction), whereas grade IIIb complications (requiring any sort of intervention needing general anesthesia) were most frequent. Screening the medical records, we identified 18 patients (~12%) who required blood transfusion. In detail, there were 8 hematomas (iTFVT, 2; dOVT, 4; combined operation, 2), 6 occluded AVFs (iTFVT, 2; dOVT, 1; combined operation, 3), 2 with impaired wound healing (dOVT, 1; combined

Table I. Patients' characteristics and risk factors

Characteristics	Total study cohort (N = 152)			Patients at DPFE (n = 38)
	iTFVT (n = 73)	dOVT (n = 35)	Combined (n = 44)	
Age, years		42.4 ± 1.4		42.9 ± 2.8
	44.8 ± 2.1	44.8 ± 3	36.5 ± 2.3	
Length of in-hospital stay, days	12.8 ± 1			10.4 ± 0.7
	12.1 ± 1.7	15.8 ± 2.3	11.8 ± 0.9	
Sex	M: 76/152 (50); F: 76/152 (50)			M: 19/38 (50) F: 19/38 (50)
	M: 33/73 (45.2) F: 40/73 (54.8)	M: 19/35 (54.3) F: 16/35 (45.7)	M: 24/44 (54.5) F: 20/44 (45.5)	
Concomitant PE before surgery		59/152 (38.8)		17/38 (44.7)
	22/73 (30.1)	14/35 (40)	23/44 (52.3)	
Concomitantly affected leg	r: 36/152 (23.7); l: 66/152 (43.4); b: 50/152 (32.9)			r: 9/38 (23.7) l: 20/38 (52.6) b: 9/38 (23.7)
	r: 19/73 (26) l: 38/73 (52) b: 16/73 (22)	r: 9/35 (25.7) l: 14/35 (40) b: 11/35 (31.4)	r: 8/44 (18.2) l: 13/44 (29.5) b: 23/44 (52.3)	
AVF	ss: 110/152 (72.4); bs: 42/152 (27.6)			ss: 27/38 (71.1) bs: 11/38 (28.9)
	ss: 62/73 (84.9) bs: 11/73 (15.1)	ss: 23/35 (65.7) bs: 12/35 (34.3)	ss: 25/44 (56.8) bs: 19/44 (43.2)	
Anticoagulation therapy, months		37.7 ± 6.1		48.2 ± 11.9
	69.4 ± 8.1	32.7 ± 11.6	50 ± 13.6	

Risk factors	Total study cohort (N = 152)					Patients at DPFE (n = 38)
				Log regression		
	iTFVT (n = 73)	dOVT (n = 35)	Combined (n = 44)	Mortality	Patency	
Obesity		19/152 (12.5)				6/38 (15.8)
	8/73 (11)	4/35 (11.4)	7/44 (15.9)	.92	.39	
Immobilization		97/152 (63.8)				23/38 (60.5)
	48/73 (65.8)	21/35 (60)	28/44 (63.6)	.75	.43	
Smoking		30/152 (19.7)				10/38 (26.3)
	16/73 (21.9)	4/35 (11.4)	10/44 (22.7)	.51	.17	
Carcinoma		23/152 (15.1)				3/38 (7.9)
	11/73 (15.1)	7/35 (20)	5/44 (11.4)	.58	.41	

AVF, Arteriovenous fistula; *b*, both; *bs*, both sides; *dOVT*, direct open venous thrombectomy; *DPFE*, detailed phlebologic follow-up examination; *iTFVT*, indirect transfemoral venous thrombectomy; *l*, left; *PE*, pulmonary embolism; *r*, right; *ss*, single side.
Patients' basic characteristics are presented for the total study cohort, the surgical subgroups, and the DPFE cohort separately. Arteriovenous fistula was constructed on the side of iliac vein thrombosis. A logistic regression analysis (Hosmer-Lemeshow test) was applied to analyze whether risk factors for inferior vena cava thrombosis (total, n = 152) are associated with patient mortality, patency, or post-thrombotic syndrome rate. Data are presented as mean ± standard error of the mean or frequency distribution (%).

operation, 1), 1 intestinal obstruction (combined operation), 1 peritonitis (dOVT), and 36 recurrent thromboses (iTFVT, 20; dOVT, 6; combined operation, 10).

Applying CDU and CT scans, 36 patients with recurrent thromboses were identified. In detail, we observed 33 recurrent iliac vein thromboses. Of these, 23 recurrent thromboses also affected the femoral veins and 6 the popliteal veins. Whereas there were no isolated recurrent thromboses in the femoral or popliteal veins, four isolated recurrent IVCTs were observed. In accordance with extension of the proximal recurrent thrombosis in the IVC, 19 iTFVTs and eight dOVTs were performed as repeated operations. Nine of the recurrent thrombosis patients showed limited extension and mild clinical symptoms and underwent conservative management. A second additional recurrent thrombosis after repeated surgery occurred in 11 patients. For these, four iTFVTs and one dOVT were performed as second repeated operations, whereas six patients underwent conservative management.

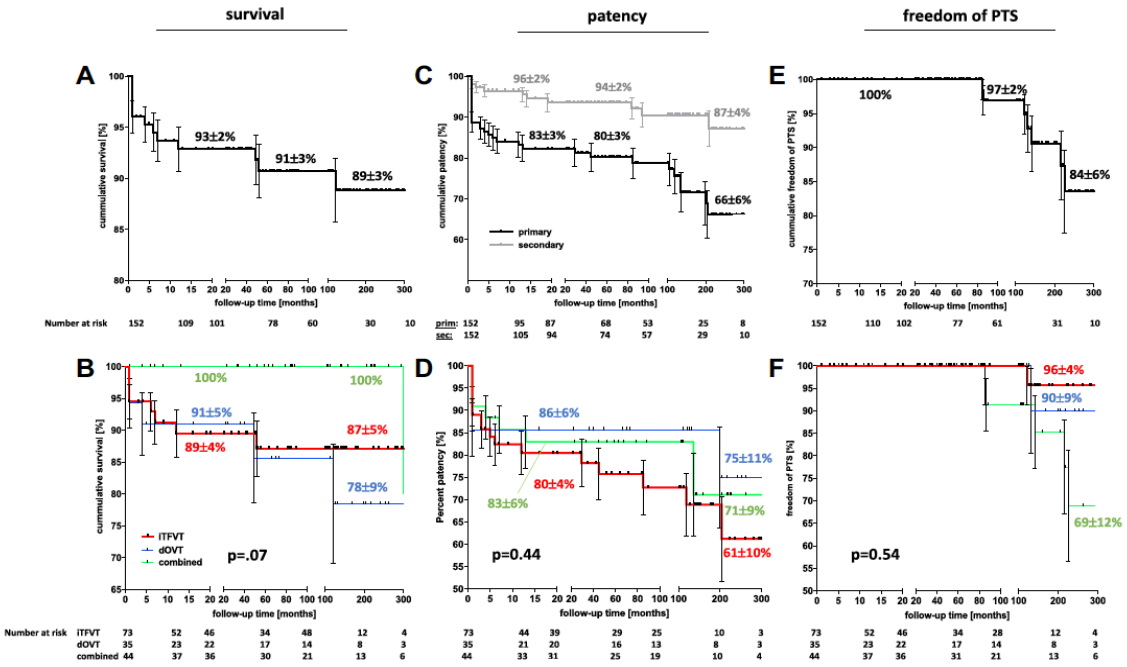

Fig 2. Kaplan-Meier estimator for patient follow-up outcomes. Data are ±standard error of the mean. Post-thrombotic syndrome (*PTS*) was defined inconsistently during the study period. For patients who attended the detailed phlebologic follow-up examination (DPFE; n = 38), a Villalta score of ≥5 was considered PTS. For the remaining patients (n = 114), PTS needed to be mentioned in the list of diagnoses of the latest archived medical records of collaborating general practitioners or of the outpatient department. **A,** Kaplan-Meier estimator for patient survival. Patients' 1-, 5-, and 25-year survival rates are presented. **B,** Subgroup-specific Kaplan-Meier estimator for patient survival. Patients' 1- and 25-year survival rates are presented for each subgroup. *dOVT,* Direct open venous thrombectomy; *iTFVT,* indirect transfemoral venous thrombectomy. **C,** Kaplan-Meier estimator for primary and secondary patency rates for inferior vena cava thrombosis (IVCT). Recurrent thrombosis after primary surgery was diagnosed using compression duplex ultrasound (CDU) or computed tomography (CT) scans. Patency rates at 1 year, 5 years, and 25 years are presented. **D,** Subgroup-specific Kaplan-Meier estimator for primary patency rates. Patients' 1- and 25-year primary patency rates are presented for each subgroup. **E,** Kaplan-Meier estimator for freedom from PTS. The 1-, 5-, and 25-year freedom from PTS rates are presented. **F,** Subgroup-specific Kaplan-Meier estimator for freedom from PTS. Patients' 25-year freedom from PTS rates are presented for each subgroup. **A, C,** and **E:** n = 152. **B, D,** and **F:** n = 73 for iTFVT, n = 35 for dOVT, n = 44 for combined procedures; log-rank (Mantel-Cox) test was applied. No significant differences were found between subgroups. *P* values are shown.

DPFE. Patients were invited to attend a DPFE at the outpatient department. Along with the invitation, patients were asked to file an SF-36 questionnaire.

We received 48 questionnaires, resulting in a 53% return rate (48/90) of mailed questionnaires and 27% (48/180) for the entire patient cohort. Patients with IVCT who underwent open surgical venous thrombectomy considered their physical and social functioning worse than did the German normative control group. Nevertheless, there was no difference for the mental and physical component summary scores between cohorts (Table III).

There were 38 patients (38/180 [21%]) who presented for a DPFE. The mean follow-up time at clinical examination for this subgroup of patients was 145.3 ± 15 months. All of these patients were screened for coagulation disorders. Antithrombin III deficiency (3/38 [7.9%]) was the most common coagulation disorder. We could not identify an association between coagulation disorders and follow-up patency or PTS (Table IV).

At clinical examination, patients received detailed assessment of lower limb veins for reflux and occlusion (Supplementary Table, online only). Next, patients were classified on the basis of their clinical symptoms according to the Villalta score and CEAP clinical classes. Using the Villalta score, 10 of 38 (26%) patients received a score of ≥5. When the CEAP clinical classes were used, 15 patients (15/38 [39%]) were subclassified for classes ≥C3 (Table V).

Table II. Postsurgery complications according to the Clavien-Dindo classification

Grade	Total study cohort (N = 152)			Patients at DPFE (n = 38)
	iTFVT (n = 73)	dOVT (n = 35)	Combined (n = 44)	
0		106/152 (69.7)		25/38 (65.8)
	55/73 (75.3)	22/35 (62.9)	30/44 (68.2)	
I		8/152 (5.3)		4/38 (10.5)
	4/73 (5.5)	3/35 (8.6)	1/44 (2.3)	
II		10/152 (6.6)		3/38 (7.9)
	3/73 (4.1)	2/35 (5.7)	(5/44 11.4)	
IIIa		2/152 (1.3)		0/38 (0)
	0/73 (0)	0/35 (0)	2/44 (4.5)	
IIIb		20/152 (13.2)		6/38 (15.8)
	7/73 (9.6)	6/35 (17.1)	6/44 (13.6)	
IVa		1/152 (0.7)		0/38 (0)
	1/73 (1.4)	0/35 (0)	0/44 (0)	
IVb		0/152 (0)		0/38 (0)
	0/73 (0)	0/35 (0)	0/44 (0)	
V		5/152 (3.3)		0/38 (0)
	3/73 (4.1)	2/35 (5.7)	0/44 (0)	

dOVT, Direct open venous thrombectomy; *DPFE*, detailed phlebologic follow-up examination; *iTFVT*, indirect transfemoral venous thrombectomy.
Data are presented as frequency distribution (%). Distribution of complications was similar between surgical subgroups.

DISCUSSION

This single-center study reports clinical patient outcomes after iTFVT and dOVT for IVCT during a 25-year follow-up period. We included 152 patients, with 38 patients presenting for a DPFE with assessment of PTS symptoms. As noted before, patient survival was satisfactory, and patency rates were similar to those of modern endovascular interventional approaches. Applying the Villalta score, freedom from PTS after 25 years was 84% using Kaplan-Meier estimation and 26.3% after 12 years using detailed phlebologic examination.

To date, there is no specific recommendation for the duration of long-term anticoagulation for IVCT. It is well established that a recurrent thrombosis is a significant risk factor for development of PTS. The Recurrent Venous thromboembolism Risk Stratification Evaluation (REVERSE) study has demonstrated the importance of therapeutic anticoagulation in reducing the long-term

Table III. The 36-Item Short Form Health Survey (SF-36) scores for patients at detailed phlebologic follow-up (DPFE)

	Physical functioning	Role physical	Bodily pain	General health perceptions	Energy/ vitality	Social functioning	Role emotional	Mental health	Physical component score	Mental component score
IVCT										
Mean score	74.1	79.5	71.9	62.3	58.1	80.5	83.3	72.8	46.7	48.1
SEM	4.0	5.0	4.2	3.0	2.9	3.2	4.5	2.7	5.0	1.7
German normative data										
Mean score	83.6	80.3	77.2	66.0	61.8	87.7	87.7	72.8	49.3	49.4
Difference in means	9.5	0.8	5.3	3.7	3.7	7.2	4.4	0	2.6	1.3
Analysis										
Levene test	0.16	0.97	0.84	0.77	0.42	<.05	0.11	0.31	0.78	0.13
P value, *t*-test	<.05[a]	.84	.21	.22	.22	<.05[a]	.34	.99	.58	.66

IVCT, Inferior vena cava thrombosis; *SEM*, standard error of the mean.
Eight domain scores of the SF-36 and two summary scales (physical component and mental component) are presented for patients after indirect transfemoral or direct open venous thrombectomy with temporary arteriovenous fistula for IVCT. Physical and social functioning scores were significantly lower vs German normative data, whereas there was no difference for the physical and mental component summary scores. Data were analyzed for homogeneity of variances (Levene test), and Student or Welch *t*-test was applied accordingly.
[a] $P < .05$ IVCT vs German normative data.

Table IV. Coagulation disorders of patients at detailed phlebologic follow-up (DPFE; N = 38)

	Frequency distribution	%	*P* value	
			Association with patency	Association with PTS
APC resistance	2/38	5.3	.78	.11
Prothrombin mutation	1/38	2.6	.74	.59
Antithrombin III deficiency	3/38	7.9	.55	.69
MTHFR mutation	1/38	2.6	.74	.59
Antiphospholipid antibody	0/38	0	–	–
Protein C deficiency	2/38	5.3	.53	.97
Protein S deficiency	2/38	5.3	.78	.97
Factor VII deficiency	0/38	0	–	–
Factor V Leiden thrombophilia	2/38	5.3	.78	.97
Elevated factor VIII level	0/38	0	–	–
Hyperfibrinogenemia	2/38	5.3	.78	.97
Homocysteinemia	0/38	0	–	–

APC, Activated protein C; *PTS*, post-thrombotic syndrome.
At clinical follow-up examination, patients were screened for coagulation disorders. The χ^2 test with Yates continuity correction was used to determine the association of anticoagulation disorders with patency or PTS in the long term.

incidence of PTS.[15,16] The American College of Chest Physicians suggests anticoagulation for 3 to 6 months for provoked proximal DVT and up to 12 months for unprovoked proximal DVT.[16] Notably, prolonged anticoagulation in the early years of the study may have caused a clinical advantage for this subgroup of patients, generating less recurrent thrombosis and increased patency, thus potentially biasing outcomes.

In the case of IVCT, the authors believe that there is a higher risk for recurrent thrombosis compared with proximal DVT patients, given the large amount of structurally damaged post-thrombotic vein wall area. In this study, we found that our cohort received anticoagulation for a mean of 37.7 ± 6.1 months. Considering this and in line with current guidelines, the authors advise that anticoagulation should be administrated for at least 12 months, in particular after open surgical venous thrombectomy, which can cause additional damage to vein valves.[16] Thereafter, patients might benefit from interdisciplinary management to further optimize the duration of anticoagulation, thereby minimizing the risk for development of PTS.

Table V. Villalta score and Clinical, Etiology, Anatomy, and Pathophysiology (*CEAP*) classification results at the detailed phlebologic follow-up (DPFE; N = 38)

	Frequency distribution	%
Villalta score		
None (≤5)	28/38	73.7
Mild disease (5-9)	4/38	10.5
Moderate disease (10-14)	4/38	10.5
Severe disease (≥15)	2/38	5.3
CEAP class		
C0	11/38	29
C1	7/38	18.4
C2	5/38	13.2
C3	7/38	18.4
C4a	5/38	13.2
C4b	1/38	2.6
C5	2/38	5.3
C6	0/38	0

At clinical examination, patients were categorized and scored according to the CEAP classification and the Villalta score based on clinical findings.

During the last two decades, there has been a scientific debate about the benefits and complications of IVC filters in this context. Interestingly, placement rates are 25 times lower in Europe than in the United States, reflecting a considerable difference in expertise.[12] Considering procedure-, postprocedure-, and retrieval-related complications, such as tilted implantation or incomplete filter opening, filter migration and thrombosis, and IVC injury during retrieval, our department intentionally decided not to use retrievable IVC filters for iTFVT.[17] Instead, placement of a temporary occlusion balloon above the renal veins combined with a temporary elevation of positive end-expiratory pressure and a supine anti-Trendelenburg position was used to prevent PE. Conspicuously, the study's procedure-related PE rate was as low as 2.6%, suggesting the effectiveness of this approach.

Previous studies have already evaluated surgical thrombus removal and systemic thrombolysis and proved both approaches to be effective in preventing PTS.[18-21] Considering available surgical approaches, the majority of authors focus on minimally invasive iliofemoral methods, in which a Fogarty catheter is advanced

through an inguinal venotomy to remove the thrombus. In the case of extensive IVCT, this approach bears elevated risks of incomplete thrombus removal and should be performed only after placement of an occlusion catheter proximal to the IVCT through the contralateral side before Fogarty maneuvers. In contrast, dOVT is much more invasive. Both procedures should always be combined with a temporary AVF.[22,23] In this study, either procedure or both procedures were performed on the basis of the extension of the IVCT. Interestingly, we did not find a difference between the surgical approaches in terms of survival, patency, or freedom from PTS rates. Consequently, we conclude that whenever physicians decide to treat an IVCT using open surgical approaches and the burden of IVCT allows either procedure, surgeons should decide on the basis of their personal preference and skill set as clinical outcomes appear similar.

As Comerota et al[24] correlated PTS development to residual thrombus burden, complete thrombus removal seems vital for patients' long-term benefit. Intraoperative venography may help establish whether this has occurred after intervention. However, that planar imaging technique is prone to missing residual thrombus. Given that recent advances in CT imaging have reduced the radiation dose, it seems plausible to suggest routine CT scans after surgical venous thrombectomy to establish irrefutable results, although this was not done in the study.

Modern, less invasive approaches have gained prominence within the last decades, such as CDT, pharmacomechanical CDT (PCDT), and pharmacomechanical thrombectomy. In comparing CDT and PCDT with anticoagulation alone, both approaches are thought to be effective in preventing PTS long term when used for iliofemoral DVT.[25,26] However, Alkhouli et al[27] reported a considerably elevated risk for PE (12.1% vs 7.8%), intracranial hemorrhage (1.6% vs 0.2%), and acute renal failure (13.9% vs 9.4%) when using CDT for treatment of IVCT. In addition, patients treated with CDT require continuous clinical bleeding observation by medical professionals combined with prolonged intensive care unit stay, which leads to the patient's discomfort.[12] Regardless of the invasiveness of iTFVT and dOVT, severe complications (Clavien-Dindo grade ≥IIIa) are uncommon,[12] acting in favor of these procedures. Despite in-hospital stays lasting as long as 13 days on average for open surgical venous thrombectomy, specific material-related cost-intensive endovascular approaches are still more expensive on final analysis.[12]

Besides major procedure-related complications, patency rates should also be taken into consideration in deciding on the best therapeutic approach. Our study reports a survival rate of 91%, with primary and secondary patency rates of 80% and 94% at 5 years after surgery. A study by Ye et al[28] cited 3-year primary and secondary patency rates of 63% and 83% using PCDT for IVCT. Moreover, comparing the outcome of our study with others, open surgical venous thrombectomy for iliofemoral DVT has been suggested to have a 3-year patency rate of 86%.[29] Patency rates for iTFVT and dOVT are comparable to previously reported outcomes using similar surgical procedures and are slightly better compared with patency rates using endovascular approaches such as CDT.

In summary, endovenous therapy bears significant risk of recurrent thrombosis and incomplete clot removal. Considering the presented data, the authors believe that lessons learned from endovenous approaches may act as an impetus for re-establishing open surgical venous thrombectomy.

The most severe long-term complication for patients is the development of relevant PTS, with venous ulceration at worst. PTS dramatically impairs the patient's quality of life. Notably, this study provides the longest follow-up period of analyzing surgical approaches for IVCT to date by covering >25 years. As such, it is important to diagnose PTS on the basis of objective scores. As the CEAP classification does not have an agreed-on cutoff, the Subcommittee on Control of Anticoagulation of the International Society on Thrombosis and Hemostasis suggests routine use of the Villalta score for establishing an appropriate diagnosis and that the score should be considered the "gold standard."[30,31] This study found a 25-year freedom from PTS of 84% (PTS rate of 16%) using Kaplan-Meier estimations and a PTS rate of 26.3% for patients who attended the DPFE at a mean follow-up of 12 years. Using the Villalta score, frequently used endovascular approaches found PTS rates of 13% after 26 months for PCDT and 41% for CDT in patients with IVCT or proximal DVT.[28,32] Considering these results, iTFVT and dOVT might improve the risk for development of clinically relevant PTS long term compared with modern endovascular techniques.

Nevertheless, it is certainly the case that patients might prefer endovascular minimally invasive approaches as these procedures cause less access site tissue damage and have been shown to reduce the risk of significant blood loss.[33] This is in line with our study, as we report a considerable blood transfusion rate of ~12%. Equipment availability for low-invasiveness procedures, along with interventionalists' expertise, is gradually expanding. For this reason, it is likely that patient outcomes will improve for these techniques in the near future. However, evidence proving the superiority of endovascular techniques regarding patient outcomes is not yet available.

The acceptance and relevance of any therapy always depend on patient satisfaction. Therefore, the patient's HRQOL would seem of utmost interest. Our study suggests that open surgical approaches for IVCT affect patients' physical and social functioning, whereas overall mental health and physical health seem similar to those found in German normative data when the SF-36

questionnaire is used. In general, patient-based quality of life measures correlate with physicians' objective assessments of clinical PTS symptoms.[4] Broholm et al[34] demonstrated that venous reflux and occluded veins are the main contributors favoring impaired HRQOL for patients with iliofemoral DVT. The fear of social stigmatization due to visible ulcerations, along with widespread disease-specific knowledge about long-term complications, might explain impaired social functioning in our patient collective.

This study has major limitations. The retrospective design potentially biased reported outcomes. Only patients with valid contact information were available for objective data acquisition and Villalta scoring, thus limiting the power of the study. Furthermore, the majority of patients were enrolled early in the study, which might have resulted in a significant selection bias due to shifts in patients' age and comorbidities. Reported PTS rates might also be biased as objective criteria to diagnose PTS were not applied consistently during the study period. Exact Villalta score calculation based on objective clinical symptoms could be obtained only for patients attending the DPFE, whereas the remaining patients were screened for PTS on the basis of their latest archived medical records. In addition, our reported results might incorporate a timing bias, meaning that patient scoring and record analysis were performed at a given time point, although patients might have suffered from PTS symptoms at some prior time point. Our conclusions may also be somewhat compromised, given that only 21% of the entire patient cohort was available for a DPFE, and only 27% filed an SF-36 questionnaire, even though basic characteristics were similar between the entire study cohort and patients at DPFE.

CONCLUSIONS

Open surgical venous thrombectomy delivers satisfactory patient outcomes regarding patency and long-term PTS. Even though patients' preferences might favor endovascular interventional therapies, open surgery remains an option for patients who either reject or are ineligible for these approaches. In particular, emergency situations with fulminant PE might still require the skill set and knowledge of a trained surgeon capable of performing indirect or direct surgical approaches for the most beneficial patient outcomes.

AUTHOR CONTRIBUTIONS

Conception and design: MW, KA, HS, MD
Analysis and interpretation: MW, CD, KA, JM, WI, NE, JS
Data collection: MW, CD, KA, YMJ
Writing the article: MW, CD, NE, JS
Critical revision of the article: MW, CD, KA, YMJ, JM, WI, JS, HS, MD
Final approval of the article: MW, CD, KA, YMJ, JM, WI, NE, JS, HS, MD
Statistical analysis: MW, CD, YMJ, WI, MD
Obtained funding: Not applicable
Overall responsibility: MW

REFERENCES

1. Coon WW, Willis PW, Keller JB. Venous thromboembolism and other venous disease in the Tecumseh community health study. Circulation 1973;48:839-46.
2. Anderson FA Jr, Wheeler HB, Goldberg RJ, Hosmer DW, Patwardhan NA, Jovanovic B, et al. A population-based perspective of the hospital incidence and case-fatality rates of deep vein thrombosis and pulmonary embolism. The Worcester DVT Study. Arch Intern Med 1991;151:933-8.
3. White RH. The epidemiology of venous thromboembolism. Circulation 2003;107:I4-8.
4. Kahn SR, Hirsch A, Shrier I. Effect of postthrombotic syndrome on health-related quality of life after deep venous thrombosis. Arch Intern Med 2002;162:1144-8.
5. Stein PD, Matta F, Yaekoub AY. Incidence of vena cava thrombosis in the United States. Am J Cardiol 2008;102:927-9.
6. Patel R, Choksi D, Chaubal A, Pipaliya N, Ingle M, Sawant P. Renal vein and inferior vena cava thrombosis: a rare extra-splanchnic complication of acute pancreatitis. ACG Case Rep J 2016;3:e172.
7. Sitwala PS, Ladia VM, Brahmbhatt PB, Jain V, Bajaj K. Inferior vena cava anomaly: a risk for deep vein thrombosis. N Am J Med Sci 2014;6:601-3.
8. Chee YL, Culligan DJ, Watson HG. Inferior vena cava malformation as a risk factor for deep venous thrombosis in the young. Br J Haematol 2001;114:878-80.
9. Sen CK, Gordillo GM, Roy S, Kirsner R, Lambert L, Hunt TK, et al. Human skin wounds: a major and snowballing threat to public health and the economy. Wound Repair Regen 2009;17:763-71.
10. Heit JA, Silverstein MD, Mohr DN, Petterson TM, O'Fallon WM, Melton LJ 3rd. Risk factors for deep vein thrombosis and pulmonary embolism. Arch Intern Med 2000;160:809.
11. Prandoni P, Lensing AW, Prins MH, Frulla M, Marchiori A, Bernardi E, et al. Below-knee elastic compression stockings to prevent the post-thrombotic syndrome. Ann Intern Med 2004;141:249.
12. Alkhouli M, Morad M, Narins CR, Raza F, Bashir R. Inferior vena cava thrombosis. JACC Cardiovasc Interv 2016;9:629-43.
13. Turpie G, Levine N, Hirsh J, Ginsberg S, Cruickshank M, Jay R, et al. Tissue plasminogen activator (rt-PA) vs heparin in deep vein thrombosis. Results of a randomized trial. Chest 1990;97:172-5.
14. Goldhaber SZ, Meyerovitz MF, Green D, Vogelzang RL, Citrin P, Heit J, et al. Randomized controlled trial of tissue plasminogen activator in proximal deep venous thrombosis. Am J Med 1990;88:235-40.
15. Chitsike RS, Rodger MA, Kovacs MJ, Betancourt MT, Wells PS, Anderson DR, et al. Risk of post-thrombotic syndrome after subtherapeutic warfarin anticoagulation for a first unprovoked deep vein thrombosis: results from the REVERSE study. J Thromb Haemost 2012;10:2039-44.
16. Kearon C, Akl EA, Comerota AJ, Prandoni P, Bounameaux H, Goldhaber SZ, et al. Antithrombotic therapy for VTE disease: Antithrombotic Therapy and Prevention of Thrombosis, 9th ed: American College of Chest Physicians Evidence-Based Clinical Practice Guidelines. Chest 2012;141:e419S-96S.
17. Grewal S, Chamarthy MR, Kalva SP. Complications of inferior vena cava filters. Cardiovasc Diagn Ther 2016;6:632-41.

18. Comerota AJ, Aldridge SC. Thrombolytic therapy for deep venous thrombosis: a clinical review. Can J Surg 1993;36:359-64.
19. Schweizer J, Kirch W, Koch R, Elix H, Hellner G, Forkmann L, et al. Short- and long-term results after thrombolytic treatment of deep venous thrombosis. J Am Coll Cardiol 2000;36:1336-43.
20. Wagenhäuser MU, Sadat H, Dueppers P, Meyer-Janiszewski YK, Spin JM, Schelzig H, et al. Open surgery for iliofemoral deep vein thrombosis with temporary arteriovenous fistula remains valuable. Phlebology 2018;33:600-9.
21. Dueppers P, Grabitz K, Li Y, Schelzig H, Wagenhäuser MU, Duran M. Surgical management of iliofemoral vein thrombosis during pregnancy and the puerperium. J Vasc Surg Venous Lymphat Disord 2016;4:392-9.
22. Neglén P, Nazzal MM, al-Hassan HK, Christenson JT, Eklöf B. Surgical removal of an inferior vena cava thrombus. Eur J Vasc Surg 1992;6:78-82.
23. Kniemeyer HW, Sandmann W, Schwindt C, Grabitz K, Torsello G, Stühmeier K. Thrombectomy with arteriovenous fistula for embolizing deep venous thrombosis: an alternative therapy for prevention of recurrent pulmonary embolism. Clin Investig 1993;72:40-5.
24. Comerota AJ, Grewal N, Martinez JT, Chen JT, Disalle R, Andrews L, et al. Postthrombotic morbidity correlates with residual thrombus following catheter-directed thrombolysis for iliofemoral deep vein thrombosis. J Vasc Surg 2012;55:768-73.
25. Razavi MK, Wong H, Kee ST, Sze DY, Semba CP, Dake MD. Initial clinical results of tenecteplase (TNK) in catheter-directed thrombolytic therapy. J Endovasc Ther 2002;9:593-8.
26. Sugimoto K, Hofmann LV, Razavi MK, Kee ST, Sze DY, Dake MD, et al. The safety, efficacy, and pharmacoeconomics of low-dose alteplase compared with urokinase for catheter-directed thrombolysis of arterial and venous occlusions. J Vasc Surg 2003;37:512-7.
27. Alkhouli M, Zack CJ, Zhao H, Shafi I, Bashir R. Comparative outcomes of catheter-directed thrombolysis plus anticoagulation versus anticoagulation alone in the treatment of inferior vena caval thrombosis. Circ Cardiovasc Interv 2015;8:e001882.
28. Ye K, Qin J, Yin M, Liu X, Lu X. Outcomes of pharmacomechanical catheter-directed thrombolysis for acute and subacute inferior vena cava thrombosis: a retrospective evaluation in a single institution. Eur J Vasc Endovasc Surg 2017;54:504-12.
29. Pokrovskiĭ AV, Ignat'ev IM, Gradusov EG, Bredikhin RA. [Open thrombectomy in acute iliofemoral venous thrombosis]. Angiol Sosud Khir 2017;23:177-84.
30. Kahn SR, Partsch H, Vedantham S, Prandoni P, Kearon C; Subcommittee on Control of Anticoagulation of the Scientific and Standardization Committee of the International Society on Thrombosis and Haemostasis. Definition of post-thrombotic syndrome of the leg for use in clinical investigations: a recommendation for standardization. J Thromb Haemost 2009;7:879-83.
31. Soosainathan A, Moore HM, Gohel MS, Davies AH. Scoring systems for the post-thrombotic syndrome. J Vasc Surg 2013;57:254-61.
32. Enden T, Haig Y, Kløw NE, Slagsvold CE, Sandvik L, Ghanima W, et al. Long-term outcome after additional catheter-directed thrombolysis versus standard treatment for acute iliofemoral deep vein thrombosis (the CaVenT study): a randomised controlled trial. Lancet 2012;379:31-8.
33. Martinez Trabal JL, Comerota AJ, LaPorte FB, Kazanjian S, DiSalle R, Sepanski DM. The quantitative benefit of isolated, segmental, pharmacomechanical thrombolysis (ISPMT) for iliofemoral venous thrombosis. J Vasc Surg 2008;48:1532-7.
34. Broholm R, Sillesen H, Damsgaard MT, Jørgensen M, Just S, Jensen LP, et al. Postthrombotic syndrome and quality of life in patients with iliofemoral venous thrombosis treated with catheter-directed thrombolysis. J Vasc Surg 2011;54:18S-25S.

Submitted Aug 1, 2018; accepted Nov 7, 2018.

Additional material for this article may be found online at www.jvsvenous.org.

Journal of Vascular Surgery: Venous and Lymphatic Disorders
May 2019

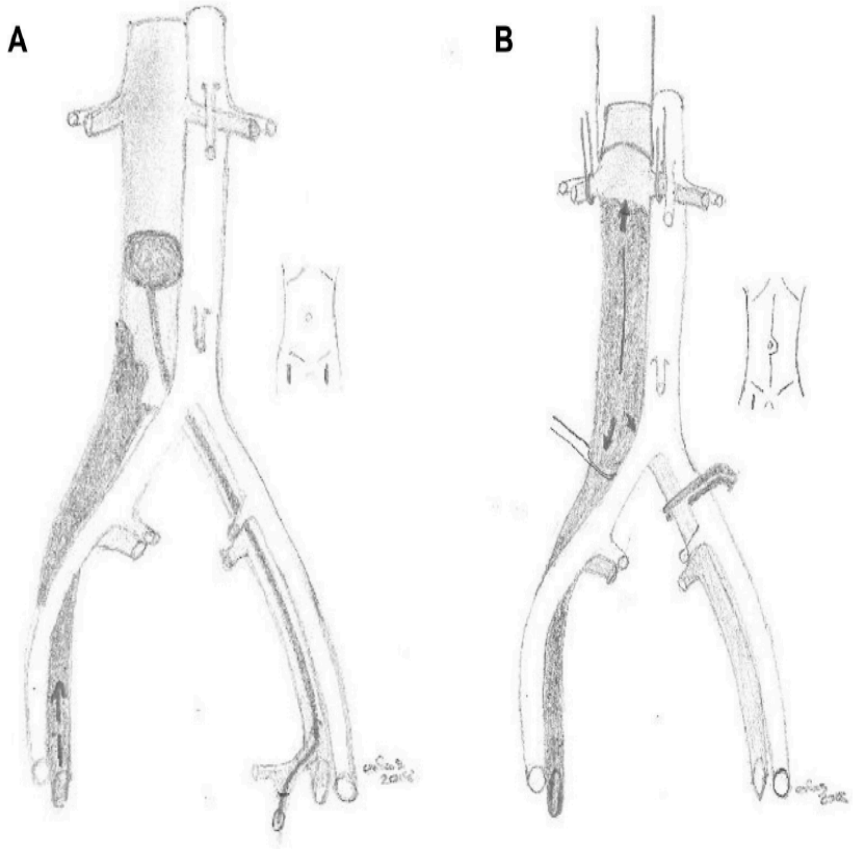

Supplementary Fig (online only). Surgical approaches. **A,** Indirect transfemoral venous thrombectomy (iTFVT). Inferior vena cava thrombosis (IVCT) with deep venous thrombosis (DVT) of the right iliac and femoral veins. Bilateral inguinal incision with exposure of all relevant structures including femoral artery and veins. An occlusion balloon is advanced over the left inguinal approach and placed proximal to the thrombus in the inferior vena cava (IVC). Thereafter, Fogarty maneuvers (*arrows*) are performed for complete thrombus removal. The final thrombectomy maneuver is performed with the occlusion balloon over the left inguinal approach to completely remove residual and mobilized thrombus. **B,** Direct open venous thrombectomy (dOVT). Extensive thrombus burden with extension of the IVCT to the renal vein level. Median laparotomy is performed to expose the aorta and the IVC. Temporary vessel loops are used to control venous backflow over the renal veins, the IVC, and the thrombosed common iliac vein. The contralateral common iliac vein is clamped. Direct thrombectomy is performed using venotomy of the IVC, followed by retrograde Fogarty maneuvers (*arrows*). Additional inguinal incision on the thrombosed side or additional abdominal incision combining dOVT and iTFVT was necessary for 44 patients (conversion rate from iTFVT to dOVT, n = 35 patients; dOVT to iTFVT, n = 9 patients). An arteriovenous fistula (AVF) was established for both procedures to augment blood flow on the sides of the thrombosed iliac veins during a period of 3 months.

Journal of Vascular Surgery: Venous and Lymphatic Disorders
Volume 7, Number 3

Supplementary Table (online only). Compression duplex ultrasound (CDU) for patients at detailed phlebologic follow-up (DPFE; N = 38)

	Affected leg (reflux/total)	Contralateral leg (reflux/total)	Affected leg (occlusion/total)	Contralateral leg (occlusion/total)
Common femoral vein and iliac veins (iliofemoral trunk)	7/38 (18.4)	2/38 (5.3)	5/38 (13.2)	3/38 (7.9)
Femoral vein	2/38 (5.3)	1/38 (2.6)	1/38 (2.6)	3/38 (7.9)
Deep femoral vein	0/38 (0)	0/38 (0)	0/38 (0)	0/38 (0)
Popliteal vein	4/38 (10.5)	3/38 (7.9)	1/38 (2.6)	1/38 (2.6)
Posterior tibial vein	0/38 (0)	0/38 (0)	0/38 (0)	0/38 (0)
Anterior tibial vein	0/38 (0)	0/38 (0)	0/38 (0)	0/38 (0)
Fibular vein	0/38 (0)	0/38 (0)	0/38 (0)	0/38 (0)
Great saphenous vein	10/38 (26.3)	8/38 (21.1)	0/38 (0)	0/38 (0)
Small saphenous vein	2/38 (5.3)	0/38 (0)	0/38 (0)	0/38 (0)

Data are presented as frequency distribution (%).

5. Fazit

Funktionales Geweberemodeling spielt bei vielen gefäßmedizinischen Krankheitsbildern eine maßgebende Rolle. In der Pathogenese des AAA ist das Geweberemodeling kausal beteiligt und steht in reziproker Beziehung zur Inflammation. Nikotin bedingt durch das Remodeling der aortalen Gefäßwand eine differentielle Steifigkeitsentwicklung in thorakalen und abdominellen Aortensegmenten. Für eine Zunahme der Gefäßsteifigkeit spielt neben der Elastinfragmentierung die anteilige Verteilung von Kollagen innerhalb der einzelnen Wandschichten eine wesentliche Rolle, so dass eine automatisierte Auswertung richtungsweisend ist. Die enge Verzahnung von Geweberemodeling und Inflammation zeigt sich in vielsprechenden anti-inflammatorischen therapeutischen Ansätzen.

Das Geweberemodeling während der physiologischen Wundheilung sowie bei ischämisch bedingten Wunden beruht maßgeblich auf dem funktionalen Zusammenspiel zellulärer Subprozesse. Dies wird durch eine suffiziente Sauerstoffversorgung des Wundgebiets ermöglicht. CBH inhibieren essentielle zelluläre Subprozesse der physiologischen Wundheilung wie Zellproliferation, -migration und die Kontraktion der EZM schon bei kurzen Expositionszeiten. GBH zeigen diese Effekte nicht in gleicher Weise. Die Auswirkungen der Hämostyptika sind dabei nicht ausschließlich durch die degradationsbedingte Azidose zu erklären, sondern könnten partiell auch auf parallel anfallende Endprodukte der Degradation beruhen. Um ein konstant ausreichendes Sauerstoffangebot für das Geweberemodeling ischämisch-bedingter Wunden zu gewährleisten, existieren konservative Therapieansätze wie die intravenöse Prostglandin E1 Infusion. Die TcPO2, als Index für das lokale Sauerstoffangebot, kann bei Positionierung 15-20 cm proximal der ischämisch-bedingten Wunde und nach Normierung mit herznahen TcPO2 Werten den Erfolg der Therapie effektiv dokumentieren.

Das PTS führt als Folgeerkrankung einer IFDVT und/oder einer ICVT zu hoher Morbidität und beruht auf einem dysfunktionalen Geweberemodeling in betroffenen Venensegmenten. Offen chirurgische Therapieverfahren zur frühen Entfernung des proximalen Thrombus führen im Vergleich zu endovaskulären Therapieansätzen zu einer vergleichbaren PTS Inzidenz und erscheinen methodisch sicher. Aufgrund ihrer

Invasivität sind sie in einem modernen Therapiesettings nur in bestimmten Situationen anzuwenden. Die Sorge der sozialen Stigmatisierung bei Auftreten eines schweren PTS stellt eine wesentliches Morbiditätsmerkmal für betroffene Patienten dar.

Die vorgelegten Arbeiten zeigen die zentrale Relevanz des Geweberemodelings in vaskulären Erkrankungen auf. In experimentellen und klinischen Untersuchungen wurden relevante Erkenntnisse für die dargestellten Krankheitsbilder erarbeitet und potentielle therapeutische Angriffspunkte für klinische Therapiemöglichkeiten formuliert.

6. Abkürzungsverzeichnis

AAA = abdominelles Aortenaneurysma
ANG II = Angiontensin II
Apoe(−/−) = Apolipoprotein E-defizient
AV-Fistel = arterio-venöse Fistel
α-SMA = α-smooth muscle actin
BMI = body-mass index
bzw. = beziehungsweise
ca. = zirka
CBH = Zellulose-basierte Hämostyptika
CDT = catheter-directed thrombolysis
CEAP = clinical, etiological, anatomical, and pathophysiological
cm = Zentimeter
CTLS = CT-gesteuerte lumbale Symapthikolyse
DMP = distaler Messpunkt
dOVT = direkte offene venöse cavale Thrombektomie
DPFE = detaillierte phlebologische Nachuntersuchung
ELISA = Enzyme-linked Immunosorbent Assay
ERK = extracellular-signal-regulated kinase
EZM = extrazelluläre Matrix
FGF-2 = Fibroblast Growth Factor-2
GBH = Gelatine-basierte Hämostyptika
GUI = Graphical User Interface
h = Stunde
H&E = Hematoxylin und Eosin
HRQOL = Health-related quality of life
ICH = Immunhistochemie
IFDVT = iliofemorale Venenthrombose
IL-10 = Interleukin-10
IL-6 = Interleukin-6
ILT = intraluminaler Thrombus
iTFVT = indirekte transfemorale venöse Thrombektomie
IVCT = Thrombose der V. cava inferior

kg = Kilogramm

MAPK = mitogen-activated protein kinase

miRNA = mirko-RNA

MMP = Matrix-Metalloproteinase

MTT = 3-(4,5-Dimethylthiazol-2-yl)-2,5-diphenyltetrazoliumbromid

o.g. = oben genannten

ONRC = oxidierte nicht regenerierte Zellulose

ORC = oxidierte regenerierte Zellulose

pAVK = periphere arterielle Verschlusskrankheit

PBS = phosphate-buffered saline

PCDT = pharmacomechanical catheter-directed thrombolysis

PMN = polymorphkernige neutrophile Granulozyten

PMP = proximaler Messpunkt

PPE = Porcine Pancreas Elastase

PSR = Pikro-Siriusrot

PTS = post-thrombotisches Syndrom

PWV = Pulswellengeschwindigkeit

RPI = regionale Perfusionsindex (RPI)

SEM = Standardfehler des Mittwertes

TcPO2 = transkutane Sauerstoffspannung

TGF-β = transforming growth factor-β

TNF-α = Tumor necrosis factor-alpha

T_{reg} = Regulatorische T-Zellen

TVT = tiefe Venenthrombose

u.a. = unter anderem

V. = Vena

VEGF = Vascular Endothelial Growth Factor

7. Literaturverzeichnis

1 Robert S, Gicquel T, Victoni T, *et al.* Involvement of matrix metalloproteinases (MMPs) and inflammasome pathway in molecular mechanisms of fibrosis. *Biosci Rep* 2016; **36**: e00360–e00360.

2 Yue B. Biology of the extracellular matrix: an overview. *J Glaucoma* 2014; **23**: S20-3.

3 Grinnell F, Fukamizu H, Pawelek P, Nakagawa S. Collagen processing, crosslinking, and fibril bundle assembly in matrix produced by fibroblasts in long-term cultures supplemented with ascorbic acid. *Exp Cell Res* 1989; **181**: 483–91.

4 Barczyk M, Carracedo S, Gullberg D. Integrins. *Cell Tissue Res* 2010; **339**: 269–80.

5 Geiger B, Yamada KM. Molecular architecture and function of matrix adhesions. *Cold Spring Harb Perspect Biol* 2011; **3**: a005033–a005033.

6 Wolfenson H, Lavelin I, Geiger B. Dynamic regulation of the structure and functions of integrin adhesions. *Dev Cell* 2013; **24**: 447–58.

7 Mack M. Inflammation and fibrosis. *Matrix Biol* 2018; **68**–**69**: 106–21.

8 Madri JA, Graesser D, Haas T. The roles of adhesion molecules and proteinases in lymphocyte transendothelial migration. *Biochem Cell Biol* 1996; **74**: 749–57.

9 Owen CA, Campbell EJ. The cell biology of leukocyte-mediated proteolysis. *J Leukoc Biol* 1999; **65**: 137–50.

10 Niestrawska JA, Regitnig P, Viertler C, Cohnert TU, Babu AR, Holzapfel GA. The role of tissue remodeling in mechanics and pathogenesis of abdominal aortic aneurysms. *Acta Biomater* 2019; **88**: 149–61.

11 Gonzalez AC de O, Costa TF, Andrade Z de A, Medrado ARAP. Wound healing - A literature review. *An Bras Dermatol* 2016; **91**: 614–20.

12 Shaw TJ, Martin P. Wound repair at a glance. *J Cell Sci* 2009; **122**: 3209–13.

13 Henke PK, Varma MR, Deatrick KB, *et al.* Neutrophils modulate post-thrombotic vein wall remodeling but not thrombus neovascularization. *Thromb Haemost* 2006; **95**: 272–81.

14 Deatrick KB, Luke CE, Elfline MA, *et al.* The effect of matrix metalloproteinase 2 and matrix metalloproteinase 2/9 deletion in experimental post-thrombotic vein wall remodeling. *J Vasc Surg* 2013; **58**: 1375-1384.e2.

15 Sprynger M, Willems M, Van Damme H, Drieghe B, Wautrecht JC, Moonen M. Screening Program of Abdominal Aortic Aneurysm. *Angiology* 2019; **70**: 407–13.

16 Sweeting MJ, Thompson SG, Brown LC, Powell JT, RESCAN collaborators. Meta-analysis of individual patient data to examine factors affecting growth and rupture of small abdominal aortic aneurysms. *Br J Surg* 2012; **99**: 655–65.

17 Hirsch AT, Haskal ZJ, Hertzer NR, *et al.* ACC/AHA 2005 Practice Guidelines for the Management of Patients With Peripheral Arterial Disease (Lower Extremity, Renal, Mesenteric, and Abdominal Aortic). *Circulation* 2006; **113**: e463-654.

18 Kent KC, Zwolak RM, Egorova NN, *et al.* Analysis of risk factors for abdominal aortic aneurysm in a cohort of more than 3 million individuals. *J Vasc Surg* 2010; **52**: 539–48.

19 von Beckerath O, Schrader S, Katoh M, Luther B, Santosa F, Kröger K. Mortality in endovascular and open abdominal aneurysm repair - trends in Germany. *Vasa* 2018; **47**: 43–8.

20 Shimizu K, Mitchell RN, Libby P. Inflammation and cellular immune responses in abdominal aortic aneurysms. *Arterioscler Thromb Vasc Biol* 2006; **26**: 987–94.

21 Manning MW, Cassis LA, Daugherty A. Differential effects of doxycycline, a broad-spectrum matrix metalloproteinase inhibitor, on angiotensin II-induced atherosclerosis and abdominal aortic aneurysms. *Arterioscler Thromb Vasc Biol* 2003; **23**: 483–8.

22 Satta J, Haukipuro K, Kairaluoma MI, Juvonen T. Aminoterminal propeptide of type III procollagen in the follow-up of patients with abdominal aortic aneurysms. *J Vasc Surg*

1997; **25**: 909–15.
23 Ailawadi G, Moehle CW, Pei H, *et al.* Smooth muscle phenotypic modulation is an early event in aortic aneurysms. *J Thorac Cardiovasc Surg* 2009; **138**: 1392–9.
24 Kunieda T, Minamino T, Nishi J-I, *et al.* Angiotensin II induces premature senescence of vascular smooth muscle cells and accelerates the development of atherosclerosis via a p21-dependent pathway. *Circulation* 2006; **114**: 953–60.
25 Maegdefessel L, Spin JM, Raaz U, *et al.* miR-24 limits aortic vascular inflammation and murine abdominal aneurysm development. *Nat Commun* 2014; **5**: 5214.
26 Maegdefessel L, Azuma J, Toh R, *et al.* Inhibition of microRNA-29b reduces murine abdominal aortic aneurysm development. *J Clin Invest* 2012; **122**: 497–506.
27 Haller SJ, Crawford JD, Courchaine KM, *et al.* Intraluminal thrombus is associated with early rupture of abdominal aortic aneurysm. *J Vasc Surg* 2018; **67**: 1051-1058.e1.
28 Coulombe PA. Wound epithelialization: accelerating the pace of discovery. *J Invest Dermatol* 2003; **121**: 219–30.
29 Norgren L, Hiatt WR, Dormandy JA, Nehler MR, Harris KA, Fowkes FGR. Inter-Society Consensus for the Management of Peripheral Arterial Disease (TASC II). *J Vasc Surg* 2007; **45**: S5–67.
30 Nelzén O, Bergqvist D, Lindhagen A. The prevalence of chronic lower-limb ulceration has been underestimated: results of a validated population questionnaire. *Br J Surg* 1996; **83**: 255–8.
31 Ploeg AJ, Lardenoye J-WP, Peeters M-PFMV, Hamming JF, Breslau PJ. Wound complications at the groin after peripheral arterial surgery sparing the lymphatic tissue: a double-blind randomized clinical trial. *Am J Surg* 2009; **197**: 747–51.
32 Lee ES, Santilli SM, Olson MM, Kuskowski MA, Lee JT. Wound infection after infrainguinal bypass operations: multivariate analysis of putative risk factors. *Surg Infect (Larchmt)* 2000; **1**: 257–63.
33 Exton RJ, Galland RB. Major groin complications following the use of synthetic grafts. *Eur J Vasc Endovasc Surg* 2007; **34**: 188–90.
34 Olinic D-M, Spinu M, Olinic M, *et al.* Epidemiology of peripheral artery disease in Europe: VAS Educational Paper. *Int Angiol* 2018; **37**: 327–34.
35 Smolderen KG, Wang K, de Pouvourville G, *et al.* Two-year vascular hospitalisation rates and associated costs in patients at risk of atherothrombosis in France and Germany: highest burden for peripheral arterial disease. *Eur J Vasc Endovasc Surg* 2012; **43**: 198–207.
36 Schäfer M, Werner S. Cancer as an overhealing wound: an old hypothesis revisited. *Nat Rev Mol Cell Biol* 2008; **9**: 628–38.
37 Werner S, Grose R. Regulation of wound healing by growth factors and cytokines. *Physiol Rev* 2003; **83**: 835–70.
38 Reinke JM, Sorg H. Wound repair and regeneration. *Eur Surg Res* 2012; **49**: 35–43.
39 Wang P-H, Huang B-S, Horng H-C, Yeh C-C, Chen Y-J. Wound healing. *J Chin Med Assoc* 2018; **81**: 94–101.
40 Tuderman L, Myllylä R, Kivirikko KI. Mechanism of the prolyl hydroxylase reaction. 1. Role of co-substrates. *Eur J Biochem* 1977; **80**: 341–8.
41 Sorg H, Tilkorn DJ, Hager S, Hauser J, Mirastschijski U. Skin Wound Healing: An Update on the Current Knowledge and Concepts. *Eur Surg Res* 2017; **58**: 81–94.
42 Lindholm C, Searle R. Wound management for the 21st century: combining effectiveness and efficiency. *Int Wound J* 2016; **13 Suppl 2**: 5–15.
43 Heng MCY. Wound healing in adult skin: aiming for perfect regeneration. *Int J Dermatol* 2011; **50**: 1058–66.
44 Opalenik SR, Davidson JM. Fibroblast differentiation of bone marrow-derived cells during wound repair. *FASEB J* 2005; **19**: 1561–3.

45 Gurtner GC, Werner S, Barrandon Y, Longaker MT. Wound repair and regeneration. *Nature* 2008; **453**: 314–21.

46 Ende-Verhaar YM, Tick LW, Klok FA, *et al.* Post-thrombotic syndrome: Short and long-term incidence and risk factors. *Thromb Res* 2019; **177**: 102–9.

47 Baldwin MJ, Moore HM, Rudarakanchana N, Gohel M, Davies AH. Post-thrombotic syndrome: a clinical review. *J Thromb Haemost* 2013; **11**: 795–805.

48 Kahn SR, Ducruet T, Lamping DL, *et al.* Prospective evaluation of health-related quality of life in patients with deep venous thrombosis. *Arch Intern Med* 2005; **165**: 1173–8.

49 Deatrick KB, Elfline M, Baker N, *et al.* Postthrombotic vein wall remodeling: preliminary observations. *J Vasc Surg* 2011; **53**: 139–46.

50 Wakefield TW, Strieter RM, Wilke CA, *et al.* Venous thrombosis-associated inflammation and attenuation with neutralizing antibodies to cytokines and adhesion molecules. *Arterioscler Thromb Vasc Biol* 1995; **15**: 258–68.

51 Sood V, Luke CE, Deatrick KB, *et al.* Urokinase plasminogen activator independent early experimental thrombus resolution: MMP2 as an alternative mechanism. *Thromb Haemost* 2010; **104**: 1174–83.

52 Deatrick KB, Obi A, Luke CE, *et al.* Matrix metalloproteinase-9 deletion is associated with decreased mid-term vein wall fibrosis in experimental stasis DVT. *Thromb Res* 2013; **132**: 360–6.

53 Deatrick KB, Eliason JL, Lynch EM, *et al.* Vein wall remodeling after deep vein thrombosis involves matrix metalloproteinases and late fibrosis in a mouse model. *J Vasc Surg* 2005; **42**: 140–8.

54 Franzeck UK, Schalch I, Jäger KA, Schneider E, Grimm J, Bollinger A. Prospective 12-year follow-up study of clinical and hemodynamic sequelae after deep vein thrombosis in low-risk patients (Zürich study). *Circulation* 1996; **93**: 74–9.

55 Bergan JJ, Schmid-Schönbein GW, Smith PDC, Nicolaides AN, Boisseau MR, Eklof B. Chronic venous disease. *N Engl J Med* 2006; **355**: 488–98.

56 Nicolaides AN, Hussein MK, Szendro G, Christopoulos D, Vasdekis S, Clarke H. The relation of venous ulceration with ambulatory venous pressure measurements. *J Vasc Surg* 1993; **17**: 414–9.

57 Araki CT, Back TL, Padberg FT, *et al.* The significance of calf muscle pump function in venous ulceration. *J Vasc Surg* 1994; **20**: 872–7; discussion 878-9.

58 Welkie JF, Comerota AJ, Katz ML, Aldridge SC, Kerr RP, White J V. Hemodynamic deterioration in chronic venous disease. *J Vasc Surg* 1992; **16**: 733–40.

59 Chiasakul T, Cuker A. The case for catheter-directed thrombolysis in selected patients with acute proximal deep vein thrombosis. *Blood Adv* 2018; **2**: 1799–802.

60 Filippidis FT, Laverty AA, Gerovasili V, Vardavas CI. Two-year trends and predictors of e-cigarette use in 27 European Union member states. *Tob Control* 2017; **26**: 98–104.

61 Raaz U, Schellinger IN, Chernogubova E, *et al.* Transcription Factor Runx2 Promotes Aortic Fibrosis and Stiffness in Type 2 Diabetes Mellitus. *Circ Res* 2015; **117**: 513–24.

62 Raaz U, Zollner AM, Schellinger IN, *et al.* Segmental Aortic Stiffening Contributes to Experimental Abdominal Aortic Aneurysm Development. *Circulation* 2015; **131**: 1783–95.

63 Azuma J, Asagami T, Dalman R, Tsao PS. Creation of murine experimental abdominal aortic aneurysms with elastase. *J Vis Exp* 2009; **23**: pii: 1280.

64 Daugherty A, Manning MW, Cassis LA. Angiotensin II promotes atherosclerotic lesions and aneurysms in apolipoprotein E-deficient mice. *J Clin Invest* 2000; **105**: 1605–12.

65 Rhee M-Y, Na S-H, Kim Y-K, Lee M-M, Kim H-Y. Acute effects of cigarette smoking on arterial stiffness and blood pressure in male smokers with hypertension. *Am J Hypertens* 2007; **20**: 637–41.

66 Ikonomidis I, Vlastos D, Kourea K, *et al.* Electronic Cigarette Smoking Increases Arterial Stiffness and Oxidative Stress to a Lesser Extent Than a Single Conventional Cigarette:

An Acute and Chronic Study. *Circulation* 2018; **137**: 303–6.
67 Lyle AN, Raaz U. Killing Me Unsoftly: Causes and Mechanisms of Arterial Stiffness. *Arterioscler Thromb Vasc Biol* 2017; **37**: e1–11.
68 Wegner KA, Keikhosravi A, Eliceiri KW, Vezina CM. Fluorescence of Picrosirius Red Multiplexed With Immunohistochemistry for the Quantitative Assessment of Collagen in Tissue Sections. *J Histochem Cytochem* 2017; **65**: 479–90.
69 Velidandla S, Gaikwad P, Ealla KKR, Bhorgonde KD, Hunsingi P, Kumar A. Histochemical analysis of polarizing colors of collagen using Picrosirius Red staining in oral submucous fibrosis. *J Int oral Heal JIOH* 2014; **6**: 33–8.
70 Coleman R. Picrosirius red staining revisited. *Acta Histochem* 2011; **113**: 231–3.
71 Lattouf R, Younes R, Lutomski D, *et al.* Picrosirius red staining: a useful tool to appraise collagen networks in normal and pathological tissues. *J Histochem Cytochem* 2014; **62**: 751–8.
72 Carty CS, Soloway PD, Kayastha S, *et al.* Nicotine and cotinine stimulate secretion of basic fibroblast growth factor and affect expression of matrix metalloproteinases in cultured human smooth muscle cells. *J Vasc Surg* 1996; **24**: 927–34; discussion 934-5.
73 Jacob-Ferreira ALB, Palei ACT, Cau SB, *et al.* Evidence for the involvement of matrix metalloproteinases in the cardiovascular effects produced by nicotine. *Eur J Pharmacol* 2010; **627**: 216–22.
74 Goergen CJ, Barr KN, Huynh DT, *et al.* In vivo quantification of murine aortic cyclic strain, motion, and curvature: implications for abdominal aortic aneurysm growth. *J Magn Reson Imaging* 2010; **32**: 847–58.
75 Wolinsky H, Glagov S. Comparison of abdominal and thoracic aortic medial structure in mammals. Deviation of man from the usual pattern. *Circ Res* 1969; **25**: 677–86.
76 Hickson SS, Butlin M, Graves M, *et al.* The relationship of age with regional aortic stiffness and diameter. *JACC Cardiovasc Imaging* 2010; **3**: 1247–55.
77 Zhang J, Zhao X, Vatner DE, *et al.* Extracellular Matrix Disarray as a Mechanism for Greater Abdominal Versus Thoracic Aortic Stiffness With Aging in Primates. *Arterioscler Thromb Vasc Biol* 2016; **36**: 700–6.
78 Ramella M, Bernardi P, Fusaro L, *et al.* Relevance of inflammation and matrix remodeling in abdominal aortic aneurysm (AAA) and popliteal artery aneurysm (PAA) progression. *Am J Transl Res* 2018; **10**: 3265–75.
79 Fiorentino DF, Bond MW, Mosmann TR. Two types of mouse T helper cell. IV. Th2 clones secrete a factor that inhibits cytokine production by Th1 clones. *J Exp Med* 1989; **170**: 2081–95.
80 Commins S, Steinke JW, Borish L. The extended IL-10 superfamily: IL-10, IL-19, IL-20, IL-22, IL-24, IL-26, IL-28, and IL-29. *J Allergy Clin Immunol* 2008; **121**: 1108–11.
81 Fiorentino DF, Zlotnik A, Mosmann TR, Howard M, O'Garra A. IL-10 inhibits cytokine production by activated macrophages. *J Immunol* 1991; **147**: 3815–22.
82 Péguet-Navarro J, Moulon C, Caux C, Dalbiez-Gauthier C, Banchereau J, Schmitt D. Interleukin-10 inhibits the primary allogeneic T cell response to human epidermal Langerhans cells. *Eur J Immunol* 1994; **24**: 884–91.
83 Chernoff AE, Granowitz E V, Shapiro L, *et al.* A randomized, controlled trial of IL-10 in humans. Inhibition of inflammatory cytokine production and immune responses. *J Immunol* 1995; **154**: 5492–9.
84 Tiemessen MM, Jagger AL, Evans HG, van Herwijnen MJC, John S, Taams LS. CD4+CD25+Foxp3+ regulatory T cells induce alternative activation of human monocytes/macrophages. *Proc Natl Acad Sci U S A* 2007; **104**: 19446–51.
85 Rateri DL, Howatt DA, Moorleghen JJ, Charnigo R, Cassis LA, Daugherty A. Prolonged infusion of angiotensin II in apoE(-/-) mice promotes macrophage recruitment with continued expansion of abdominal aortic aneurysm. *Am J Pathol* 2011; **179**: 1542–8.

86 Liu G, Ma H, Qiu L, *et al.* Phenotypic and functional switch of macrophages induced by regulatory CD4+CD25+ T cells in mice. *Immunol Cell Biol* 2011; **89**: 130–42.

87 Lindeman JHN, Abdul-Hussien H, van Bockel JH, Wolterbeek R, Kleemann R. Clinical trial of doxycycline for matrix metalloproteinase-9 inhibition in patients with an abdominal aneurysm: doxycycline selectively depletes aortic wall neutrophils and cytotoxic T cells. *Circulation* 2009; **119**: 2209–16.

88 Henderson EL, Geng YJ, Sukhova GK, Whittemore AD, Knox J, Libby P. Death of smooth muscle cells and expression of mediators of apoptosis by T lymphocytes in human abdominal aortic aneurysms. *Circulation 1999*; **99**: 96–104.

89 Meng X, Yang J, Zhang K, *et al.* Regulatory T cells prevent angiotensin II-induced abdominal aortic aneurysm in apolipoprotein E knockout mice. *Hypertens (Dallas, Tex 1979)* 2014; **64**: 875–82.

90 Velnar T, Bailey T, Smrkolj V. The wound healing process: an overview of the cellular and molecular mechanisms. *J Int Med Res* 2009; **37**: 1528–42.

91 Probst S, Seppänen S, Gerber V, Hopkins A, Rimdeika R, Gethin G. EWMA Document: Home Care-Wound Care: Overview, Challenges and Perspectives. *J Wound Care* 2014; **23 Suppl 5a**: S1–41.

92 Nussbaum SR, Carter MJ, Fife CE, *et al.* An Economic Evaluation of the Impact, Cost, and Medicare Policy Implications of Chronic Nonhealing Wounds. *Value Health* 2018; **21**: 27–32.

93 Silhi N. Diabetes and wound healing. *J Wound Care* 1998; **7**: 47–51.

94 Pierpont YN, Dinh TP, Salas RE, *et al.* Obesity and surgical wound healing: a current review. *ISRN Obes* 2014; **20**: 2014:638936

95 Young ME. Malnutrition and wound healing. *Heart Lung* 1988; **17**: 60–7.

96 Garg A. Pathophysiology of tobacco use and wound healing. *Dent Implantol Update* 2010; **21**: 1–4.

97 Wang AS, Armstrong EJ, Armstrong AW. Corticosteroids and wound healing: clinical considerations in the perioperative period. *Am J Surg* 2013; **206**: 410–7.

98 Merino J, Planas A, Elosua R, *et al.* Incidence and Risk Factors of Peripheral Arterial Occlusive Disease in a Prospective Cohort of 700 Adult Elderly Men Followed for 5 Years. *World J Surg* 2010; **34**: 1975–9.

99 Sundaram C, Keenan A. Evolution of hemostatic agents in surgical practice. *Indian J Urol* 2010; **26**: 374.

100 Frantz VK. ABSORBABLE COTTON, PAPER AND GAUZE : (OXIDIZED CELLULOSE). *Ann Surg* 1943; **118**: 116–26.

101 Pierce A, Wilson D, Wiebkin O. Surgicel: macrophage processing of the fibrous component. *Int J Oral Maxillofac Surg* 1987; **16**: 338–45.

102 Lewis KM, Spazierer D, Urban MD, Lin L, Redl H, Goppelt A. Comparison of regenerated and non-regenerated oxidized cellulose hemostatic agents. *Eur Surg* 2013; **45**: 213–20.

103 Alpaslan C, Alpaslan GH, Oygur T. Tissue reaction to three subcutaneously implanted local hemostatic agents. *Br J Oral Maxillofac Surg* 1997; **35**: 129–32.

104 Kim S-D, Hong S-L, Kim M-J, *et al.* Effectiveness of hemostatic gelatin sponge as a packing material after septoplasty: A prospective, randomized, multicenter study. *Auris Nasus Larynx* 2018; **45**: 286–90.

105 Padalhin AR, Lee B-T. Hemostasis and Bone Regeneration Using Chitosan/Gelatin-BCP Bi-layer Composite Material. *ASAIO J* 2019; **65:** 620-62

106 Gazzeri R, Galarza M, Conti C, De Bonis C. Incidence of thromboembolic events after use of gelatin-thrombin-based hemostatic matrix during intracranial tumor surgery. *Neurosurg Rev* 2018; **41**: 303–10.

107 Vyas KS, Saha SP. Comparison of hemostatic agents used in vascular surgery. *Expert Opin Biol Ther* 2013; **13**: 1663–72.

108 Echave M, Oyagüez I, Casado MA. Use of Floseal®, a human gelatine-thrombin matrix sealant, in surgery: a systematic review. *BMC Surg* 2014; **14**: 111.

109 Sundaram CP, Keenan AC. Evolution of hemostatic agents in surgical practice. *Indian J Urol* 2010; **26**: 374–8.

110 Zoucas E, Göransson G, Bengmark S. Comparative evaluation of local hemostatic agents in experimental liver trauma: a study in the rat. *J Surg Res* 1984; **37**: 145–50.

111 Pober JS, Cotran RS. The role of endothelial cells in inflammation. *Transplantation* 1990; **50**: 537–44.

112 Schreml S, Szeimies RM, Prantl L, Karrer S, Landthaler M, Babilas P. Oxygen in acute and chronic wound healing. *Br J Dermatol* 2010; **163**: 257–68.

113 Lewis KM, Spazierer D, Urban MD, Lin L, Redl H, Goppelt A. Comparison of regenerated and non-regenerated oxidized cellulose hemostatic agents. *Eur Surg* 2013; **45**: 213–20.

114 Spangler D, Rothenburger S, Nguyen K, Jampani H, Weiss S, Bhende S. In vitro antimicrobial activity of oxidized regenerated cellulose against antibiotic-resistant microorganisms. *Surg Infect (Larchmt)* 2003; **4**: 255–62.

115 Ibrahim MM, Chen L, Bond JE, *et al.* Myofibroblasts contribute to but are not necessary for wound contraction. *Lab Invest* 2015; **95**: 1429–38.

116 Froehlich JE, Anastassiades TP. Role of pH in fibroblast proliferation. *J Cell Physiol* 1974; **84**: 253–60.

117 Akyol N, Akpolat N. Effects of intraoperative oxidated regenerated cellulose on wound healing reaction after glaucoma filtration surgery: a comparative study with Interceed and Surgicel. *Indian J Ophthalmol 2008*; **56**: 109–14.

118 Liu S-A, Cheng C-C, Chen J-S, Hung Y-W, Chen F-J, Chiu Y-T. Effect of oxidized regenerated cellulose on the healing of pharyngeal wound: an experimental animal study. *J Chin Med Assoc* 2012; **75**: 176–82.

119 Varkey M, Ding J, Tredget EE. Fibrotic Remodeling of Tissue-Engineered Skin with Deep Dermal Fibroblasts Is Reduced by Keratinocytes. *Tissue Eng Part A* 2014; **20:** 716-27

120 Hart J, Silcock D, Gunnigle S, Cullen B, Light ND, Watt PW. The role of oxidised regenerated cellulose/collagen in wound repair: effects in vitro on fibroblast biology and in vivo in a model of compromised healing. *Int J Biochem Cell Biol* 2002; **34**: 1557–70.

121 Krishnan LK, Mohanty M, Umashankar PR, Lal AV. Comparative evaluation of absorbable hemostats: advantages of fibrin-based sheets. *Biomaterials* 2004; **25**: 5557–63.

122 Pierce AM, Wiebkin OW, Wilson DF. Surgicel: its fate following implantation. *J Oral Pathol* 1984; **13**: 661–70.

123 Dimitrijevich SD, Tatarko M, Gracy RW, *et al.* In vivo degradation of oxidized, regenerated cellulose. *Carbohydr Res* 1990; **198**: 331–41.

124 Lan WC, Lan WH, Chan CP, Hsieh CC, Chang MC, Jeng JH. The effects of extracellular citric acid acidosis on the viability, cellular adhesion capacity and protein synthesis of cultured human gingival fibroblasts. *Aust Dent J* 1999; **44**: 123–30.

125 Huang S, He P, Xu D, Li J, Peng X, Tang Y. Acidic stress induces apoptosis and inhibits angiogenesis in human bone marrow-derived endothelial progenitor cells. *Oncol Lett* 2017; **14**: 5695–702.

126 Huang C, Jacobson K, Schaller MD. MAP kinases and cell migration. *J Cell Sci* 2004; **117**: 4619–28.

127 Denton CP, Khan K, Hoyles RK, *et al.* Inducible lineage-specific deletion of TbetaRII in fibroblasts defines a pivotal regulatory role during adult skin wound healing. *J Invest Dermatol* 2009; **129**: 194–204.

128 Balzer K, Bechara G, Bisler H, *et al.* Reduction of ischaemic rest pain in advanced peripheral arterial occlusive disease. A double blind placebo controlled trial with iloprost. *Int Angiol 1991*; **10**: 229–32.

129 Brock FE, Abri O, Baitsch G, *et al.* [Iloprost in the treatment of ischemic tissue lesions in

diabetics. Results of a placebo-controlled multicenter study with a stable prostacyclin derivative]. *Schweiz Med Wochenschr* 1990; **120**: 1477–82.
130 Norgren L, Alwmark A, Angqvist KA, *et al.* A stable prostacyclin analogue (iloprost) in the treatment of ischaemic ulcers of the lower limb. A Scandinavian-Polish placebo controlled, randomised multicenter study. *Eur J Vasc Surg* 1990; **4**: 463–7.
131 Trübestein G, Ludwig M, Diehm C, Gruss JD, Horsch S. [Prostaglandin E1 in stage III and IV arterial occlusive diseases. results of a multicenter study]. *Dtsch Med Wochenschr* 1987; **112**: 955–9.
132 Reiter M, Bucek RA, Stümpflen A, Minar E. Prostanoids for intermittent claudication. *Cochrane database Syst Rev* 2004; **(1):** CD000986.
133 Bombor I, Wissgott C, Andresen R. Lumbar sympathicolysis in patients with severe peripheral artery disease: hemodynamics of the lower limbs determined by near-infrared spectroscopy, color coded duplex sonography, and temperature measurement. *Clin Med Insights Cardiol* 2014; **8**: 29–36.
134 Kahn SR, Partsch H, Vedantham S, Prandoni P, Kearon C, Subcommittee on Control of Anticoagulation of the Scientific and Standardization Committee of the International Society on Thrombosis and Haemostasis. Definition of post-thrombotic syndrome of the leg for use in clinical investigations: a recommendation for standardization. *J Thromb Haemost* 2009; **7**: 879–83.
135 STAIN M, SCHONAUER V, MINAR E, *et al.* The post-thrombotic syndrome: risk factors and impact on the course of thrombotic disease. *J Thromb Haemost* 2005; **3**: 2671–6.
136 Kahn SR, Shrier I, Julian JA, *et al.* Determinants and time course of the postthrombotic syndrome after acute deep venous thrombosis. *Ann Intern Med* 2008; **149**: 698–707.
137 Galanaud JP, Holcroft CA, Rodger MA, *et al.* Predictors of post-thrombotic syndrome in a population with a first deep vein thrombosis and no primary venous insufficiency. *J Thromb Haemost* 2013; **11**: 474–80.
138 Jaff MR, McMurtry MS, Archer SL, *et al.* Management of Massive and Submassive Pulmonary Embolism, Iliofemoral Deep Vein Thrombosis, and Chronic Thromboembolic Pulmonary Hypertension. *Circulation* 2011; **123**: 1788–830.
139 Kearon C, Akl EA, Comerota AJ, *et al.* Antithrombotic therapy for VTE disease: Antithrombotic Therapy and Prevention of Thrombosis, 9th ed: American College of Chest Physicians Evidence-Based Clinical Practice Guidelines. *Chest* 2012; **141**: e419S-e496S.
140 Elliot MS, Immelman EJ, Jeffery P, *et al.* A comparative randomized trial of heparin versus streptokinase in the treatment of acute proximal venous thrombosis: an interim report of a prospective trial. *Br J Surg* 1979; **66**: 838–43.
141 Comerota AJ. Venous thrombectomy and arteriovenous fistula versus anticoagulation in the treatment of iliofemoral venous thrombosis. *J Vasc Surg* 1992; **15**: 887–9.
142 Ockert S, von Allmen M, Heidemann M, Brusa J, Duwe J, Seelos R. Acute Venous Iliofemoral Thrombosis: Early Surgical Thrombectomy Is Effective and Durable. *Ann Vasc Surg* 2018; **46**: 314–21.
143 Stein PD, Matta F, Yaekoub AY. Incidence of vena cava thrombosis in the United States. *Am J Cardiol* 2008; **102**: 927–9.
144 Plate G, Eklöf B, Norgren L, Ohlin P, Dahlström JA. Venous thrombectomy for iliofemoral vein thrombosis--10-year results of a prospective randomised study. *Eur J Vasc Endovasc Surg* 1997; **14**: 367–74.
145 Prandoni P, Lensing AW, Cogo A, *et al.* The long-term clinical course of acute deep venous thrombosis. *Ann Intern Med* 1996; **125**: 1–7.
146 Vedantham S, Goldhaber SZ, Julian JA, *et al.* Pharmacomechanical Catheter-Directed Thrombolysis for Deep-Vein Thrombosis. *N Engl J Med* 2017; **377**: 2240–52.
147 Enden T, Haig Y, Kløw N-E, *et al.* Long-term outcome after additional catheter-directed thrombolysis versus standard treatment for acute iliofemoral deep vein thrombosis (the

CaVenT study): a randomised controlled trial. *Lancet (London, England)* 2012; **379**: 31–8.
148 Grommes J, Strijkers R, Greiner A, Mahnken AH, Wittens CHA. Safety and Feasibility of Ultrasound-accelerated Catheter-directed Thrombolysis in Deep Vein Thrombosis. *Eur J Vasc Endovasc Surg* 2011; **41**: 526–32.
149 Engelberger RP, Stuck A, Spirk D, *et al.* Ultrasound-assisted versus conventional catheter-directed thrombolysis for acute iliofemoral deep vein thrombosis: 1-year follow-up data of a randomized-controlled trial. *J Thromb Haemost* 2017; **15**: 1351–60.
150 Du G-C, Zhang M-C, Zhao J-C. Catheter-directed thrombolysis plus anticoagulation versus anticoagulation alone in the treatment of proximal deep vein thrombosis - a meta-analysis. *Vasa* 2015; **44**: 0195–202.
151 Casey ET, Murad MH, Zumaeta-Garcia M, *et al.* Treatment of acute iliofemoral deep vein thrombosis. *J Vasc Surg* 2012; **55**: 1463–73.
152 Kahn SR, Comerota AJ, Cushman M, *et al.* The Postthrombotic Syndrome: Evidence-Based Prevention, Diagnosis, and Treatment Strategies. *Circulation* 2014; **130**: 1636–61.
153 Dueppers P, Grabitz K, Li Y, Schelzig H, Wagenhäuser MU, Duran M. Surgical management of iliofemoral vein thrombosis during pregnancy and the puerperium. *J Vasc Surg Venous Lymphat Disord* 2016; **4**: 392–9.
154 Alkhouli M, Morad M, Narins CR, Raza F, Bashir R. Inferior Vena Cava Thrombosis. *JACC Cardiovasc Interv* 2016; **9:** 629-43
155 Ye K, Qin J, Yin M, Liu X, Lu X. Outcomes of Pharmacomechanical Catheter-directed Thrombolysis for Acute and Subacute Inferior Vena Cava Thrombosis: A Retrospective Evaluation in a Single Institution. *Eur J Vasc Endovasc Surg* 2017; **54**: 504–12.
156 Alkhouli M, Zack CJ, Zhao H, Shafi I, Bashir R. Comparative outcomes of catheter-directed thrombolysis plus anticoagulation versus anticoagulation alone in the treatment of inferior vena caval thrombosis. *Circ Cardiovasc Interv* 2015; **8**: e001882.
157 Broholm R, Sillesen H, Damsgaard MT, *et al.* Postthrombotic syndrome and quality of life in patients with iliofemoral venous thrombosis treated with catheter-directed thrombolysis. *J Vasc Surg* 2011; **54**: 18S-25S.
158 Kumar R, Rodriguez V, Matsumoto JMS, *et al.* Health-related quality of life in children and young adults with post-thrombotic syndrome: Results from a cross-sectional study. *Pediatr Blood Cancer* 2014; **61**: 546–51.

8. Abbildungsverzeichnis

9. Publikationsverzeichnis

Originalarbeiten:

Wagenhäuser MU, Pietschmann MF, Sievers B, Docheva D, Schieker M, Jansson V, Muller PE. Collagen type I and decorin expression in tenocytes depend on the cell isolation method. BMC Musculoskelet Disord. 2012; 13(1):140.

Pietschmann MF, **Wagenhäuser MU,** Docheva D, Gülecyüz MF, Jansson V, Müller P.E. The long head of the biceps tendon is a suitable cell source for tendon tissue regeneration. Arch Med Sci. 2014; 10(3):587-96.

Wagenhäuser MU, Pietschmann MF, Docheva D, Gülecyüz MF, Jansson V, Müller P.E. Müller. Assessment of essential characteristics of two different scaffolds for tendon in situ regeneration. Knee Surg Sports Traumatol Arthrosc. 2015; 23(4):1239-46.

Wagenhäuser MU, Rückert F, Niedergethmann M, Grützmann R, Saeger HD. Distribution of characteristic mutations in native ductal adenocarcinoma of the pancreas and pancreatic cancer cell lines. Cell Biol: Res Ther. 2:1. doi:10.4172/2324-9293.1000104

Sagban TA, Scharf RE, **Wagenhäuser MU,** Oberhuber A, Schelzig H, Grabitz K, Duran M. Elevated risk of thrombophilia in agenesis of the vena cava as a factor for deep vein thrombosis. Orphanet J Rare Dis. 2015; 21;10:3.

Wagenhäuser MU, Herma KB, Sagban TA, Dueppers P, Schelzig H, Duran M: Long-term results of open repair of popliteal artery aneurysm. Ann Med Surg (Lond). 2015; 4:58–63.

Wagenhäuser MU, Duran M, Dueppers P, Witte M, Schelzig H, Oberhuber A. Preliminary results of transcutaneous oxygen pressure measurement as effective monitoring for conservative therapy in peripheral occlusive disease. Ital J Vasc Endovasc Surg. 2015; 22(4):163-70.

Ficklscherer A, Stapf J, Meissner KM, Niethammer T, Lahner M, **Wagenhäuser M,** Mueller PE, Petschmann MF, Jansson V. Testing the feasibility and saftey of a Ninetendo Wii gaming console in orthopedic rehabilitation: A pilot randomized controlled study. Arch Med Sci. 2016; 12(6):1273-1278.

Dueppers P, Grabitz K, Li Y, Schelzig H, **Wagenhäuser MU,** Duran M: Surgical management of iliofemoral vein thrombosis during pregnancy and the puerperium. J Vasc Surg Venous Lymphat Disord. 2016; 4(4):392-9.

Wagenhäuser MU, Mulorz J, Ibing W, Simon F, Spin JM, Schelzig H, Oberhuber A: Oxidized (non)-regenerated cellulose affects fundamental cellular processes of wound healing. Sci Rep. 2016; 25;6:32238.

Wagenhäuser MU, Meyer-Janiszewski YK, Dueppers P, Spin JM, Floros N, Schelzig H, Duran M. Chronic Mesenteric Ischemia: Patient Outcomes Using Open Surgical Revascularization. Dig Surg. 2017; 34(4):340-349.

Floros N, Papadakis M**, Wagenhäuser MU,** Duran M, Schelzig H, Oberhuber A. Outcomes after open-surgery for inflammatory abdominal aortic aneurysm: a 10-year single-centre experience. Ann Vasc Surg. 2017; 43:144-15.

Mulorz J, **Wagenhäuser MU,** Janiszewski YK, Dueppers P, Simon F, Schelzig H, Duran M. Retrograde aortomesenteric Bypass with left-retrorenal route - "French Bypass" in 16 cases of chronic mesenteric ischemia. Ann Vasc Surg. 2017; 44:381-386.

Wagenhäuser MU, Sadat H, Dueppers P, Meyer-Janiszewski YK, Spin JM, Schelzig H, Duran M. Open surgery for iliofemoral deep vein thrombosis with temporary arteriovenous fistula remains valuable. Phlebology. 2018; 33(9):600-609.

Güleçyüz MF, Kraus-Petersen M, Schröder C, Ficklscherer A, **Wagenhäuser MU,** Braun C, Müller PE, Pietschmann MF. The Primary Stability of a Bioabsorbable Poly-L-Lactic Acid Suture Anchor for Rotator Cuff Repair Is Not Improved with Polymethylmethacrylate or Bioabsorbable Bone Cement Augmentation. HSS J. 2018; 14(1):15-22.

Toyama K, Spin JM Deng AC, Ke W, Yoshino T, **Wagenhäuser MU,** Nguyen H, Huang TT, Uwe Raaz U, Adam M, Jagger A, Tsao PS. microRNA-Mediated Therapy Modulating Blood-Brain Barrier Disruption Improves Vascular Cognitive Impairment. Arterioscler Thromb Vasc Biol. 2018; 38(6):1392-1406.

Adam M, Kooreman N, Jagger A, **Wagenhäuser MU,** Mehrkens D, Wang Y, Yosuke Kayama Y, Toyama K, Raaz U, Schellinger IN, Maegdefessel L, Spin JM, Hamming JF, Quax PHA, Baldus S, Wu JC, Tsao PS. Systemic upregulation of IL-10 using a non-immunogenic vector reduces abdominal aortic aneurysm growth and dissection rate. Arterioscler Thromb Vasc Biol. 2018; 38(8):1796-1805.

Wagenhäuser MU, Schellinger IN, Yoshino T, Toyama K, Kayama Y, Deng A, Guenther SP, Petzold A, Mulorz J, Mulorz P, Hasenfuß G, Ibing W, Elvers M, Schuster A, Ramasubramanian AK, Adam M, Schelzig H, Spin JM, Raaz U, Tsao PS. Chronic Nicotine Exposure Induces Murine Aortic Remodeling and Stiffness Segmentation-Implications for Abdominal Aortic Aneurysm Susceptibility. Front Physiol. 2018; 31;9:1459.

Nguyen DM, **Wagenhäuser MU,** Mehrkens D, Adam M, Tsao PS, Ramasubramanian AK. An Automated Algorithm to Quantify Collagen Distribution in Aortic Wall. J Histochem Cytochem. 2019; 67(4):267-274.

Dueppers P, Duran M, Floros N, Schelzig H, **Wagenhäuser MU,** Oberhuber A. The JOTEC iliac branch device for exclusion of hypogastric artery aneurysms-ABRAHAM study. J Vasc Surg. 2019; 70(3):748-755.

Wagenhäuser MU, Dimopoulos C, Antakyali K, Meyer-Janiszewski YK, Mulorz J, Ibing W, Ertas N, Spin JM, Schelzig H, Duran M. Clinical outcomes after direct and indirect surgical venous thrombectomy for inferior vena cava thrombosis. J Vasc Surg Venous Lymphat Disord. 2019; 7(3):333-343.e2.

Toyama K, Spin JM, Suzuki Y, Deng AC, **Wagenhäuser MU,** Yoshino Y, Mulorz J, Shuang L, Tsao PS, Masaki M. Controlled isoflurane anesthesia exposure is required for reliable behavioral testing in murine surgical models. J Pharmacol Sci. 2019; 140(1):106-108.

Wagenhäuser MU, Garabet W, van Bonn M, Ibing W, Mulorz J, Rhee YH, Spin JM, Dimopoulos C, Oberhuber A, Schelzig H, Simon F. Time-dependent effects of cellulose and gelatin-based hemostats on cellular processes of wound healing. Arch Med Sci. 2020; doi:10.5114/aoms.2020.92830.

Case studies:

Wagenhäuser MU, Ertas N, Sagban TA, Witte M, Hoffmann T, Schelzig H, Oberhuber A. A 61 year old man with disseminated intravascular coagulation: a case report. Ann Vasc Surg. 2014; 28(6):1566.e17-22.

Dueppers P, Jankowiak S, Schelzig H, **Wagenhäuser MU,** Oberhuber A: Spontaneous rupture of an isolated iliac artery dissection in a young man because of cystic medial degeneration Erdheim-Gsell. Ann Vasc Surg 2015; 29:596.e11–3.

Dueppers P, Schelzig H, **Wagenhäuser MU,** Oberhuber A: Crossover Thrombectomy of Hypogastric Arteries. Ann Vasc Surg 2015; 29:1689–92.

Rhee YH, Busch L, Sansone R, Kelm M, Ertas N, Floros N, Schelzig H, Mulorz, J, **Wagenhäuser MU.** Endovascular Occlusion of a Proximal Renal Arteriovenous Fistula with concomitant Aneurysm Formation for Rupture Prevention: A Case Report. Case Rep Vasc Med. 2019; 31;2019:8530641.

Reviews:

Wagenhäuser MU, Sagban TA, Witte M, Duran M, Schelzig H, Oberhbuber A. Isolated dissection of the superior mesenteric artery treated using open emergency surgery. World J Emerg Surg. 2014; 14;9:47.

Simon F, Oberhuber A, Floros N, Busch A, **Wagenhäuser MU,** Schelzig H, Duran M. Acute Limb Ischemia-Much More Than Just a Lack of Oxygen. Int J Mol Sci. 2018; 26;19(2): 374.

Knapsis A, Schelzig H, **Wagenhäuser MU.** Traumatische Gefäßverletzungen. Allgemein- und Viszeralchirurgie up2date 2019; 13(03): 207-222.

Dueppers P, Floros N, Schelzig H, **Wagenhaeuser MU,** Simon F, Oberhuber A. Konservative Therapie der peripheren arteriellen Verschlusserkrankung. Gefässchirurgie 2019; 24(5);431–440.

Simon F, **Wagenhäuser MU,** Busch A, Schelzig H, Gombert A. Arteriogenesis of the Spinal Cord-The Network Challenge. Cells. 2020; 22;9(2): 501.

10. Lebenslauf

Persönliche Daten

Name:	Dr. med. Markus Udo Wagenhäuser
Klink:	Klink für Gefäß- und Endovaskularchirurgie
Geburtsdatum:	07.10.1983
Staatsangehörigkeit	deutsch

Schulbildung

1990-1994	Klosterschule Dachau (Grundschule)
1994-1997	Josef-Effner-Gymnasium Dachau
1997-1999	Ignaz-Taschner-Gymnasium Dachau
1999-2000	Aarden-Lawn-School in Henley in Arden, UK (GCSE)
2000-2003	Ignaz-Taschner-Gymnasium Dachau (Abitur)

Studium

2004-2006	Friedrich-Alexander-Universität Erlangen (vorklinischer Abschnitt)
2006-2011	Ludwig-Maximilians-Universität München (klinischer Abschnitt)

praktisches Jahr

02/2010-06/2010	Schulthess Klinik, Universität Zürich (Orthopädie)
06/2010-10/2010	Victoria Hospital Wynberg, Kapstadt, Südafrika (Innere Medizin)
10/2010-02/2010	Krankenhaus Ingolstadt, Deutschland (Chirurgie)

wissenschaftliche/klinische Tätigkeiten

09/2011-01/2013	Klinik für Viszeral-, Thorax- und Gefäßchirurgie, Universitätsklinikum Dresden, Campus Carl-Gustav Carus, wissenschaftlicher Mitarbeiter
06/2013-11/2015	Klinik für Gefäß- und Endovaskularchirurgie Universitätsklinikum

	Düsseldorf (Heinrich-Heine-Universität), wissenschaftlicher Mitarbeiter
11/2015 – 3/2018	Postdoc, Tsao Lab, Cardiovascular Institute, Stanford University, CA, USA
3/2018 – aktuell	Klinik für Gefäß- und Endovaskularchirurgie Universitätsklinikum Düsseldorf (Heinrich-Heine-Universität), wissenschaftlicher Mitarbeiter
4/2020:	Facharzt für Gefäßchirurgie

wissenschaftliche Preise

2014:	Doktoranden-Preis der Deutschen Gesellschaft für Gefäßchirurgie und Gefäßmedizin als Betreuer von cand med. Joscha Mulorz 2014 (Hamburg 2014)
2015:	Posterpreis der European Society of Vascular Surgery, Spring meeting Frankfurt, 2015
2017:	Travel & Exchange Ideas Award Winners, Cardiovascular Institute, Stanford University, CA, USA
2018:	Young Investigator Award der österreichischen Gesellschaft für Gefässchirurgie
2019:	Doktoranden-Preis der Deutschen Gesellschaft für Gefäßchirurgie und Gefäßmedizin als Betreuer von cand med. Hyun Yae Rhee (Mannheim 2019)

Drittmittel

2015:	Forschungsstipendium der Deutschen Gesellschaft für Gefäßchirurgie und Gefäßmedizin; „Einfluss von Hämostyptika auf die molekularen Regulationsmechanismen einzelner Wundheilungsphasen“
2015:	DFG Forschungsstipendium zur Inanspruchnahme bei Prof. Philip S. Tsao, Cardiovasular Institute, Stanford University School of Medicine; „Stimulationsmechanismen und micro-RNA-abhängige Regulation von Inflammasomen in Aortenaneurysmen“ (WA 3533/2-1)
2018:	Stiftung für Altersforschung der Heinrich-Heine-Universität Düsseldorf; „Einfluss von Thrombozyten auf die Osteopontin und Gefäßsteifigkeits-Genexpression in Aortenaneurysma-relevanten Zelllinien unter Hypoxie“
2019:	Deutsches Zentrum für Herz-Kreislauf-Forschung e.V.; “The role of intraluminal thrombus derived non---coding RNAs in the hypoxic micromilieu of the growing abdominal aortic aneurysm wall”
2020:	Forschungskommission der Medizinischen Fakultät der Heinrich-Heine-Universität Düsseldorf, Förderlinie Ib Anschubförderung; “Tightening

endothelial junctions to prevent aortic dissections – a non-coding RNA-based approach”

2020: DFG Einzelantrag; “Einfluss der Thrombozyten-Erythrozyten Interaktionen auf die Thrombose und die Progression des abdominalen Aortenaneurysmas: Mechanismen und Konsequenzen" (WA 3533/3-1)

11. Danksagung

Die Erstellung einer wissenschaftlichen Arbeit ist nie das Werk einer einzelnen Person. Es ist jetzt an der Zeit, mich bei allen Menschen zu bedanken, die mir die Erstellung meiner Habilitationsschrift ermöglicht und mich über Jahre hinweg mit Diskussionen und Kritik sowie mit positiver Energie und ihren Optimismus unterstützt und begleitet haben.

Mein ganz besonderer Dank gilt meinem Mentor und Förderer Herrn **Hubert Schelzig**, der mir die Durchführung meiner wissenschaftlichen Ideen ermöglicht und mich bei allen Vorhaben unterstützt. Seine thematischen und wissenschaftlichen Hinweise haben wesentlich zum Gelingen der Arbeit beigetragen. Sein Rat war und ist für mich in jeder Hinsicht ein verlässlicher Kompass.

Mein großer Dank gilt Herrn **Alexander Oberhuber** und Frau **Margitta Elvers**, die mich beide in Ihre Arbeitsgruppen aufnahmen und mit denen ich konstruktiv und produktiv zusammenarbeitete.

Ich bedanke mich zudem besonders bei meinem amerikanischen Mentor Herrn **Philip Tsao** und seiner Arbeitsgruppe. Sie nahmen mich ohne Vorbehalt als Postdoc auf und waren bereit, in meine wissenschaftliche Ausbildung zu investieren. Sein großer wissenschaftlicher Fundus und sein Umgang mit Mitarbeitern, Kollegen und Partnern hat bei mir einen nachhaltigen Eindruck hinterlassen. Er war und ist für meine Arbeiten ein wichtiger Taktgeber.

Mein ganz besonderer Dank gilt **meiner Familie**. Für sie waren die vergangenen Jahre nicht minder aufregend. Sie hat mich mit Zuversicht unterstützt und hat für meine Anliegen zu jeder Tag- und Nachzeit ein offenes Ohr. Ich bedanke mich zudem bei meiner Lebenspartnerin Frau **Isabelle Honnes**, die oft auf mich verzichten musste und mir stets Mut zusprach, wenn er gebraucht wurde.

Mein Dank gilt Herrn **Joscha Mulorz.** Die Zusammenarbeit mit ihm bereitet mir riesen Spaß und große Freude. Sein Enthusiasmus war und ist begeisternd. Mit der Zeit wurde

er zu einem Freund. Ich freue mich, mit ihm auch in Zukunft Ideen zu entwickeln und zu verfolgen.

Ich möchte mich auch bei Frau **Wiebke Ibing** bedanken. Ihr empathisches Verhalten ist für mich vorbildhaft und ihr Optimismus ist ein unersetzlicher Wegbegleiter. Ohne Ihre Unterstützung wären die Arbeiten nicht möglich gewesen. Wir werden noch lange und kollegial zusammenarbeiten.

Abschließend bedanke ich mich bei allen, die zum Gelingen der Arbeiten beigetragen haben. Ich bin für jede einzelne Anregung und für jeden damit verbundenen Moment dankbar.